Geneeskundige Stichting Koningin Elisabeth
Fondation Médicale Reine Elisabeth
Königin-Elisabeth-Stiftung für Medizin
Queen Elisabeth Medical Foundation

Verslag – Rapport – Bericht – Report

2019

G.S.K.E. – F.M.R.E. – K.E.S.M. – Q.E.M.F.

www.fmre-gske.be
www.fmre-gske.eu
www.fmre-gske.com

Geneeskundige Stichting Koningin Elisabeth
2019
Inleiding verslag activiteiten van de GSKE – FMRE

De Geneeskundige Stichting Koningin Elisabeth ondersteunt onderzoek in de neurowetenschappen en kent elk jaar prijzen toe aan teams van onderzoekers die zich onderscheiden door hun innovatief werk.

De academische sessie in 2019, georganiseerd op 28 mei, in aanwezigheid van H.K.H. Prinses Astrid, de voorzitter van de senaat, professor J. Brotchi en de minister van Volksgezondheid Maggie De Block, evenals tal van politieke en wetenschappelijke persoonlijkheden, prijsgevers en onderzoekers was de gelegenheid om prijzen uit te reiken aan volgende teams:

- de Prijs Ernest Solvay aan Prof. Dr. Ir. Simon De Meyer, PhD (KU Leuven – campus Kulak Kortrijk)
- de Prijs Elisabeth Vreven aan Prof. Thomas Voets (KU Leuven)
- de Prijs CBC Banque aan Prof. Dr. Veerle Baekelandt, PhD (KU Leuven)
- de Prijs Janine et Jacques Delruelle aan Prof. Dr. Luc Leybaert, MD, PhD (UGent)

Tijdens deze sessie presenteerde Professor Richard Frakowiak een conferentie over een neuro-wetenschappelijk onderwerp “Advances in Human Brain Studies with Neuroimaging”. Deze opmerkelijke conferentie werd zeer gewaardeerd en de presentatie (PPT bestand) is beschikbaar op onze site (https://www.fmre-gske.be/pdf/uitreiking19c.pdf).

Op het einde van het jaar, op 17 oktober 2019, stelde een bezoek aan de laboratoria van de KU Leuven – Campus Kulak Kortrijk, H.K.H. Prinses Astrid, vergezeld door leden van de Raad van Bestuur, de wetenschappelijk directeur, de heer Denis Solvay en vele autoriteiten en de leden van de universiteit, in staat om het werk te ontdekken van professor dr. Ir. Simon De Meyer, die dit jaar de Ernest Solvay prijs ontving.

We danken zeer hartelijk H.K.H. Prinses Astrid voor Haar aanwezigheid op de wetenschappelijke dag en het bezoek aan de laboratoria van de KU Leuven – Campus Kulak Kortrijk. We danken de leden van de Raad van Bestuur enn het Wetenschappelijk Comité voor het werk dat zij verrichten ten voordele van de neurowetenschappelijke onderzoekers in ons land die dankzij de prijsgevers de ontwikkeling van Neurowetenschappen kunnen voortzetten.

Prof. dr. Jean-Marie Maloteaux,
wetenschappelijk directeur
Brussel, 30 december 2019

Fondation Médicale Reine Elisabeth
2019
Introduction rapport d'activités de la FMRE – GSKE

La Fondation Médicale Reine Élisabeth soutient la recherche en Neurosciences et délivre des Prix chaque année à des équipes de chercheurs qui se sont illustrés par leurs travaux innovants.

La séance académique en 2019, organisée le 28 mai, en présence de S.A.R. la Princesse Astrid, du Président du Sénat le Professeur J. Brotchi et de la Ministre de la santé Maggie De Block, de même que de très nombreuses personnalités politiques et scientifiques, de mécènes et de chercheurs fut l'occasion de remettre des prix aux équipes suivantes :

- le Prix Ernest Solvay au Prof. Dr. Ir. Simon De Meyer, PhD (KU Leuven – campus Kulak Courtrai)
- le Prix Élisabeth Vreven au Prof. Thomas Voets (KU Leuven)
- le Prix CBC Banque au Prof. Dr. Veerle Baekelandt, PhD (KU Leuven)
- le Prix Janine et Jacques Delruelle au Prof. Dr. Luc Leybaert, MD, PhD (UGent)

Au cours de cette séance, le Professeur Richard Frackowiack a présenté une conférence sur un thème de Neurosciences : "advances in Human Brain Studies with Neuroimaging". Cette remarquable conférence fut hautement appréciée et la présentation (fichier ppt) est disponible sur notre site (https://www.fmre-gske.be/pdf/uitreiking19c.pdf).

En fin d'année, le 17 octobre 2019, une visite des laboratoires de la KU Leuven – Campus Kulak Courtrai a permis à S.A.R. la Princesse Astrid accompagnée de membres du Conseil d'administration, du Directeur scientifique, de Monsieur Denis Solvay et de nombreuses autorités et membres de l'Université de découvrir les travaux du Professeur Dr. Ir. Simon De Meyer, qui a reçu le Prix Ernest Solvay au cours de cette année.

Nous remercions vivement S.A.R. la Princesse Astrid pour sa présence à la journée scientifique et à la visite des laboratoires de la KU Leuven – Campus Kulak Courtrai. Nous remercions les membres du Conseil d'Administration et du Comité Scientifique pour le travail qu'ils accomplissent au bénéfice des chercheurs en neurosciences de notre pays qui grâce aux mécènes peuvent poursuivre le développement des Neurosciences.

Prof. dr. Jean-Marie Maloteaux,
directeur scientifique
Bruxelles, 30 décembre 2019

Universiteiten met onderzoeksprogramma's die gesteund worden door de G.S.K.E.

Universités ayant des programmes de recherche subventionnés par la F.M.R.E.

Universities having research programs supported by the Q.E.M.F.

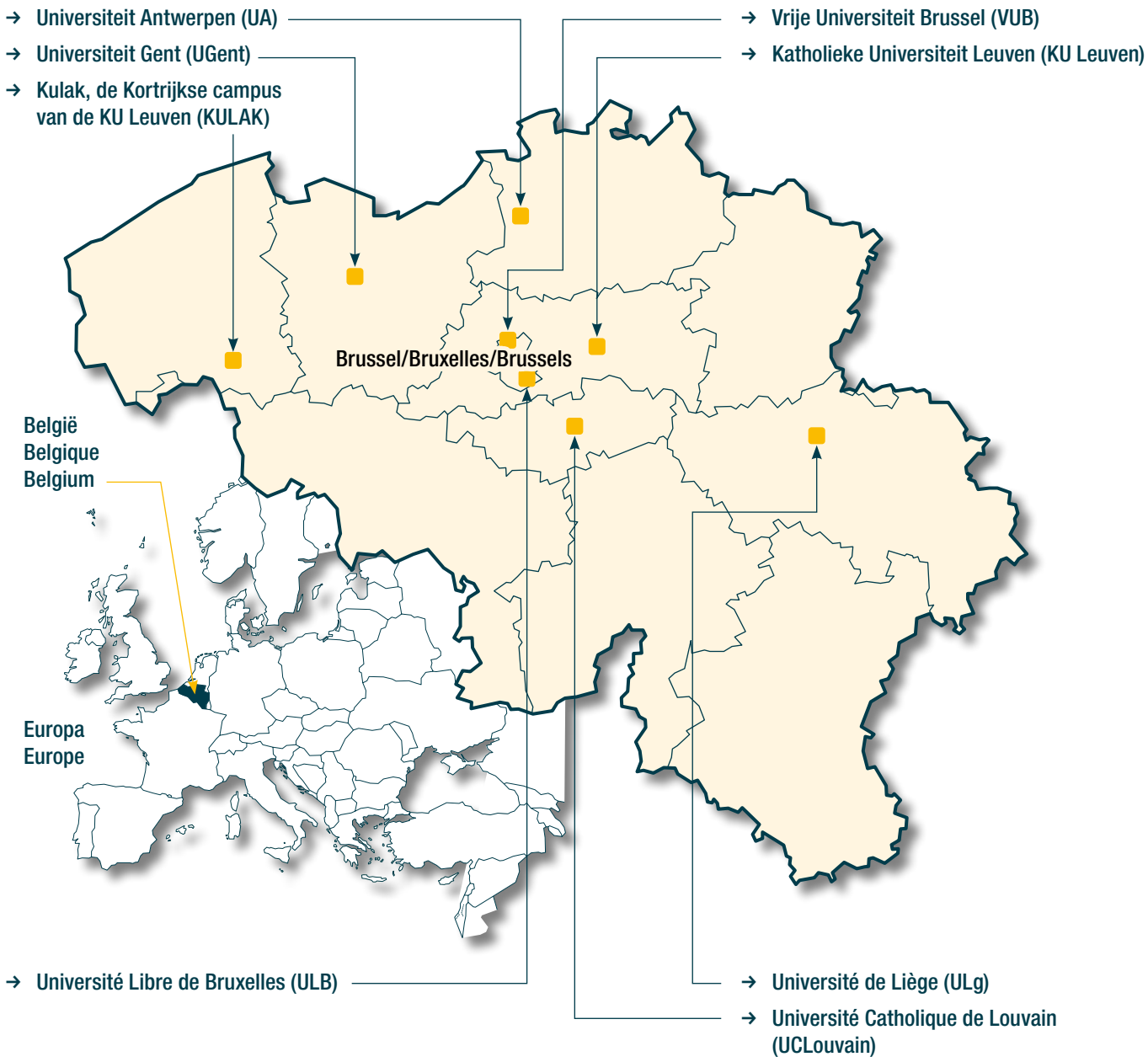

Onderzoeksprogramma's gefinancierd door de G.S.K.E. - Programma 2017-2019

Programmes de recherche subventionnés par la F.M.R.E. - Programme 2017-2019

Q.E.M.F. funded research projects - Program 2017-2019

KU Leuven

- **Prof. dr. Baekelandt Veerle, PhD**
  The role of alpha-synuclein aggregation, spreading and neuroinflammation in Parkinson's disease and related disorders.
- **Prof. dr. Ir De Meyer Simon**
  Neutrophil extracellular traps: novel targets for neuroprotection in stroke.
- **Prof. dr. De Strooper Bart, MD. PhD**
  The study of the initial cellular phase of Alzheimer's disease.
- **Prof. Goris An, PhD**
  Unraveling the BAFF pathway towards targeted treatment of multiple sclerosis.
- **Prof. dr. Vandenberghe Wim, MD. PhD**
  LRRK2, Rab10 and mitochondrial quality control in Parkinsons's disease.
- **Prof. dr. Vangheluwe Peter, PhD**
  Neuroprotection by lysosomal transport mechanisms in Parkinson's disease.
- **Prof. dr. Verfaillie Catherine**
  Unraveling the role of TREM2 mutations in Alzheimer's disease using human Pluripotent Stem Cells.
- **Prof. Voets Thomas**
  Unraveling the role of TRMP3 in neuropathic and inflammatory pain.

UA

- **Prof. dr. Timmerman Vincent, PhD**
  Unravelling the novel molecular pathways contributing to distal hereditary motor neuropathy caused by mutant HSPB8 with the aim to identify potential therapeutic targets.

UCLouvain

- **Prof. Fadel Tissir, PhD**
  Development and malformations of the cerebral cortex: role of the diaphanous 3 gene.

UGent

- **Prof. dr. Leybaert Luc, MD. PhD**
  Exploring the role of astroglial Cx43 hemichannels as therapeutic targets in stroke.
- **Prof. dr. Geert van Loo, PhD**
  Microglia, inflammasomes and multiple sclerosis.
- **Prof. dr. Vonck Kristl**
  The role of locus coeruleus noradrenergic neurons in the mechanism of vagus nerve stimulation and the effect of selective activation of these neurons in epilepsy.

ULB

- **Prof. Vanhollebeke Benoit, PhD**
  Organ-wide analysis of brain neurovascular communication in real-time and at single-cell resolution.

ULg

- **Dr. Nguyen Laurent, PhD**
  Deciphering the role of protein ubiquitination in human cortical malformation and hearing impairment.

VUB

- **Prof. dr. De Bundel Dimitri, PhD**
  Chemogenetic interrrogation of neuromedin U involvement in stress-induced psychopathology.

Final reports of the university research groups, supported by the Queen Elisabeth Medical Fondation in collaboration with the following professors and doctors (2017–2019)

Geneeskundige Stichting Koningin Elisabeth
Fondation Médicale Reine Elisabeth
Königin-Elisabeth-Stiftung für Medizin
Queen Elisabeth Medical Foundation

Final report of the research group of

Prof. dr. Baekelandt Veerle, PhD

Katholieke Universiteit Leuven (KU Leuven)

Principal investigator

Prof. dr. Baekelandt Veerle, PhD
Laboratory for Neurobiology and Gene Therapy
Division of Molecular Medicine K.U.Leuven –
Faculty of Medicine Kapucijnenvoer 33 VCTB+5
B-3000 Leuven
Belgium
Tel.: +32 16 37 40 61
Fax: +32 16 33 63 36
E-mail: Veerle.Baekelandt@kuleuven.be

Table of contents

The role of α-synuclein aggregation, spreading and neuroinflammation in Parkinson's disease and related disorders

1. Summary

Misfolded protein aggregates are a common feature of several neurodegenerative diseases, although the major protein component and the affected brain regions differ for each neurodegenerative disorder, e.g. α-synuclein (αSYN) in Parkinson's disease (PD), amyloid-β (Aβ)/Tau in Alzheimer's disease (AD) and huntingtin in Huntington's disease. Familial forms of neurodegenerative disorders are often linked to mutations that change the aggregation propensity of the disease-related protein, suggesting that protein misfolding and aggregation are likely to play a decisive role in the pathogenesis of neurodegenerative diseases. A distinctive pattern of pathological changes throughout the brain has been described for all the major neurodegenerative diseases[1,2]. The recent discovery of the transmissible nature of amyloidogenic proteins puts forward a hypothesis of a pathogenic trigger that spreads throughout the nervous system, underlying the progression of the disease[3]. Furthermore, evidence is emerging that these protein aggregates can adopt distinct conformations or 'strains' with remarkable differences in their structural and phenotypic traits, both in AD and PD[4-7]. Now, often referred to as prion-like diseases, the transmissibility and seeding mechanisms of these amyloidogenic proteins are the subject of intense research.

Synucleinopathies are determined by the formation of αSYN-rich deposits but segregate in distinct pathological phenotypes and diagnostic criteria including PD, Dementia with Lewy bodies (DLB) and Multiple System Atrophy (MSA). However, why αSYN inclusions are found in diseases that present with different phenotypic traits remains unresolved.

PD is the most common neurodegenerative movement disorder affecting approximately 10 million people worldwide. The neuropathological hallmarks of PD are the deposition of misfolded protein aggregates, predominantly composed of αSYN, in distinct brain regions and the progressive degeneration of dopaminergic neurons in the substantia nigra pars compacta (SNpc), subsequently leading to striatal dopamine depletion, which is responsible for the classical motor symptoms.

Nevertheless, several questions remain unanswered regarding the cause of neuronal cell death and the role of misfolded protein aggregates in PD. It has been postulated that neuroinflammatory processes might play a crucial role in the pathogenesis of PD and other neurodegenerative disorders[8,9]. Numerous post-mortem, brain imaging, epidemiological and animal studies have documented the involvement of the innate and adaptive immunity in neurodegeneration[10-14]. Whether these inflammatory processes are directly involved in the etiology of PD or represent secondary consequences of nigrostriatal pathway injury is the subject of intensive research. Immune alterations in response to extracellular αSYN may play a critical role in modulating Parkinson's disease progression.

We hypothesized that distinct phenotypes in synucleinopathies might correlate to heterogeneity in αSYN strains in patients. We also postulated that neuroinflammatory processes are closely involved in αSYN transmission and neurotoxicity. To date, a parallel comparison of αSYN assemblies derived from well-stratified patients with distinct synucleinopathies, aiming to reveal the existence and relevance of distinct αSYN strains in the human brain, is still missing. To fill this gap and establish a molecular basis for the different synucleinopathies, we examined the structural-functional relationship of αSYN aggregates directly derived from the human brain. We exploited the capacity of αSYN aggregates found in the brain of patients suffering from PD, MSA or DLB to seed and template monomeric human αSYN *in vitro* via a protein misfolding cyclic amplification assay. We found that the resulting αSYN fibrillar assemblies are structurally distinct. A careful comparison of the properties of total brain homogenates and *in vitro* amplified αSYN fibrillar assemblies upon inoculation in the rat brain demonstrates that

the intrinsic structure of αSYN fibrils dictates synucleinopathies characteristics. We show that MSA strains are significantly more potent in inducing motor deficits, nigrostriatal neurodegeneration, αSYN pathology, spreading, and inflammation, reflecting the aggressive nature of this disease. In contrast, DLB strains display no or only very modest neuropathological features under our experimental conditions. Collectively, our data show that αSYN strains, derived from the human brain, have distinct structural features and govern neuropathological and immunological properties *in vivo*. This further confirms the existence and the role of αSYN strains in the human brain and their relevance in synucleinopathies. Ongoing projects include the characterization of αSYN in models for MSA. A better understanding of the role of intercellular transmission and neuroinflammation in αSYN-linked neurodegeneration will contribute to the early diagnosis, prevention and the development of novel therapeutic strategies and compounds for synucleinopathies and other ageing-related disorders.

2. Scientific progress

WP1. Characterization of seeding and spreading properties of patient-derived αSYN assemblies

In WP1 we aim to bridge the gap between preclinical studies using recombinant protein and the human pathology. To this end, we tested patient-derived *in vitro* amplified αSYN assemblies in the rodent brain and compared those to recombinant αSYN assemblies for disease-inducing properties in terms of αSYN spreading and pathology.

1.1. Isolation and in vitro characterization of patient-derived αSYN assemblies

Brain samples of patients with PD, MSA and DLB obtained from the UK Brain Bank via Prof. S. Gentleman (Imperial College London, UK; n=6/group) have been extensively characterized from a clinicopathological point of view. These samples were transferred to the group of our collaborator Prof. R. Melki (CNRS, France) who has isolated, purified and characterized the different ***αSYN*** assemblies present *in vitro*. He also implemented a Protein Misfolding Cyclic Amplification (PMCA) assay for Lewy bodies containing tissues to amplify the αSYN assemblies *in vitro*.

The resulting αSYN fibrillar assemblies were imaged by transmission electron microscopy (TEM) and their limited proteolytic patterns upon exposure to Proteinase K were analyzed by SDS-PAGE. TEM analysis revealed disease-specific differences in the shape of the fibrils. PD patient-derived αSYN fibrils obtained by PMCA exhibited a flat appearance, resembling that of the fibrillar polymorph “Ribbons”. Those derived from MSA patients were cylindrical and thin. Finally, those derived from DLB patients were indistinguishable from the fibrillar polymorph “Fibrils” (Fig. 1a). Furthermore, PMCA-derived PD and MSA αSYN fibrils exhibited similar limited proteinase K degradation patterns that differed from those derived from DLB patients (Fig. 1b). Limited proteolysis patterns of PD and MSA patient-derived αSYN fibrils resembled that of the fibrillar polymorph “Ribbons” while the proteolysis pattern of DLB patient-derived αSYN fibrils was similar to the fibrillar polymorph “Fibrils”. We conclude from these observations that fibrils derived from patients developing one given synucleinopathy have comparable fingerprints and morphology. We further conclude that despite the fact that PD, MSA and DLB patient-derived αSYN fibrils have different shapes, PD and MSA patient-derived fibrils have a similar limited proteolysis pattern, distinct from that of DLB patient-derived fibrils.

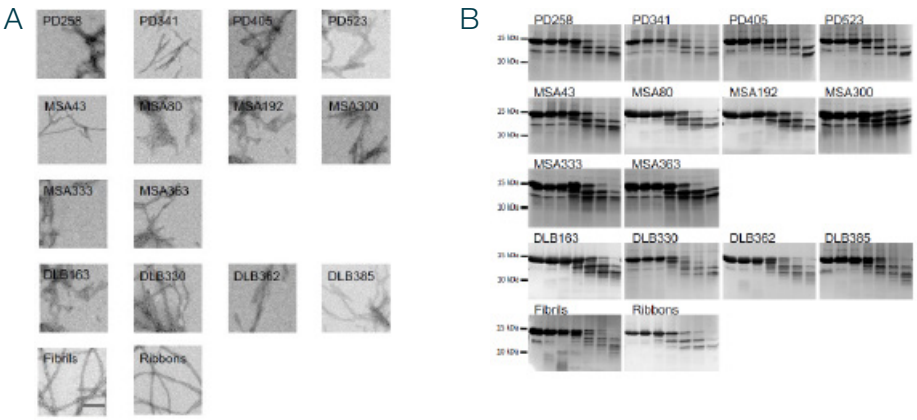

Figure 1 – Characterization of PMCA-amplified patient-derived αSYN assemblies.
(a) Electron micrographs of αSYN assemblies obtained after the 3rd cycle of amplification by PMCA from PD, MSA and DLB patients and from de novo generated αSYN Fibrils and Ribbons. Scale bar = 200 nm.
(b) Limited proteolytic patterns of αSYN assemblies obtained after the 3rd cycle of amplification by PMCA from PD, MSA and DLB patients and from de novo generated αSYN Fibrils and Ribbons. Monomeric αSYN concentration is 100 µM. Proteinase K concentration is 3.8µg/ml. Samples were withdrawn from the reaction before PK addition (lane most to the left), immediately after PK addition (second lane from left) and at time 1, 5, 15, 30 and 60 min from left to right in all panels. PAGE analysis was performed as described in the methods section and the gels were stained with Coomassie blue. The molecular weight markers are shown on the left.

1.2. Cellular characterization of patient-derived αSYN strains

We next assessed the seeding capacity of the distinct PMCA-amplified αSYN fibrillar strains in a human H4 neuroglioma cell line expressing αSYN-YFP. Recombinant αSYN fibrils, used as a positive control, gave rise to YFP^+ $P\alpha SYN^+$ intracellular inclusions in H4 cells (Fig. 2a). Exposure of H4 cells to all αSYN strains for 24h led to αSYN aggregation as quantified by the number of YFP^+ puncta per H4 cell nucleus (Fig. 2a, b). No such aggregation was observed upon exposure of H4 cells to PMCA control samples (Fig. 2a, b) or brain homogenates (Fig. 2d). Aggregated αSYN-YFP co-localized to a large extent with PαSYN aggregates, however no differences were detected between PD, MSA and DLB patient-derived fibrils (Fig. 2c). These data demonstrate that the PMCA-amplified αSYN strains seed monomeric αSYN aggregation in cell culture. Exposure of primary cortical neurons for 10 days to the different PMCA-amplified αSYN fibrillar strains, but not control samples, led to the formation of phosphorylated αSYN deposits (Fig. 2e). Interestingly, we observed a distinct phosphorylation pattern for the different PMCA-amplified αSYN fibrillar strains. Neurons exposed to MSA and PD patient-derived fibrils presented PαSYN positive neurites whereas those exposed to fibrils derived from DLB patients had diffuse PαSYN deposits within the soma, surrounding the nucleus. These findings further suggest that distinct PMCA-amplified αSYN strains seed the aggregation of endogenous αSYN to different extents.

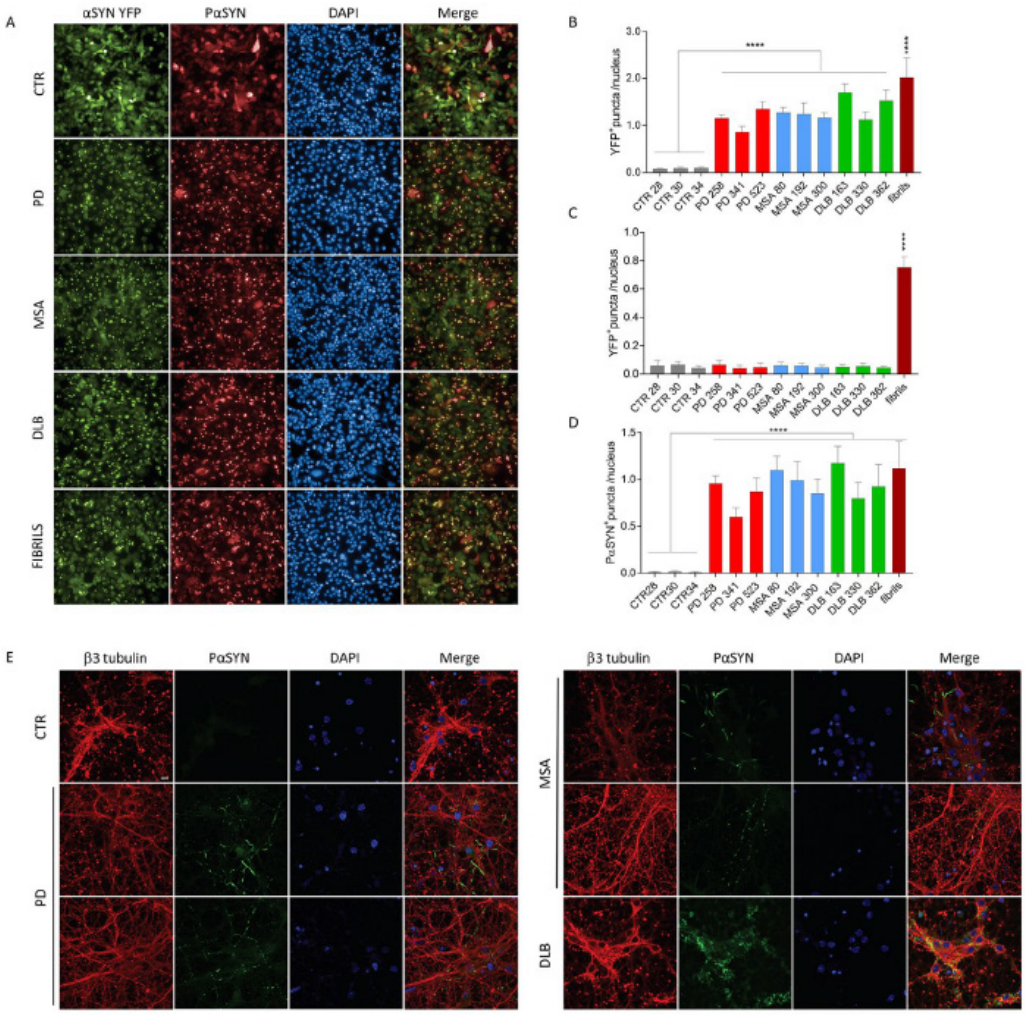

Figure 2 – Characterization of PMCA-amplified αSYN strains in cellular models
(a) Representative photomicrographs of the human neuroglioma (H4) cells stably expressing αSYN-YFP upon administration of the different PMCA-amplified αSYN strains (175 nM; green) or recombinant αSYN fibrils (175 nM; green) stained for PαSYN (red). DAPI was used to visualize the nuclei (blue). (b) The number of YFP+ puncta per nucleus in H4 cells (presented in panel a) was quantified 24h after incubation with the different PMCA-amplified αSYN strains. (c) The number of PαSYN+ puncta per nucleus in H4 cells (presented in panel a) was quantified 24h after incubation with the different PMCA-amplified αSYN strains. (d) The number of YFP+ puncta per nucleus in H4 cells was quantified 24h after incubation with total brain homogenates. Results shown as mean ± SEM (**** $p < 0.0001$ for one-way ANOVA with Tukey's post-hoc analysis, n=3 patients per condition). (e) Representative photomicrographs of the primary cortical neurons after incubation with the different PMCA-amplified αSYN strains for 10 days stained for the neuronal marker β3-tubulin (red) and for PαSYN (green). DAPI was used to visualize the nuclei (blue). This experiment was repeated three times. Scale bar represents 10 μm.

1.3. In vivo characterization of patient-derived αSYN strains

Intracerebral inoculation of PD, MSA and DLB patient-derived αSYN strains trigger changes in motor behavior

To determine whether the distinct characteristics of αSYN strains reflect *in vivo*, we inoculated brain homogenates from PD, MSA and DLB patients in parallel with pure PMCA-amplified αSYN assemblies derived from those patients into the rat SN in absence or presence of an rAAV2/7 vector encoding human αSYN (Fig. 3a). A total of 12-16 animals per group was included in this study, representing 4-6 patients per condition and 3 animals per patient. To monitor behavioral performance, we subjected the animals to the cylinder test on a monthly basis for five months (Fig. 4b). Neither the brain homogenates nor the PMCA-amplified assemblies induced significant motor deficits in naive animals within the experimental time frame (Fig. 3c, e). When we combined patient-derived material with rAAV-mediated αSYN expression, clear motor deficits developed progressively over time from 3 months post injection and onwards. The MSA patient brain homogenates induced the most prominent motor deficits compared to the CTR patients (MSA, 11 ± 4 % remaining forepaw use versus CTR, 36 ± 7 %, Fig. 3d). Animals

injected with rAAV-αSYN alone or together with PMCA-amplified αSYN assemblies derived from CTR, PD or MSA patients presented similar motor deficits (Fig. 3f). Surprisingly the animals injected with PMCA-amplified αSYN assemblies derived from DLB patients did not display detectable motor deficits. To rule out any technical issues we inoculated an additional group of animals with PMCA-amplified αSYN assemblies derived from DLB and MSA patients (n=8-12 animals per condition) and similar results were obtained (data not shown). We conclude from these findings that rats robustly develop motor deficits only when brain homogenates from PD, MSA and DLB patients, and to a much lesser extent PMCA-amplified αSYN assemblies derived from those cases, are delivered into their SN in the presence of additional soluble human αSYN supplied by a rAAV-αSYN expression vector.

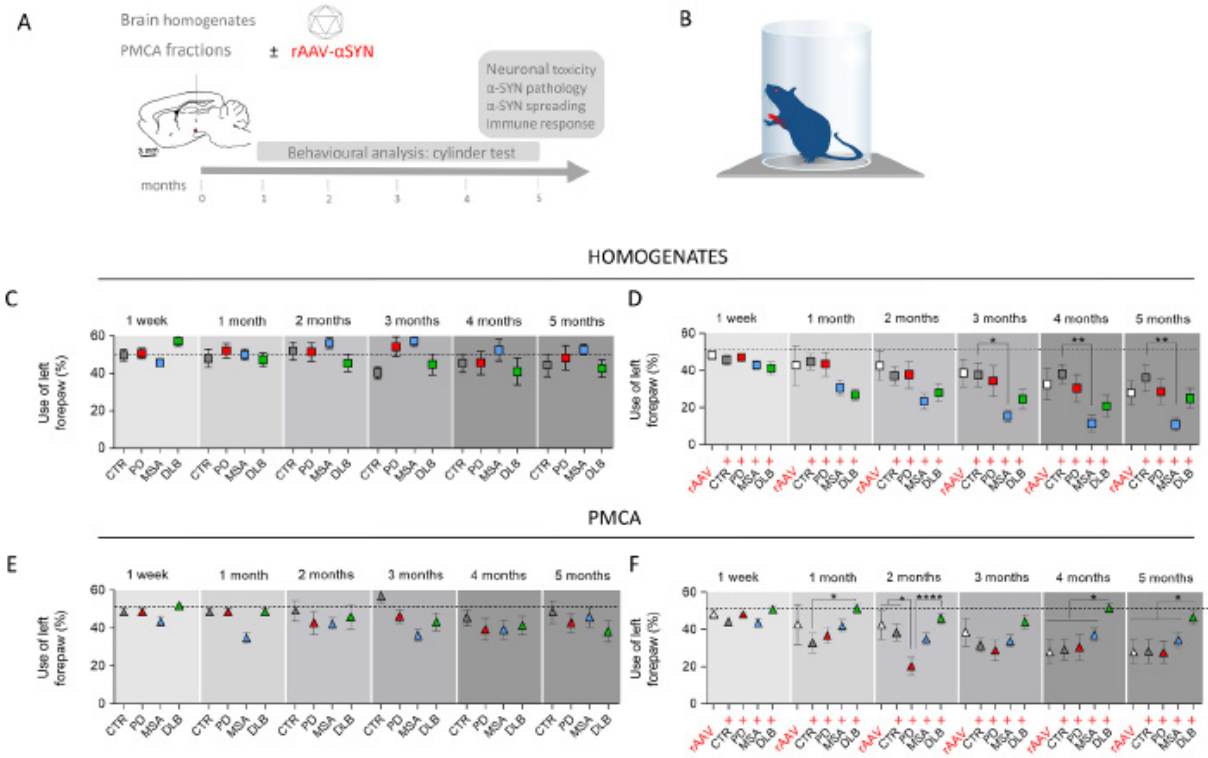

Figure 3 – Assessment of motor deficits after intracerebral inoculation of the different patient-derived homogenates and PMCA-amplified αSYN strains in absence or presence of rAAV2/7-mediated αSYN expression.
(a) Schematic representation of the experimental set-up. Rats were inoculated with the different patient-derived brain homogenates or PMCA-amplified αSYN strains in absence or presence of human αSYN expression. Animals were subjected to the cylinder test on a monthly basis. The *in vivo* behavior of the distinct human αSYN strains was characterized by assessing neuronal toxicity, αSYN pathology, spreading of αSYN pathology and inflammatory response at the final time point of 150 days. (b) Schematic drawing illustrating the set-up of the cylinder test to assess motor behavior. (c-d) Alterations in motor behavior after inoculation of PD, MSA, DLB patient-derived homogenates and age-matched controls in absence (c) or presence of rAAV2/7-mediated overexpression of αSYN (rAAV) (d) were assessed using the cylinder test. (e-f) Alterations in motor behavior after inoculation of PD, MSA or DLB-derived PMCA-amplified αSYN assemblies in absence (e) or presence of rAAV-αSYN overexpression (f) were assessed using the cylinder test. Results shown as mean ± SEM (* $p < 0.05$, ** $p < 0.01$, **** $p < 0.0001$ for two-way ANOVA with Tukey's post-hoc analysis, n= 4-6 patients per group and n=3 per patient). A total of 12-16 animals per group was included in this study.

PD, MSA and DLB patient-derived αSYN strains exhibit distinct dopaminergic neurotoxicity

Nigral inoculation of brain homogenates in naive rats led to a decrease in the number of tyrosine hydroxylase (TH)-positive neurons with the MSA and DLB groups having the highest proportion of neuronal loss (41 ± 5% and 49 ± 8 % respectively) compared to the PD and CTR groups (27 ± 7% and 28 ± 4% respectively) at the final time point of 150 days (Fig. 4a). AAV-mediated expression of human αSYN resulted in 25 ± 5 % nigral dopaminergic cell loss. Upon co-injection with brain homogenates, additional cell loss was observed for the MSA and PD groups (74 ± 3% and 61 ± 6% respectively) but not for the DLB and CTR groups (44 ± 6% and 30 ± 12%; Fig. 5b, c). Nigral inoculation of PMCA-amplified αSYN assemblies in naive rats only induced mild dopaminergic cell loss (ranging from 21-28 %) with no differences between the different experimental groups (Fig. 4d). In line with the results obtained with brain homogenates, combining rAAV-αSYN expression with PMCA-amplified MSA and

PD assemblies had an additive effect (62 ± 4 % and 53 ± 6 % respectively) unlike PMCA-amplified DLB and CTR assemblies (26 ± 5 % and 14 ± 3 %; Fig. 4e, f). Quantifications of striatal dopaminergic nerve terminals further revealed that inoculation of both the brain homogenates or the PMCA-amplified αSYN assemblies in naive rats did not induce a significant striatal lesion at the final time point of 150 days (Fig. 4g, i). However, upon inoculation of brain homogenates in the presence of rAAV-αSYN, significant striatal lesions were induced for all diseases with the most prominent loss for MSA patient brain homogenates (60 ± 8%, Fig. 4h). Similarly, prominent striatal lesions were observed in animals co-injected with rAAV-αSYN and PMCA-amplified assemblies from PD and MSA patients but not from DLB patients (Fig. 4j).

PD, MSA and DLB patient-derived αSYN strains induce distinct αSYN pathology and spreading

To assess αSYN pathology, we first analyzed the number of phosphorylated αSYN (PαSYN) positive nigral neurons. Injection of PD, MSA and DLB patient brain homogenates or PMCA-amplified assemblies in naive rats resulted in a low number of PαSYN positive dopaminergic neurons (Fig. 5a, left). In contrast, combining rAAV-driven αSYN expression with PD, MSA and DLB patient brain homogenates or PMCA-amplified assemblies led to overall increased numbers of PαSYN positive cells (Fig. 5a, right). Interestingly, the number of nigral PαSYN positive cells was significantly higher in animals of the MSA group when compared to the PD, DLB or CTR groups (Fig. 5b, Fig. 5a). This marked PαSYN pathology is in line with the observed severe motor deficits and prominent nigral cell loss (Fig. 3d and 4b). Intriguingly, a significantly lower number of PαSYN positive cells was observed when rAAV-αSYN was co-injected with PMCA-amplified DLB assemblies (Fig. 5c). DLB brain-derived PMCA assemblies appeared to reduce the number of PαSYN cells (Fig. 5c, Fig. 8b). The latter results are altogether in agreement with the limited effect of DLB patient-derived PMCA assemblies on motor behavior (Fig. 3f) and nigral and striatal cell loss (Fig. 4e and j). We further examined the presence of PαSYN pathology in other cell types such as astrocytes (data not shown) and oligodendrocytes (Fig 5d) but we only found PαSYN positive neuronal inclusions.

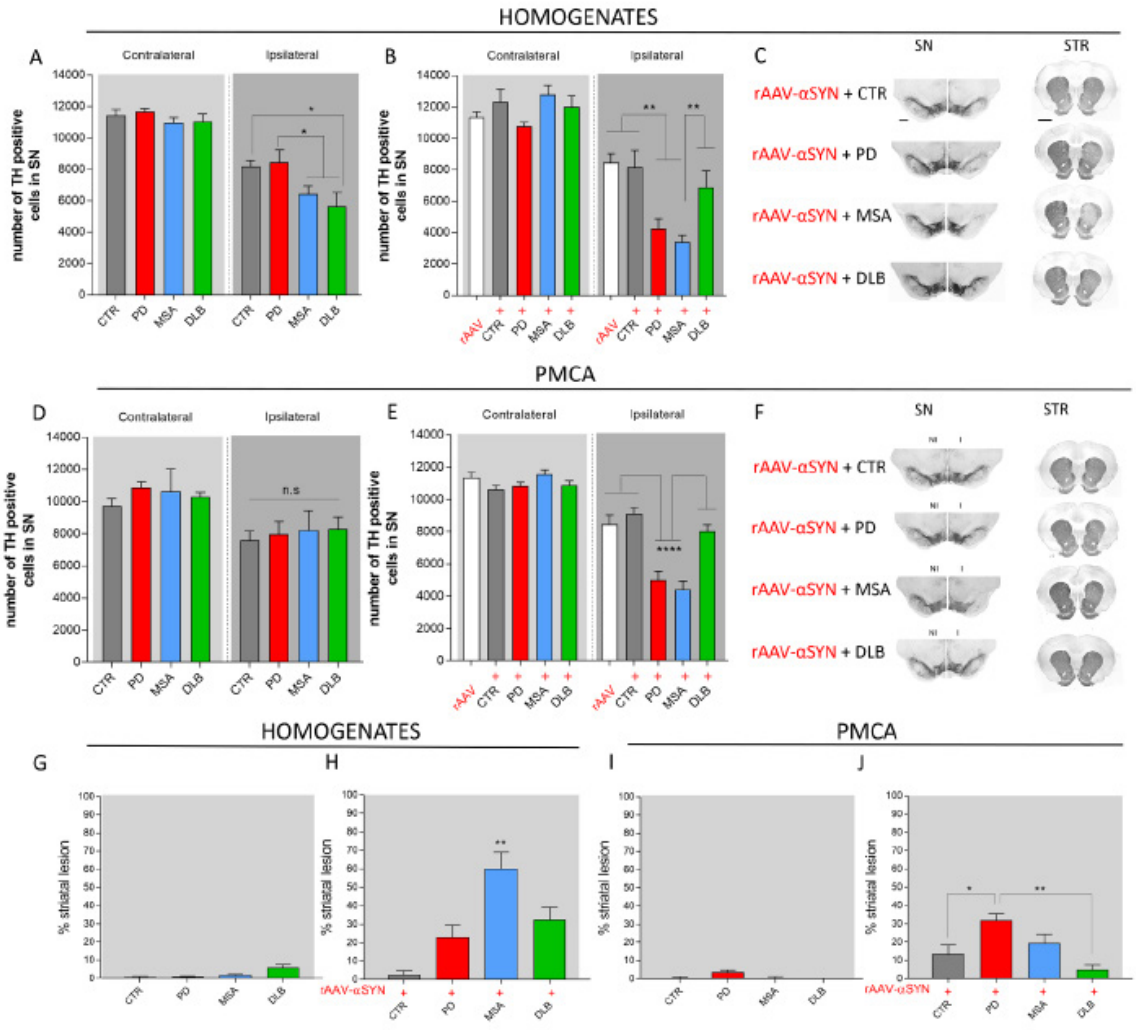

Figure 4 - Dopaminergic neurodegeneration after intracerebral inoculation of different patient-derived homogenates and PMCA-amplified αSYN strains in absence or presence of rAAV2/7-mediated αSYN expression.
(a-b) Stereological quantification of the number of TH⁺ cells in the rat SN five months after inoculation of patient-derived homogenates in absence (a) or presence (b) of rAAV2/7-αSYN overexpression (rAAV). (c) Representative images of TH staining in the SN and striatum five months after co-injection of the patient-derived homogenates and human αSYN overexpression. Scale bar represents 400 µm. (d-e) Stereological quantification of the number of TH⁺ cells in the rat SN five months after inoculation of PMCA-amplified αSYN in absence (d) or presence (e) of rAAV2/7-αSYN overexpression. (f) Representative images of TH staining in the SN and striatum five months after co-injection of PMCA-amplified αSYN assemblies and human αSYN expression. Scale bar represents 1000 µm. Results shown as mean ± SEM (* $p < 0.05$, ** $p < 0.01$, **** $p < 0.0001$ for two-way ANOVA with Bonferroni post-hoc analysis, n=4-6 patients per group and n=3 per patient). A total of 12-16 animals per group was included in this study. (g-h) TH striatal lesion was assessed five months after inoculation of patient-derived homogenates in absence (g) or presence (h) of rAAV2/7-αSYN overexpression. (i-j) TH striatal lesion was assessed five months after inoculation of PMCA-amplified αSYN assemblies in absence (i) or presence (j) of rAAV2/7-αSYN overexpression. Results shown as mean ± SEM (* $p < 0.05$, ** $p < 0.01$, **** $p < 0.0001$ for one-way ANOVA with Tukey's post-hoc analysis, n=4-6 patients per group and n=3 per patient). A total of 12-16 animals per group was included in this study. I, injected; NI, non-injected; n.s., not significant; SN, substantia nigra; STR, striatum.

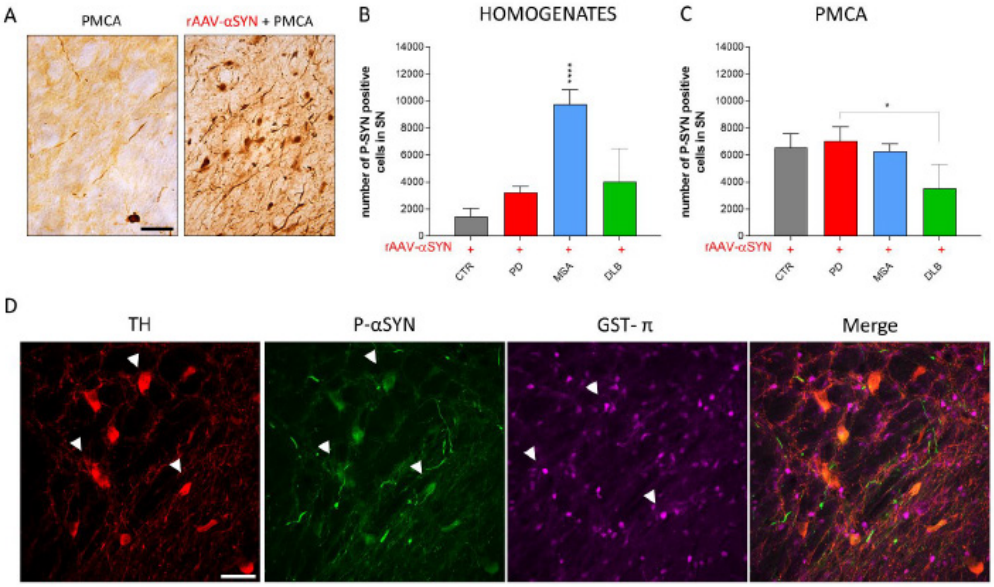

Figure 5 - Assessment of αSYN pathology after intracerebral inoculation of different patient-derived homogenates and PMCA-amplified αSYN assemblies in association with rAAV2/7-mediated αSYN expression. (a) Representative images of a P-S129 αSYN staining in the SN five months after co-injection of PMCA-amplified MSA strains in absence (left) or presence (right) of rAAV2/7-αSYN overexpression. Scale bar = 50 µm. (b-c) Stereological quantification of the number of PαSYN+ cells in the SN five months after co-injection of patient-derived homogenates (b) or PMCA-amplified αSYN assemblies (c) with rAAV2/7-αSYN overexpression. Results shown as mean ± SEM (* $p < 0.05$, **** $p < 0.0001$ for one-way ANOVA with Tukey's post-hoc analysis, n=4-6 patients per group and n=3 per patient). A total of 12-16 animals per group was included in this study. (d) Representative images of dopaminergic neurons (TH, in red), αSYN phosphorylated at Ser129 (P-S129 αSYN, in green) and oligodendrocytes (GST-π, in magenta) in the SN five months after inoculation of PMCA-amplified MSA strains in association with rAAV2/7-mediated overexpression of αSYN. White arrowheads represent on the one hand neuronal cell bodies (red) co-localizing with P-S129 αSYN staining (green) and on the other hand oligodendroglia cell bodies (magenta) in the absence of co-localization with P-S129 αSYN (green). Scale bar represents 50 µm.

Next, we assessed the spreading pattern of pathological αSYN within the brain following injection of PD, MSA and DLB patient brain homogenates and the corresponding PMCA-amplified assemblies with or without rAAV-driven αSYN expression (Fig. 6 and Fig. 7). For patient brain homogenates, αSYN phosphorylation patterns in brain regions connected to the injection site were only seen upon co-injection with rAAV-αSYN (Fig. 6a, b). Pathological αSYN deposits were more abundant for all diseases compared to controls but most prominent in animals injected with MSA patient brain homogenates. Both PαSYN positive cells as well as PαSYN positive neurites were observed in the dorsal caudate putamen. A considerable number of PαSYN positive cells and very few PαSYN positive neurites were observed in the SN (Fig. 6a). Interestingly, PMCA-amplified assemblies induced an overall more pronounced PαSYN pathology compared to the patient brain homogenates. The sole injection of PMCA-amplified MSA assemblies induced the most prominent spreading of pathological αSYN deposits in the regions almost similar to those observed with combined injection of rAAV-αSYN and MSA patient brain homogenates (the caudate putamen and the lateral part of the SN, Fig. 7a, c). However, PαSYN positive neurites were more abundant than PαSYN positive cells. Furthermore, co-injection of rAAV-αSYN and PMCA-amplified MSA assemblies led to a more severe phenotype (Fig. 7b, d). Here, both PαSYN positive cells and PαSYN positive neurites were found in the different brain regions examined. Again, PMCA-amplified DLB assemblies with or without rAAV-αSYN induced very low levels of PαSYN pathology in the striatum, similar to the CTR animals.

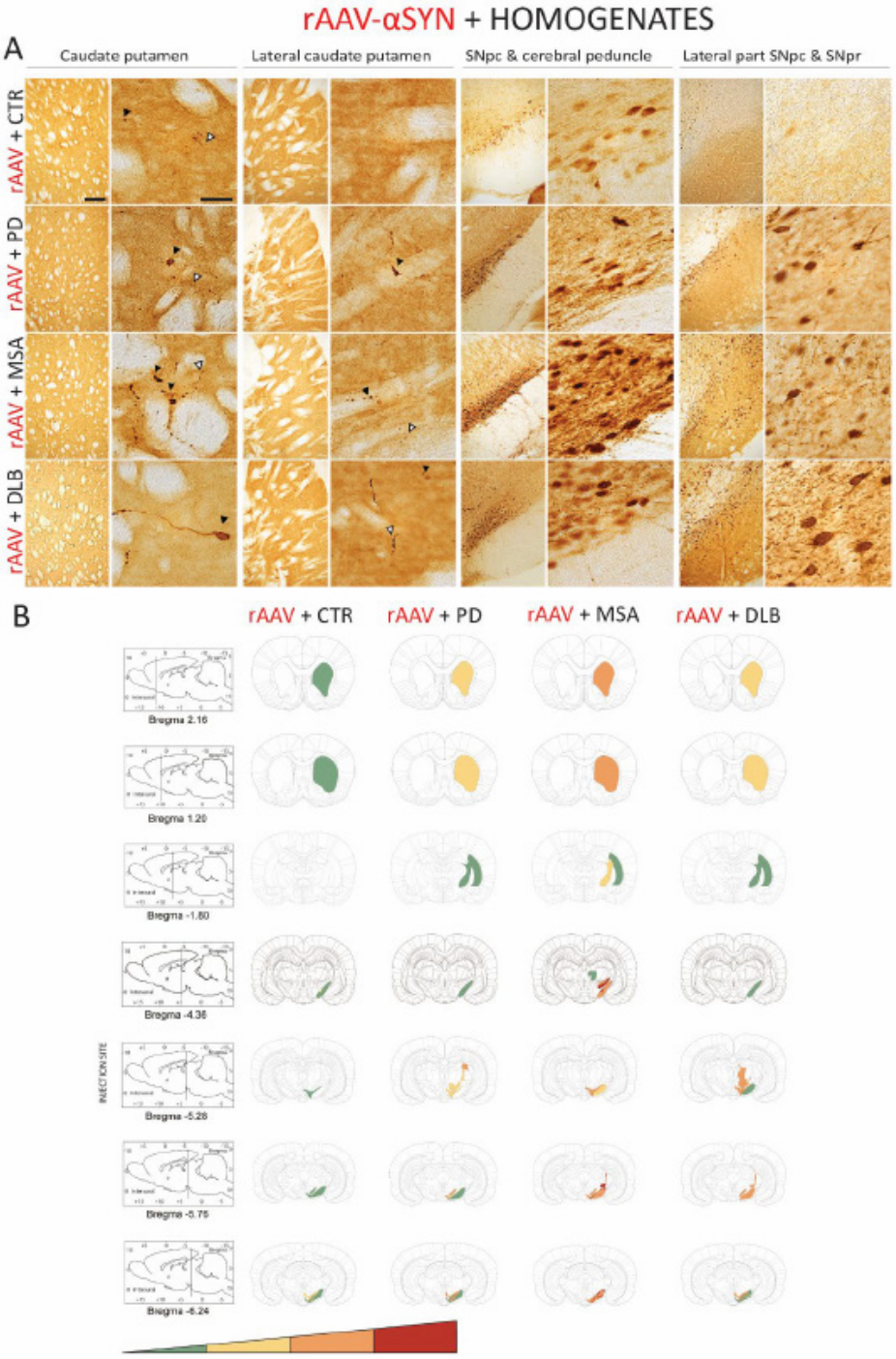

Figure 6 - Spreading of αSYN pathology after inoculation of different patient-derived homogenates in association with rAAV2/7-αSYN expression. (a) Representative photomicrographs of PαSYN pathology in four different brain regions five months after co-injection of patient-derived homogenates and rAAV2/7-αSYN overexpression. The selected brain regions are the following: (1) and (2) adjacent sections of caudate putamen (CPu); (3) SNpc and cerebral peduncle (cp); (4) lateral part of the SNpc and SNpr. Black arrows represent PαSYN-positive cells and open arrows show PαSYN-positive outgrowths. Scale bars represent 200 µm (left) and 50 µm (right). (b) Heat map for the spreading of αSYN pathology towards different brain regions. The heat map ranges from low (green) tot very high (red). A total of 3 animals per group was included. The data were presented as heat maps to semi-quantitatively illustrate the distribution of αSYN pathology throughout the brain. Each panel represents a coronal plane (bregma 2.16, 1.20, -1.80, -4.36, -5.28, -5.76, -6.24 mm) for each group. The left column presents sagittal views of the corresponding coronal planes.

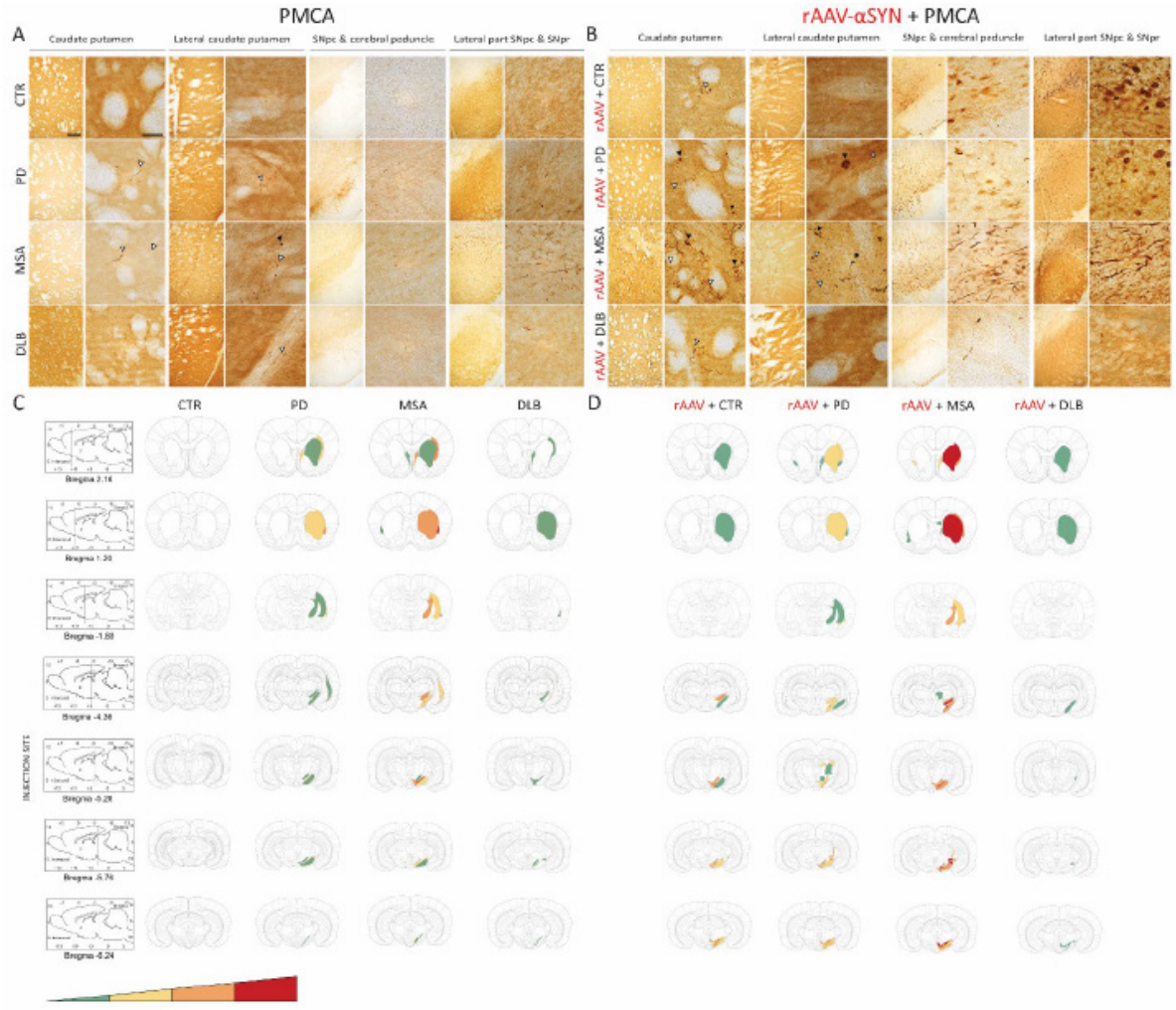

Figure 7 - Spreading of αSYN pathology after inoculation of different PMCA-amplified αSYN strains without or with rAAV2/7-mediated αSYN expression.
(a-b) Representative photomicrographs of PαSYN pathology in four different brain regions five months after inoculation of PMCA-amplified αSYN assemblies without (a) or with (b) rAAV2/7-αSYN expression. The selected brain regions are the following: (1) and (2) adjacent sections of caudate putamen (CPu); (3) SNpc and cerebral peduncle (cp); (4) lateral part of the SNpc and SNpr. Black arrows represent PαSYN-positive cells and open arrows show PαSYN-positive outgrowths. Scale bars represents 200 µm (left) and 50 µm (right). (c-d) Heat map for the spreading of αSYN pathology towards different brain regions after inoculation of PMCA-amplified αSYN assemblies without (c) or with (d) rAAV2/7-αSYN expression. The heat map ranges from low (green) tot very high (red). A total of 3 animals per group was included. The data were presented as heat maps to semi-quantitatively illustrate the distribution of αSYN pathology throughout the brain. Each panel represents a coronal plane (bregma 2.16, 1.20, -1.80, -4.36, -5.28, -5.76, -6.24 mm) for each group. The left column presents sagittal views of the corresponding coronal planes.

WP2. Elucidation of the role of the immune system in αSYN spreading and neurotoxicity

Evidence is emerging that α***SYN*** can adopt distinct conformations, also referred to as 'strains', which are characterized by remarkable differences in structural and phenotypic features[4,5]. Therefore, presentation of different αSYN assemblies (monomers, oligomers or fibrils) to the innate immune system and the subsequent immune response might be a driving force in the disease, although the exact αSYN strains which might trigger this inflammatory response have not yet been identified[3].

2.1. Characterization of the microglial response to different αSYN assemblies

In this part of the WP, we have studied the phenotype of BV2 cells (immortalized murine microglial cell line) and primary microglia in response to exogenous administration of recombinant αSYN assemblies including oligomers and two different fibrillar αSYN strains, called fibrils and ribbons. Fibrils and ribbons display distinct structural properties and present different toxicity and propagation propensity in cell

culture[4]. We found that both αSYN fibrils and ribbons induce the classical pro-inflammatory microglial phenotype and suppress the alternative repair state in BV2 cells, as characterized by the expression of anti-inflammatory markers (data not shown).
To further define the microglial inflammatory response with respect to the different recombinant αSYN assemblies, we extended our study to primary microglia isolated from the mouse brain. We administered αSYN monomers, oligomers and two distinct fibrillar αSYN strains to primary microglia (Figure 8). Treatment with BSA was used as a negative control, whereas administration of LPS and IL4 was included as positive control for the pro- and anti-inflammatory profile, respectively. In order to assess the uptake of the different αSYN assemblies, we performed double immunocytochemistry for αSYN and the microglial marker Iba1 24 hours after administration of the αSYN strains. As shown in Figure 8, the different αSYN assemblies were taken up by primary microglia. However, qualitative analysis of confocal images revealed a stronger signal for αSYN 'fibrils' and 'ribbons' indicating that they might be internalized by microglial cells more efficiently than monomeric and monomeric αSYN.

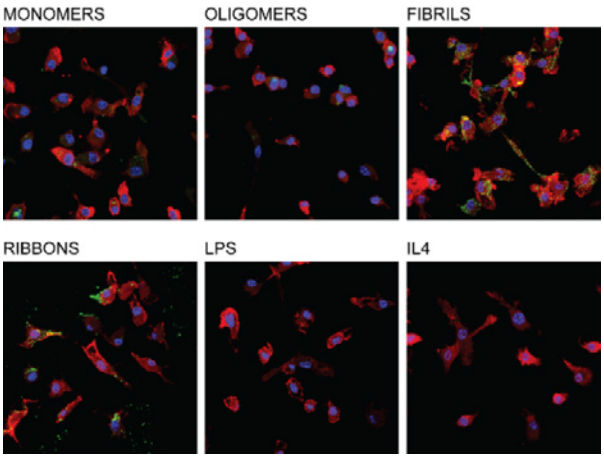

Figure 8 - Uptake of different αSYN assemblies by murine primary microglia. Double immunofluorescent staining for human αSYN (green) and murine Iba1 (red) of primary microglia treated with different αSYN strains for 24 hours. αSYN 'fibrils' and 'ribbons' display the strongest signal. LPS and IL4 treatment were included as positive control for the proinflammatory and anti-inflammatory profile, respectively. Scale bar = 50 µm.

More thorough analysis on the uptake and degradation of αSYN assemblies was performed over time, from 2 hours up to 24 hours post treatment. This confirmed that both fibrillar αSYN strains are taken up more easily and degraded more slowly by microglial cells than monomeric and oligomeric αSYN based on immunocytochemistry staining. Uptake of Alexa 488 labeled αSYN assemblies by $CD11b^+$ $CD45^+$ primary microglia was further assessed by flow cytometric analysis. The percentage of αSYN positive microglial cells was substantially increased upon exposure to 'fibrils' and 'ribbons' in comparison to αSYN monomers and oligomers (Figure 9).

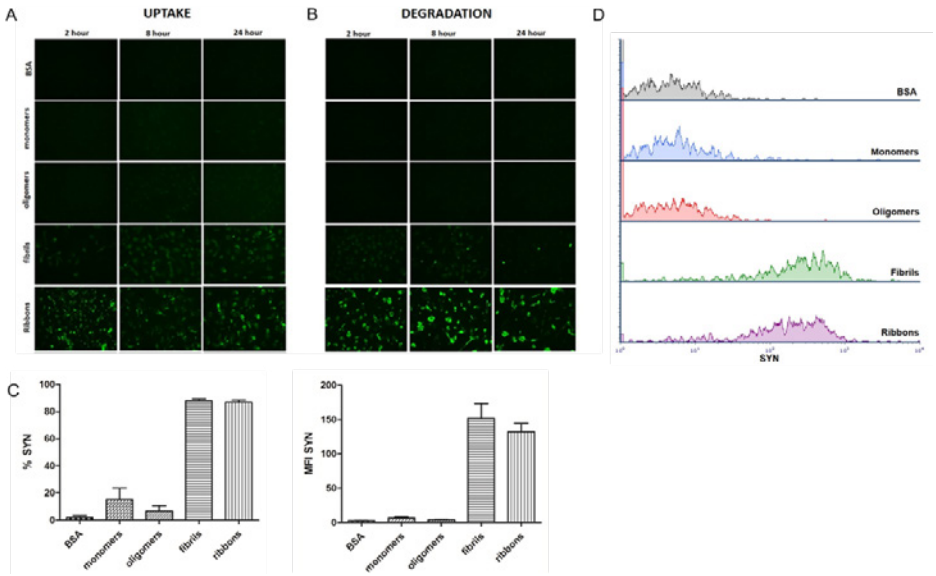

Figure 9 - Detailed uptake and degradation by murine primary microglia. A-B. Immunocytochemistry staining for αSYN (green) of primary microglia treated with different αSYN strains up to 24 hours. C-D. Representative histograms depicting αSYN uptake by CD11b+ CD45+ microglial cells assessed by flow cytometry. BSA was used as a negative control.

Microglial proinflammatory response in reaction to the different αSYN assemblies was further examined. We found that the expression of TNFα, IL1β and IL6 was strongly upregulated upon administration of αSYN 'fibrils' and 'ribbons' while expression of those markers remained stable after treatment with monomeric and oligomeric αSYN (Figure 10). In line with the results previously obtained in BV2 cells, primary microglia showed a pronounced proinflammatory response but only towards the fibrillar αSYN polymorphs.

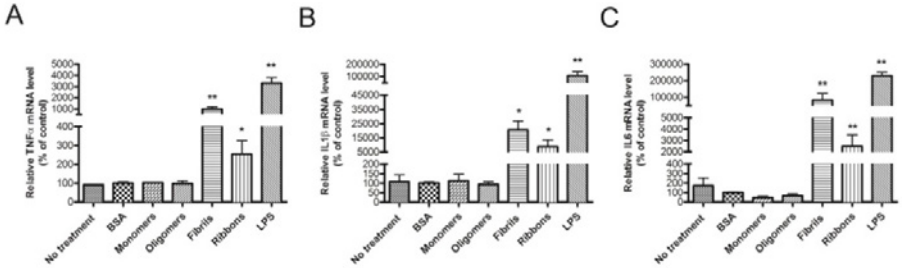

Figure 10 - Characterization of the proinflammatory response in primary microglia upon treatment with different αSYN assemblies. Quantification of mRNA levels of TNFα (A), IL1β (B) and IL6 (C) in murine primary microglia upon administration of the two different fibrillar αSYN forms ('fibrils' and 'ribbons', 1μM each) or oligomeric αSYN (1 μM). LPS treatment (2.5 mg/ml) was used as positive control. Untreated cells and cells treated with BSA (1 μM) were included as negative controls. Mean ± SEM are shown (n=3). * $p < 0.05$, ** $p < 0.01$.

2.2. Characterization of the microglial response to distinct αSYN assemblies in vivo

In order to study the microglial immune response to different αSYN assemblies *in vivo*, we have stereotactically injected αSYN monomers, oligomers and the two fibrillar αSYN strains into the SN of adult mice. Mice injected with BSA were included as a negative control. Two days post injection, we sacrificed the animals and performed immunohistochemical analysis using the CD11b antibody in order to visualize the microglial cells (Figure 11). As a result, we observed an increase in the number of CD11b positive cells in the injected side of the brain upon exposure to αSYN 'fibrils' and 'ribbons' compared to control animals injected with BSA. A less pronounced microglial response was detected upon administration of αSYN oligomers, while CD11b positive cells were almost undetectable in animals injected with αSYN monomers. Our results suggest that microglial activation in response to fibrillar αSYN assemblies *in vivo* is more pronounced in comparison to monomeric and oligomeric species.

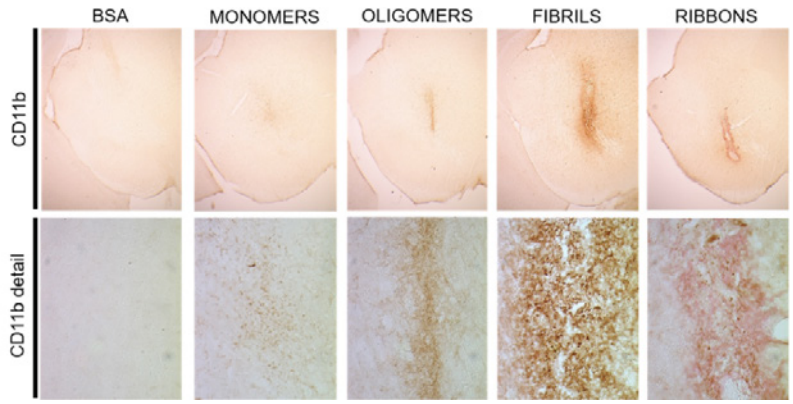

Figure 11 - Characterization of the microglial response upon stereotactic injection of different αSYN assemblies in the mouse SN. Immunohistochemical staining for CD11b showing the presence of microglia, two days after injection of recombinant αSYN strains in the SN. BSA was injected as a negative control.

2.3. The involvement of inflammatory cells in SYN spreading

The discovery of misfolded αSYN protein aggregates with different structural characteristics, that could account for the distinct pathological traits within synucleinopathies and which amplify in a "prion-like" fashion[15-18], has led us to consider that pathogenic αSYN might be hijacking the activation and mobilisation mechanism of the peripheral immune system to reach and disseminate within the CNS. Therefore, we assessed the impact of peripheral inflammation on αSYN spreading in order to understand the participation of the immune system in αSYN pathology.

The results presented here show that intraperitoneal LPS injection combined with intravenous administration of two different recombinant αSYN pathogenic strains (fibrils or ribbons) in wild-type mice, induces an increase in brain resident microglia and promotes the recruitment of leukocytes towards the brain (Figure 12A) and the spinal cord (Figure 12C). When further characterising the phenotypic traits of the peripheral cells trafficking to the CNS, we identified neutrophils and professional antigen presenting cells among innate myeloid leukocytes (data not shown), as well as a distinct migration of $CD4^+$ and $CD8^+$ T cell subsets after administration of αSYN strains, which was most prominent in the brain for ribbons compared to fibrils (Figure 12B, D). Moreover, LPS-primed inflammatory monocytes proved to be the major source of CNS-associated phagocytes after systemic challenge with αSYN strains. In the brain, fibrils induced a stronger response compared to ribbons, while the effect in the spinal cord was similar for both αSYN strains (Figure 12A, C). Interestingly, we noticed that LPS priming favoured αSYN spreading towards the brain and spinal cord, as observed by an upregulation of $αSYN^+$-expressing microglia and inflammatory monocytes (Figure 12E, F).

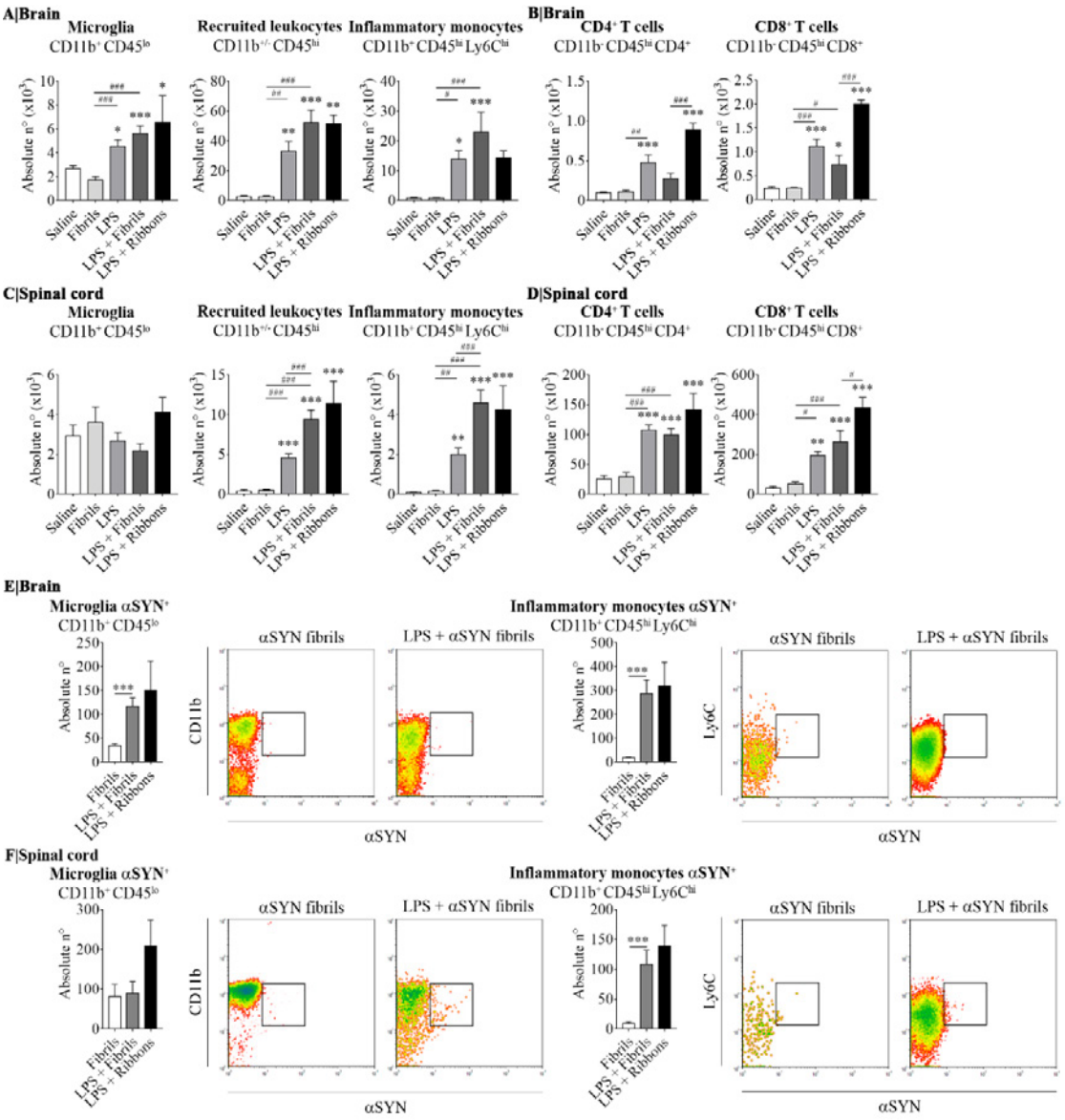

Figure 12 – Flow cytometric analysis of inflammatory cells in the brain and spinal cord after peripheral administration of aSYN assemblies combined with interaperitoneal LPS. Twelve hours after the last injection, mice were euthanised and immune cells were isolated from either whole brain **(A, B)** or spinal cord **(C, D)** and stained for subsequent flow cytometric analysis. Absolute numbers of CD11b^{+} CD45^{lo} microglial cells, CD11b$^{+/-}$ CD45^{hi} recruited cells, CD11b^{+} CD45^{hi} Ly6C^{hi} inflammatory monocytes, CD11b^{-} CD45^{hi} CD4^{+} and CD11b^{-} CD45^{hi} CD8^{+} lymphocytes were assessed by flow cytometry. Absolute numbers of αSYN-internalized CD11b^{+} CD45^{lo} microglial cells or CD11b^{+} CD45^{hi} Ly6C^{hi} inflammatory monocytes purified from brain **(E)** or spinal cord **(F)**, were assessed by flow cytometry. Results are representative of two independent experiments combined (n= 3-4 animals per group). Representative CD11b vs. αSYN and Ly6C vs. αSYN density-plots illustrate the gating analysis strategy employed for microglial cells and inflammatory monocytes, when gated in CD45^{lo} or CD45^{hi} cells respectively. Data are expressed as mean ± s.e.m. Means between groups were compared with one-way analysis of variance followed by a Tukey's *post hoc* test. Statistical significance levels were set as follows: $^{*/\#}$ if $p < 0.05$, $^{**/\#\#}$ if $p < 0.01$, and $^{***/\#\#\#}$ if $p < 0.001$. The asterisks indicate the comparison against the saline-treated group. (Peralta Ramos et al. Frontiers in Immunology January 2019).

2.4. PD, MSA and DLB patient-derived αSYN strains trigger a differential immune response

To investigate whether distinct αSYN strains may act as antigens altering immune tolerance, provoking neuroinflammation and subsequent deleterious reactions, we investigated the presence of different immune-related cells in the brain. In naive animals, injection of different brain homogenates or PMCA-amplified αSYN strains did not induce a detectable Iba1-positive microglial response at the final time point of 150 days (data not shown). However, in the presence of human αSYN, we detected a pronounced additive immune response. Remarkably, the overall immune response to PMCA-amplified αSYN assemblies from PD, MSA and DLB patients was more significant compared to the corresponding brain homogenates. When comparing diseases, MSA-derived material induced the

strongest immune response, followed by PD and DLB (Fig. 13). More specifically, co-injection of PD or MSA brain homogenates or PMCA-amplified αSYN strains with rAAV-αSYN resulted in a significantly higher number of Iba1-positive cells and the presence of large phagocytic reactive microglia (Fig. 13a, b). MHC II expression was triggered by injection of PD, MSA and DLB material, with the strongest expression for samples originating from MSA patients (Fig. 13a, b). Since microglial upregulation of MHC II is suggestive of an adaptive immune response, we further examined the affected areas for CD4 (T helper) and CD8 (cytotoxic)-T cells infiltration. An increase in the number of CD4- and CD8-positive T cells paralleled MHCII expression (Fig. 13a, b).

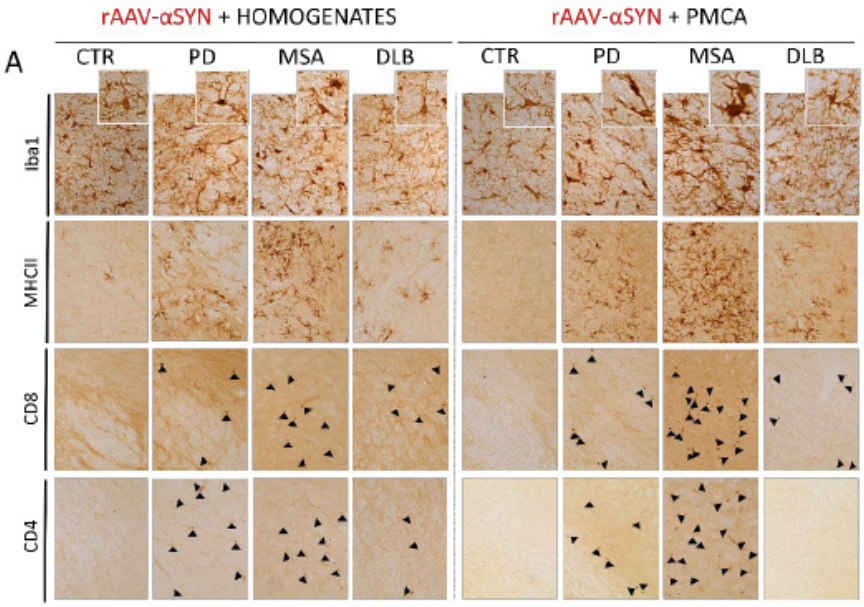

B

	rAAV-αSYN + HOMOGENATES				rAAV-αSYN + PMCA			
	CTR	PD	MSA	DLB	CTR	PD	MSA	DLB
Iba1 (ameboid)	+	++	++	+	+	++	+++	++
MHCII	-	+	++	+	-	++	+++	+
CD4	-	++	++	+	-	++	+++	-
CD8	-	+	++	+	-	++	++++	+

Fig. 13 - Assessment of immune response after inoculation of different patient-derived homogenates and PMCA-amplified αSYN strains in association with rAAV2/7-mediated αSYN expression.
(a) Representative photomicrographs of the immune response stained for Iba1 (microglia), MHCII (reactive microglia), CD4 (T helper cells) and CD8 (cytotoxic T cells) in the SN five months after co-injection of different patient-derived homogenates (left) or PMCA-amplified αSYN assemblies (right) with rAAV2/7-αSYN overexpression. Cells immunoreactive for CD4 and CD8 are marked with black arrows. Scale bar Iba1 = 50 µm, MHCII – CD4 = 100 µm. (b) Table with scoring system for the different immune markers Iba1, MHCII, CD4 and CD8 in the rat SN five months after inoculation with patient-derived homogenates (left) or PMCA-amplified αSYN assemblies (right) combined with human αSYN expression. The scoring system ranges from not present (-) to abundantly present (++++). A total of 3 animals per group was included. The data were presented as a table with scoring system to demonstrate the presence of an inflammatory response in the rat SN.

3. Follow-up projects

Multiple system atrophy (MSA) is histopathologically characterized by the presence of αSYN deposits in glial cells of the central and peripheral nervous system. Different subtypes of the disease are described and can either be parkinsonian (MSA-P) or cerebellar (MSA-C). It is still not known why MSA, that invariably presents with αSyn oligodendrogliopathy, is clinically so heterogeneous. It has been shown that oligodendrocytes in MSA brain impact the seeding of soluble αSYN into unique and highly toxic

protein assemblies. We are now further investigating if within this unique MSA environment, different αSYN high molecular weight assemblies can seed distinct MSA phenotypes in vivo in a strain-dependent manner.
To do this, we have taken 2 approaches in parallel : on the one hand we focused on the development of a viral vector-mediated αSYN rat model, and on the other hand we have characterized αSYN strains in an existing transgenic mouse model for MSA.

3.1. Characterization of αSYN strains in a viral vector-based model for MSA
We have developed and validated AAV vectors for specific and robust transgene expression in oligodendrocytes in vivo. (Peelaerts*, de Brito* et al, in preparation). In order to achieve specific expression in oligodendrocytes in rat brain, we compared multiple promoters specific for mature oligodendrocytes in combination with different serotype capsids. The rAAV2/9 serotype in combination with the MAG promoter gave the best results (Fig. 14).

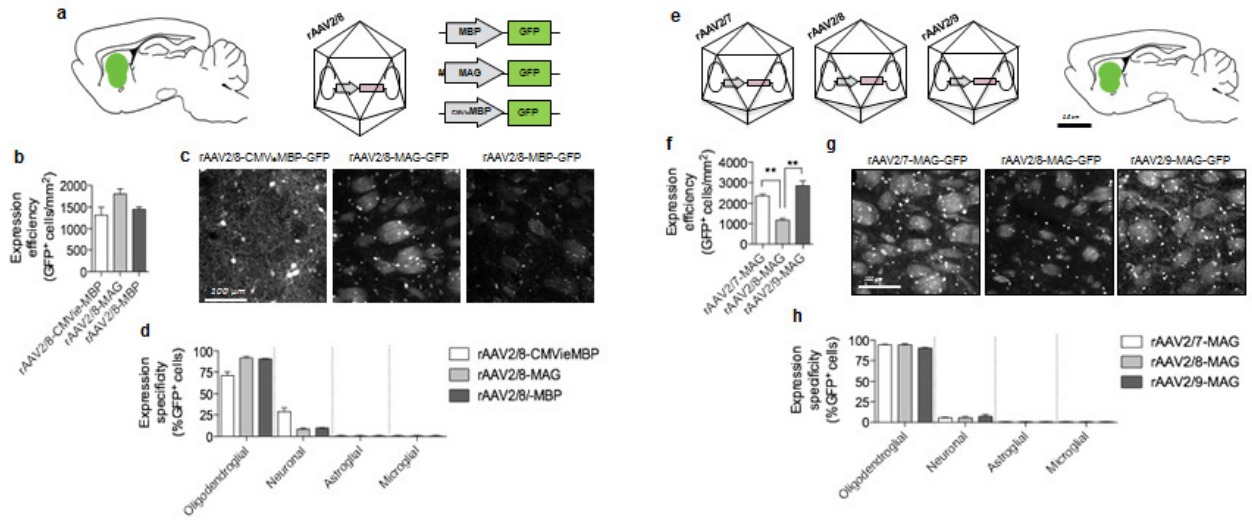

Figure 14. Initial side-by-side comparison of viral vector-mediated overexpression of eGFP in different cell types *in vivo*.
a. schematic representation of the injected brain area, an AAV viral vector particle and the used constructs, b. expression efficiency for the 3 different promoters quantified as GFP positive cell density, c. immunohistological staining for GFP expressed from the 3 different promoters, d. expression specificity of the 3 different promoters quantified for oligodendrocytes, neurons, astrocytes and microglia, e. Schematic representation of the 3 different viral vector particles and the injected brain area, f. expression efficiency for the 3 different serotypes quantified as GFP positive cell density, g. immunohistological staining for GFP expressed from the 3 different AAV serotypes, h. expression specificity for the 3 different serotypes quantified for oligodendrocytes, neurons, astrocytes and microglia (Peelaerts, de Brito et al., in preparation)

Next, we generated viral vectors encoding for human alpha-synuclein specifically in oligodendrocytes. rAAV2/9-MAG vectors encoding hαSYN or GFP (as control) were stereotactically injected in the striatum of Sprague Dawley rats. The animals were followed for 5 months and assessed for motor behavior with the cylinder test. Then the brains were perfused for further histological analysis. Analysis is still ongoing including myelin density and oligodendroglial cells by luxol fast blue staining, MBP and olig2+ cells, as well as dopaminergic and striatal neuronal integrity by TH and NeuN staining followed by stereological quantifications. Neuropathological characterization will consist of immunostainings for phosphorylated Ser129 αSYN and the aggresome marker p62.
In the meantime, the PMCA amplified strains from PD, DLB and MSA patients, as well as age-matched controls have been injected in rat striatum in parallel with brain homogenates from the same patients (5 µg/rat). The underlying hypothesis is that different strains will present distinct capacities to propagate

and induce PD-, DLB- or MSA-like features depending on their origin and seeding environment. More specifically, we will investigate uptake of different αSYN assemblies after stereotactic injection (n=8-10/group) and subsequent spreading to connected anatomical regions by detailed immunostaining and confocal microscopy. Motor and sensorimotor behavioral deficits will be analyzed by different behavioral assays (e.g. cylinder test, rotarod test, adhesive removal test) between 2 weeks and 5 months after injection. Upon completion of behavioral studies, animals will be sacrificed and the brains will be microdissected into specific brain regions for further detailed characterization as described above.

3.2. Characterization of αSYN strains in a transgenic model for MSA

In a second approach we have injected two well-characterized but distinct recombinant αSYN strains (fibrils and ribbons) unilaterally in the striatum of transgenic MSA mice that constitutively express αSYN under the oligodendrocyte-specific promoter of the proteolipid protein (PLP). We allowed the MSA mice to age for 9 months and subjected them to different behavioral tests at 3, 6 and 9 months after injection. At 9 months after injection, we detected a significant worsening of MSA mice exposed to fibrils compared to the ribbons and control groups (data not shown). In addition we found that fibrils cause severe neuronal damage and demyelination whereas ribbons inflicted more severe glial pathology (Fig 15) (Torre-Muruzabal, Peelaerts et al, in preparation).

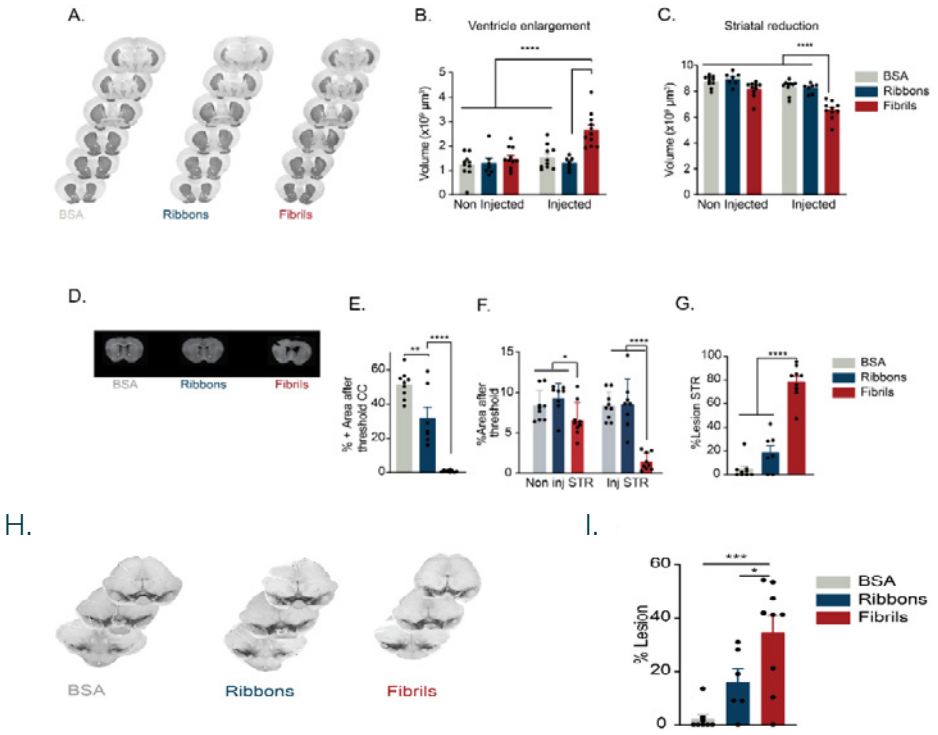

Figure 15. Injection of recombinant αSYN fibrils in MSA transgenic mice induces brain atrophy, demyelination and dopaminergic neurodegeneration.

A-C Representative images and quantification of ventricle enlargement and striatal volume

D-G representative images and quantification of demyelination in the corpus callosum (CC) and striatum

H-I Representative images and quantification of TH-positive neurons in the substantia nigra

In addition, fibrils triggered extensive recruitment of activated and pro-inflammatory macrophagic cells from the periphery into affected brain areas. Fibrils can therefore augment MSA neuropathology via direct neurotoxic and indirect peripheral responses. It thus seems that the resulting disease phenotype not only depends on the host genotype but both the protein strain and the host environment in which αSYN seeds and propagates. In addition, we found a yet undescribed role for the peripheral immune response in MSA, which might be potential therapeutic target for MSA.

4. Scientific output

4.1. Publications

- Gelders G., Baekelandt V. and Van der Perren A. (2018) Linking Neuroinflammation and Neurodegeneration in Parkinson's disease. *Journal of Immunology Research*, 2018:4784268 (IF 3.3)
- Peralta Ramos JM, Iribarren P, Bousset L, Melki R, Baekelandt V, Van der Perren A (2019) Peripheral inflammation regulates CNS immune surveillance through the recruitment of inflammatory monocytes upon systemic α-synuclein administration. *Frontiers in Immunology,* 10:80. (IF 5.5)
- Torre-Muruzabal T, Devoght J, Van den Haute C, Brône B, Van der Perren A, Baekelandt V. (2019) Chronic nigral neuromodulation aggravates behavioral deficits and synaptic changes in an α-synuclein based rat model for Parkinson's disease. *Acta Neuropathol Commun.*; 7(1):160 (IF 5.9)
- van Veen S#, Martin S#, Van den Haute C, Benoy V, Lyons J, Vanhoutte R, Kahler JP, Decuypere J-P, Gelders G, Lambie E, Swinnen JV, Annaert W, Agostinis P, Ghesquière B, Verhelst S, Baekelandt V, Eggermont J, Vangheluwe P (2019) ATP13A2 deficiency disrupts lysosomal polyamine export. *Nature*, in press (IF 43.1).
- Van der Perren A*, Gelders G*, Fenyi A*, Bousset L, Brito F, Peelaerts W, Van den Haute C, Gentleman S, Melki R*, Baekelandt V*. Patient-derived α-synuclein strains display distinct functional characteristics in cells and in vivo. *Acta Neuropathol , under revision* (IF 18.2)
- Peelaerts W.*, Brito F.*, Van den Haute C., Steiner J., Brundin P., Baekelandt V. Widespread, specific and efficient transgene expression in oligodendrocytes after intracerebral and intracerebroventricular delivery of viral vectors in vivo. *In preparation*
- Torre-Muruzabal T*, Peelaerts W*, Camacho-Garcia S, Bousset L, Melki R, Stefanova N and Baekelandt V. Alpha-synuclein strains promote distinct multiple system atrophy pathologies via central and peripheral mechanisms in vivo. *In preparation*

4.2. Presentations at conferences and meetings

- Van Der Perren A, Gelders G, Macchi F, Peelaerts W, Bousset L, Van Den Haute C, Melki R and Baekelandt V. Differential response of microglia to distinct alpha-synuclein assemblies. Alzheimer Disease & Parkinson's Disease (ADPD) meeting, Vienna, Austria, March 29 - April 2 2017. Poster presentation
- Van Der Perren A, Gelders G, Macchi F, Peelaerts W, Bousset L, Van Den Haute C, Melki R and Baekelandt V. Differential response of microglia to distinct alpha-synuclein assemblies.Venusberg Meeting on Neuroinflammation, Bonn, Germany, May 11-15 2017. Poster presentation
- Van Der Perren A, Gelders G, Macchi F, Peelaerts W, Bousset L, Van Den Haute C, Melki R and Baekelandt V. Differential response of microglia to distinct alpha-synuclein assemblies. 12th National Congress of the Belgian Society for Neuroscience, Ghent, Belgium, May 22 2017. Poster presentation
- Van Der Perren A, Gelders G, Macchi F, Peelaerts W, Bousset L, Van Den Haute C, Melki R and Baekelandt V. Differential response of microglia to distinct alpha-synuclein assemblies. 20 years of alpha-synuclein in Parkinson's disease and other related synucleinopathies. "From the bedside to the bench and back to the patient". Athens, Greece, September 7-10 2017. Poster presentation
- Van Der Perren A, Gelders G, Macchi F, Peelaerts W, Bousset L, Van Den Haute C, Melki R and Baekelandt V. Differential response of microglia to distinct alpha-synuclein assemblies. Neuroscience meeting (SFN), Washington DC, US, November 9-15 2017. Selected for dynamic poster presentation
- Van Der Perren A, Gelders G, Macchi F, Peelaerts W, Bousset L, Van Den Haute C, Melki R and Baekelandt V. Differential response of microglia to distinct alpha-synuclein assemblies. Keystone Meeting, Keystone, US, June 17-21 2018. Poster presentation
- Gelders G, CAJAL Advanced Neuroscience Training Programme: Neuroinflammation and How to Study It, Bordeaux, France, June 25 – July 7 2018. Summer School
- Van Der Perren A, Gelders G, Fenyi A, Bousset L, Brito F, Peelaerts W, Gentleman S, Melki R, Baekelandt V. In vivo characterization of distinct patient-derived alpha-synuclein strains. Cold Spring Harbor, New York, US, November 28 – December 1 2018. Poster presentation
- Van Der Perren A, Gelders G, Fenyi A, Bousset L, Brito F, Peelaerts W, Gentleman S, Melki R, Baekelandt V. In vivo characterization of distinct patient-derived alpha-synuclein strains. AD/PD 2019, Lisbon, Portugal, March 26-31 2019. Selected for oral presentation

Invited lectures

- Baekelandt V. Systemic transmission of alpha-synuclein strains. Invited speaker at «20 years of alpha-synuclein in Parkinson's Disease and related synucleinopathies: from the bedside to the bench and back to the patient», Athens, Greece, 7-10 Sept 2017
- Baekelandt V. Modeling alpha-synuclein aggregation, propagation and neurotoxicity in rodent brain. Invited speaker at the Research Summer School within the EU-Project BrainMatTrain, Galway, Ireland, 9-10 Oct 2017

– Baekelandt V. Modeling alpha-synuclein aggregation, propagation and neurotoxicity in rodent brain. Invited speaker at the NECTAR meeting, Dublin, Ireland, 6-8 Dec 2017
– Baekelandt V. Synuclein Meeting 2019 : Where we are and where we need to go, Porto, Portugal, 1-4 Sept 2019. Invited speaker

4.3. PhD degrees related to this project

– Geraldine Gelders (2016- planned June 2020) Unraveling the role of the immune system in alpha-synuclein transmission and neurotoxicity in vivo. (V. Baekelandt promotor, A. Van der Perren copromotor). *Supported by the GSKE*
– Teresa Torre Muruzabal (2016- planned June 2020) The effect of synaptic activity on alpha-synuclein pathogenesis in a model for Parkinson's Disease. (V. Baekelandt promotor, A. Van der Perren copromotor) FWO-sb fellowship
– Jianmin Si (2016- planned in 2020) Impact of ATP13A2 on alpha-synuclein neurotoxicity. (V. Baekelandt promotor) DBOF fellowship
– Filipa de Brito (2017- planned end 2020) Investigating the role of alpha-synuclein strains in synucleinopathies. (V. Baekelandt promotor) FWO-sb fellowship
– Diego Cabezudo (2018-) Investigation of the role of LRRK2 in α-synuclein-induced neurotoxicity and neuroinflammation in models for Parkinson's disease (V. Baekelandt promotor, Evy Lobbestael copromotor). FWO fellowship

5. References

1. Braak, H. & Braak, E. Neuropathological stageing of Alzheimer-related changes. *Acta Neuropathol* **82**, 239-259 (1991).
2. Braak, H. *et al.* Staging of brain pathology related to sporadic Parkinson's disease. *Neurobiol Aging* **24**, 197-211 (2003).
3. Hansen, C. *et al.* α-Synuclein propagates from mouse brain to grafted dopaminergic neurons and seeds aggregation in cultured human cells. *J Clin Invest* **121**, 715-725, doi:10.1172/JCI43366 (2011).
4. Bousset, L. *et al.* Structural and functional characterization of two alpha-synuclein strains. *Nat Commun* **4**, 2575, doi:10.1038/ncomms3575 (2013).
5. Peelaerts, W. *et al.* α-Synuclein strains cause distinct synucleinopathies after local and systemic administration. *Nature* **522**, 340-344, doi:10.1038/nature14547 (2015).
6. Guo, J. L. *et al.* Distinct α-synuclein strains differentially promote tau inclusions in neurons. *Cell* **154**, 103-117, doi:10.1016/j.cell.2013.05.057 (2013).
7. Stöhr, J. *et al.* Distinct synthetic Aβ prion strains producing different amyloid deposits in bigenic mice. *Proc Natl Acad Sci U S A* **111**, 10329-10334, doi:10.1073/pnas.1408968111 (2014).
8. Hirsch, E. C. & Hunot, S. Neuroinflammation in Parkinson's disease: a target for neuroprotection? *Lancet Neurol* **8**, 382-397, doi:10.1016/S1474-4422(09)70062-6 (2009).
9. Gelders, G., Baekelandt, V. & Van der Perren, A. Linking Neuroinflammation and Neurodegeneration in Parkinson's Disease. *J Immunol Res* **2018**, 4784268, doi:10.1155/2018/4784268 (2018).
10. Heneka, M. T. *et al.* NLRP3 is activated in Alzheimer's disease and contributes to pathology in APP/PS1 mice. *Nature* **493**, 674-678, doi:10.1038/nature11729 (2013).
11. McGeer, P. L., Itagaki, S., Boyes, B. E. & McGeer, E. G. Reactive microglia are positive for HLA-DR in the substantia nigra of Parkinson's and Alzheimer's disease brains. *Neurology* **38**, 1285-1291 (1988).
12. Holmans, P. *et al.* A pathway-based analysis provides additional support for an immune-related genetic susceptibility to Parkinson's disease. *Hum Mol Genet* **22**, 1039-1049, doi:10.1093/hmg/dds492 (2013).
13. Tansey, M. G. & Goldberg, M. S. Neuroinflammation in Parkinson's disease: its role in neuronal death and implications for therapeutic intervention. *Neurobiol Dis* **37**, 510-518, doi:10.1016/j.nbd.2009.11.004 (2010).
14. Gerhard, A. *et al.* In vivo imaging of microglial activation with [11C](R)-PK11195 PET in idiopathic Parkinson's disease. *Neurobiol Dis* **21**, 404-412, doi:10.1016/j.nbd.2005.08.002 (2006).
15. Li, J. Y. *et al.* Lewy bodies in grafted neurons in subjects with Parkinson's disease suggest host-to-graft disease propagation. *Nature medicine* **14**, 501-503, doi:10.1038/nm1746 (2008).
16. Kordower, J. H., Chu, Y., Hauser, R. A., Freeman, T. B. & Olanow, C. W. Lewy body-like pathology in long-term embryonic nigral transplants in Parkinson's disease. *Nature medicine* **14**, 504-506, doi:10.1038/nm1747 (2008).
17. Olanow, C. W. & Prusiner, S. B. Is Parkinson's disease a prion disorder? *Proc Natl Acad Sci U S A* **106**, 12571-12572, doi:10.1073/pnas.0906759106 (2009).
18. Peelaerts, W. *et al.* alpha-Synuclein strains cause distinct synucleinopathies after local and systemic administration. *Nature* **522**, 340-344, doi:10.1038/nature14547 (2015).

Geneeskundige Stichting Koningin Elisabeth
Fondation Médicale Reine Elisabeth
Königin-Elisabeth-Stiftung für Medizin
Queen Elisabeth Medical Foundation

Final report of the research group of

Prof. dr. De Bundel Dimitri, PhD

Vrije Universiteit Brussel (VUB)

Principal investigator

Prof. dr. Dimitri De Bundel

Co-investigators

Prof. dr. Ilse Smolders
Prof. dr. Ann Van Eeckhaut

Research Group Experimental Pharmacology, Center for Neurosciences
Department of Pharmaceutical and Pharmacological Sciences
Vrije Universiteit Brussel
Laarbeeklaan 103
1090 Brussels

Neuromedin U involvement in stress-induced psychopathology

1. Stress and the hypothalamus-pituitary-adrenal axis

The brain is the central organ for adaptation to psychobiological stressors because it determines what is threatening, stores relevant memories, and regulates physiological and behavioural responses (1). These allostatic responses enable an organism to actively adapt to its changing environment and achieve stability. Activation of the hypothalamus-pituitary-adrenal-axis (HPA axis) is a key physiological allostatic process characterized by release of corticotropin-releasing hormone (CRH) from the hypothalamic paraventricular nucleus (PVH), adrenocorticotropic hormone (ACTH) from the pituitary and glucocorticoids such as cortisol and corticosterone (CORT) from the adrenal cortex (1). Release of glucocorticoids initiates a series of cardiovascular, metabolic and behavioural coping mechanisms. However, when allostatic load exceeds the physiological regulatory capacity, due to the unpredictable or uncontrollable nature of stressors, HPA axis activity can become maladaptive, leading to inappropriate physiological and behavioural responses that may impede coping and recovery (1, 2). Not surprisingly, stress has been identified as a major risk factor for the development of cardiovascular, metabolic and mental disorders (3-5). More specifically, excessive HPA axis activation following stress exposure is associated with alterations in neuronal activity, changes in spine morphology, dendritic remodelling, suppression of dentate gyrus neurogenesis, and inappropriate behavioural responses that are proposed to be core features in the aetiology of psychiatric disorders such as post-traumatic stress disorder and major depression (6). Neuropeptides are typically released by discrete neuronal populations and may enable diversified physiological and behavioural responses to a wide range of stressors through their specific projections in the brain.

Position	**1**	**2**	**3**	**4**	**5**	**6**	**7**	**8**	**9**	**10**	**11**	**12**	**13**	**14**	**15**	**16**	**17**	**18**	**19**	**20**	**21**	**22**	**23**	**24**	**25**
Human NMU-25	Phe	Arg	Val	Asp	Glu	Glu	Phe	Gln	Ser	Pro	Phe	Ala	Ser	Gln	Ser	Arg	Gly	Tyr	**Phe**	**Leu**	**Phe**	**Arg**	**Pro**	**Arg**	**Asn**	NH_2
Rat NMU-23	Tyr	Lys	Val	Asn	Glu	*	–	Tyr	Gln	Gly	Pro	*	–	Val	Ala	Pro	Ser	Gly	Gly	Phe	**Phe**	**Leu**	**Phe**	**Arg**	**Pro**	**Arg**	**Asn**	NH_2
Mouse NMU-23	Phe	Lys	Ala	*	–	Glu	*	–	Tyr	Gln	Ser	Pro	Ser	Val	Gly	Gln	Ser	Lys	Gly	Tyr	**Phe**	**Leu**	**Phe**	**Arg**	**Pro**	**Arg**	**Asn**	NH_2

Figure 1. *The structure of NMU in distinct species. The highly conserved C-terminus is shown in bold. Structural homology between human, rat and mouse sequences is emphasized by elongation with gaps represented by an asterix (*). Adapted from (7)*

2. Neuromedin U and the stress response

Neuromedin U (NMU) is a neuropeptide coded by the *Nmu* gene showing a remarkable amino acid sequence homology across mammals (7), suggesting a strong evolutionary pressure to maintaining its structure and function (Figure 1). The C-terminal amidated heptapeptide is entirely conserved in mammals and the C-terminal amidated octapeptide NMU-8 exerts the same biological effects as its longer endogenous isoforms, NMU-25 in humans or NMU-23 in rodents (7). NMU-like immunoreactivity has been detected in neurons of the brain, spinal cord and mesenteric plexus (7). NMU activates two G-protein coupled receptors: NMUR1 receptors that are mainly expressed in the periphery and NMUR2 receptors that are mainly expressed in the brain and spinal cord (8, 9). NMU was previously demonstrated to modulate food intake and stress responsiveness through activation of hypothalamic NMUR2 receptors (8, 10-13). Nevertheless, precise anatomical knowledge remains lacking and in-depth insight in the role of NMU systems in the brain remains hampered by the lack of specific and sensitive research tools. For this reason, we developed a knock-in mouse model expressing Cre recombinase under the Nmu promotor to enable a highly specific expression of proteins for anatomical and physiological characterization of NMU-producing cells based on tools exploiting Cre-lox recombination.

3. Results

3.1. Effects of NMU-8 on stress responsiveness and HPA axis activity in C57BL6/J mice

We aimed to provide a better understanding of how NMU-8 influences various aspects of the stress response by studying the effects of intracerebroventricular NMU-8 administration on stress-related behaviour and activity of HPA axis in male C57BL/6J mice. We investigated these NMU-8 effects when mice remained in their home cage and when they were challenged by exposure to forced swim stress. NMU-8 administration resulted in increased grooming behaviour in mice that remained in their home cage and in a significant increase in c-Fos immunoreactivity in the PVH and ARC. Surprisingly, NMU-8 administration significantly decreased plasma corticosterone concentrations. Furthermore, NMU-8 administration increased immobility in the forced swim test in both naïve mice and mice that were previously exposed to swim stress. These findings were in contrast to a previous study (14). The effect of NMU-8 on c-Fos immunoreactivity in the PVH was dependent on previous exposure to swim stress given that we observed no significant changes in mice exposed for the first time to swim stress. In contrast, in the ARC we observed a significant increase in c-Fos immunoreactivity regardless of previous stress exposure. Interestingly, NMU-8 administration also significantly decreased plasma corticosterone concentrations in mice that were exposed to single forced swim stress, while this effect was no longer observed when mice were exposed to forced swim stress for a second time. Taken together, our data indicate that NMU-8 regulates stress responsiveness and suggests that its effects depend on previous stress exposure. The results of this study have now been published in Hormones and Behavior (15).

3.2. Neuroanatomical characterization of NMU-expressing cells in the central nervous system

We generated a *B6.NmuCre-IRES-Nmu* knock-in mouse model constitutively expressing a Cre recombinase in NMU-producing cells in collaboration with Dr. Peter Boyd (GeneOway, France). This was achieved by insertion of Cre-IRES-Nmu cDNA in frame with the ATG coding sequence of the *Nmu* gene on chromosome 5qC3.3. We obtained offspring of crossings between heterozygous *B6.NmuCre-IRES-Nmu* mice and homozygous B6.*ROSA26RCL-ZsGreen1* reporter mice that harbour a targeted mutation of the ROSA26 gene locus with a loxP-flanked STOP cassette preventing transcription of a CAG promotor-driven enhanced green fluorescent protein (ZsGreen1). In a first series of experiments we characterized the distribution of ZsGreen1 expression cells. ZsGreen1 expression appeared stable and consistent in both male and female *Nmu:ZsGreen1* mice (Figure 2). Nevertheless, we observed a wider distribution pattern of ZsGreen1 compared to the pattern of NMU mRNA expression in rodents (16,17). In mice specifically, NMU mRNA was previously detected in subregions of the hypothalamus, notably the suprachiasmatic nucleus (SCN), arcuate nucleus (ARC), dorsomedial hypothalamus (DMH), ventromedial hypothalamus (VMH) and medial eminence (ME) (17). In the hypothalamus of *Nmu:ZsGreen1 mice,* the distribution of ZsGreen1 cells was strikingly similar, but we also detected ZsGreen1 cells beyond the hypothalamus, notably throughout the cortex, but also the midbrain, and specific clusters of cells in the lateral hypothalamus (LH) and the medial amygdala (MEA) (Figure 2).

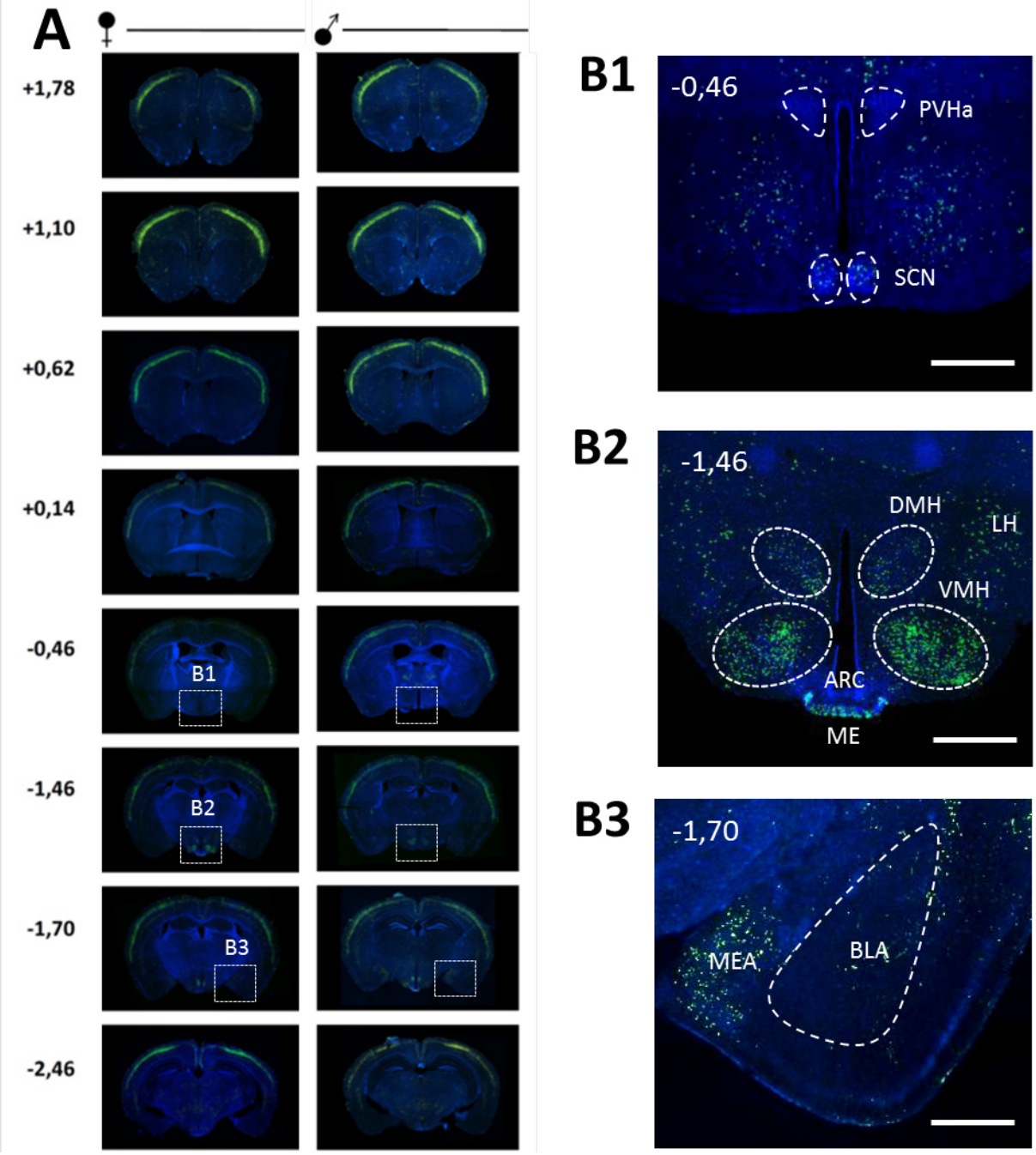

Figure 2. *Distribution of ZsGreen1 expression in coronal brain sections obtained from Nmu:ZsGreen1 mice. Numbers denote neuroanatomical coordinates relative to bregma. Abbreviations: anterior paraventricular hypothalamus (PVHa), suprachiasmatic nucleus (SCN), dorsomedial hypothalamus (DMH), ventromedial hypothalamus (VHM), lateral hypothalamus (LH), arcuate nucleus (ARC), medial eminence (ME), medial amygdala (MEA), basolateral amygdala (BLA). Scale bar 300* µm.

The notion that the distribution pattern of ZsGreen1 appears wider compared to studies using *in situ* hybridization is not surprizing. The Cre recombinase is expressed constitutively. While this enable high sensitivity, it also leads to accumulation of the green fluorescent protein across development. Therefore, ZsGreen1 may be expressed in cells where the NMU promotor is no longer active. We initially attempted to validate the NMU promotor-dependent expression of Cre recombinase in our mouse model using fluorescence in-situ hybridization (FISH). Hereto, we have cloned antisense RNA probes based on distinct designed primer pairs that hybridize to NMU mRNA of the mouse. The best probe was selected for further characterization but we were unable to obtain a reliable signal for NMU mRNA due to low NMU mRNA expression levels and inadequate sensitivity of the used FISH system. We therefore opted

for a different strategy. Presently, experiments are ongoing to determine NMU mRNA expression in *Nmu:ZsGreen1 mice* using the Automated RNAScope system.

To further facilitate the description of ZsGreen1 expression in *Nmu:ZsGreen1 mice,* we are presently optimizing a CUBIC (clear unobstructed brain imaging cocktails and computational analysis) protocol for whole-brain imaging using the ZEISS Lightsheet Z1 fluorescence microscope which was recently installed at our university (FWO Hercules HERC45).

3.3. Chemogenetic modulation of hypothalamic NMU neurons.

We are also investigating the behavioural effects of direct manipulation of NMU expressing cells in the mouse hypothalamus using chemogenetic intervention. We obtained the commercially available adeno-associated viral (AAV) control vector AAV8-DIO-mCherry and DREADD (Designer Receptor Exclusively Activated by Designer Drugs) vectors AAV8-DIO-hM3Dq-mCherry or AAV8-DIO-hM4Di-mCherry. These vectors use a Cre-dependent expression system based on a double-inverted open (DIO) reading frame sequence, to drive expression of a red fluorescent protein (mCherry) and engineered human muscarinic receptors, hM4Di (Gi-coupled) or hM3Dq (Gq-coupled) DREADDs specifically by Cre-containing neurons, in our case NMU neurons (Figure 3). We carried out initial experiments demonstrating that mCherry is expressed in *ZsGreen1* expressing neurons of *Nmu:ZsGreen1* mice following local infusion of the AAV8-DIO-mCherry control vector into the hypothalamus (Figure 3). It should be noted that while mCherry cells expressed ZsGreen1, not all ZsGreen1 cells expressed mCherry. This indicates that in adult mice, the NMU promotor is active in a more restricted population of cells compared to all cells expressing ZsGreen1. Moreover, when injecting viral vectors into the VMH, expression of mCherry could be observed in the VMH, LH and MEA. Further optimization of the injection procedure may therefore be necessary.

We carried out pilot experiments (n=3/4 per group) to demonstrate the feasibility of the chemogenetic strategy for manipulation of NMU neurons. We compared the expression of the immediate early gene c-Fos, a marker of neuronal activity, following administration of vehicle or the DREADD agonist clozapine-N-oxide (CNO, 3 mg/kg) in *B6.NmuCre-IRES-Nmu* knock-in mice previously injected in VMH with the control vector or with vectors driving the excitatory DREADD hM3Dq or the inhibitory DREADD hM4Di. In these experiments, mCherry was expressed in the VMH but also in adjacent brain regions previously demonstrated to contain NMU cells. Our preliminary experiments suggest that chemogenetic activation of NMU cells increases c-Fos expression in the VMH and other hypothalamic subregions. The quantification of c-Fos with co-labelling for mCherry to identify successfully transfected cells is presently ongoing.

We also performed pilot experiments (n = 3/5 per group) to understand how chemogenetic manipulation of VMH NMU cells affects homecage activity, food intake and anxiety-sensitive exploratory activity in the open field test and elevated plus maze test (Figure 4). We carried out additional labelling of mCherry and only included subjects where the VMH of both hemispheres was successfully transfected.

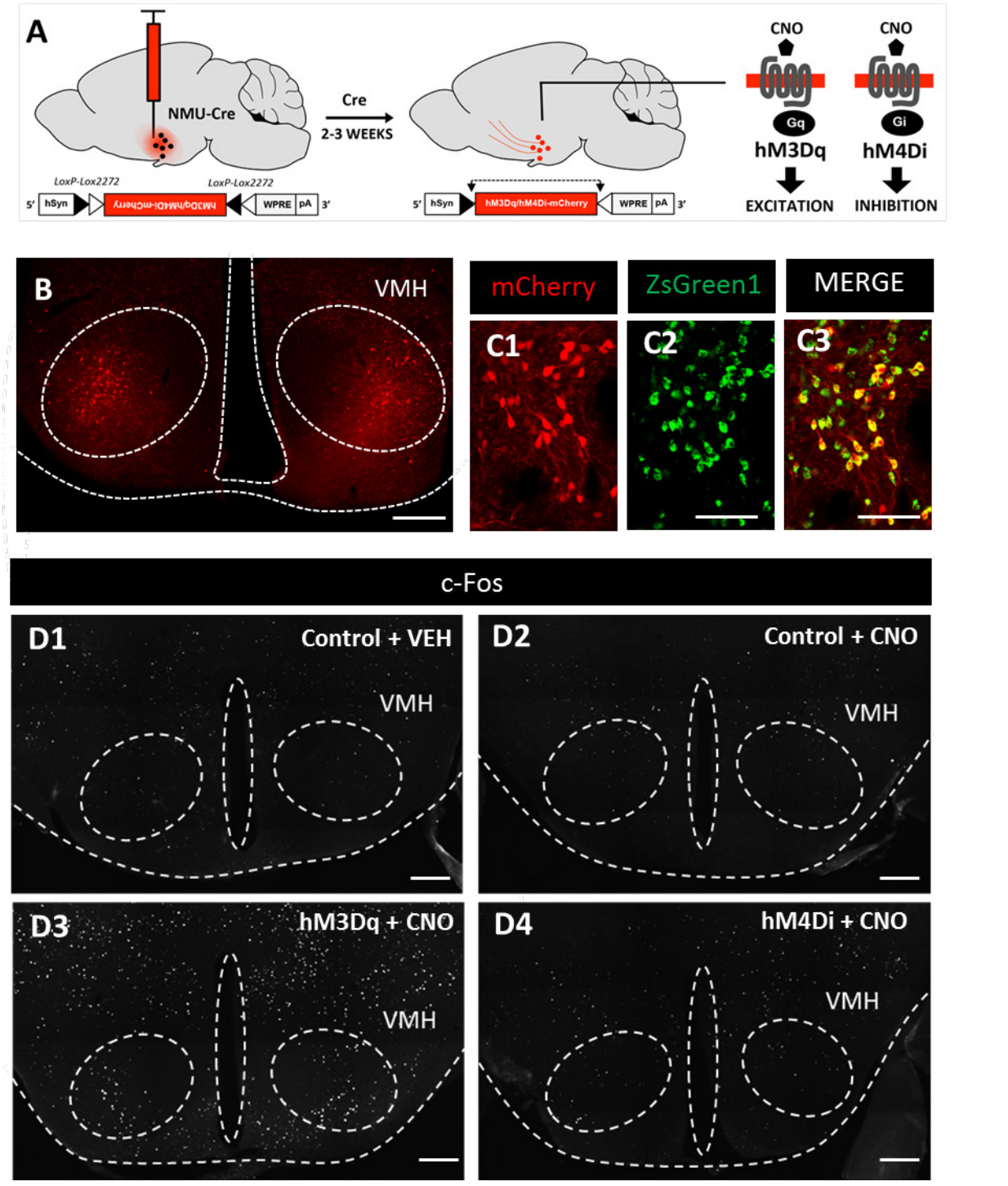

Figure 3. *Validation of chemogenetic manipulation in NMU-Cre mice. (A) Chemogenetic strategy to drive the expression of excitatory (hM3Dq) DREADDs or inhibitory (hM4Di) DREADDs specifically in hypothalamic NMU neurons. Expression is based on local infusion of an AAV8 viral vector and recombination of the DIO sequences (LoxP-Lox2272) by Cre expressed in NMU neurons leading to expression of a red fluorescent protein (mCherry) and the DREADD of choice. Systemic injection of clozapine-N-oxide (CNO) specifically activates the DREADDs and excites or inhibits the neurons in which they are expressed. (B) Image showing expression of mCherry in mice injected with control vector. (C1-3) Co-localization of mCherry and ZsGreen1 in the hypothalamus of Nmu:ZsGreen1 mice injected with AAV8-DIO-mCherry control virus. (D1-4) Expression of the immediate early gene c-Fos following administration of vehicle (VEH) or clozapine-N-Oxide (CNO) in NMU-Cre mice injected with control vector, hM3Dq vector or hM4Di vector. Scale bar 100* µm.

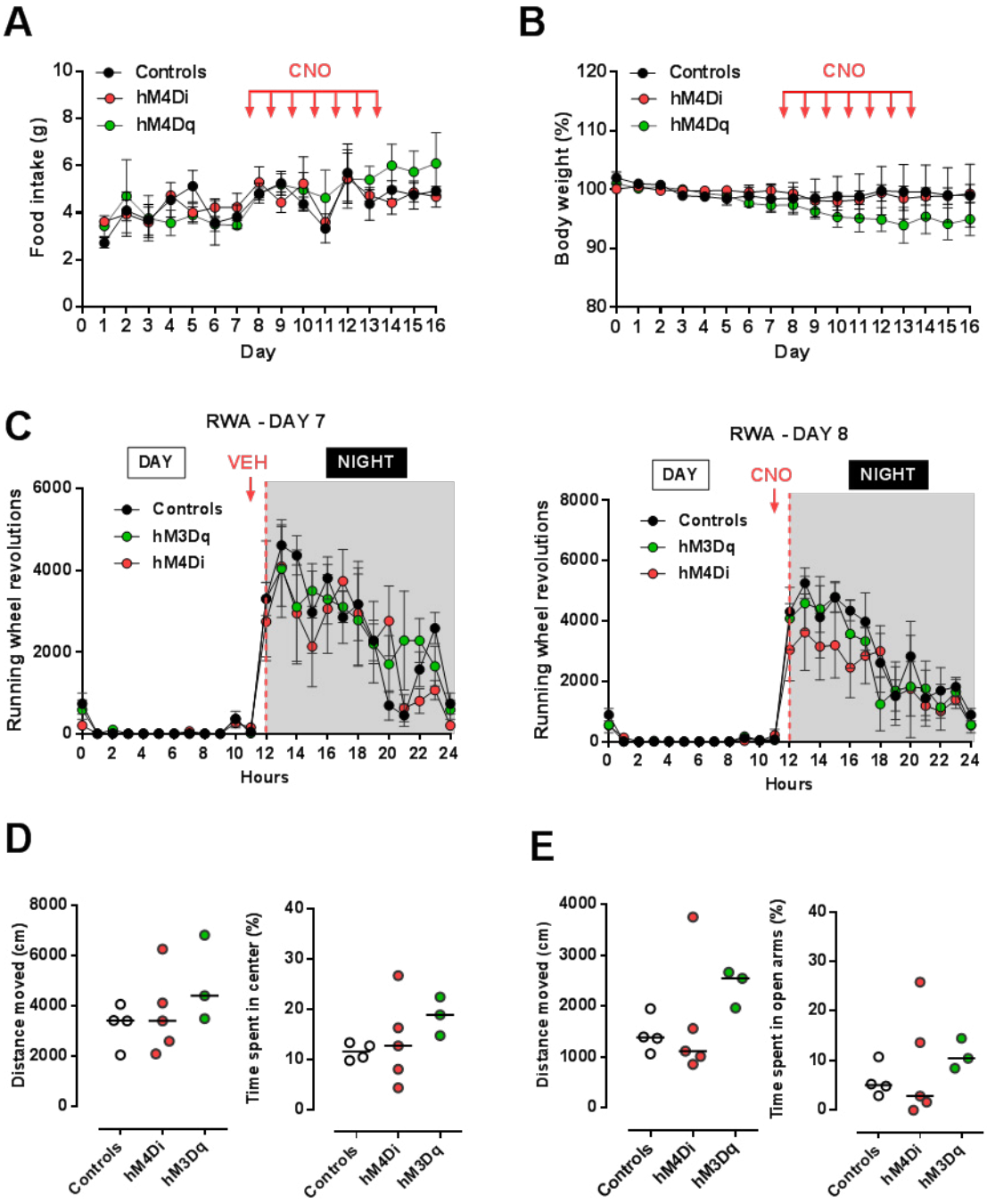

Figure 4. *Effects of chemogenetic manipulation of hypothalamic NMU cells on food intake (A), body weight (B), running wheel activity (C), exploratory activity in the open field test (D) and in the elevated plus maze test (D) in male NMU-Cre mice injected with control vector, hM3Dq vector or hM4Di vector.*

This proposed project is technically challenging. Despite previous setbacks with the production of *NMU-Cre mice* and with FISH for NMU mRNA, we now have preliminary data that demonstrate the technical feasibility of the project in our laboratory and that will generate additional questions regarding the role of NMU. We have recruited a post-doctoral researcher who is working on this project since September 2019. This will enable us to expand our preliminary findings on chemogenetic manipulation of hypothalamic NMU cells more rapidly and to explore the effects on other stress-related behaviours such as the forced swim test. We hope to complete our experiments regarding the description of hypothalamic NMU cells and the effects of chemogenetic manipulation of these cells on mouse behaviour by the end of 2020.

3.4. Optimization of nanoUHPLC-MS/MS parameters for NMU quantification

We proposed to investigate NMU release in targeted brain areas following direct manipulation of NMU-containing neurons. We will adopt an optogenetic approach using Cre-dependent expression of channel rhodopsin (ChR2), a yellow light-sensitive cation channel, in *B6.NmuCre-IRES-Nmu* mice. ChR2 expression will permit stimulating NMU-containing cells at a specific frequency (1-20 Hz) using an implanted optical fibre connected to an appropriate light-source. NMU release will be determined by intracerebral microdialysis and miniaturized UHPLC-MS/MS. We have acquired a NanoAcquity NanoUPLChip (IonKey) system coupled to the most recent and most sensitive triple quadrupole mass spectrometer (Xevo TQ-QS; both Waters) through funding from the Hercules Foundation (HERC36), opening new opportunities to obtain unpreceded sensitivity in very small sample volumes (≤ 20 µL). We aim to develop a microchip-electrospray ionization (ESI)-tandem mass spectrometry (MS/MS) method with detection limits in the low picomolar range (attomole on column) for the quantification NMU in volume-restricted samples, namely mouse brain microdialysates. The development of this method for the quantification of endogenous, sub-picomolar levels of neuropeptide in small sample volumes remains very demanding. Optimization of all chromatographic, ionization and MS/MS parameters is crucial to obtain the highest sensitivity possible.

One of the causes of lower sensitivity is that the peptide ion current is divided amongst multiple charge states that are commonly observed in ESI. The acquisition of multiple charge states splits the available ion current for the peptide into parts which is severely detrimental for quantitative and sensitive analyses. Moreover, sensitivity is negatively affected by a more pronounced increased background noise level when monitoring multiple transitions at the time. Supercharging agents allow modifying the maximal charge state and the corresponding distribution of charges, thereby potentially increasing the number of ions reaching the detector in selected reaction monitoring mode. The tetravalent charged precursor of NMU was selected as charge state of interest based on its abundancy and the production of stable fragment ions, suitable for quantification. We examined the effect of different superchargers and their simultaneous presence on the ionization of NMU and defined optimal conditions for signal to noise ratio for a given concentration. The results of this study are published in Talanta (18).

Although ESI is extensively used as ionization source, poor ionization and transmission efficiency are reported. Therefore, Waters has developed a new atmospheric pressure ionization source, UniSpray, which is built up by a high velocity spray arising from a grounded nebulizer that impacts asymmetrically on a cylindrical target held at high voltage (Figure 5). Although ESI and UniSpray display an analogous ionization of analytes, Unispray possesses some additional mechanisms that contribute to enhanced ionization and ion transmission efficiency. The source has already been evaluated for the analysis of a broad range of small molecules. For many of these compounds, sensitivity improvements have been reported with UniSpray compared to ESI. As earlier research only focused on small molecules, our study aimed to evaluate the LC-MS performance of the UniSpray source in comparison with ESI for seven neuropeptides, including NMU. In this way, our results may provide better insights into the potential applications and advantages of this source for quantitative peptide analysis.

Initially, optimal MS parameters were determined for both sources by direct infusion of a reference peptide, neurotensin. During this step, also the position of the spray emitter was optimized based on visual observations, as it can affect source stability and sensitivity. The highest signal intensity with the UniSpray source was indeed obtained when the spray impacted on the upper right quadrant of the rod. Next, the best overall capillary/impactor voltage was determined by injection of a mix containing seven neuropeptides, including NMU, on the LC-MS/MS system. An optimal capillary/impactor voltage of 2 kV was chosen and applied in the following experiments. Furthermore, higher total signal intensities were observed with UniSpray for all seven neuropeptides. Limit of quantification and linear range were determined and compared between both sources by construction of calibration curves (10 – 4000 nM).

Moreover, as matrix effects are regularly seen with ESI, it was investigated whether this is also observed for UniSpray. For this purpose, a post-column infusion method was applied to evaluate the matrix effects of protein-precipitated human plasma and microdialysate on the ionization of the investigated neuropeptides. Finally, the effect of the supercharging agents m-nitrobenzyl alcohol, dimethyl sulfoxide and sulfolane on the ionization of the neuropeptides was examined with both sources. Although the use of supercharging agents can be advantageous to modify the charge state distribution, an individual approach for each peptide is demanded. A paper discussing the obtained results will be soon submitted for publication.

4. References

1. McEwen BS, et al. (2015) Mechanisms of stress in the brain. Nature neuroscience 18(10):1353-1363.
2. Koolhaas JM, et al. (2011) Stress revisited: a critical evaluation of the stress concept. Neuroscience and biobehavioral reviews 35(5):1291-1301.
3. Steptoe A (2016) Diabetes: Stress resilience and risk of type 2 diabetes mellitus. Nature reviews. Endocrinology 12(4):189-190.
4. Steptoe A & Kivimaki M (2012) Stress and cardiovascular disease. Nature reviews. Cardiology 9(6):360-370.
5. Pittenger C & Duman RS (2008) Stress, depression, and neuroplasticity: a convergence of mechanisms. Neuropsychopharmacology : official publication of the American College of Neuropsychopharmacology 33(1):88-109.
6. McEwen BS et al. (2016) Stress Effects on Neuronal Structure: Hippocampus, Amygdala, and Prefrontal Cortex. Neuropsychopharmacology : official publication of the American College of Neuropsychopharmacology 41(1):3-23.
7. Brighton PJ et al. (2004) Neuromedin U and its receptors: structure, function, and physiological roles. Pharmacological reviews 56(2):231-248.
8. Howard AD, et al. (2000) Identification of receptors for neuromedin U and its role in feeding. Nature 406(6791):70-74.
9. Gartlon J, et al. (2004) Localisation of NMU1R and NMU2R in human and rat central nervous system and effects of neuromedin-U following central administration in rats. Psychopharmacology 177(1-2):1-14.
10. Zeng H, et al. (2006) Neuromedin U receptor 2-deficient mice display differential responses in sensory perception, stress, and feeding. Molecular and cellular biology 26(24):9352-9363.
11. Peier A, et al. (2009) The antiobesity effects of centrally administered neuromedin U and neuromedin S are mediated predominantly by the neuromedin U receptor 2 (NMUR2). Endocrinology 150(7):3101-3109.
12. Graham ES, et al. (2003) Neuromedin U and Neuromedin U receptor-2 expression in the mouse and rat hypothalamus: effects of nutritional status. Journal of neurochemistry 87(5):1165-1173.
13. Hanada R, et al. (2001) A role for neuromedin U in stress response. Biochemical and biophysical research communications 289(1):225-228.
14. Tanaka & Telgedy (2014). Neurotransmissions of antidepressant-like effects of neuromedin U-23 in mice. Behav Brain Res. 259(1):196-9.
15. De Prins A et al. (2019) Effects of neuromedin U-8 on stress responsiveness and hypothalamus-pituitary-adrenal axis activity in male C57BL/6J mice. Horm Behav. 30:104666
16. Howard AD et al. (2000) Identification of receptors for neuromedin U and its role in feeding. Nature. 406(6791):70-4.
17. Graham ES et al. (2003) Neuromedin U and Neuromedin U receptor-2 expression in the mouse and rat hypothalamus: effects of nutritional status. J Neurochem. 87(5):1165-73.
18. Van Wanseele Y et al. (2019) Assessing mixtures of supercharging agents to increase the abundance of a specific charge state of Neuromedin U. Talanta. 198:206-214. doi: 10.1016/j.talanta.2019.01.098. Epub 2019 Jan 29.

5. Publications acknowledging support from G.S.K.E.

Research papers

2019

- De Prins A, Allaoui W, Medrano Moya M, Van Eeckhaut A, Ballet S, Smolders I, De Bundel D. Effects of neuromedin U-8 on stress responsiveness and hypothalamus-pituitary-adrenal axis activity in male C57BL/6J mice. Horm Behav. 2019 Dec 30:104666. doi: 10.1016/j.yhbeh.2019.104666. [Epub ahead of print]
- De Prins A, Van Eeckhaut A, Smolders I, Tourwé D, Ballet S. Neuromedin U and Structural Analogs: an Overview of Their Structure, Function and Selectivity. Curr Med Chem. 2019 Sep 16. doi: 10.2174/0929867326666190916143028. [Epub ahead of print]
- Van Wanseele Y, Bongaerts J, Segers K, Viaene J, De Bundel D, Vander Heyden Y, Smolders I, Van Eeckhaut A.Assessing mixtures of supercharging agents to increase the abundance of a specific charge state of Neuromedin U. Talanta. 2019 Jun 1;198:206-214. doi: 10.1016/j.talanta.2019.01.098. Epub 2019 Jan 29.

2018

- Bongaerts J, De Bundel D, Mangelings D, Smolders I, Vander Heyden Y, Van Eeckhaut A. Sensitive targeted methods for brain metabolomics studies in microdialysis samples. J Pharm Biomed Anal. 2018 Nov 30;161:192-205. doi: 10.1016/j.jpba.2018.08.043. Epub 2018 Aug.23. Review.
- De Prins A, Martin C, Van Wanseele Y, Tömböly C, Tourwé D, Caveliers V, Holst B, Van Eeckhaut A, Rosenkilde MM, Smolders I, Ballet S. Synthesis and in Vitro Evaluation of Stabilized and Selective Neuromedin U-1 Receptor Agonists. ACS Med Chem Lett. 2018 Apr 23;9(5):496-501. doi: 10.1021/acsmedchemlett.8b00105. eCollection 2018 May 10.
- De Prins A, Martin C, Van Wanseele Y, Skov LJ, Tömböly C, Tourwé D, Caveliers V, Van Eeckhaut A, Holst B, Rosenkilde MM, Smolders I, Ballet S. Development of potent and proteolytically stable human neuromedin U receptor agonists. Eur J Med Chem. 2018 Jan 20;144:887-897. doi: 10.1016/j.ejmech.2017.12.035. Epub 2017 Dec 14.

2017

- Van Wanseele Y, Viaene J, Van den Borre L, Dewachter K, Vander Heyden Y, Smolders I, Van Eeckhaut A. LC-method development for the quantification of neuromedin-like peptides. Emphasis on column choice and mobile phase composition. J Pharm Biomed Anal 2017 137, 104-112 2017; published online Epub Apr 15 (10.1016/j.jpba.2017.01.014).
- Van Wanseele Y, Maes K, Lanckmans K, Van Schoors J, Smolders I, Van Eeckhaut A. Surface and Solvent Dependent Adsorption of Three Neuromedin-Like Peptides in Glass and Plastic Syringes. Chromatographia, 2017; published online Epub October 12 (10.1007/s10337-017-3397-9).

Doctoral theses

- Development and biological evaluation of neuromedin U analogs as tools for functional elucidation: focus on stress-related disorders. An De Prins, VUB PRESS 2019.
- Miniaturized UHPLC-MS/MS for the in vivo quantification of neuropeptides in microdialysis samples. Yannick Van Wanseele, VUB PRESS 2019.

Geneeskundige Stichting Koningin Elisabeth
Fondation Médicale Reine Elisabeth
Königin-Elisabeth-Stiftung für Medizin
Queen Elisabeth Medical Foundation

Final report of the research group of

Prof. dr. Ir. De Meyer Simon

Katholieke Universiteit Leuven
(KU Leuven – Kulak)

Principal investigator

Prof. dr. ir. Simon De Meyer
Laboratory for Thrombosis Research
IRF Life Sciences Department of Cardiovascular Sciences
KU Leuven Kulak
E. Sabbelaan 53
8500 Kortrijk
Belgium
Tel.: +32 56 24 62 32
Fax: +32 56 24 69 97
E-mail: simon.demeyer@kuleuven-kortrijk.be
www.kuleuven-kulak.be/irf/thrombosis

Table of contents

Neutrophil extracellular traps: Novel targets for neuroprotection in stroke?

1. Introduction of the project

Ischemic stroke is one of the leading causes of death and sustained disability worldwide. Blockade of blood flow to the brain by an occlusive thrombus leads to irreversible damage of the associated brain tissue. The **enormous clinical, economic and social burden** of ischemic stroke is in strong contrast with the **limited treatment options** that are currently available. Despite the huge clinical need, only one pharmacological intervention is currently approved: early thrombolysis using the fibrinolytic agent tissue plasminogen activator (t-PA). However, t-PA can only be administered in the limited time window of 4.5 hours post-stroke onset due to the unacceptable risk of cerebral bleeding when treatment is delayed. As a consequence, t-PA treatment is available to less than 10% of patients.[1] Most remarkably, t-PA results in recanalization only in less than half of the patients that receive it and factors that contribute to this so-called **'t-PA resistance'** are not well understood.[2] Furthermore, although timely recanalization of the occluded cerebral artery is fundamental to salvage threatened ischemic brain tissue, reperfusion of the ischemic territory itself can also seriously exacerbate tissue damage by **reperfusion injury**. This problem does not only occur after successful thrombolysis but also often complicates stroke outcome after successful mechanical thrombectomy. Even though reperfusion injury significantly accelerates neurodegeneration, the underlying cellular and molecular interactions are still poorly understood**.**

It has become clear that both thrombotic and inflammatory pathways are involved in ischemic brain damage, known as "thrombo-inflammation".[3] Without a doubt, neutrophils and especially **neutrophil extracellular traps (NETs)** have recently led to a paradigm shift in various fields. NETs have been discovered by Brinkmann et al. as a novel mechanism by which neutrophils contribute to the innate immune response.[4] Indeed, as a result of a unique form of cell death, dubbed "NETosis", neutrophils **release their chromatin** that is lined with granular components, creating fibrous nets with antimicrobial properties that prevent microorganisms from spreading (Figure 1). Although much of the cell biological mechanisms of NETosis are still being characterized, one essential step is histone citrullination by peptidylarginine deiminase 4 (PAD4).

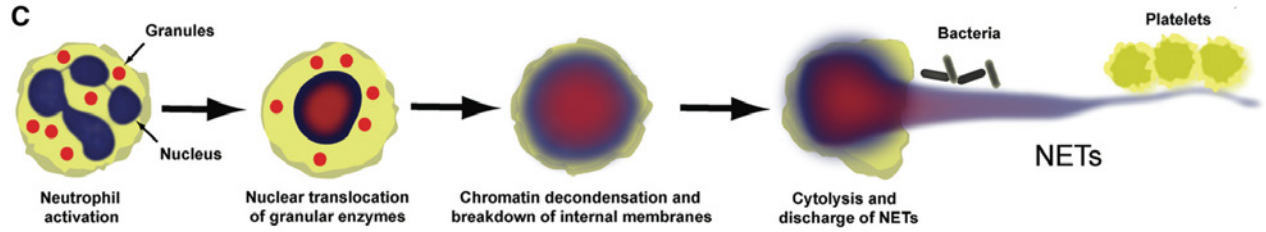

Figure 1: Scheme of NET formation (NETosis) *[5] Enzymes such as PAD4 from granules (red) translocate to the nucleus (blue) and facilitate chromatin decondensation. Internal membranes break down and cytolysis releases NETs_*

PAD4 enters the nucleus to modify histones via hypercitrullination of specific arginine residues on histones H3 and H4. This results in a loss of positive charge from the transformed arginine residues allowing chromatin decondensation (figure 1). Apart from their role in immunity, it has become clear that NETs are also strongly implicated in various thrombotic and thrombo-inflammatory pathologies.[6]

At the start of this project, as good as nothing was known yet about the potential effects of NETs in stroke-associated brain damage. Therefore, this project was aimed at elucidating the potential involvement of NETs in the pathophysiology of ischemic stroke, both in acute phase and in the reperfusion phase, in order to develop novel neuroprotective strategies in stroke management.

2. Main results

In order investigate the potential involvement of NETs in stroke pathophysiology, four delineated work packages (WP) were defined:

- WP1: Nets in thrombi obtained from stroke patients
- WP2: Prothrombolytic capacity of DNAse-1
- WP3: NETs in a mouse model of tMCAO
- WP4: NETs markers in plasma of stroke patients

In this results section, an overview is given of the main findings that were obtained with support of the GSKE grant in the 2017-2019 period.

WP 1: NETs in thrombi obtained from stroke patients

The goal of this work package was to assess the presence of NETs in thrombi retrieved from ischemic stroke patients. Recent studies demonstrate that NETs can form a scaffold for platelets and pro-thrombotic plasma proteins and consequently participate in both arterial and venous thrombus formation.[7-10] We recently summarized the field in a topical review, with support of GSKE funding.[11] It is surprising how little is known about the exact composition of thrombi that cause ischemic stroke. Yet, such information is crucial for designing efficient and safe thrombolytic strategies, and potentially explain the above-mentioned t-PA-resistance. To investigate the presence of NETs in thrombi from ischemic stroke patients, we took the advantage of the unique opportunity offered by the emergence of cerebral thrombectomy in the clinic. In collaboration of AZ Groeninge hospital in Kortrijk (Prof. Tommy Andersson and Dr. Olivier Francois), more than 250 thrombi retrieved from stroke patients have been collected. This unique collection allowed us to perform an in-depth study on the make-up and architecture of stroke thrombi with a focus on neutrophils and their NETs. The main observations are described below and showed for the first time the presence of NETs in ischemic stroke thrombi.

Finding 1: Neutrophils are abundant in ischemic stroke thrombi

Classically, blood clots are thought to be formed mainly by platelets, fibrin and trapped red blood cells. Upon examination of the stroke thrombi, however, H&E stainings revealed a large number of leukocytes, visible as nucleated cells in all thrombus specimens (Fig. 2A, 2B and 2E). To specifically assess the presence of neutrophils, we stained thrombi samples for the granulocyte marker CD66b (Fig. 2A, 2C and 2F) and for neutrophil elastase (NE, Fig. 2A, 2D and 2G). Neutrophils were abundant in all 68 thrombi, with varying amounts (Fig. 2J and 2K). No differences in neutrophil counts were observed between thrombi with different etiology (Fig. 2J). Interestingly, older thrombi (> 1 day) contained significantly higher amounts of neutrophils (8726 ± 4493 per mm^2) compared to fresh thrombi (< 1 day) (5292 ± 2551 per mm^2, $p < 0.001$, Fig. 2K). In conclusion, these results clearly show a high cellular load of ischemic stroke thrombi with a specific abundance of neutrophils.

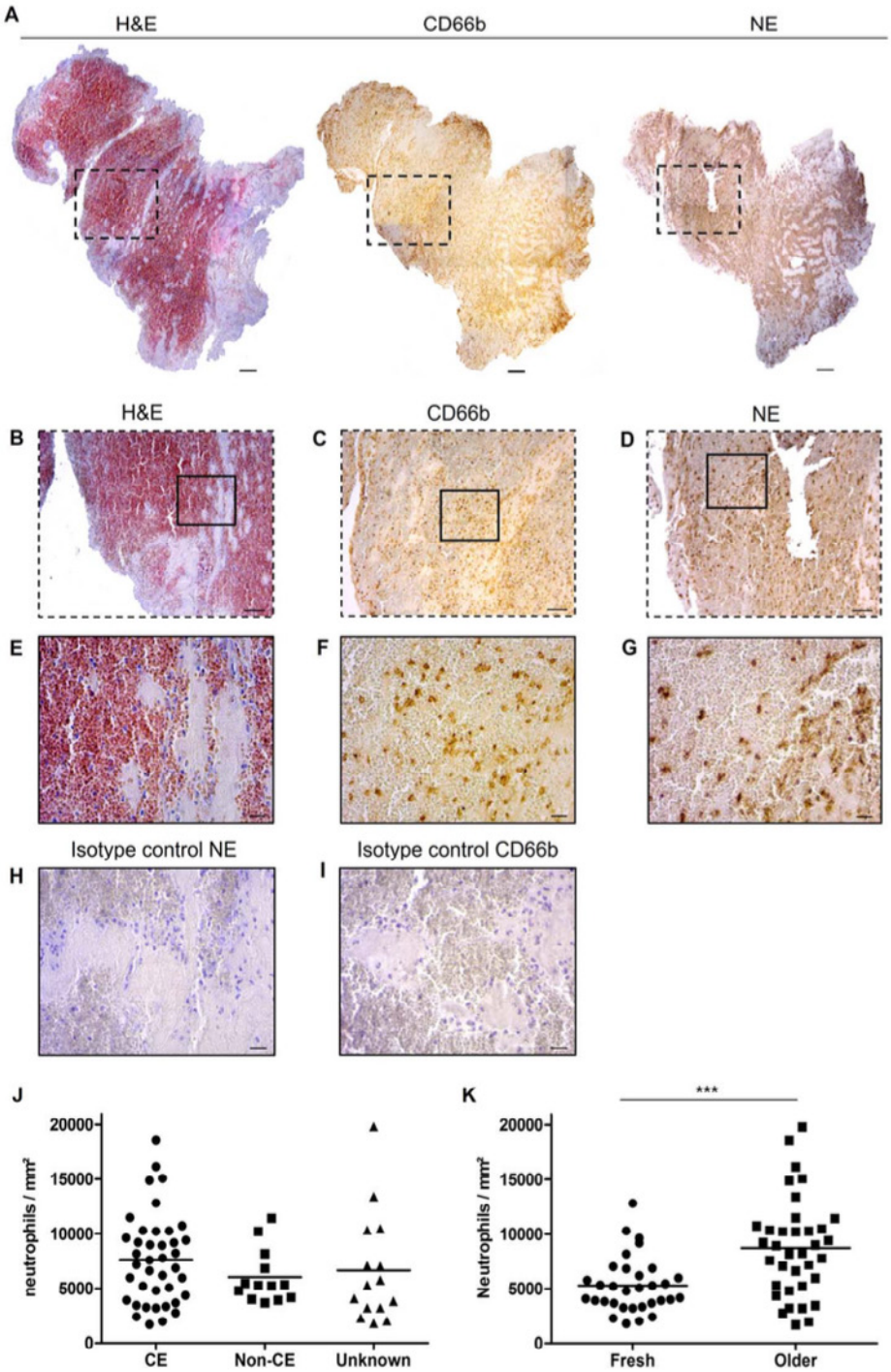

Figure 2: Neutrophils are abundant in ischemic stroke thrombi*. To visualize the presence of neutrophils, sections of thrombi retrieved from ischemic stroke patients were stained with H&E and with antibodies against CD66b and neutrophil elastase (NE). Panel (A) shows representative composite images of one thrombus stained for H&E (left), CD66b (middle) and NE (right) (scale bar: 100 µm.). Magnifications show the presence of leukocytes on H&E staining (B) and in particular neutrophils via either CD66b (C) or NE (D) staining. Scale bar: 50 µm. Larger magnifications of these areas are shown for H&E (E), CD66b (F) and NE (G). Scale bar: 10 µm. Isotype control staining is shown for NE (H) and CD66b (I). Scale bar: 10 µm. Neutrophil numbers in thrombi were quantified and are presented according to stroke etiology (J) (CE: cardioembolic, non-CE: non-cardioembolic) and thrombus age (K) (fresh: < 1 day, older: > 1 day). *** p < 0.001. Published in Annals of Neurology.*[12]

Finding 2: NETs are a structural hallmark of all ischemic stroke thrombi

Careful analysis of H&E staining sometimes revealed prominent extracellular nucleic acid-rich areas that were located in neutrophil-rich zones (Fig. 3A). We hypothesized that these structures could be NETs. To confirm this hypothesis, thrombus sections were also stained for citrullinated H3 histones (H3Cit), a defining marker of NETs. These stainings revealed that the areas containing extracellular nucleic acids

visible by H&E indeed are rich in citrullinated histones (Fig. 3B). Typically, these extensive networks also stained positive for neutrophil elastase, further demonstrating their neutrophil origin (Fig. 3C).

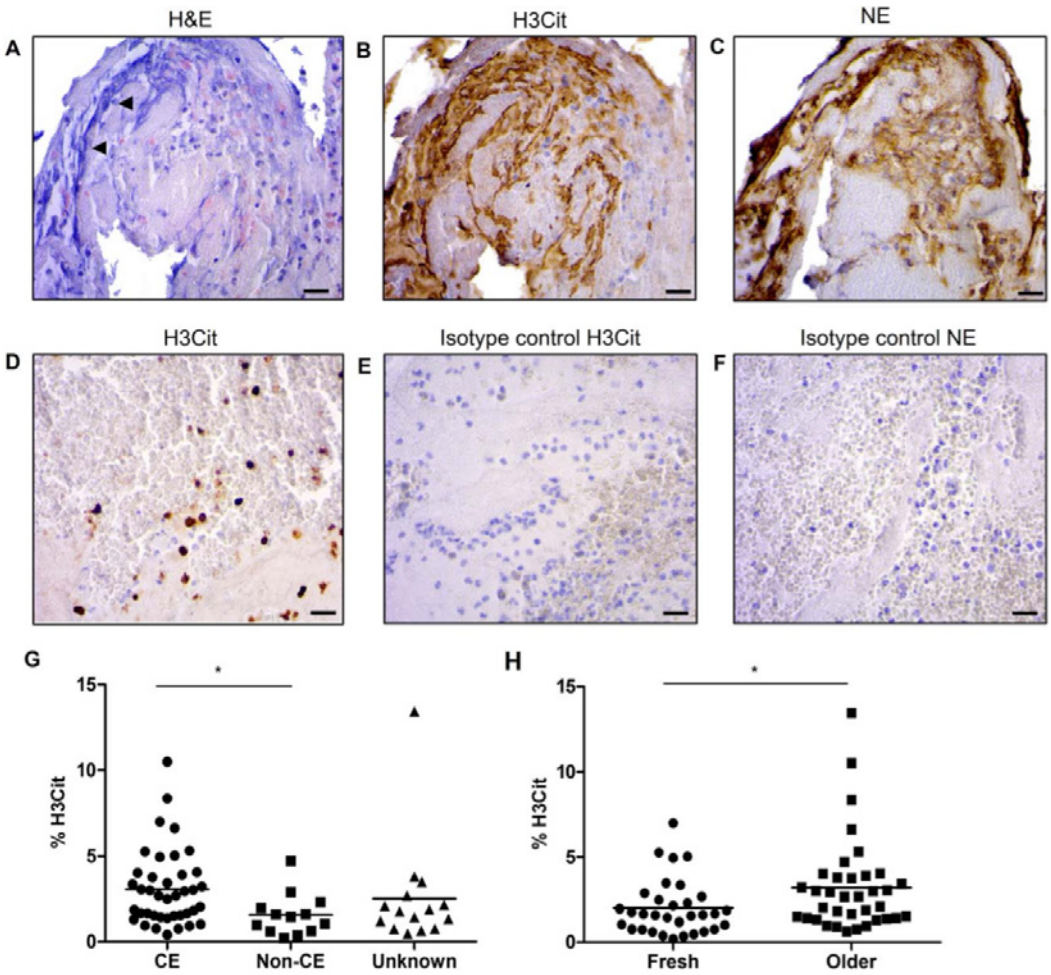

Figure 3: Citrullinated histones reveal the presence of NETs in ischemic stroke thrombi*. The presence of citrullinated histones was analyzed via immunohistochemistry using an antibody against H3Cit. Extracellular zones of nuclear material were often observed on H&E stainings (A, arrow heads). These chromatin strands corresponded with areas staining positive for H3Cit (B, brown staining) and NE (C, brown staining). In other places, no extracellular structures were visible and H3Cit-positive signal was observed only intracellularly, indicative of early NETosis processes (D). No H3Cit nor NE signal was present on isotype control stainings (E and F). Scale bars: 10 µm. H3Cit-positive signal was present in all thrombi and quantification of H3Cit staining per thrombus is shown according to stroke etiology (G) (CE: cardioembolic, non-CE: non-cardioembolic) or thrombus age (H) (fresh: < 1 day, older: > 1 day). * p < 0.05. Published in Annals of Neurology.*[12]

H3Cit-positive signal was found in all investigatyed thrombi, indicating that NETs are a common component of ischemic stroke thrombi. Besides the presence of neutrophils that had already formed extracellular fibrous NET structures (as e.g. shown in Fig. 3B), thrombi typically also contained neutrophils in the initiation phase of NETosis. These neutrophils show H3Cit-positive chromatin that was still inside cells that had not bursted yet, hence the term intracellular (Fig. 3D). H3Cit quantification showed a broad range of NET amounts among different thrombi (Fig 3G and 3H). Of note, thrombi of cardioembolic origin contained nearly double the amount of NETs compared to non-cardioembolic thrombi ($p<0.05$, Fig. 3G). Furthermore, older thrombi showed significantly higher amounts of H3Cit compared to fresh thrombi (Fig. 3H). These data undeniably showed for the first time that NETs are an important structural feature of ischemic stroke thrombi.

Finding 3: fluorescent stainings confirm the presence of NETs in ischemic stroke thrombi and further illustrate the presence of various stages of NETosis

To further confirm the presence of NETs and origin of citrullinated histones, immunofluorescent stainings were performed combining H3Cit with the granulocyte marker CD66b and a DNA dye (DAPI). Fluorescent co-staining of H3Cit together with CD66b and extracellular DNA further corroborate the abundance of decondensed DNA networks containing citrullinated histones that originate from CD66b positive cells (Fig. 4). In line with the immunohistochemical stainings, fluorescent staining also showed neutrophils in the initial stages of NETosis (Fig. 4A), with sometimes even only one nuclear lobe containing H3Cit positive chromatin (middle row of Fig. 4A) and neutrophils that had already fully ejected their decondensated chromatin into the extracellular space (Fig. 4B). Neutrophil origin of extracellular DNA was also confirmed by immunofluorescent co-staining with neutrophil elastase (not shown, see publication). In conclusion, these results clearly show the abundant presence of NETs in ischemic stroke thrombi and NETs are present in various phases of NETosis.

Finding 4: RBC-rich and platelet-rich areas form distinct structural components of stroke thrombi

Given our findings on the abundant presence of leukocytes in stroke thrombi we aimed to further characterize the specific cellular or molecular distribution of these leukocytes and extracellular DNA in stroke thrombi. We analyzed 177 thrombi from patients with ischemic stroke who were treated by thrombectomy. All thrombi were stained with Haemtoxylin and Eosoin (H&E) and Martius Scarlet Blue (MSB) to visualize their general organization (Figure 5). H&E allows identification of fibrin/platelet aggregates (pink), RBCs (red) and nucleated cells (dark blue), whereas MSB staining selectively demonstrates the presence of fibrin (dark pink/red), RBCs (yellow) and collagen (blue). These studies revelad that stroke thrombi typically contain two distinct types of thrombus material: (i) RBC-rich/fibrin-poor material that appears red on H&E stainings and yellow on MSB stainings and (ii) RBC-poor/fibrin-rich areas that appear as light pink areas on H&E staining and pink to red areas on MSB stainings. Interestingly, blood platelets are only present in the RBC-poor/fibrin-rich areas and not in the RBC-rich areas, as shown via platelet-specific immunostaining (Figure 5). Based on these clear and distinct differences, RBC-rich/fibrin-poor areas will be referred to as RBC-rich (R), whereas the term platelet-rich (P) will be used to indicate the RBC-poor/fibrin-rich/platelet-rich areas.

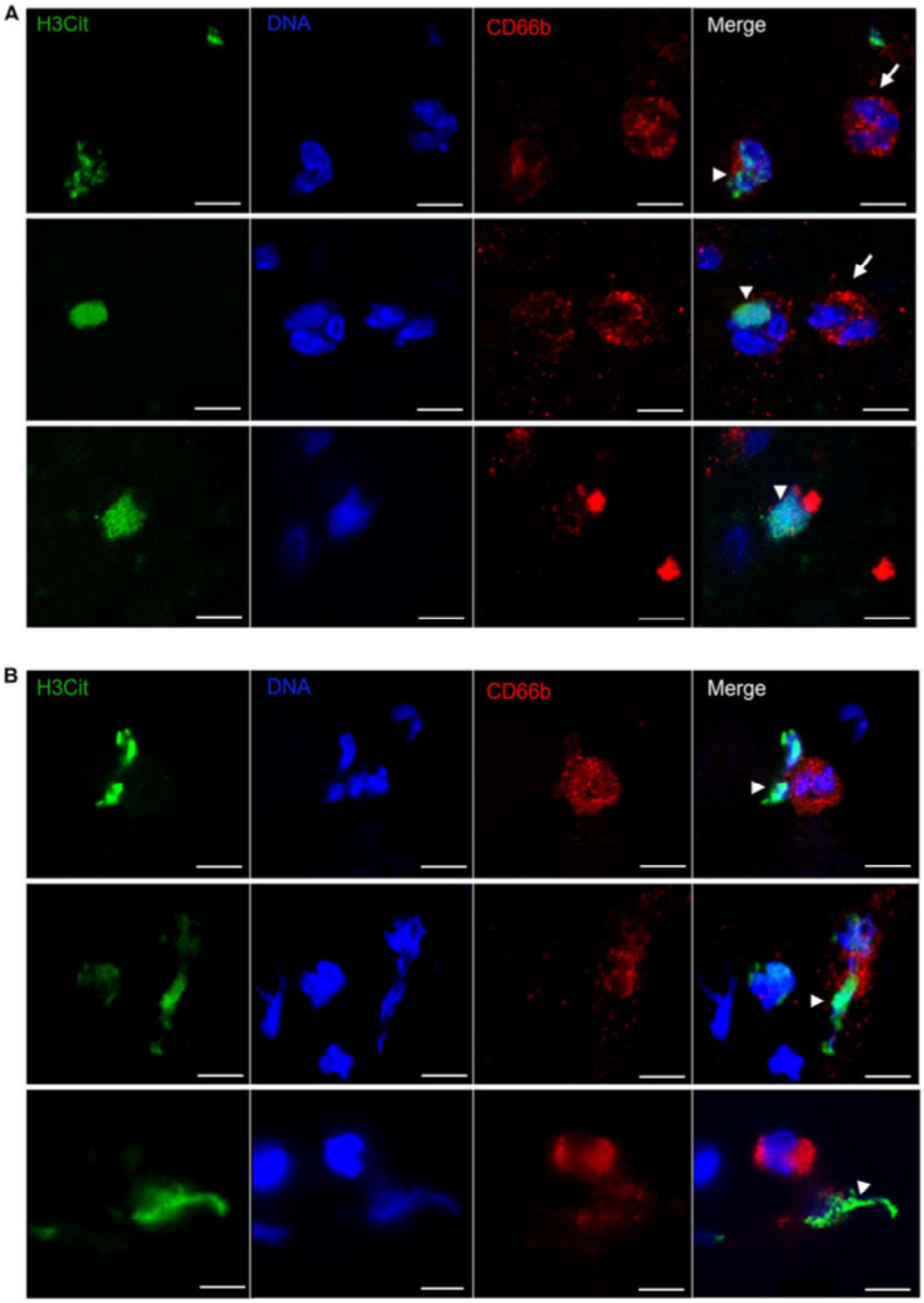

Figure 4: Immunofluorescent identification of NETs in stroke thrombi. *NETs were visualized in human ischemic stroke thrombi by co-staining of the granulocyte marker CD66b (red) with H3Cit (green) and DNA (DAPI, blue). (A) Three representative images of neutrophils at the initial stage of NET formation. H3Cit positive signal is only detected inside the cell (arrowhead). Neutrophils without citrullinated histones are also shown (arrows). (B) Three representative images of neutrophils that underwent complete NETosis. Neutrophils released their decondensated chromatin in the extracellular space. Arrowheads indicate extracellular co-staining of DNA with H3Cit. Scale bar: 5 µm. Published in Annals of Neurology.*[12]

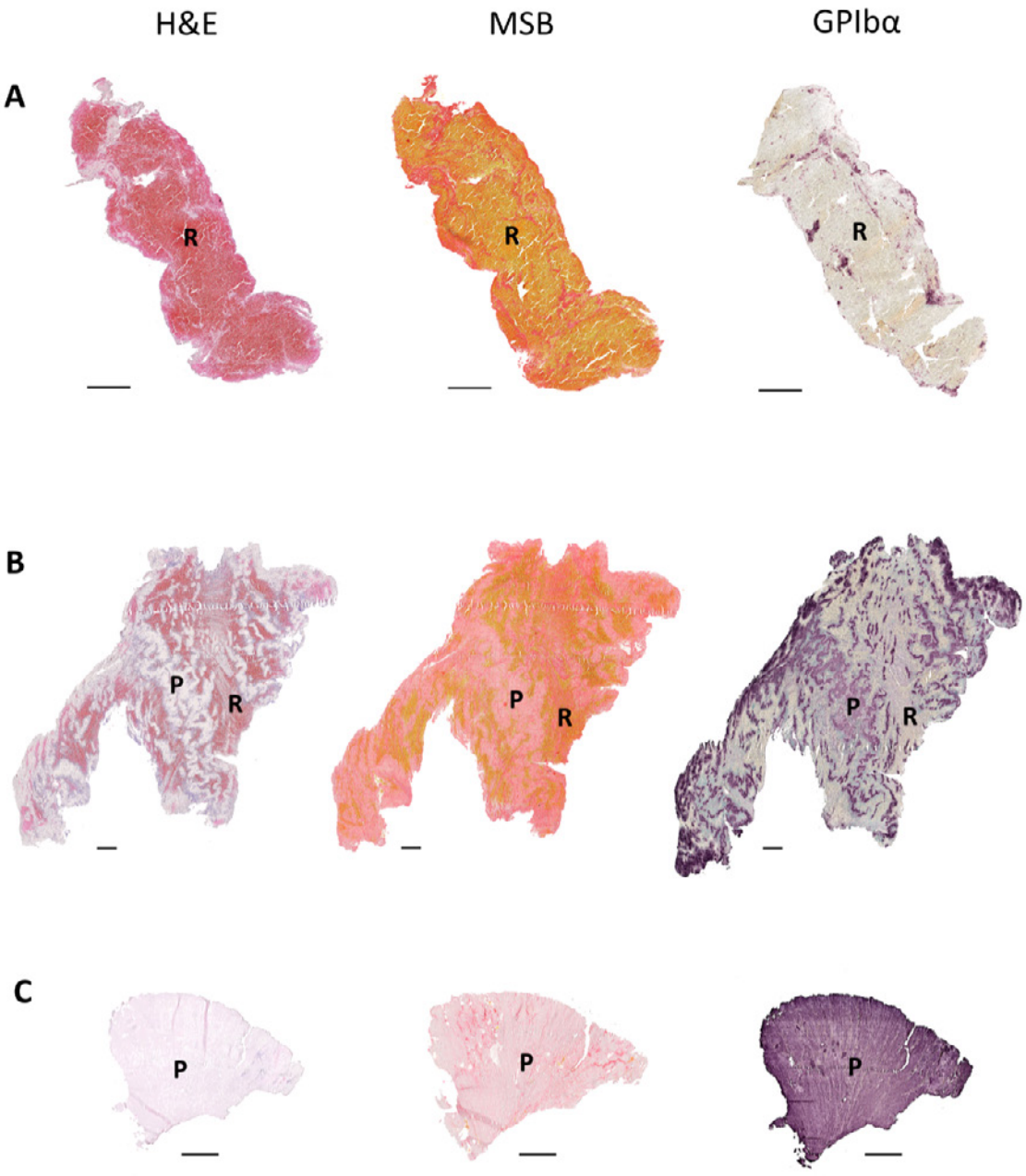

Figure 5: Stroke thrombi typically consist of RBC-rich areas and platelet-rich areas. *Consecutive thrombus sections were stained with H&E, MSB and an anti-GPIbα antibody. Classical H&E staining (left) was used to visualize overall thrombus composition and organization. On H&E staining, RBC-rich areas appear red on H&E stainings whereas RBC-poor areas appear light pink. On MSB staining (middle), red areas show the presence of fibrin, whereas red blood cells (RBC) appear yellow. Platelets (purple) were immunohistochemically stained using an anti-GPIbα antibody (right). Overall, stroke thrombi consist of two distinct areas: RBC-rich areas, indicated by R, and platelet-rich areas, indicated by P. Examples of representative thrombi are shown, which are RBC-rich/platelet-poor (A), mixed (B) and RBC-poor/platelet-rich (C). Scale = 500 µm. Published in Haematologica* [13]

Finding 5: Leukocytes and DNA are mainly present on the interface between RBC-rich en platelet-rich areas

Remarkably, we observed that leukocytes are primarily found on the interface between red blood cell-rich and platelets-rich areas (Figure 6). Besides their specific presence on these boundary zones, leukocytes are also abundantly present within the platelet-rich zones. In contrast, leukocytes are not common in RBC-rich areas, where, if present, they are homogenously distributed throughout the RBCs (Figure 6).

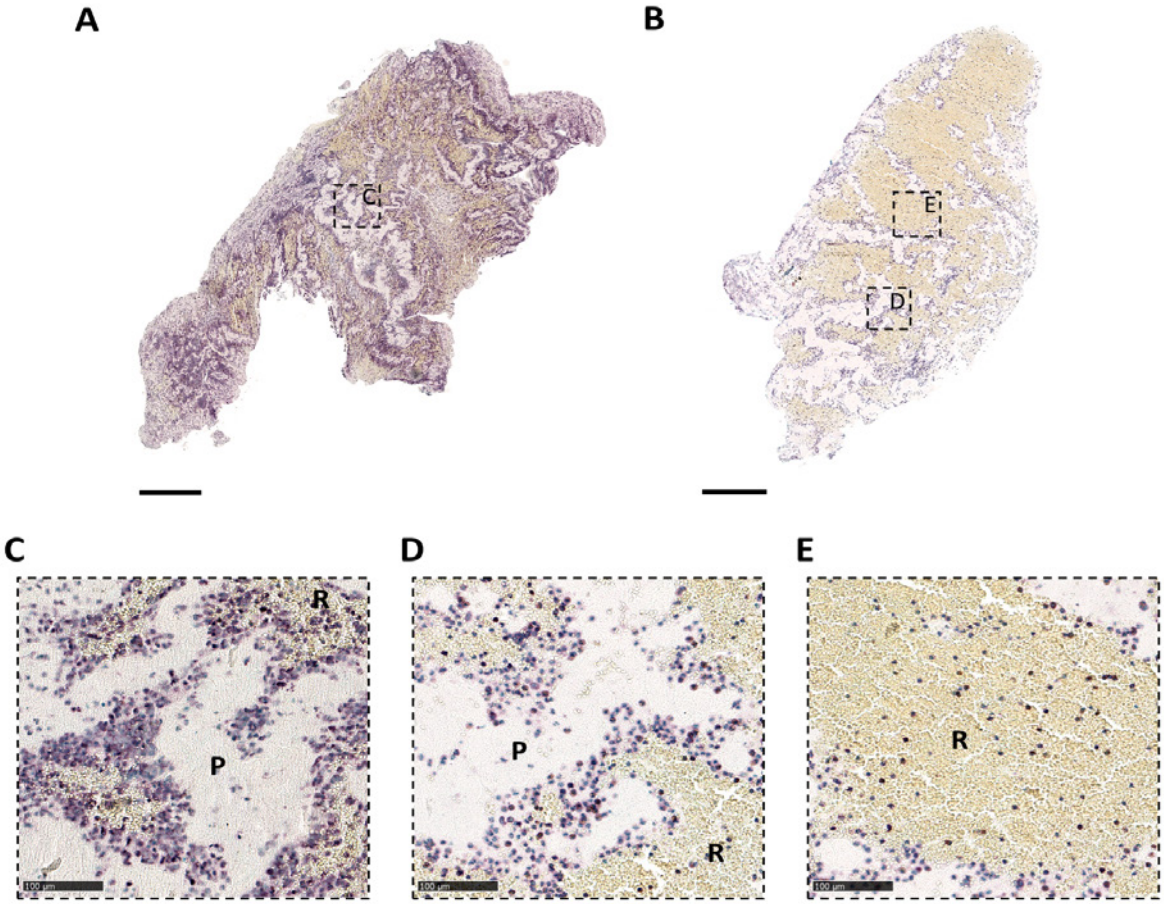

Figure 6: Leukocytes accumulate in platelet-rich areas and on the interface between platelet-rich and RBC-rich areas*. Stroke thrombi were immunohistochemically analyzed for leukocytes (purple). (A-B) Two representative images of a stroke thrombi stained for leukocytes (purple). (C-E) Magnifications show that leukocytes tend to accumulate in platelet-rich areas (C) or on the boundary areas between platelet-rich and RBC-rich areas (D), whereas leukocytes are homogenously spread within RBC-rich areas (E). Scale bar = 500 µm for A and B and 100 µm in panels C-E. P = platelet-rich area, R = red blood cell-rich area. Published in Haematologica.* [13]

To further examine the presence and internal organization of DNA networks in stroke thrombi, we optimized and performed a highly sensitive Feulgen's DNA staining on a subset of 100 stroke thrombi. Strikingly, large extracellular DNA networks were seen throughout the majority of thrombi. Again, similar to the presence of neutrophils, abundant amounts of extracellular DNA were particularly observed in the platelet-rich areas and in the boundary areas between platelet-rich and RBC-rich regions (Figure 7). No extracellular DNA was found within the RBC-rich regions. In conclusion, leukocytes and networks of extracellular DNA were found specifically on the interface of the platelet-rich and RBC-rich regions and in the platelet-rich regions.

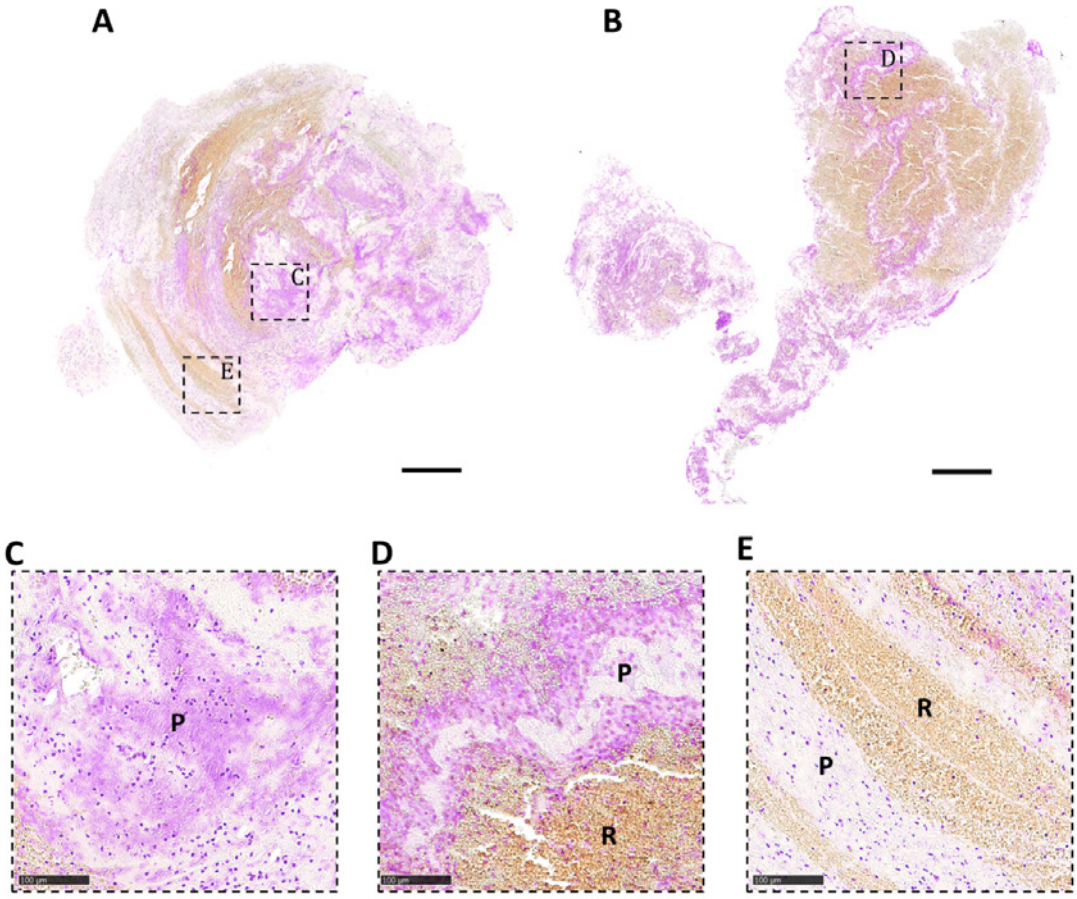

Figure 7: Extracellular DNA accumulates in platelet-rich areas and on the interface between platelet-rich and RBC-rich areas*. Stroke thrombi were stained using a Feulgen's reaction to visualize intra/extracellular DNA (pink). (A-B) Two representative images of stroke thrombi stained for DNA (pink). (C-E) Magnifications show that extracellular DNA tends to accumulate within platelet-rich areas (C) or on the boundary areas between platelet-rich and RBC-rich areas (D). No extracellular DNA is observed in RBC-rich areas (E). Scale bar = 500 µm for A and B and 100 µm in panels C-E. P = platelet-rich area, R = red blood cell-rich area. Published in Haematologica.* [13]

WP 2: Pro-thrombolytic capacity of DNase-1

Our findings from WP1 could have important therapeutic consequences in the stroke clinic. Since use of t-PA leads to the dissolution of occluding thrombi in some cases, but not in others, we believe that factors other than fibrin are involved in thrombus stability and thus contribute to t-PA resistance. Such newly identified factors can become promising targets for thrombolytic therapy. We recently showed that von Willebrand confers t-PA resistance to cerebral thrombi and that the von Willebrand factor-cleaving protease ADAMTS13 has a pro-thrombolytic activity that may become useful in stroke.[14] Based on our novel findings that NETs and extracellular DNA is abundant in ischemic stroke thrombi, we hypothesized that extracellular DNA traps are a stabilizers of thrombi and that targeting these DNA traps might enhance overall thrombolysis. The goal of this work package therefore was to test the capacity of DNase-1 to support acute thrombolytic activity by disassembling extracellular DNA traps in stroke thrombi.

Finding: DNase 1 promotes ex vivo lysis of ischemic stroke thrombi

Given our observations that NETs can form extensive DNA networks in stroke thrombi, we reasoned that pharmacological breakdown of NETs could enhance thrombus dissolution. To test this, two equal parts of fresh patient thrombi were submitted to ex vivo lysis by t-PA (1 µg/ml) or by a combination of t-PA (1 µg/ml) and DNase 1 (100 IE/ml) for 120 min at 37°C. Thrombus lysis was calculated in function of time as percentage of thrombus weight compared to the original weight (Figure 8). Standard t-PA alone induced gradual, partial lysis of the thrombi (residual weight at 120 min was 62.84 % ± 20.59 %

of original thrombus weight). Strikingly, addition of DNase 1 to t-PA significantly accelerated ex vivo lysis compared to t-PA alone, reducing the thrombus weight at 120 min to 40.65 % ± 27.25 % ($p < 0.01$). These findings show for the first time that DNase 1 can promote stroke thrombus dissolution and provide proof-of-concept to target NETs as a novel pro-thrombolytic strategy.

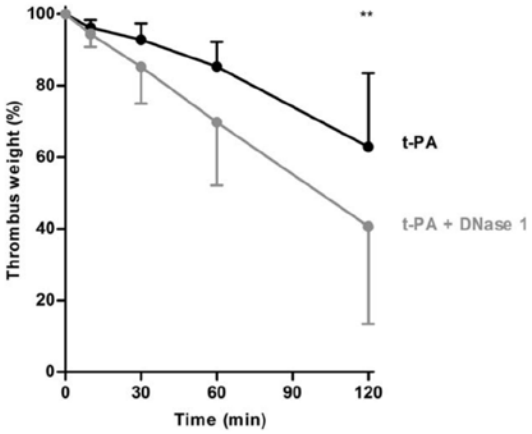

Figure 8: DNase 1 promotes ex vivo lysis of ischemic stroke thrombi. *For ex vivo lysis of thrombi (n=8) retrieved from ischemic stroke patients, 2 equal parts were used. The thrombus parts were incubated for 120 min at 37°C in the presence of either t-PA alone (black) or t-PA plus DNase 1 (grey). Thrombus weight % of original weight) was measured at time points 0, 10, 30, 60 and 120 minutes. Data are represented as mean with SD (** $p < 0.01$). Published in Annals of Neurology.*[12]

WP 3: NETs-formation in a mouse model of transient middle cerebral artery occlusion

In this WP, the goal was to assess whether NETs also form in progressive ischemic brain damage during ischemia and reperfusion in mice. Pathogenic mechanisms underlying this reperfusion injury are not completely understood but involve a complex interplay of thrombo-inflammatory processes.[3] We recently showed that NET formation worsened outcome in mouse models of myocardial ischemia/reperfusion.[15] The role of NETs in (mouse models of) cerebral ischemia/reperfusion brain damage is far from clear. To clarify the potential involvement of NETs in cerebral ischemia/reperfusion injury, we used an established model of transient middle cerebral artery occlusion.[16] In this model, a silicon-coated monofilament is used to temporary (typically 1 hour) block the right middle cerebral artery of the mouse. After withdrawal of the monofilament, blood flow to the brain is restored and a reperfusion is allowed for 23 hours. Using flow cytometry of single cell suspensions of the harvested brains after stroke, we established that neutrophils are abundantly recruited in the ipsilateral hemisphere (figure 9A). Strikingly, using detailed immunohistochemical analysis of mouse stroke brains we found that NETs are indeed formed in the brain early during the reperfusion phase (Figure 9B and 9C). Our first sets of data show time-dependent and lesion-specific accumulation of neutrophils, citrullinated histones and NETs (the latter staining positive for the neutrophil marker Ly6G, citrullinated histones and DNA, Figure 9B and 9C). Many of the NETs are found intravascularly although NETs are also found in the parenchyma. These data document the formation of NETs in the early phase cerebral ischemia/reperfusion injury. We are currently in the process of further mapping the spatio-temporal characteristics of NETosis in the mouse brain but these first data already strongly support the biological importance of NETs formation in stroke and further support the use of DNase-1 in cerebral ischemia/reperfusion injury as we demonstrated previously. [17]

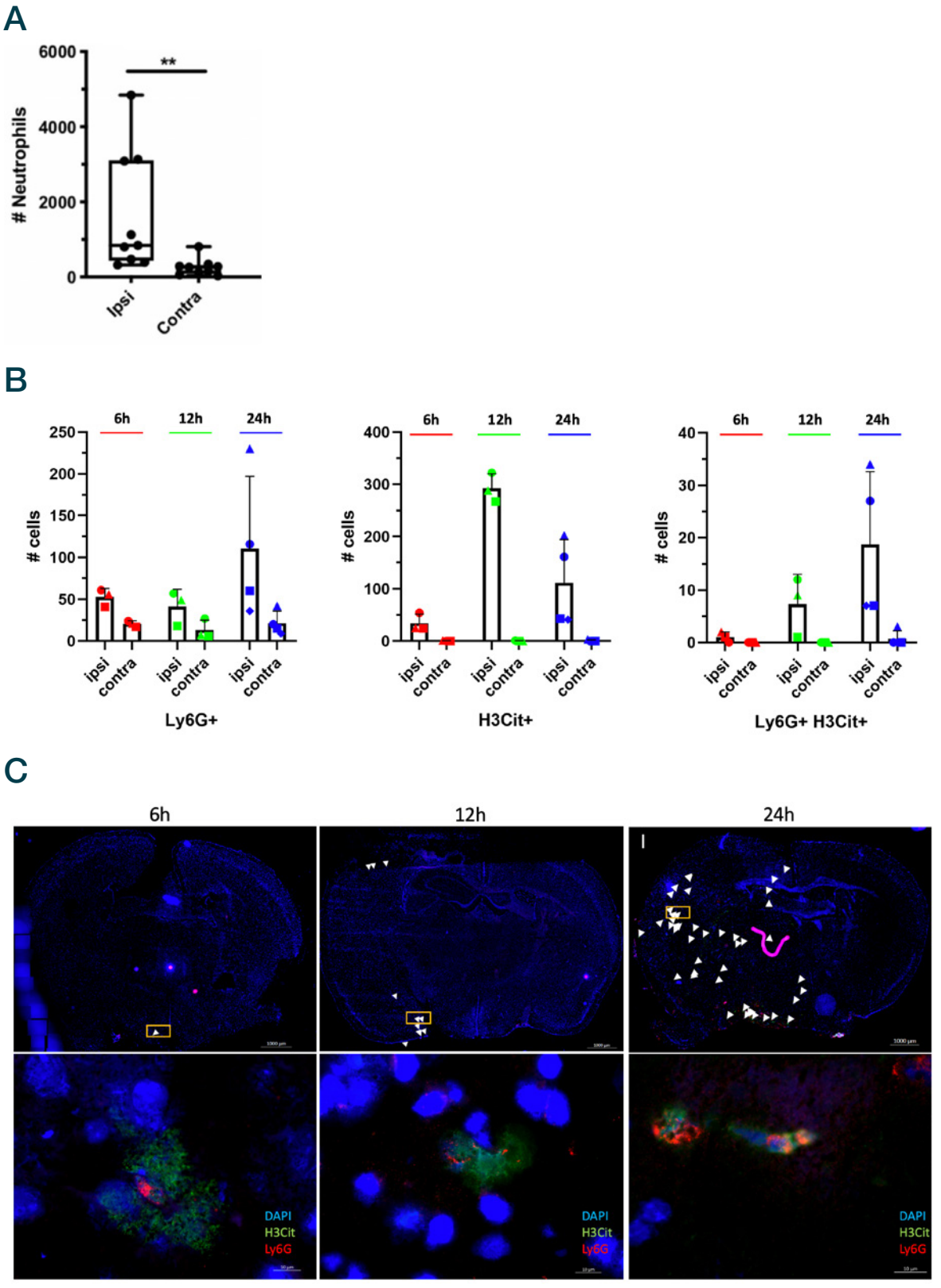

Figure 9: Neutrophils and NETs in a mouse model of cerebral ischemia/reperfusion injury. *Transient focal cerebral ischemia was induced by 60 minutes occlusion of the right middle cerebral artery (tMCAO), followed by 23 hours of reperfusion in C57Bl/6 mice. Panel A shows the assessment of neutrophil ($CD45^{high}$; $CD11b^{+}$; $Ly6G^{+}$) recruitment to each hemisphere as determined via flow cytometry. Total amount of neutrophils are represented as box plots showing all data points and the median value, **, $p<0.01$. Panel B shows the quantification of neutrophils (left), citrullinated histone-postive cells (middle) and NETs (right), based in immunohistochemical staining. Quantifications are performed by counting three complete sections per mouse brain for three independent animals. Each dot represents one animal, Panel C shows representative stainings counted in panel B. White arrowheads show the presence of NETs (magnifications shown in the lower panels). Part of these results are currently under revision in Haematologica.*

WP 4: NETs markers in plasma of stroke patients

In this WP, the goal was to investigate the presence of established circulating biomarkers of NETs (cell-free DNA, nucleosomes) in stroke patients. Such NETs -markers were recently shown to be increased in a variety of pathological conditions, such as sepsis, small vessel vasculitis, venous thrombosis and coronary atherosclerosis[6,18] but almost nothing is known yet about circulating NETs markers in stroke patients. We therefore assessed plasma of different groups of stroke patients (and healthy controls) and determined levels of NETs biomarkers. We found a striking presence of circulating NETs makers in stroke patients.

Finding 1: Cell-free DNA is elevated in stroke patients

As a first maker, we tested cell-free DNA in a large cohort of stroke patients and healthy volunteers (cohort samples were obtained through our collaboration with Prof. C. Kleinschnitz, Würzbrug, now Essen in Germany[19]). In total, 104 patients with stroke (acute ischemic stroke (AIS) or transient ischemic attack (TIA) and 85 healthy volunteers (HV) were included in the study. Trisodium citrate anticoagulated blood was collected on day 0, 1, and 3 in patients with stroke, and once in HV between 08.00 and 12.00 hours from an antecubital vein using a 21-gauge butterfly needle. Cell-free DNA in plasma was analyzed using PicoGreen and quantified via a DNA standard curve. Interestingly, patients with ischemic stroke presented with significantly higher levels of circulating DNA (compared to healthy volunteers) and this was true for day 0, 1 and 3 of stroke (Figure 10).

Finding 2: Nucleosome levels are elevated in stroke patients

Using the same cohorts of patients and healthy volunteers, we also measured the presence of free circulation nucleosomes, which are also indicative of NETs formation. Nucleosome levels were determined via ELISA. Similar to cell-free DNA, we again observed that stroke patients have significant increased circulating nucleosome levels compared to healthy volunteers (Figure 11). These results are line with our previous data showing that plasma nucleosome levels are elevated in mice after stroke, which could potentially be derived from NETs that are formed in the ischemic area.[17] Thus, in this work package, we show that stroke patients have increased numbers of NETs markers in their circulation, further established in the clinical relevance of NETs in ischemic stroke. Since all clinical data of our patient cohort is available, we are in the process of correlating levels of circulating NETs markers with clinical parameters such as treatment success, morbidity, disability and mortality.

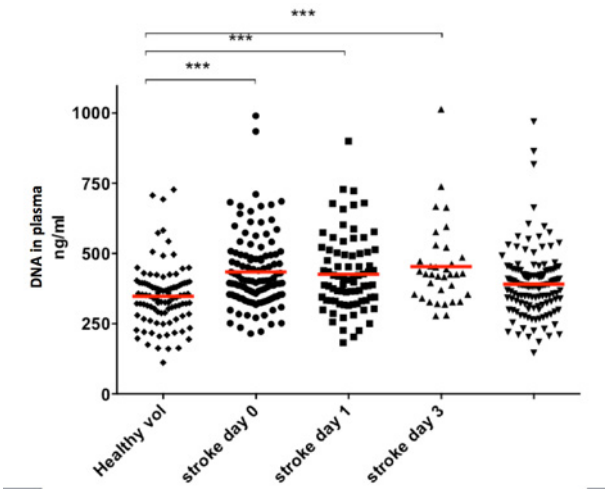

Figure 10: Plasma DNA levels are increased in patients with ischemic stroke. *In total, 104 patients with stroke and 85 healthy volunteers were included in the study. Trisodium citrate anticoagulated blood was collected on day 0, 1, and 3 in patients with stroke, and once in HV Cell-free DNA in plasma was analyzed using PicoGreen and quantified via a DNA standard curve. Unpublished results.*

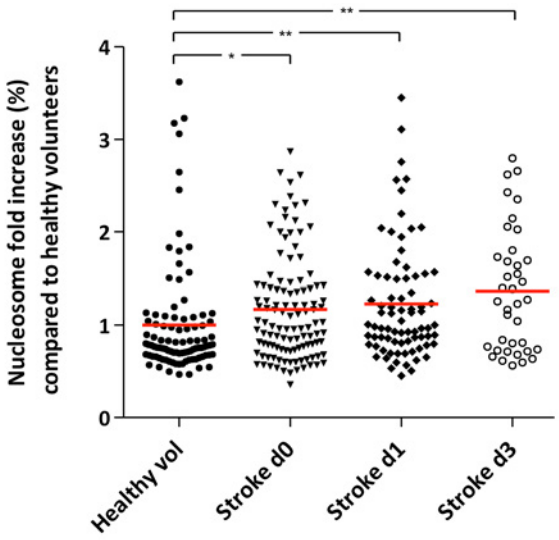

Figure 11: Nucleosome levels are increased in patients with ischemic stroke. *In total, 104 patients with stroke and 85 healthy volunteers were included in the study. Trisodium citrate anticoagulated blood was collected on day 0, 1, and 3 in patients with stroke, and once in HV nucleosome levels in plasma was analyzed using a commerical nucleosome detection kit. Unpublished results.*

3. Scientific relevance and impact

During the course of this GSKE project, important novel insights have been generated. We demonstrated for the first time the presence of NETs in ischemic stroke thrombi and found that their presence is correlated with cardioembolic etiology as well as with thrombus organization. Targeting NETs with DNase-1 successfully improved ex vivo thrombolysis, calling for further investigation of DNase-1-based strategies to improve thrombus dissolution and prevent excessive neurodegeneration in acute ischemic stroke. We found that extracellular DNA-structures are a common structural feature of ischemic stroke thrombi that specifically localize in and around platelet-rich areas. In addition, we found that NETs are also generated in vivo during cerebral ischemia/reperfusion in mouse models of stroke. Finally, we could show that NET's markers are elevated in stroke patients, further underscoring a direct clinical link between NETs and stroke pathology.

Given the serious limitations in current stroke therapy, the clinical implications of our findings could be of high relevance for acute ischemic stroke management. Our detailed histological analysis reveals different structural features in ischemic stroke thrombi that could be highly relevant for developing efficient pharmacological thrombolysis strategies. Serving as a thrombotic scaffold, NETs and extracellular DNA most likely contributes to overall thrombus stability and might confer resistance to fibrinolytic therapy thereby exacerbating ischemic stroke neurodegeneration. The presence of fibrin and DNA could explain why the current 'one size fits all' therapy aiming only at fibrinolysis via t-PA is not always sufficient in patients. Strikingly, extracellular DNA traps have been shown to change the structure of fibrin, rendering it more resistant to mechanical and enzymatic destruction.[20] DNase-1 already is a safe, low-cost, FDA-approved drug routinely used for cystic fibrosis to clear extracellular DNA in the lungs. Combination of DNase-1 with t-PA could potentially allow decreasing the dose of t-PA utilized, limiting its side effects and potentially increasing its therapeutic time window. Even a small prolongation of the therapeutic window for safe thrombolytic therapy would already help hundreds of thousands of patients each year. This would allow a drastic reduction of the current burden caused by the negative side-effects of t-PA. Additional studies are needed to further assess this hypothesis and are planned in the future.

Importantly, targeting of NETs (e.g. using DNase-1) could become a therapeutic strategy that kills two birds with one stone. Indeed, whereas DNase-1 could promote efficient lysis of the occluding blood clot in the patient upon arrival in the hospital, it could also become a promising drug to reduce the reperfusion injury subsequent to blood clot removal. Our results indeed indicate that NETs are formed when blood flow is restored in the ischemic brain. NETs appear in early phase of reperfusion and peak at 24 hours (later timepoints are currently under investigation. A significant amount of these NETs is present intravascularly. We hypothesize that NETs can promote thrombo-inflammatory processes that result in hypoperfusion of the microcirculation of the affected brain tissue, leading to secondary infarct growth. This idea is strongly supported by our previous findings showing that DNase-1 has a protective effect in a mouse model of cerebral ischemia/reperfusion injury.[18] Hence, besides its potential prothrombolytic activity that could promote fast restoration of blood vessel patency, DNase-1 could additionally reduce subsequent reperfusion injury and thus improve neurological outcome in ischemic stroke.

Taken together, this grant from GSKE helped us to establish a novel role of NETs in ischemic stroke pathophysiology and allowed us to develop a novel promising treatment avenue for stroke patients based on targeting extracellular DNA traps.

4. Output

The results that were obtained with support of the GSKE led to various output, visibility and novel collaborations. In the following section an overview of the most important output achievements is given.

Papers with GSKE acknowledgement derived from this grant:

- Laridan E., Denorme F., Desender L., François O., Deckmyn H., Vanhoorelbeke K., **De Meyer SF**. (2017). Neutrophil extracellular traps in ischemic stroke thrombi. *Annals of Neurology*, *82* (2): 223-232. (Impact factor: 10.24).
- Brouwer PA., Brinjikji W., **De Meyer SF**. (2018). Clot Pathophysiology Why Is It Clinically Important? *Neuroimaging clinics of North America*, *28* (4), 611-623. (Impact factor: 1.28).
- Laridan E., Martinod K., **De Meyer SF**. (2019) Neutrophil extracellular traps in thrombosis. *Seminars in Thrombosis and Haemotasis*. 45 (1), 86-93. (Impact factor: 3.3)
- Staessens S., Denorme F., François O., Desender L., Dewaele T., Vanacker P., Deckmyn H., Vanhoorelbeke K. (2019). Andersson T., **De Meyer S.F**. Structural analysis of ischemic stroke: histological indications for therapy resistance. (2019). *Haematologica*. Epub ahead of print. (Impact factor: 7.6)
- Staessens S, Fitzgerald S, Andersson T, Clarençon F, Denorme F, Gounis MJ, Hacke W, Liebeskind DS, Szikora I, van Es A, Brinjikji W, Doyle KM, **De Meyer SF**. (2019) Histological stroke clot analysis after thrombectomy: Technical aspects and recommendations. *International Journal of Stroke.* doi: 10.1177/1747493019884527 Epub ahead of print. (Impact factor: 4.5)
- Denorme F, Vanhoorelbeke K, **De Meyer SF**. (2019), von Willebrand Factor and Platelet Glycoprotein Ib: A Thromboinflammatory Axis in Stroke. *Frontiers in Immunology – Inflammation*. doi.org/10.3389/fimmu.2019.02884, Epub ahead of print. (Impact factor 4.7)
- Staessens S, **De Meyer SF**. (2019), Thrombus Heterogeneity in Ischemic Stroke. Platelets. (invited review, under revision, impact factor: 3.1)
- Denorme F., Martinod K., Vandenbulcke A., Denis C.V., Lenting P.J., Deckmyn H., Vanhoorelbeke K. and **De Meyer S.F**. VWF A1 domain mediates thrombo-inflammation through recruitment of monocytes, neutrophils and T-cells in murine stroke. (under revision in *Haematologica* IF 7.6)
- Olivier François*, Senna Staessens*, Linda Desender, Tom Dewaele, Peter Vanacker, Raf Sciot, Karen Vanhoorelbeke, Tommy Andersson, **Simon F. De Meyer** (* contributed equally) Histological analysis of a thrombectomy-resistant ischemic stroke thrombus: a case report. (*submitted in Annals of Neurology, impact factor 9.5*)

Awards:

The results obtained from this GSKE grant have been awarded at many occasions:

- *2017* ***Eberhard F. Mammen Young Investigator Award*** *(to my PhD student Elodie Laridan*).
  The Eberhard F. Mammen Young Investigoar Awards (up to a total of six in any year) are given for the "Best presentation or meeting abstract by a young investigator — as presented or delivered to an international or large regional meeting on a topic related to the fields of thrombosis and hemostasis and whose subject matter is determined to be in the spirit of Dr. Mammen." (Dr Mammen was the Founding Editor of '*Seminars in Thrombosis & Hemostasis*').
- ***Prize Baron Marc Verstraete for the study of hemato-angiology (Royal Academy for Medicine of Belgium)***,
  This five-annual Prize was awarded to Simon F De Meyer for his research that reveals novel insights on ischemic stroke, including NETs (Brussels, Belgium 2017)
- ***ISTH Young Investigator Award*** *(to my PhD student Elodie Laridan*).
  The Young Investigator Awards of the International Society of Thrombosis and Hemostasis are given to the highest scored abstracts of the bi-annual international meeting of the ISTH. Elodie Laridan received this award for her presentation "Neutrophil extracellular traps in thrombi retrieved from ischemic stroke patients" during the 2017 ISTH meeting in Berlin.
- *2018* ***Paul Capel Prize*** *of the BSTH (to my PhD student Senna Staessens*).
  The Paul Capel Prize of the Belgian Society of Thrombosis and Hemostasis is given to the best presentation of the annual international meeting of the BSTH. Senna Staessens received this prize for his presentation " Dense fibrin, von Willebrand factor and extracellular DNA are specific structural hallmarks of platelet-rich regions of ischemic stroke thrombi " during the 2018 BSTH.
  2018 ***Prize for best clinical contribution*** *at research day of the Department of Cardiovascluar Sciences, KU Leuven (to my PhD student Senna Staessens*).
- ***ISTH Young Investigator Award*** *(to my PhD student Senna Staessens*).
  The Young Investigator Awards of the International Society of Thrombosis and Hemostasis are given to the highest scored abstracts of the bi-annual international meeting of the ISTH. Senna Staessens received this award for his presentation "**Dense fibrin, von Willebrand factor and extracellular DNA are specific structural hallmarks of platelet-rich areas in ischemic stroke thrombi**" during the 2019 ISTH meeting in Melbroune, Australia.

– *2019* ***Paul Capel Prize*** *of the BSTH (to my PhD student Senna Staessens).*
  The Paul Capel Prize of the Belgian Society of Thrombosis and Hemostasis is given to the best oral presentation of the annual international meeting of the BSTH. Senna Staessens received this prize for his presentation "Histological analysis of a thrombectomy-resistant ischemic stroke thrombus: a case report" during the 2019 BSTH.
– 2019 GSKE Ernest Solvay Prize (to Simon F. De Meyer)
  Awarded by GSKE to award progress made within the GSKE grant period.

Invited lectures:

The scientific results from this grant have been well received in the international community as is reflected by the many invitations I received to present this work at international conferences. These invitations include:

– 2nd Thrombosis Meeting, February 2017 Freiburg, Germany (invited speaker)
– Haematology Lectures Program, Erasmus Medical Center, May 2017, Rotterdam, The Netherlands (invited speaker)
– International Society on Thrombosis and Hemostasis Congress, July 2017, Berlin, Germany (invited speaker)
– The 9th Bari International Conference, September 2017, Bari, Italy (invited speaker)
– GFHT meeting, October 2017, Caen, France (invited speaker - Plenary Lecture)
– 14th Congress of the World Federation of Interventional and Therapeutic Neuroradiology, October 2017, Budapest, Hungary (invited speaker - Plenary Lecture)
– 3rd Neuravi Clot summit, December 2017, Amsterdam, The Netherlands (invited speaker)
– ECMINT 1.3 European Course on Minimally Invasive Neurological Therapy, December 2017, Oxford, UK (invited speaker)
– 2017 meeting of the Belgian Society of Interventional and Therapeutic Neuroradiology, December 2017, Brussels, Belgium (invited speaker)
– 4th European Stroke Organisation Conference, May 2018, Gôteborg, Sweden (invited speaker)
– International Society on Thrombosis and Hemostasis SSC meeting, July 2018, Dublin, Ireland (invited speaker)
– 4th EUPLAN platelet conference, September 2018, Bruges, Belgium (co-organizer)
– 11th World Stroke Congress, October 2018, Montreal, Canada (invited speaker, co-convener)
– Annual Meeting of the Irish Haematology Society, October 2018, Cork, Ireland (invited speaker - Plenary Lecture)
– 14th International Symposium on Thrombolysis, Thrombectomy and Acute Stroke Therapy, October 2018, Houston, Texas (invited speaker)
– European Stroke Course on Minimally Invasive Neuroradiological Therapy, November 2018, Prague, Czech Republic (invited speaker)
– 5th International Symposium on Collaterals in the Brain, December 2018, Los Angeles, USA (invited speaker)
– Clot Summit, December 2018, Los Angeles, USA (invited speaker)
– 3rd Conference of the European Society for Microcirculation / European Vascular Biology Organization, April 2019, Maastricht, The Netherlands (invited speaker)
– International Society on Thrombosis and Hemostasis Congress, July 2019, Melbourne, Australia (invited speaker)
– SLICE meeting, October 2019, Nice, France (invited speaker)
– 15th Congress of the World Federation of Interventional and Therapeutic Neuroradiology, October 2019, Naples, Italy (invited speaker - Plenary Lecture)
– European Stroke Course on Minimally Invasive Neuroradiological Therapy, November 2019, Prague, Czech Republic (invited speaker)
– 61st annual meeting of the American Society for Hematology (ASH), December 2019, Orlando, USA (invited speaker)
– ECMINT 3.3 European Course on Minimally Invasive Neurological Therapy, December 2019, Oxford, UK (invited speaker)

5. References

1. Hacke W, Kaste M, Bluhmki E, et al. Thrombolysis with alteplase 3 to 4.5 hours after acute ischemic stroke. *N. Engl. J. Med.* 2008;359(13):1317–1329.
2. Rha J-H, Saver JL. The impact of recanalization on ischemic stroke outcome: a meta-analysis. *Stroke*. 2007;38(3):967–973.
3. De Meyer SF, Denorme F, Langhauser F, et al. Thromboinflammation in Stroke Brain Damage. *Stroke*. 2016;47(4):1165–1172.
4. Brinkmann V, Reichard U, Goosmann C, et al. Neutrophil extracellular traps kill bacteria. *Science*. 2004;303(5663):1532–1535.
5. Fuchs TA, Brill A, Wagner DD. Neutrophil extracellular trap (NET) impact on deep vein thrombosis. *Arteriosclerosis, Thrombosis, and Vascular Biology*. 2012;32(8):1777–1783.
6. Martinod K, Wagner DD. Thrombosis: tangled up in NETs. *Blood*. 2014;123(18):2768–2776.
7. Fuchs TA, Brill A, Duerschmied D, et al. Extracellular DNA traps promote thrombosis. *Proc. Natl. Acad. Sci. U.S.A.* 2010;107(36):15880–15885.
8. Brill A, Fuchs TA, Savchenko AS, et al. Neutrophil extracellular traps promote deep vein thrombosis in mice. *J Thromb Haemost*. 2012;10(1):136–144.
9. Oklu R, Albadawi H, Watkins MT, et al. Detection of extracellular genomic DNA scaffold in human thrombus: implications for the use of deoxyribonuclease enzymes in thrombolysis. *J Vasc Interv Radiol*. 2012;23(5):712–718.
10. Brühl von M-L, Stark K, Steinhart A, et al. Monocytes, neutrophils, and platelets cooperate to initiate and propagate venous thrombosis in mice in vivo. *Journal of Experimental Medicine*. 2012;209(4):819–835.
11. Laridan E, Martinod K, De Meyer S. Neutrophil Extracellular Traps in Arterial and Venous Thrombosis. *Semin. Thromb. Hemost.* 2019;45(01):086–093.
12. Laridan E, Denorme F, Desender L, et al. Neutrophil extracellular traps in ischemic stroke thrombi. *Ann Neurol*. 2017;82(2):223–232.
13. Staessens S, Denorme F, François O, et al. Structural analysis of ischemic stroke thrombi: histological indications for therapy resistance. *Haematologica*. 2019.
14. Denorme F, Langhauser F, Desender L, et al. ADAMTS13-mediated thrombolysis of t-PA–resistant occlusions in ischemic stroke in mice. *Blood*. 2016;127(19):2337–2345.
15. Savchenko AS, Borissoff JI, Martinod K, et al. VWF-mediated leukocyte recruitment with chromatin decondensation by PAD4 increases myocardial ischemia/reperfusion injury in mice. *Blood*. 2014;123(1):141–148.
16. Verhenne S, Denorme F, Libbrecht S, et al. Platelet-derived VWF is not essential for normal thrombosis and hemostasis but fosters ischemic stroke injury in mice. *Blood*. 2015;126(14):1715–1722.
17. De Meyer SF, Suidan GL, Fuchs TA, Monestier M, Wagner DD. Extracellular chromatin is an important mediator of ischemic stroke in mice. *Arteriosclerosis, Thrombosis, and Vascular Biology*. 2012;32(8):1884–1891.
18. Fuchs TA, Hovinga JAK, Schatzberg D, Wagner DD, Lämmle B. Circulating DNA and myeloperoxidase indicate disease activity in patients with thrombotic microangiopathies. *Blood*. 2012;120(6):1157–1164.
19. Kraft P, Drechsler C, Gunreben I, et al. Von Willebrand Factor Regulation in Patients with Acute and Chronic Cerebrovascular Disease: A Pilot, Case–Control Study. *PLoS ONE*. 2014;9(6):e99851.
20. Longstaff C, Varjú I, Sótonyi P, et al. Mechanical stability and fibrinolytic resistance of clots containing fibrin, DNA, and histones. *J. Biol. Chem.* 2013;288(10):6946–6956.

Geneeskundige Stichting Koningin Elisabeth
Fondation Médicale Reine Elisabeth
Königin-Elisabeth-Stiftung für Medizin
Queen Elisabeth Medical Foundation

Final report of the research group of

Prof. dr. De Strooper Bart, MD. PhD

Katholieke Universiteit Leuven (KU Leuven)

Principal investigator

Prof. dr. De Strooper Bart, MD. PhD
VIB Center for Brain and Disease Research
Herestraat 49
3000 Leuven
Belgium
Tel.: +32 495 77 10 44
E-mail: Bart.Destrooper@vib.be

Hilde Govaert
Administrative Director
hilde.govaert@kuleuven.vib.be

Wei-Ting Chen
Postdoctoral Researcher
weiting.chen@kuleuven.vib.be

Mark Fiers
VIB Expert Technologist
mark.fiers@kuleuven.vib.be

Katleen Craessaerts
Staff employee
katleen.craessaerts@kuleuven.vib.be

Ashley Lu
PhD student
ashley.lu@kuleuven.vib.be

Carlo Sala Frigerio
Staff scientist
carlo.salafrigerio@kuleuven.vib.be

Benjamin Pavie
Imaging Analysis Expert
benjamin.pavie@kuleuven.vib.be

The study of the initial cellular phase of Alzheimer's Disease

1. Scientific report

Alzheimer disease (AD) affects roughly 10% of the population aged 65 and up to 50% of people aged 85, while the worldwide cost was estimated € 703 billion (World Alzheimer Report 2016). Although the need for novel therapies is great, a deeper understanding of molecular and cellular mechanisms is first required to make this possible. The last few years have provided a significant paradigm shift in that regard. Failing trials in the clinic[1–4]Alois Alzheimer described the neuropathology of the disease that was to bear his name. 1 Subsequently, our understanding of Alzheimer disease (AD show that the postulated linear relationship between amyloid peptide (Aβ) accumulation, neuronal degeneration and dementia is no longer tenable[4,5]. On the other hand, we see a shift from the classical neurocentric view[6] towards a more integrated view[4] incorporating astroglia and microglia, mainly because the majority of newly identified AD risk genes[7–12] are expressed in these cells. Gene expression profiles show that microglial[13,14] and astroglial[15–17] cells adopt many different states in AD, which might explain their disparate roles in the development and progression of the pathology[18].

We have made enormous progress over the last three years, also thanks to the support from the GSKE to map what we called in 2016 "the cellular phase of Alzheimer's Disease"[19]. We have implemented over the three years three novel technologies that allow asking now questions on the pathogenic cellular mechanisms in a complete novel and exciting way. These are single cell sequencing[20], spatial transcriptomics analysis (Chen et al., submitted) and finally creation of human-mouse chimeric mice[21] allowing to study human microglia in the context of the brain.

We have published a series of high impact papers that describe the first results of these approaches and which have provided a strong foundation for functional studies on a treasure of novel pathways and drug targets relevant to inflammation and neurodegeneration in Alzheimer's disease. All the findings have been highlighted and discussed on Alz Forum. We summarize below the different publications that acknowledge the support of GSKE, and highlight the major finding in each work from a basic science and/or translational point of view.

1.1. Spatial transcriptomics reveal microglia-astroglia crosstalk in the amyloid-β plaque cell niche of Alzheimer's disease

The linear cause-consequence relationship linking amyloid-β peptide (Aβ) accumulation to neuronal dysfunction in Alzheimer disease (AD) is gradually replaced by the concept that Aβ initiates complex inflammatory-like cellular alterations that progressively become Aβ independent and lead to brain dyshomeostasis. Little is known about the pathophysiology of this cellular phase of AD. We use here two orthogonal technologies, Spatial Transcriptomics and *in situ* sequencing (figure), to analyse the transcriptome changes in cells in the amyloid-β plaque niche in a knock-in mouse model for AD. We identify a multicellular co-expressed gene network of 57 Plaque-Induced Genes (PIGs) that define a series of co-ordinated and spatially restricted microglia, astroglia and oligodendrocyte responses to progressing amyloid plaques encompassing complement, oxidative stress and inflammation. A separate oligodendrocyte network suggests abnormal myelination. Spatial Transcriptomics provides an unprecedented approach to untangle the dysregulated cellular network in the vicinity of pathogenic hallmarks of AD and other brain diseases. The work demonstrates the increasing interaction of the PiGs when exposed more strongly to amyloid plaques and provide several

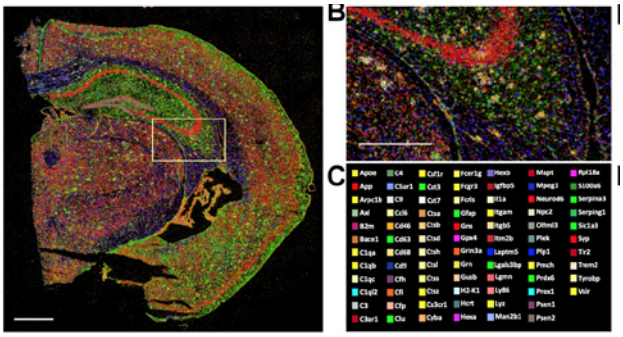

novel drug targets that should allow to modulate the astroglia/microglia response to amyloid plaques. This is a very active area of research in the field.

1.2. Novel Alzheimer risk genes determine the microglia response to amyloid-β but not to TAU pathology

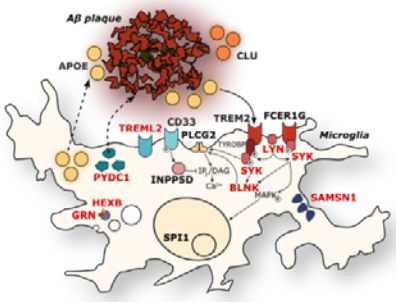

Genetic variants even when not reaching genome-wide significance still add to the genetic risk of developing Alzheimer's disease (AD) as assessed by polygenic risk scores. Whether and how such subthreshold risk loci translate into relevant disease pathways, is unknown. We investigate here the involvement of AD risk variants in the transcriptional responses of two AD mouse models: APPswe/PS1^{L166P} (APPtg) and Thy-TAU22 (TAUtg). A unique gene expression module, highly enriched for AD risk genes, is specifically responsive to Aβ but not to TAU pathology. We identify in this module 7 established AD (*APOE*, *CLU*, *INPP5D* aka SHIP1, *CD33* (Siglech in mice), *PLCG2*, *SPI1* and *FCER1G*) and 11 risk genes implicated in AD in GWAS without reaching genome wide significance (*GPC2, TREML2, SYK, GRN, SLC2A5, SAMSN1, PYDC1, HEXB, RRBP1, LYN* and BLNK), that become significantly upregulated when exposed to Aβ (see figure). Single microglia sequencing confirms that Aβ, not TAU, pathology induces a marked transcriptional change in microglia, resulting in increased proportions of activated response microglia. Moreover, 15 of these 18 AD risk genes are expressed in microglia, with 7 significantly higher expressed in homeostatic microglia. We conclude that genetic risk of AD functionally translates into different microglia pathway responses to Aβ pathology. This insight puts an important part of the AD genetic risk downstream of the amyloid pathway but upstream of TAU pathology.

1.3. The major risk factors for Alzheimer's disease: Age, Sex and Genes, modulate the microglia response to Aβ plaques

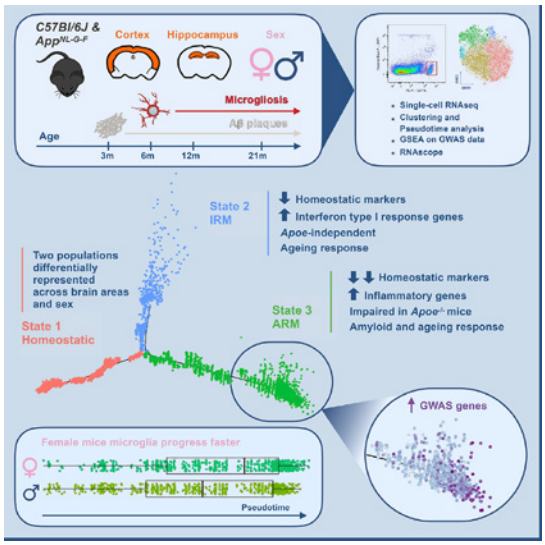

Microglia are involved in Alzheimer's disease (AD) by adopting activated phenotypes. How ageing in the absence or presence of β-amyloid (Aβ) deposition in different brain areas affects these phenotypes and whether sex and AD risk genes are involved, remains largely unknown. Here we analyzed the gene expression profiles of more than 10,000 individual microglia cells isolated from cortex and hippocampus of male and female *App*$^{NL-G-F}$ at 4 different stages of Aβ deposition and in age-matched control mice. Microglia adopt two major activated states (figure), both during normal aging and during exposure to Aβ. The activated response microglia (ARM) is enhanced by amyloid plaques, is composed of specialized subgroups overexpressing MHC type II and tissue repair genes (*Dkk2*, *Gpnmb*, *Spp1*), induced upon prolonged Aβ exposure, and is strongly enriched with AD risk genes. Microglia in female mice advance faster in the activation trajectories. Similar activated states were also found in a second AD model and in human brain. Abolishing the expression of *Apoe*, the major genetic risk factor for AD, impairs the ARM response, while the second response type, enriched for interferon response genes, remains unaffected. Our data indicate that ARMs are the converging point of multiple AD risk factors.

1.4. Stem cell derived human microglia transplanted in mouse brain to study human disease

While genetics highlight the role of microglia in Alzheimer's disease (AD), one third of putative AD-risk genes lack adequate mouse orthologs. Here, we successfully engraft human microglia derived from embryonic stem cells in the mouse brain. The cells recapitulate transcriptionally human primary microglia *ex vivo (figure)* and show expression of human specific AD-risk genes. Oligomeric Amyloid-β induces a divergent response in human vs. mouse microglia. This model can be used to study the role of microglia in neurological diseases. ESC-derived human microglia transplanted into mouse brain represents clearly a step forward to model part of the GWAS defined risk of AD. Despite certain limitations that should be considered (e.g. lack of adaptive immune system, variability in the grafting efficiency of different pluripotent stem cells, iPSC), we anticipate that our approach will be widely applicable to study other neurological diseases. The use of human H9 cells in combination with CRISPR/Cas9 technology opens unanticipated possibilities to model human specific genetic aspects of brain disease.

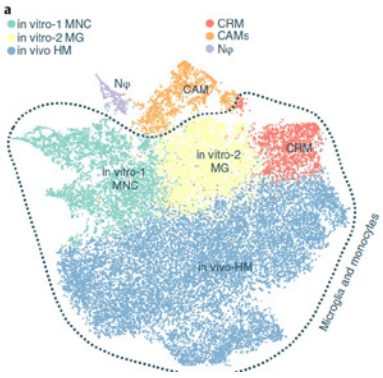

1.5. Secreted Amyloid-β Precursor Protein Functions as a $GABA_BR1a$ Ligand to Modulate Synaptic Transmission

The Amyloid-β Precursor Protein (APP) is central to the pathogenesis of Alzheimer's disease, yet its physiological function remains unresolved. Increasing evidence suggests that APP has a synaptic function mediated by an unidentified receptor for the shed APP ectodomain (sAPP). Here we show that sAPP binds the gamma-aminobutyric acid type B receptor subunit 1a (GABABR1a), which predominantly localizes to synaptic boutons. This interaction is direct and mediated by a conserved peptide stretch in the extension domain of APP and the sushi 1 domain specific to the GABABR1a subunit. sAPP-GABABR1a binding suppresses basal synaptic transmission and augments short-term facilitation in hippocampal synapses via inhibition of synaptic vesicle release (figure). Further, a 17 amino acid peptide corresponding to the GABABR1a binding region within APP reversibly suppresses spontaneous neuronal activity in vivo. Our findings identify GABABR1a as a synaptic receptor for sAPP and reveal a physiological role for sAPP in regulating GABABR1a function to modulate synaptic transmission.

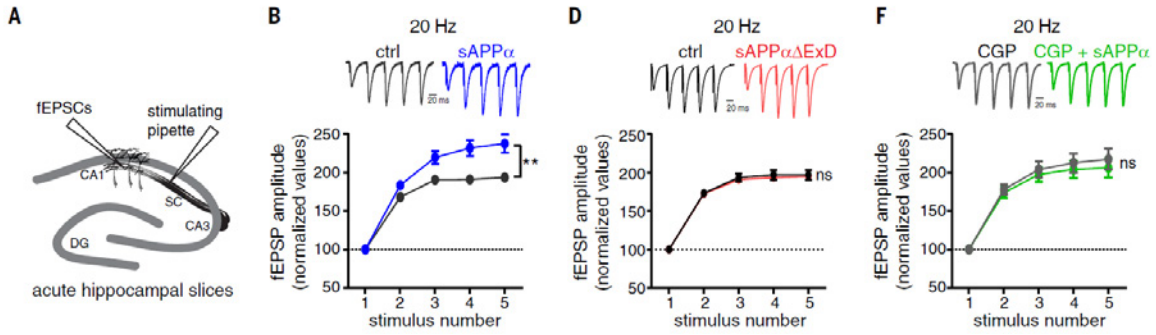

1.6. Contribution of GABAergic interneurons to amyloid-β plaque pathology in an APP knock-in mouse model

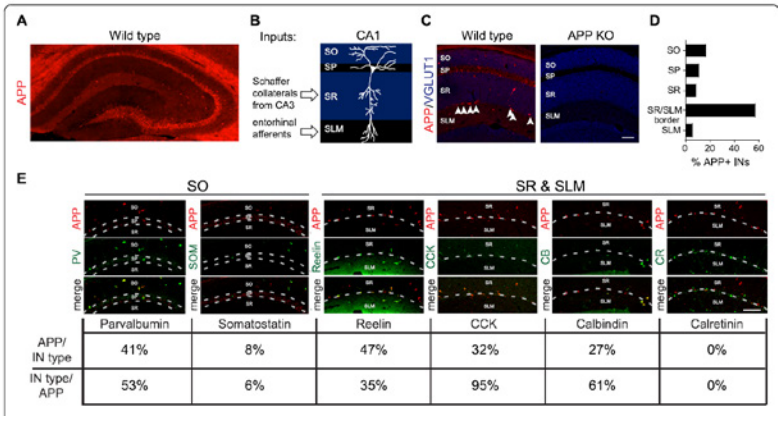

	Parvalbumin	Somatostatin	Reelin	CCK	Calbindin	Calretinin
APP/ IN type	41%	8%	47%	32%	27%	0%
IN type/ APP	53%	6%	35%	95%	61%	0%

The amyloid-β (Aβ) peptide, the primary constituent of amyloid plaques found in Alzheimer's disease (AD) brains, is derived from sequential proteolytic processing of the Amyloid Precursor Protein (APP). However, the contribution of different cell types to Aβ deposition has not yet been examined in an in vivo, non-overexpression system. Here, we show that endogenous APP is highly expressed in a heterogeneous subset of GABAergic interneurons throughout various laminae of the hippocampus (figure), suggesting that these cells may have a profound contribution to AD plaque pathology. We then characterized the laminar distribution of amyloid burden in the hippocampus of an APP knock-in mouse model of AD. To examine the contribution of GABAergic interneurons to plaque pathology, we blocked Aβ production specifically in these cells using a cell type-specific knock-out of BACE1. We found that during early stages of plaque deposition, interneurons contribute to approximately 30% of the total plaque load in the hippocampus. The greatest contribution to plaque load (75%) occurs in the stratum pyramidale of CA1, where plaques in human AD cases are most prevalent and where pyramidal cell bodies and synaptic boutons from perisomatic-targeting interneurons are located. These findings reveal a crucial role of GABAergic interneurons in the pathology of AD. Our study also highlights the necessity of using APP knock-in models to correctly evaluate the cellular contribution to amyloid burden since APP overexpressing transgenic models drive expression in cell types according to the promoter and integration site and not according to physiologically relevant expression mechanisms.

1.7. PARL deficiency in mouse causes Complex III defects, coenzyme Q depletion, and Leigh-like syndrome

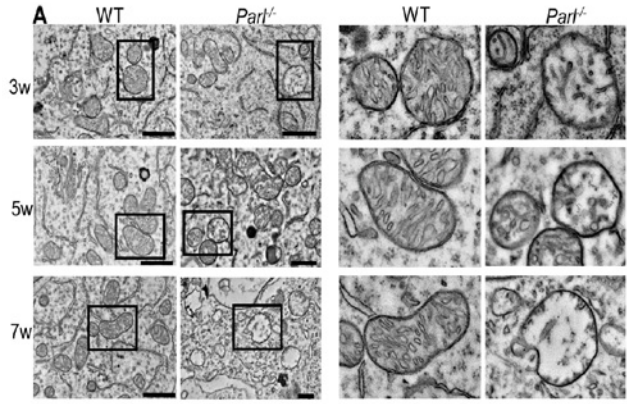

The mitochondrial intramembrane rhomboid protease Parl has been implicated in diverse functions *in vitro*, but its physiological role in vivo remains unclear. Here we show that Parl ablation in mouse causes a striking necrotizing encephalomyelopathy similar to Leigh syndrome, a mitochondrial disease characterized by disrupted energy production. Mice with conditional Parl deficiency in the nervous system, but not in muscle, develop a similar phenotype as germline Parl knockouts demonstrating the vital role of Parl in neurological homeostasis. Genetic modification of two major Parl substrates, Pink1 and Pgam5, do not modify this severe neurological phenotype. Parl-/- brain mitochondria are affected by severe ultrastructural changes (figure), and defects in Complex III activity, coenzyme Q biosynthesis, and mitochondrial calcium metabolism. Parl is necessary for the stable expression of Ttc19, required for Complex III activity, and of Coq4, essential in coenzyme Q biosynthesis. Thus, Parl plays a previously overseen constitutive role in the maintenance of the respiratory chain in the nervous system, and its deficiency causes progressive mitochondrial dysfunction, structural abnormalities and Leigh-like syndrome

1.8. microRNA-132 restores adult hippocampal neurogenesis and memory deficits in Alzheimer's disease

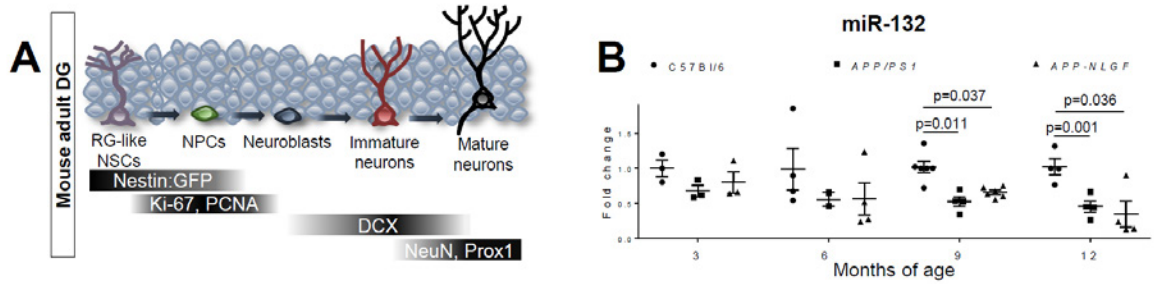

Adult hippocampal neurogenesis (AHN) is functionally linked to mnemonic and cognitive plasticity in humans and rodents. In Alzheimer's disease (AD), the process of generating new neurons at the hippocampal neurogenic niche is impeded, but the mechanisms involved are unknown. Here we identify miR-132, one of the most consistently downregulated microRNAs in AD, as a potent regulator of AHN, exerting cell-autonomous proneurogenic effects in the adult neurogenic niche. Using distinct AD mouse models (figure), cultured human primary and established neural stem cells, and human patient material, we demonstrate that AHN is directly impacted by AD pathology. miR-132 replacement in adult mouse AD hippocampus restores AHN and relevant memory deficits. Our findings corroborate the significance of AHN in AD and reveal the possible therapeutic significance of targeting miR-132 in neurodegeneration.

1.9. The role of astroglia in Alzheimer's disease: pathophysiology and clinical implications. (review)

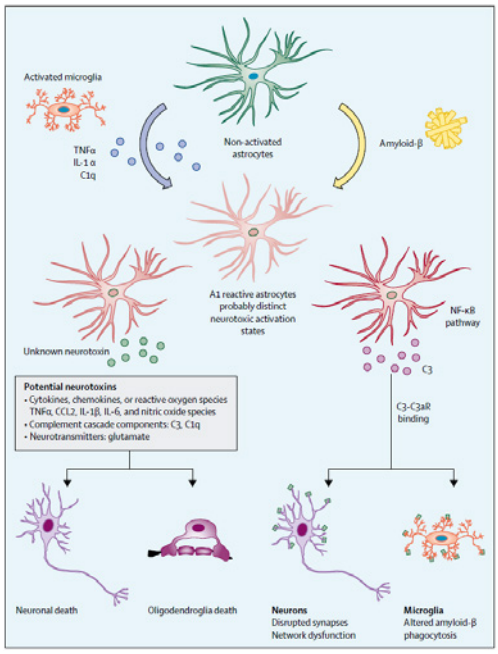

Astrocytes, also called astroglia, maintain homoeostasis of the brain by providing trophic and metabolic support to neurons. They recycle neurotransmitters, stimulate synaptogenesis and synaptic neurotransmission, form part of the blood–brain barrier, and regulate regional blood flow. Although astrocytes have been known to display morphological alterations in Alzheimer's disease for more than a century, research has remained neurocentric. Emerging evidence suggests that these morphological changes reflect functional alterations that affect disease. Genetic studies indicate that most of the risk of developing late onset Alzheimer's disease, the most common form of the disease, affecting patients aged 65 years and older, is associated with genes (ie, APOE, APOJ, and SORL) that are mainly expressed by glial cells (ie, astrocytes, microglia, and oligodendrocytes). This insight has moved the focus of research away from neurons and towards glial cells and neuroinflammation. Molecular studies in rodent models suggest a direct contribution of astrocytes to neuroinflammatory and neurodegenerative processes causing Alzheimer's disease; however, these models might insufficiently mimic the human disease, because rodent astrocytes differ considerably in morphology, functionality, and gene expression. In-vivo studies using stem-cell derived human astrocytes are allowing exploration of the human disease and providing insights into the neurotoxic or protective contributions of these cells to the pathogenesis of disease. The first attempts to develop astrocytic biomarkers and targeted therapies are emerging.

2. Publications mentioning support from GSKE:

1. Rice HC, de Malmazet D, Schreurs A, Frere S, Van Molle I, Volkov AN, Creemers E, Vertkin I, Nys J, Ranaivoson FM, Comoletti D, Savas JN, Remaut H, Balschun D, Wierda KD, Slutsky I, Farrow K, **De Strooper B***, de Wit J*.
   Secreted amyloid-β precursor protein functions as a GABA(B)R1a ligand to modulate synaptic transmission. **Science**. 2019 Jan 11;363(6423).
2. Spinazzi M, Radaelli E, Horré K, Arranz AM, Gounko NV, Agostinis P, Maia TM, Impens F, Morais VA, Lopez-Lluch G, Serneels L, Navas P, **De Strooper B**.
   PARL deficiency in mouse causes Complex III defects, coenzyme Q depletion, and Leigh-like syndrome. **Proc Natl Acad Sci U S A**. **2019** Jan 2;116(1):277-286.
3. Renzo Mancuso, Johanna Van Den Daele, Nicola Fattorelli, Leen Wolfs, Sriram Balusu, Oliver Burton, Annerieke Sierksma, Yannick Fourne, Suresh Poovathingal, Amaia Arranz-Mendiguren, Carlo Sala Frigerio, Christel Claes, Lutgarde Serneels, Tom Theys, V. Hugh Perry, Catherine Verfaillie, Mark Fiers, **Bart De Strooper**.
   Stem cell derived human microglia transplanted in mouse brain to study human disease. **Nature Neuroscience 2019** pages2111–2116
4. Amaia M Arranz, **Bart De Strooper**
   The role of astroglia in Alzheimer's disease: pathophysiology and clinical implications. **Lancet Neurology 2019**: 406-414
5. Carlo Sala Frigerio, Leen Wolfs, Nicola Fattorelli, Nicola Thrupp, Iryna Voytyuk, Inga Schmidt, Renzo Mancuso, Wei-Ting Chen, Maya Woodbury, Gyan Srivastava, Thomas Möller, Eloise Hudry, Sudeshna Das, Takaomi Saido, Eric Karran, Bradley Hyman, V. Hugh Perry, Mark Fiers, **Bart De Strooper**.
   The major risk factors for Alzheimer's disease: Age, Sex and Genes, modulate the microglia response to Aβ plaques. **Cell Reports 2019**, pp 1293–1306
6. Rice HC, Marcassa G, Chrysidou I, Horré K, Young-Pearse TL, Müller UC, Saito T, Saido TC, Vassar R, de Wit J, **De Strooper B**.
   Contribution of GABAergic interneurons to amyloid-β plaque pathology in an APP knock-in mouse model. **Mol Neurodegener. 2020** Jan 8;15(1):3. doi: 10.1186/s13024-019-0356-y

In press:

7. Annerieke Sierksma, Ashley Lu,, Evgenia Salta, Renzo Mancuso, Jesus Zoco, David Blum, Luc Buée, **Bart De Strooper***, Mark Fiers*, Novel Alzheimer risk genes determine the microglia response to amyloid-β but not to TAU pathology. **Embo Mol.Med., in press**

Resubmitted to Cell

8. Wei-Ting Chen, Ashley Lu, Katleen Craessaerts, Benjamin Pavie, Carlo Sala Frigerio, Renzo Mancuso, Xiaoyan Qian, Jana Lalakova, Malte Kühnemund, Iryna Voytyuk, Leen Wolfs, An Snellinx, Sebastian Munck, Aleksandra Jurek, Jose Fernandez Navarro, Takaomi C Saido, Joakim Lundeberg, Mark Fiers, **Bart De Strooper**. Spatial and temporal transcriptomics reveal microglia-astroglia crosstalk in the amyloid-β plaque cell niche of Alzheimer's disease. https://www.biorxiv.org/content/10.1101/719930v1

Resubmitted to Cell Stem Cell

9. Evgenia Salta, Hannah Walgrave, Sriram Balusu, Elke Vanden Eynden, Sarah Snoeck, Katleen Craessaerts, Nicky Thrupp, Leen Wolfs, Katrien Horré, Yannick Fourne, Alicja Ronisz, Edina Silajdžić, Zsuzsanna Callaerts-Vegh, Rudi D'Hooge, Dietmar Rudolf Thal, Henrik Zetterberg, Sandrine Thuret, Mark Fiers, Carlo Sala Frigerio, **Bart De Strooper** microRNA-132 restores adult hippocampal neurogenesis and memory deficits in Alzheimer's disease

3. Honors over the last three years

2018 European Grand Prix for Research (France, awarded by Fondation pour la Recherche sur Alzheimer)
2018 Commander in the Order of Leopold (Belgian national honorary order)
2018 Brain Prize, awarded by the Lundbeck Foundation (Denmark)
2018 Recognized as Highly cited researcher 2018 (Clarivate, Web of Science Group)
2019 Recognized as Highly cited researcher 2019 (Clarivate, Web of Science Group)
2019 Recognized as an Expertscape World Expert in Alzheimer's disease (nº 8 worldwide), presenilins (nº1 worldwide) and Amyloid beta-Peptides (nº 4 worldwide)

Geneeskundige Stichting Koningin Elisabeth
Fondation Médicale Reine Elisabeth
Königin-Elisabeth-Stiftung für Medizin
Queen Elisabeth Medical Foundation

Final report of the research group of

Prof. Goris An, PhD

Katholieke Universiteit Leuven (KU Leuven)

Principal investigator

Prof. Goris An, PhD
KU Leuven
Department of Neurosciences
Laboratory for Neuroimmunology
Tel.: +32 16 33 07 72
E-mail: an.goris@kuleuven.be

Table of contents

Unraveling the baff pathway towards targeted treatment of multiple sclerosis

1. Summary and current status of research program

Multiple sclerosis (MS) is one of the most common neurological disorders in young adults, affecting around 10,000 people in Belgium and 2.5 million worldwide. The disease can lead to important physical as well as cognitive disability at a time that is crucial in the personal and professional development of patients. MS is characterized by three hallmarks: inflammation, demyelination and neuronal loss[1]. The aetiology is unknown but the past few years have seen exciting progress in the field.
The International Multiple Sclerosis Genetics Consortium (IMSGC), of which I am the Belgian representative, has recently identified 200 common genetic susceptibility factors for MS as well as four less common genetic susceptibility factors[2,3]. These risk factors highlight the role not only of T cells, but increasingly also of B cells in the pathogenesis of MS. In a systems immunology approach comparing multiple immunomodulatory treatments, we have previously demonstrated a unique B cell pathway, including an increase in B cell activation factor (BAFF) and transitional B cells and a decrease in memory B cells, as shared across treatments[4]. This shared B-cell related mechanism has recently been extended to other novel treatments in the literature[5-7]. Inhibiting BAFF, on the other hand, as was suggested by animal models proved to worsen MS in clinical trials but taught valuable lessons on the importance of B cells in MS[8-10]. The combination of these data point to a key role for B cells not only in the pathogenesis but also in the treatment of MS[11,12]. This is also highlighted by the choice for B cells as the topic of this year's European Charcot Foundation conference. In the project supported by a Research Grant and the **Prize Viscountess Valine de Spoelberch** from GSKE, we set out to build on these data supporting the role of a specific B-cell pathway in the treatment of MS with two aims.

1. We unravel the role of the B cell pathway in detail, investigating the different contributions of known splice-forms, soluble and membrane-bound forms of BAFF and the different receptors and co-stimulatory molecules on transitional B cells. The role of B cells in the treatment of MS is emerging, but successful and failed B-cell related clinical trials indicate that a better understanding of the B cell pathway in treatment is required to develop targeted new treatments.

   This objective led to one published manuscript, and one manuscript in preparation.

   Maya Imbrechts, Karen De Samblancx, Karlien Fierens., Ellen Brisse, Jessica Vandenhaute, Tania Mitera, Claude Libert, Ide Smets, An Goris, Carine Wouters, Patrick Matthys IFN-γ stimulates CpG-induced IL-10 production in B cells via p38 and JNK signalling pathways. *European Journal of Immunology*, 2018, 48:1506-1521. IF: 4.70, 3 citations

   Ide Smets, Teresa Prezzemolo, Maya Imbrechts, Josselyn E. Garcia-Perez, Klara Mallants, James Dooley, Stephanie Humblet-Baron, Bénédicte Dubois, Patrick Matthys, Adrian Liston*@, An Goris*@, The role of the BAFF pathway in treatment-induced B cell changes in multiple sclerosis. manuscript in preparation

2. We correlate the B cell pathway with genetic and clinical factors in order to better understand how these contribute to patient-to-patient heterogeneity in pathogenesis and response to treatment. This outcome would provide a rationale for personalized medicine.

   The correlation between genetic factors and the B cell pathway has led to two published research papers and two invited Editorials.

   Ide Smets*, Barnaby Fiddes*, Josselyn E. Garcia-Perez*, Di He*, Klara Mallants, Wenjia Liao, James Dooley, George Wang, Stephanie Humblet-Baron, Bénédicte Dubois, Alastair Compston, Joanne Jones, Alasdair Coles, Adrian Liston, Maria Ban, An Goris@, Stephen Sawcer@. Multiple sclerosis risk variants alter expression of co-stimulatory genes in B cells. *Brain*, 2018, 141:786-796. IF 11.81, 8 citations

   Vasiliki Lagou, Josselyn E. Garcia-Perez, Ide Smets, Lies Van Horebeek, Marijne Vandebergh, Liye Chen, Klara Mallants, Teresa Prezzemolo, Kelly Hilven, Stephanie Humblet-Baron, Matthieu Moisse, Philip Van Damme, Guy Boeckxstaens, Paul Bowness, Bénédicte Dubois, James Dooley, Adrian Liston*@, An Goris*@. Interrelationship between genetic control of human immune system variation and disease susceptibility. *Cell Reports*, 2018, 25, 798–810. IF 7.82, 3 citations

   Adrian Liston and An Goris. The origins of diversity in human immunity (invited News and Views feature). *Nature Immunology*, 19:209-210. IF 23.53, 3 citations

   Lies Van Horebeek and An Goris. Transcript-specific regulation in T-cells in multiple sclerosis susceptibility. *European Journal of Human Genetics*, in press (invited Comment). IF 3.65

2. Achievements

Achievement 1. Multiple sclerosis risk variants alter expression of co-stimulatory genes in B cells (Smets et al., *Brain,* 2018; awarded with the Research Prize 2018 of the Belgian Neurological Society to Ide Smets; part of the PhD obtained by Dr. Ide Smets on 25 Sept 2018; invited Comment Van Horebeek and Goris, *European Journal of Human Genetics*, in press)

1. Summary

The increasing evidence supporting a role for B cells in the pathogenesis of multiple sclerosis prompted us to investigate the influence of known susceptibility variants on the surface expression of co-stimulatory molecules in these cells. Using flow cytometry we measured surface expression of CD40 and CD86 in B cells from 68 patients and 162 healthy controls that were genotyped for the multiple sclerosis associated single nucleotide polymorphisms (SNPs) rs4810485, which maps within the CD40 gene, and rs9282641, which maps within the CD86 gene. We found that carrying the risk allele at rs4810485*T lowered the cell-surface expression of CD40 in all tested B cell subtypes (in total B cells $p \leq 5.10 \times 10^{-5}$ in patients and $\leq 4.09 \times 10^{-6}$ in controls), while carrying the risk allele rs9282641*G increased the expression of CD86, with this effect primarily seen in the naïve B cell subset ($p = 0.048$ in patients and 5.38×10^{-5} in controls). In concordance with these results analysis of RNA expression demonstrated that the risk allele rs4810485*T resulted in lower total CD40 expression ($p = 0.057$) but with an increased proportion of alternative splice-forms leading to decoy receptors ($p = 4.00 \times 10^{7}$). Finally, we also observed that the risk allele rs4810485*T was associated with decreased levels of interleukin-10 ($p = 0.020$), which is considered to have an immunoregulatory function downstream of CD40. Given the importance of these co-stimulatory molecules in determining the immune reaction that appears in response to antigen our data suggest that B cells might have an important antigen presentation and immunoregulatory role in the pathogenesis of multiple sclerosis.

2. Situation in the GSKE project

This study unraveled the mechanism of action of established MS susceptibility genes CD40 and CD86, which fall within the B-cell pathway that is the topic of this GSKE project. The study demonstrates that the CD40 MS risk variant acts through a deficit in the protective role of immunoregulatory B cells. These immunoregulatory B cells are enriched amongst early (transitional) B cells, respond to the growth factor B cell activating factor (BAFF) and produce the immunoregulatory cytokine interleukin-10.

3. Future perspectives and clinical implications

Our work demonstrated the importance of splicing in CD40 activation and the association of MS risk variants with splicing. A recent study subsequently unraveled the mechanism driving CD40 expression and correct CD40 splicing, which involves CELF1[13]. A systematic study by colleagues from Cambridge reported that many MS risk variants, including CD40, affect transcript-specific expression and splicing. We were invited to write a Comment on this manuscript to highlight this message[14].

Blocking CD40 with monoclonal anti-CD40 antibodies has been proposed as a therapy for MS based on animal models and is currently considered by pharmaceutical companies. However, the results from our study suggest that decreasing or blocking CD40 is associated with increased risk for MS instead of protection. Whereas anti-CD40 may be beneficial for more antibody-driven autoimmune diseases such as rheumatoid arthritis[15], it calls for extreme caution in applying this treatment for MS. This is completely in line with the anti-BAFF therapies, which are successful in other autoimmune diseases but failed clinical trials in MS and even worsened instead of improved MS. Both anti-CD40 and anti-BAFF limit the important role of immunoregulatory B cells in MS.

Results also suggest that if limiting the role of immunoregulatory B cells worsens disease, enhancing the protective role of immunoregulatory B cells in MS may instead be beneficial. We have previously demonstrated that several currently used and efficacious MS treatments share this as a unique mechanism of action[4]. This shared B-cell related mechanism has recently been extended to other novel treatments in the literature[5-7]. Our results especially suggest that current, promising B cell depletion therapies may increase the efficacy/safety balance if they would deplete B cells more selectively, i.e. deplete likely pathogenic B cells such as memory B cells, but spare beneficial B cells such as the immunoregulatory B cells. Our research group is currently working towards a scientific basis for this aim.

Achievement 2. Interrelationship between genetic control of human immune system variation and disease susceptibility (Lagou et al., *Cell Reports*, 2018; invited News and View item Liston and Goris, *Nature Immunology*, 2018)

1. Summary

The immune system is highly diverse, but characterization of its genetic architecture has lagged behind the vast progress made by genome-wide association studies (GWASs) of emergent diseases. Our GWAS for 54 functionally relevant phenotypes of the adaptive immune system in 489 healthy individuals identifies eight genome-wide significant associations explaining 6%–20%of variance. Coding and splicing variants in *PTPRC* and *COMMD10* are involved in memory T cell differentiation. Genetic variation controlling disease-relevant T helper cell subsets includes *RICTOR* and *STON2* associated with Th2 and Th17, respectively, and the interferon-lambda locus controlling regulatory T cell proliferation. Early and memory B cell differentiation stages are associated with variation in *LARP1B* and *SP4*. Finally, the latrophilin family member *ADGRL2* correlates with baseline pro-inflammatory interleukin-6 levels. Suggestive associations reveal mechanisms of autoimmune disease associations, in particular related to pro-inflammatory cytokine production. Pinpointing these key human immune regulators offers attractive therapeutic perspectives.

2. Situation in the GSKE project

The recent advent of in-depth immune phenotyping across large sample sizes has enabled characterization of the extent and identification of the factors shaping variation in the human immune profile[16]. Longitudinal studies have reported high levels of inter-individual variation, with low longitudinal variation and a highly elastic structure, where transient antigen-induced changes are followed by a return to the individual's unique baseline[17,18]. Twin and family-based studies provide heritability estimates of 20-40% on average, but covering a wide range across individual traits[17,19,20]. Aging contributes up to 5% of variation[17-19,21], and environmental factors include obesity, cohabitation and chronic viral infections[18,19,21]. Identification of genetic factors controlling variation in the immune system is still in the initial discovery phase, with novel and strong associations emerging from pioneer studies[17,20,21]. We performed a GWAS of up to 10,246,977 autosomal variants in 489 healthy Caucasian individuals for 54 immune phenotypes established as part of our previous study[18] The 54 functionally relevant immune phenotypes for which genetic determinants were identified in this study include B cells and B cell subsets. We identified eight regions reaching genome-wide significance ($P < 5x\ 10^{-8}$) to at least one immune phenotype.

Amongst these genome-wide significant results, we identify genetic determinants controlling B cell immunophenotypes that are of relevance for the pathogenesis of MS. In particular, an intergenic variant on chromosome 7 was associated with memory B cell differentiation, a cell type we previously implicated in the immune profile of MS[4], and expression levels in B cells implicated the adjacent *SP4* gene, which is known to downregulate expression of the B cell differentiation factor *BCL2*[22,23]. A second association for a variant near *LARP1B* was observed for KREC excision circles. KREC is a marker for the early B cells which are enriched for the immunoregulatory B cells that form the topic of this GSKE project. LARP1B is still poorly characterized but highly resembles LARP1[24]. LARP1 acts downstream of mTORC1[25,26], which, in addition to its well known role in T cell metabolism and differentiation, controls early B cell development, survival, and metabolism in mice[27]. Our data now suggest an analogous function for the homolog LARP1B in early B cell development in humans. We demonstrated that treatments known to induce the formation of early B cells, such as interferon-beta[4], increase sjKREC excision circles and decrease *LARP1B* gene expression levels. We observed an inverse correlation with increased levels of LARP1B blocking early B cell differentiation. Our data provide the first evidence translating the key importance of these genes and pathways from animals to humans, and highlight that in humans these pathways are variable in vivo in a physiological range.

3. Future perspectives and clinical implications

We have previously demonstrated that KREC is increased upon treatment with current efficacious MS treatments[4]. We currently investigate whether KREC and/or the genetic determinant associated with KREC is associated with the efficacy of MS treatments and can be used as a biomarker for treatment response in a unique longitudinal cohort of 500 newly diagnosed MS patients collected at 9 European centres as part of the EU-funded Horizon2020 project "MultipleMS". KREC has indeed been suggested as a biomarker in other immune-related diseases[28]. Such biomarkers are much needed to ensure that each patient is treated as early as possible with the best possible treatment ("precision medicine") in the current context where the clinician is faced with the choice between a whole range of MS treatments, each with their own efficacy and safety profile. Further understanding of the role of how these novel genes and pathways control B cell numbers and B cell differentiation may additionally offer novel leads for rational treatment design in the context of targeting B cells as a promising therapeutic strategy for MS.

Achievement 3. The role of BAFF and BAFF receptors in the treatment of multiple sclerosis (Imbrechts et al., *European Journal of Immunology* 2018; part of the PhD obtained by Dr. Ide Smets on 25 Sept 2018; Smets et al., manuscript in preparation)

1. Summary

1. Mechanisms of IL-10 induction in B cells (Imbrechts et al. 2018)

IL-10 is an immunoregulatory cytokine produced by B cells and has been implicated in both the risk (see Achievement 1) and treatment of MS. The production of this potent immunosuppressive cytokine must be strictly regulated to ensure a balanced immune response. IFN-γ, a key cytokine in multiple immune processes and pathologies, is known as an inhibitor of IL-10 production by monocytes and macrophages, but also has some regulatory functions. In the present study, we explored the role of IFN-γ on Toll-like receptor (TLR)-induced IL-10 production in murine peritoneal and spleen cells and in human peripheral blood mononuclear cells. IFN-γ inhibited IL-10 production induced by TLR2, TLR3, TLR4 and TLR7/8 agonists, but stimulated IL-10 production when cells were triggered with CpG oligodeoxynucleotides, a specific TLR9 agonist. The stimulatory effect of IFN-γ on TLR9-induced IL-10 was restricted to B cells. In line with the increased IL-10, B cells stimulated with CpG and IFN-γ profoundly inhibited CD4 T cell proliferation. From our experiments with recombinant BAFF and neutralising BAFF- and TACI-antibodies, we conclude that BAFF does not promote IL-10 production by CpG-stimulated B cells but that a different mechanism unrelated to BAFF is at work. Further research into the mechanisms involved, revealed that the mitogen-activated protein kinases p38 and JNK are essential players in this stimulatory effect, and that the phosphatase MKP1 – an inhibitor of p38 and JNK activity – is downregulated after combined stimulation with IFN-γ and CpG. Our data may represent a novel immunoregulatory role of IFN-γ in B cells after triggering of TLR9, by stimulating IL-10 production.

2. IL-10 and B cell related changes upon treatment in MS (ongoing work)

Interferon-beta (IFNB) and fingolimod are mechanistically distinct multiple sclerosis treatments but induce both B cell-activating factor (BAFF) and transitional B cells. To date we do not fully understand how BAFF, BAFF splice forms and BAFF receptors behave under the influence of treatment and how a BAFF increase results in a regulatory immune phenotype.

We collected a cross-sectional study population of 112 Caucasian patients (41 untreated, 42 IFNB, 29 fingolimod) diagnosed with multiple sclerosis. Using flow-cytometry, we determined B cell surface expression of BAFF-R, TACI and CD40 on the entire cohort. We used digital PCR to quantify the level of delta-BAFF, a full-length BAFF antagonizing splice form. We followed up with an *in vitro* experiment in which BAFF-stimulated and unstimulated B cells of untreated and IFNB patients were brought into culture. These cells were subjected to a flow-cytometry panel focused at B cell subsets and intracellular IL-10 production. IFNB and fingolimod induced BAFF mRNA expression as well as soluble BAFF, which correlated with a surge in transitional B cells ($P = 5.70 \times 10\text{-}6$). However, there was no net change in the ratio of delta-BAFF relative to full-length BAFF ($P \geq 0.61$). Moreover, fingolimod and to a lesser extent IFNB treatment steeply reduced the expression levels of BAFF-R ($P \leq 1.77 \times 10\text{-}5$) on B cells while TACI expression remained unaltered. As we observe this steep BAFF-R decrease as a protein on the cell surface but not at the RNA level, this suggests that receptor shedding in response to the BAFF increase is involved[29], but our data add novel insights to the mechanism of shedding compared to what has been reported previously[30]. B cells from IFNB treated patients demonstrated an elevated intracellular IL-10 production. Although transitional B-cells are the main IL10-producers, the treatment-associated IL-10 increase was seen especially in naïve B cells ($P = 8.66 \times 10\text{-}3$). However, adding BAFF stimulation to B cells did not induce intracellular IL-10 production ($P > 0.05$).

In the context of this project, we have optimized and established the novel state-of-the-art technology of single-cell RNA sequencing using the 10x Genomics platform in our laboratory (Figure). In a single-cell sequencing experiment comparing 2 fingolimod-treated and 2 untreated MS patients, we confirmed that fingolimod is associated with an increase in transitional B-cells. Notably, we observe heterogeneity

amongst the transitional B-cell cluster that goes beyond the classical B-cell subset definitions that we used in our flow cytometry work and may highlight the involvement of novel B-cell subsets in MS pathogenesis and treatment.
We conclude that IFNB and fingolimod have as only shared mechanism a shift towards transitional B cells, involving different subsets, which appears associated with changes in the expression of BAFF and its receptors.

2. Situation in the GSKE project

In Achievement 1, we demonstrated that known MS genetic risk factors act through a shortage of the immunoregulatory cytokine IL-10. We previously identified a unique B cell related pathway shared across multiple MS treatments such as interferon-beta and fingolimod. This pathway consists of an increase in transitional B cells driven by elevated B cell activating factor (BAFF) levels and a decrease in memory B cells. The same treatments are known to induce IL-10 production in B cells but the mechanism of this IL-10 induction is unknown. Our experimental data indicate that BAFF is involved in driving the shift towards transitional B-cells but not the increased IL-10 production.

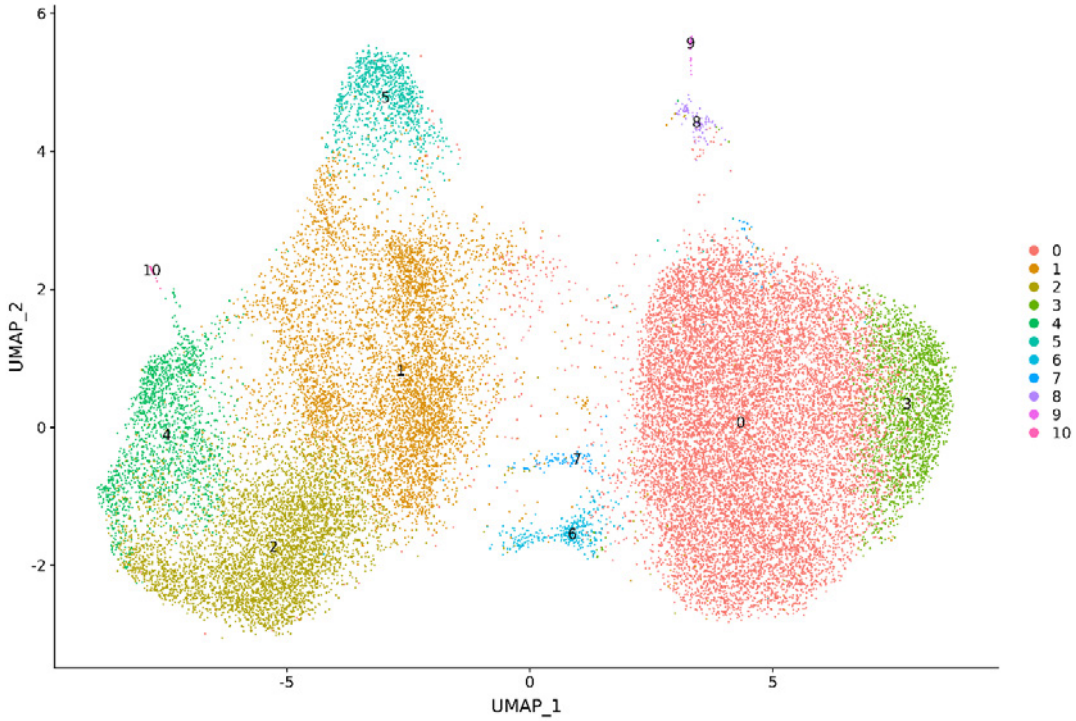

Figure. Single-cell RNA sequencing of four MS patients (two treated, two untreated) with each point represent one of 5,000 B-cells from each patient. Cells that resemble each other in terms of transcriptome are located close to each other, cells with a very different transcriptome are further apart. Bio-informatics analysis identifies 11 different B-cell clusters (colored differently), some corresponding to classical B-cell subset definitions that we used in our flow cytometry work and some highlighting potential novel subsets with relevance to MS.

3. Future perspectives and clinical implications

As we implicate BAFF in the shift towards transitional B-cells upon treatment of MS, and observe previously unknown heterogeneity in the transitional B-cell subset, we are currently characterizing the different transitional B-cell subsets using additional single-cell sequencing. An improved understanding of how BAFF and regulatory B cells have a protective role in MS, but contribute to the pathogenesis of other autoimmune diseases where auto-antibody production is a hallmark, will provide novel leads for B cell related therapeutic strategies in MS. This would allow the development of more specific B cell therapies instead of the current promising but non-selective B cell therapies, which deplete all B cells with potential safety concerns.

3. Networking and collaborations

Achievement 1 was realized in collaboration with Prof. Stephen Sawcer of Cambridge University (UK). Importantly, concordant results and conclusions were reached in both the Belgian case and UK control study populations, independent of experimental design, providing replication and robustness of our results. Dr. Ide Smets obtained the Research Prize 2018 from the Belgian Neurological Society for her publication as output of achievement 1. Achievement 3 is being realized in collaboration with Prof. Patrick Matthys (KU Leuven), who identified regulatory circuits for controlling autoimmune and autoinflammatory diseases. Building on expertise gained with GSKE support (A. Goris, 2017-2019 and Prize Viscountess Valine de Spoelberch), we have now set up a collaboration with Prof. Nathalie Cools (U Antwerpen) and have successfully applied together for an inter-university GSKE grant 2020-2022.

I recently became coordinator of the International Multiple Sclerosis Genetics Consortium (www.imsgc.org), and our research group is a member of the EU Horizon2020 Consortium MultipleMS (www.multiplems.eu).

Over the project duration, members of my research group and I attended the European Conference on the Treatment and Research in Multiple Sclerosis (ECTRIMS) in Paris, France, the MS Data Alliance Meeting in Baveno, Italy and the European Charcot Foundation Meeting in Baveno, Italy. Results from the achievements above were or will be presented at the following occasions:

- 24-October-2017: Research Community “Multiple Sclerosis” of the Research Foundation Flanders, Hasselt, Belgium
- 26-October-2017: European Conference on the Treatment and Research in Multiple Sclerosis (ECTRIMS), Paris (Travel Grant awarded to Dr. Ide Smets)
- 24-November-2017: Belgian Immunological Society, Leuven, Belgium
- 9-November-2017: Department of Human Genetics, KU Leuven, Belgium
- 6-December-2017: Neurology Department UZ Leuven, Belgium
- 15-May 2018: Yearly conference of EU Horizon2020 project “MultipleMS”
- 7-Feb 2019: Immunogenomics of Disease: Accelerating to Patient Benefit 2019, Cambridge, UK
- multiple times and locations in Belgium in 2018: lecture on MS genetics for neurologists
- 9-10-Sep 2019: Meeting International Multiple Sclerosis Genetics Consortium and MultipleMS, Stockholm, Sweden
- 4-7-Nov 2019: Visiting Professorship University Amadeo Avogadro, Novara, Italy
- 13-Dec 2019: University of Oslo, Italy

4. Relevance and future perspectives

In summary, results obtained so far strongly indicate a role of B cells in the pathogenesis as well as the treatment of MS. Our genetic and immunological studies indicate, however, that not all B cell subsets contribute equally and that novel B-cell subsets, detected by single-cell sequencing, may be involved. Whereas the memory B cell subset is thought to exert a pathogenic role, the subset of immunoregulatory B cells appears protective in the disease process and contributes to the mechanism of action of current treatments. B cell depletion therapies, in which all B cells are wiped out, are the most promising novel treatment for MS that has entered the Belgian market. B cell depletion therapies highly reduce disease activity but their long-term safety, for example with respect to susceptibility to infections, remains to be evaluated. Our data indicate that a more selective or a more targeted B cell depletion, wiping out only pathogenic B cells but sparing beneficial B cells may increase the efficacy/safety balance of MS treatment. Whereas B cell depletion therapies are promising overall, there is a group of patients for whom the treatment is not effective but may even worsen disease. B-cell related biomarkers may indicate the subset of MS patients who are most likely to benefit from B cell therapies.

Our research group currently continues on these two lines: understanding the precise role of B cell subsets towards a more targeted therapy and identifying possible B-cell related biomarkers for precision medicine, as detailed in the “Future perspectives” section of each achievement.
With GSKE support (A. Goris, 2017-2019 and Prize Viscountess Valine de Spoelberch), we focused on the role of B-cells and demonstrated an imbalance between pathogenic and immunoregulatory B-cells in MS that is amenable to treatment. Besides, it is currently generally accepted that autoimmunity against antigens expressed in the central nervous system is mediated by T-cells. With GSKE support, we implemented the novel state-of-the-art technology of single-cell RNA sequencing, and we will apply this technology also to the study of T-cells in the GSKE project 2020-2022 “Deep sequencing of myelin-reactive T-cells to elucidate new disease mechanisms and identify correlates for treatment responsiveness.”, awarded together with Prof. Nathalie Cools (U Antwerpen).

5. Financial report

As foreseen, GSKE project support has been assigned for 50% to staff and 50% to consumable costs dedicated to this project. The KU Leuven Financial Department will provide a detailed report. Staff cost in Year 1 was assigned to Ide Smets, first author of one of the GSKE-supported papers, who successfully obtained her PhD on 25 September 2018. Upon completion of her PhD, Dr. Ide Smets remains committed to this project as Neurology Resident at the University Hospitals Leuven. Staff cost in Year 2 and 3 was assigned to Klara Mallants for expert technical assistance on this project.

With the support of the Prize Viscountess Valine de Spoelberch, I was able to attract a new PhD student, Marijne Vandebergh, and thereby ensure continuity of this research line and maximally ensure that we can continue to build on the current results. As Marijne Vandebergh successfully obtained a personal PhD Fellowship of the Research Foundation Flanders (start date 01/10/2018), the budget has been re-allocated to enable us to implement the still highly expensive, genetic technology of single-cell sequencing to the study of B- and T-cells in MS. As the Figure above indicates, we have now been able to optimize and establish this novel technology and are now able to run further experiments.

6. Publications under GSKE support 2017-2019 (Research Project and Prize Viscountess Valine de Spoelberch)

* indicates shared first/senior authors and @ indicates corresponding author

- Van Horebeek L., Goris A.@ Transcript-specific regulation in T-cells in multiple sclerosis susceptibility. *European Journal of Human Genetics* (invited Comment), in press. IF 3.65
- Van Horebeek L.*, Hilven K.*, Mallants K., Van Nieuwenhuijze A., Kelkka T., Savola P., Mustjoki S., Schlenner S.M., Liston A., Dubois B., Goris A@. A robust pipeline with high replication rate for detection of somatic variants in the adaptive immune system as a source of common genetic variation in autoimmune disease. *Human Molecular Genetics*, 2019, 28:1369-1380. IF 4.54, 1 citation
- Smets I.*, Fiddes B.*, Garcia-Perez J.E.*, He D.*, Mallants K., Liao W., Dooley J., Wang G., Humblet-Baron S., Dubois B., Compston A., Jones J., Coles A., Liston A., Ban M., Goris A.@, Sawcer S.@. Multiple sclerosis risk variants alter expression of co-stimulatory genes in B cells. *Brain*, 2018, 141:786-796. IF 11.81, 8 citations
- Lagou V., Garcia-Perez J.E., Smets I., Van Horebeek L., Vandebergh M., Chen L., Mallants K., Prezzemolo T., Hilven K., Humblet-Baron S., Moisse M., Van Damme P., Boeckxstaens G., Bowness P., Dubois B., Dooley J., Liston A.*@, Goris A.*@. Interrelationship between genetic control of human immune system variation and disease susceptibility. *Cell Reports*, 2018, 25, 798–810. IF 7.82, 2 citations
- Liston A. and Goris A. The origins of diversity in human immunity (invited News and Views feature). *Nature Immunology*, 2018, 19:209-210. IF 23.53, 3 citations
- Imbrechts M., De Samblancx K., Fierens K., Brisse E., Vandenhaute J., Mitera T., Libert C., Smets I., Goris A., Wouters C., Matthys P. IFN-γ stimulates CpG-induced IL-10 production in B cells via p38 and JNK signalling pathways. *European Journal of Immunology*, 2018, 48:1506-1521. IF: 4.70, 3 citations
- Hilven K.*, Vandebergh M.*, Smets I., Mallants K., Goris A.@, Dubois B.. Genetic basis for relapse rate in multiple sclerosis: association with *LRP2* genetic variation. *Multiple Sclerosis Journal*, 2018, 24:1773-1775. IF: 5.65, 1 citation

7. Team publications within project duration 2017-2019

* indicates shared first/senior authors and @ indicates corresponding author

- Van Horebeek L., Goris A.@ Transcript-specific regulation in T-cells in multiple sclerosis susceptibility. *European Journal of Human Genetics* (invited Comment), in press. IF 3.65
- Van Horebeek L., Dubois B., Goris A., Somatic variants: new kids on the block in immunogenetics. *Trends in Genetics*, 2019, 35:935-947. IF 10.63
- The International Multiple Sclerosis Genetics Consortium. The Multiple Sclerosis Genomic Map: Role of peripheral immune cells and resident microglia in susceptibility. *Science*, 2019, 365:eaav7188. IF 41.04, 1 citation
- The International Multiple Sclerosis Genetics Consortium. A Systems Biology Approach Uncovers Cell-Specific Gene Regulatory Effects of Genetic Associations in Multiple Sclerosis. *Nat Commun*, 2019, 10:2236. IF 11.88, 4 citations
- Van Horebeek L.*, Hilven K.*, Mallants K., Van Nieuwenhuijze A., Kelkka T., Savola P., Mustjoki S., Schlenner S.M., Liston A., Dubois B., Goris A@. A robust pipeline with high replication rate for detection of somatic variants in the adaptive immune system as a source of common genetic variation in autoimmune disease. *Human Molecular Genetics*, 2019, 28:1369-1380. IF 4.54, 1 citation
- Goris A.@ and Dubois B. Leveraging human genetics to inform intervention strategies for multiple sclerosis (Invited Editorial). *Neurology* 2019, 92:735-736. IF 8.69
- Van Nieuwenhove E., Lagou V., Van Eyck L., Dooley J., Bodenhofer U., Roca C., Vandebergh M., Goris A., Humblet-Baron S., Wouters C., Liston A. (2019). Machine learning identifies an immunological pattern associated with multiple juvenile idiopathic arthritis subtypes. *Ann Rheum Dis,* 2019, 78:617-628. IF 14.30, 1 citation
- Olive M., Engvall M., Ravenscroft G., Cabrera-Serrano M., Jiao H., Bortolotti C.A., Pignataro M., Lambrughi M., Jiang H., Forrest A.R R., Benseny-Cases N., Hofbauer S., Obinger C., Battistuzzi G., Bellei M., Borsari M., Di Rocco G., Viola H.M., Hoo L.C., Cladera J., Lagerstedt-Robinson K., Xiang F., Wredenberg A., Miralles F., Jose Baiges J., Malfatti E., Romero N.B., Streichenberger N., Via C., Claeys K.G., Straathof C.S M., Goris A., Freyer C., Lammens M., Bassez G., Kere J., Clemente P., Sejersen T., Udd B., Vidal N., Ferrer I., Edstrom L., Wedell A., Laing N.G. (2019). Myoglobinopathy is an adult-onset autosomal dominant myopathy with characteristic sarcoplasmic inclusions. *Nat Commun* 2019, 10:1396. IF 11.88
- The International Multiple Sclerosis Genetics Consortium. Low-Frequency and Rare-Coding Variation Contributes to Multiple Sclerosis Risk. *Cell*, 2018, 175, 1–9. IF: 36.22, 11 citations

- Lagou V., Garcia-Perez J.E., Smets I., Van Horebeek L., Vandebergh M., Chen L., Mallants K., Prezzemolo T., Hilven K., Humblet-Baron S., Moisse M., Van Damme P., Boeckxstaens G., Bowness P., Dubois B., Dooley J., Liston A.*@, Goris A.*@. Interrelationship between genetic control of human immune system variation and disease susceptibility. *Cell Reports*, 2018, 25, 798–810. IF 7.82, 2 citations
- Liston A. and Goris A. The origins of diversity in human immunity (invited News and Views feature). *Nature Immunology*, 19:209-210. IF 23.53, 3 citations
- Imbrechts M., De Samblancx K., Fierens K., Brisse E., Vandenhaute J., Mitera T., Libert C., Smets I., Goris A., Wouters C., Matthys P. IFN-γ stimulates CpG-induced IL-10 production in B cells via p38 and JNK signalling pathways. *European Journal of Immunology*, 2018, 48:1506-1521. IF: 4.70, 3 citations
- Fenoglio C., Oldoni E., Serpente M., De Riz M.A., Arcaro M., D'Anca M., Pietroboni A.M., Calvi A., Lecchi E., Goris A., Mallants K., Dubois B., Comi C., Cantello R., Scarpini E., Galimberti D. LncRNAs expression profile in peripheral blood mononuclear cells from multiple sclerosis patients. *Journal of Neuroimmunology*, 2018, 15:129-135. IF 2.83, 3 citations
- Gille B., De Schaepdryver M., Goossens J., Dedeene L., De Vocht J., Oldoni E., Goris A., Van Den Bosch L., Depreitere B., Claeys K.G., Tournoy J., Van Damme P., Poesen K. Serum neurofilament light chain levels as a marker of upper motor neuron degeneration in patients with Amyotrophic Lateral Sclerosis. *Neuropathology and Applied Neurobiology*, 2018, 45:291-304. IF 6.88, 9 citations
- Smets I.*, Fiddes B.*, Garcia-Perez J.E.*, He D.*, Mallants K., Liao W., Dooley J., Wang G., Humblet-Baron S., Dubois B., Compston A., Jones J., Coles A., Liston A., Ban M., Goris A.@, Sawcer S.@. Multiple sclerosis risk variants alter expression of co-stimulatory genes in B cells. *Brain*, 2018, 141:786-796. IF 11.81, 8 citations
- Hilven K.*, Vandebergh M.*, Smets I., Mallants K., Goris A.@, Dubois B.. Genetic basis for relapse rate in multiple sclerosis: association with *LRP2* genetic variation. *Multiple Sclerosis Journal*, 2018, 24:1773-1775. IF: 5.65, 1 citation
- Put K., Vandenhaute J., Avau A., Van Nieuwenhuijze A., Brisse E., Dierckx T., Rutgeerts O., Garcia-Perez J., Toelen J., Waer M., Leclercq G., Goris A., Van Weyenbergh J., Liston A., De Somer L., Wouters C., Matthys P.@ (2017). Inflammatory gene expression profile and defective IFN-γ and granzyme K in natural killer cells of systemic juvenile idiopathic arthritis patients. *Arthritis & Rheumatology*, 69, 213-224. IF 9.00, 16 citations
- McLaughlin R.*, Schijven D.*, van Rheenen W., van Eijk K., O'Brien M., Project MinE GWAS Consortium, Schizophrenia Working Group of the Psychiatric Genomics Consortium, Kahn R., Ophoff R., Goris A., Bradley D., Al-Chalabi A., van den Berg L., Luykx J.@, Hardiman O.@, Veldink J.# (2017). Genetic correlation between amyotrophic lateral sclerosis and schizophrenia. *Nature Communications*, 8, 14774-14774. IF 11.88, 28 citations

8. References

1. Dendrou, C. A., Fugger, L. & Friese, M. A. Immunopathology of multiple sclerosis. *Nat Rev Immunol* **15**, 545-558 (2015).
2. The International Multiple Sclerosis Genetics Consortium. Multiple sclerosis genomic map implicates peripheral immune cells and microglia in susceptibility. *Science* **365** (2019).
3. The International Multiple Sclerosis Genetics Consortium. Low-Frequency and Rare-Coding Variation Contributes to Multiple Sclerosis Risk. *Cell* **175**, 1679-1687 e1677 (2018).
4. Dooley, J. *et al.* Immunological profiles of multiple sclerosis treatments reveal shared early B cell alterations *Neurol Neuroimmunol Neuroinflamm* **3**, e240 (2016).
5. Miyazaki, Y. *et al.* Suppressed pro-inflammatory properties of circulating B cells in patients with multiple sclerosis treated with fingolimod, based on altered proportions of B-cell subpopulations. *Clin Immunol* **151**, 127-135 (2014).
6. Schubert, R. D. *et al.* IFN-beta treatment requires B cells for efficacy in neuroautoimmunity. *J Immunol* **194**, 2110-2116 (2015).
7. Ceronie, B. *et al.* Cladribine treatment of multiple sclerosis is associated with depletion of memory B cells. *J Neurol* **265**, 1199-1209 (2018).
8. Hartung, H. P. & Kieseier, B. C. Atacicept: targeting B cells in multiple sclerosis. *Ther Adv Neurol Disord* **3**, 205-216 (2010).
9. Kappos, L. *et al.* Atacicept in multiple sclerosis (ATAMS): a randomised, placebo-controlled, double-blind, phase 2 trial. *Lancet Neurol* **13**, 353-363 (2014).
10. Sergott, R. C. *et al.* ATON: Results from a Phase II randomized trial of the B-cell-targeting agent atacicept in patients with optic neuritis. *J Neurol Sci* **351**, 174-178 (2015).
11. Krumbholz, M., Derfuss, T., Hohlfeld, R. & Meinl, E. B cells and antibodies in multiple sclerosis pathogenesis and therapy. *Nat Rev Neurol* **8**, 613-623 (2012).
12. Baker, D., Pryce, G., Amor, S., Giovannoni, G. & Schmierer, K. Learning from other autoimmunities to understand targeting of B cells to control multiple sclerosis. *Brain* **141**, 2834-2847 (2018).
13. Jiang, C. *et al.* CRISPR/Cas9 Screens Reveal Multiple Layers of B cell CD40 Regulation. *Cell Rep* **28**, 1307-1322 e1308 (2019).
14. Van Horebeek, L. & Goris, A. Transcript-specific regulation in T-cells in multiple sclerosis susceptibility. *Eur J Hum Genet* (in press).
15. Karnell, J. L. *et al.* A CD40L-targeting protein reduces autoantibodies and improves disease activity in patients with autoimmunity. *Sci Transl Med* **11** (2019).
16. Liston, A., Carr, E. J. & Linterman, M. A. Shaping Variation in the Human Immune System. *Trends Immunol* **37**, 637-646 (2016).
17. Orru, V. *et al.* Genetic variants regulating immune cell levels in health and disease. *Cell* **155**, 242-256 (2013).
18. Carr, E. J. *et al.* The cellular composition of the human immune system is maintained in multiple stable equilibriums shaped by age and cohabitation *Nat Immunol* **417**, 461-468 (2016).
19. Brodin, P. *et al.* Variation in the human immune system is largely driven by non-heritable influences. *Cell* **160**, 37-47 (2015).
20. Roederer, M. *et al.* The genetic architecture of the human immune system: a bioresource for autoimmunity and disease pathogenesis. *Cell* **161**, 387-403 (2015).
21. Aguirre-Gamboa, R. *et al.* Differential Effects of Environmental and Genetic Factors on T and B Cell Immune Traits. *Cell Rep* **17**, 2474-2487 (2016).
22. Hedrick, E., Cheng, Y., Jin, U. H., Kim, K. & Safe, S. Specificity protein (Sp) transcription factors Sp1, Sp3 and Sp4 are non-oncogene addiction genes in cancer cells. *Oncotarget* **7**, 22245-22256 (2016).
23. Nunez, G., Hockenbery, D., McDonnell, T. J., Sorensen, C. M. & Korsmeyer, S. J. Bcl-2 maintains B cell memory. *Nature* **353**, 71-73 (1991).
24. Stavraka, C. & Blagden, S. The La-Related Proteins, a Family with Connections to Cancer. *Biomolecules* **5**, 2701-2722 (2015).
25. Fonseca, B. D. *et al.* La-related Protein 1 (LARP1) Represses Terminal Oligopyrimidine (TOP) mRNA Translation Downstream of mTOR Complex 1 (mTORC1). *J Biol Chem* **290**, 15996-16020 (2015).
26. Hong, S. *et al.* LARP1 functions as a molecular switch for mTORC1-mediated translation of an essential class of mRNAs. *Elife* **6**, pii: e25237 (2017).
27. Iwata, T. N. *et al.* Conditional Disruption of Raptor Reveals an Essential Role for mTORC1 in B Cell Development, Survival, and Metabolism. *J Immunol* **197**, 2250-2260 (2016).
28. Levy-Mendelovich, S. *et al.* T and B cell clonal expansion in Ras-associated lymphoproliferative disease (RALD) as revealed by next-generation sequencing. *Clin Exp Immunol* **189**, 310-317 (2017).
29. Meinl, E., Thaler, F. S. & Lichtenthaler, S. F. Shedding of BAFF/APRIL Receptors Controls B Cells. *Trends Immunol* **39**, 673-676 (2018).
30. Smulski, C. R. *et al.* BAFF- and TACI-Dependent Processing of BAFFR by ADAM Proteases Regulates the Survival of B Cells. *Cell Rep* **18**, 2189-2202 (2017).

Geneeskundige Stichting Koningin Elisabeth
Fondation Médicale Reine Elisabeth
Königin-Elisabeth-Stiftung für Medizin
Queen Elisabeth Medical Foundation

Final report of the research group of

Prof. dr. Leybaert Luc, MD. PhD

Universiteit Gent (UGent)

Principal investigator

Prof. dr. Leybaert Luc, MD. PhD
Dept. Basic Medical Sciences
Faculty of Medicine and Health Sciences
Ghent University
Belgium
Tel.: +32 9 332 33 66
Fax: +32 16 33 09 39
E-mail: Luc.Leybaert@UGent.be

Exploring the role of astroglial Cx43 hemichannels as therapeutic targets in stroke

1. Introduction

Stroke is, like cancer, associated with a major mortality risk and is the second important cause of death, next to ischemic heart disease. The majority of strokes are caused by blood vessel obstruction, either by a clot (thrombus) or an embolism, resulting in decreased perfusion of certain brain areas and rapid development of ischemia, leading to cell injury and neuronal cell death. Current therapeutic possibilities include clot lysis by means of tissue plasminogen activator (tPA) administration within 3 hours or endovascular clot removal (endarterectomy) within 6 hours after the insult. As a result of these limited time windows and possible side effects of these treatments, a majority of patients fall outside the selection criteria to receive these treatments. Hence, there is an urgent need for further research towards identifying novel therapeutic targets and developing new treatments. The work performed in this project aims to investigate connexin proteins as potential targets to protect the brain against ischemic cell injury. Brain cells not only encompass neurons but also glial cells that are in fact more numerous than neurons (at least 3 times more numerous depending on the species). Research over the past 20 years has demonstrated that astrocytes (star shaped glial cells), which form a bridge between neurons and blood vessel cells, exert crucial functions in substrate delivery to the neurons (energy substrate, neurotransmitter precursors) and removal of end products of metabolism as well as ions, which are transferred away from active zones and transferred to the blood. This crucial role of astrocytes is, in part, facilitated by connexin proteins that form channels, called gap junctions, that connect cells to form a large glial network, called the glial syncytium (reviewed in Ref. 2, Publications under GSKE support). Gap junctions are formed by two half gap junction channels called 'hemichannels'; these hemichannels are also present in the plasma membrane in their free form, i.e. not as part of a gap junction. As such, hemichannels form non-selective pores that, when open, pass ions and molecules up to ~1.5 kDa, which may disturb cell function and lead to cell injury/cell death. The purpose of the present work is to investigate whether blocking hemichannels protects the neural tissue against post-ischemic cell injury. Over the past 10 years, the Leybaert group has provided a detailed characterization of hemichannel control by cytoplasmic Ca^{2+} and developed, based on these insights, a peptide toolset that allows to specifically modulate hemichannel function. One of these compounds is Gap19 that inhibits hemichannels composed of Cx43, the most abundant connexin in the brain that is largely present in astrocytes. Interestingly, Gap19 does not inhibit gap junctions and as such leaves the crucial physiological functions of these junctional channels intact. The work presented below reports on the second year research activities performed in the context of investigating connexin hemichannels as a potential target to protect the brain against ischemic injury. We include an account on the first year activities to provide context for the research steps performed in year 2, which have been directed at investigating the role of connexin hemichannels as a vascular as well as glial target to prevent blood-brain barrier dysfunction, thereby providing brain protection at the blood-brain interface.

2. Summary of results obtained over the 2017 and 2018 periods

We characterized a mutant Cx43 with a 'phospho-dead' MAP kinase domain and found it to phenotypically present with a loss of hemichannel function in brain astrocytes. In an animal model of permanent occlusion of the mid-cerebral artery, Cx43 MAP-kinase mutant animals (further called MK4 mice with 4 Ser to Ala modified residues) had significantly smaller brain infarcts and less cell death compared to WT animals. We tested other Cx43 phosphorylation sites (PKC, CK1) but those did not

protect against permanent brain ischemia. We also tested whether blocking hemichannels with Gap19, added as TAT-Gap19 to improve cell membrane permeation, could provide protection in WT animals. We found that this peptide gave a similar reduction in brain infarct size as observed in the Cx43 MAP-kinase mutants. Interestingly, this protection was obtained by a single i.p. administration of TAT-Gap19 2 hours after vessel occlusion, mimicking a therapeutic setting. The paper concerning this work has been expanded with data on functional recovery of the animals whereby MK4 mice showed improved behavioral performance; this paper is now in minor revision (Ref. 1, Publications under GSKE support). A one sentence summary, graphical abstract and abstract of this work are given below; a more detailed description of this part of the work is presented under 'III. Targeting connexin hemichannels to protect the brain against ischemic injury'.

Summary. The study demonstrates that astrocytic connexin43 hemichannels are largely controlled by 4 C-terminal tail located serine residues, and provides mechanistic insight on how phosphorylation of these residues affects recovery from stroke.

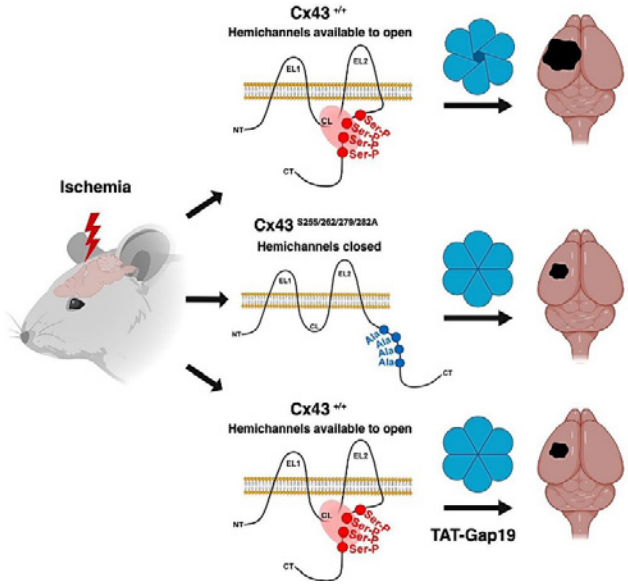

Abstract. Cx43 function is influenced by kinases that phosphorylate specific serine sites located near its C-terminus. Stroke is a powerful inducer of kinase activity, but its effect on Cx43 is unknown. We investigated the impact of wild-type (WT) and knock-in Cx43 with serine to alanine mutations at the protein kinase-C site Cx43^{S368A} (PKC), the casein kinase-1 sites Cx43$^{S325A/328Y/330A}$ (CK1) and the mitogen-activated protein kinase sites Cx43$^{S255/262/279/282A}$ (MK4), on a permanent middle cerebral artery occlusion (pMCAO) stroke model. We demonstrate that MK4 transgenic animals exhibit a significant decrease in infarct volume which was associated with significant improvement in behavioral performance. An increase in astrocyte reactivity with a concomitant decrease in microglial reactivity was observed in MK4 mice. In contrast to WT, MK4 astrocytes displayed reduced Cx43 hemichannel activity. Pharmacological blockade of Cx43 hemichannels with TAT-Gap19 significantly decreased infarct volume in WT animals. This study provides novel molecular insights and charts new avenues for therapeutic intervention associated with Cx43 function.

While this work demonstrated a crucial role of astrocytic Cx43 in protecting against brain infarct volume and cellular as well as functional recovery, we wondered whether protection by TAT-Gap19 could also involve effects at the level of the blood-brain barrier (BBB). To this purpose, we performed *in vivo* animal BBB studies in a model of inflammation-induced barrier leakage instigated by intraperitoneal lipopolysaccharide (LPS) administration. Inflammation is indeed a major, but less characterized, component of stroke pathophysiology. We found that TAT-Gap19 significantly inhibited LPS-induced

BBB leakage which was mediated by effects on both astrocytes and BBB endothelial cells, with the astrocytic contributuion being particularly potent. A detailed patch-clamp study demonstrated that peripheral (vascular) inflammation was associated with calcium-dependent Cx43 hemichannel opening in BBB endothelial cells as well as in astrocytes, the blocking of which prevented BBB failure. A more extended account of this part of the work is presented under 'IV. Targeting connexin hemichannels to protect against blood-brain barrier leakage'. This work will be further continued towards completion and publication in 2019.

3. Targeting connexin hemichannels to protect the brain against ischemic injury.

Hemichannels are composed of six connexin subunits, which are tetraspan proteins that contain two extracellular loops, one intracellular loop and N- and C-terminal domains located inside the cell (Fig. 1). Opening of Cx43 hemichannels necessitates an interaction of the C-terminal tail with the intracellular loop as demonstrated by previous work from our group (*1*). We started the present work from the observation that the C-terminal tail of Cx43 has two different domains that interact with the intracellular loop: the CT9 domain composed of the last 9 amino acids (*2-4*) of the C-terminal and the Src homology-3 (SH3) binding domain located ~100 amino acids upstream in N-terminal direction (*5*). This SH3 domain is part of a larger stretch of amino acids that contain 4 Ser residues from a MAP-kinase (MAPK) domain (Fig. 1).

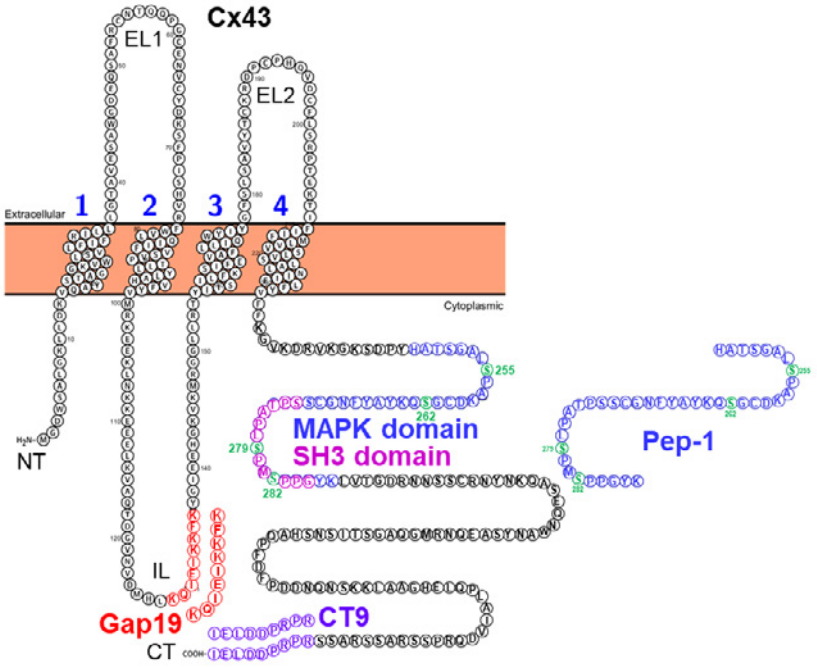

Fig. 1. Cx43 topology with indication of the CT9, SH3 and MAPK domains, and the peptides Gap19, Pep-1 and CT9. *The MAPK domain is as indicated by the Pep-1 sequence (amino acids 248-287) with the 4 Ser residues marked in green; the SH3 domain is a sub-domain within the MAPK stretch. In MK4 mice the 4 Ser residues are modified to Ala.*

To investigate whether the MAPK domain, which is larger than the SH3 domain, is also involved in hemichannel regulation, we performed experiments on Cx43 in which the 4 Ser residues in the MAPK domain (S255, S262, S279 & S282 – marked green in Fig. 1) were each modified to Ala rendering this domain 'phospho-dead'; these MAPK phosphorylation null mutants are further referred to as MK4. In collaboration with the group of Dr. P. Lampe (Translational Research Program, Fred Hutchinson Cancer Research Center, Seattle, USA) we obtained transgenic MK4 mutant mice and performed single channel patch-clamp experiments on Cx43 hemichannel function. In astrocytes isolated from WT animals, hemichannel openings were triggered by a small increase of the intracellular Ca^{2+} concentration ($[Ca^{2+}]_i$)

from 50 to 200 nM at normal resting potential of -70 mV (Fig. 2A). Gap19, a nonapeptide derived from the cytoplasmic loop of Cx43 (Fig. 1), which was previously shown by our group to inhibit hemichannel activity without inhibiting gap junctions (*6*), abolished the unitary current activities (Fig. 2A). All-point histograms furthermore indicated a unitary conductance in the range of 230-245 pS, i.e. in the range of ~220 pS reported for Cx43 hemichannels (*7, 8*) (Fig. 2B). As illustrated in Fig. 2C, charge transfer mediated by hemichannels was negligible at 50 nM $[Ca^{2+}]_i$, but was significantly enhanced at 200 nM $[Ca^{2+}]_i$ and was reduced to the basal level by Gap19 (in these experiments we could use the non-TAT version as it was applied in the whole-cell patch pipette (Fig. 2C). Remarkably, in astrocytes isolated from MK4 Cx43 phosphorylation-null mutant animals, 200 nM $[Ca^{2+}]_i$ stimulation did not trigger any hemichannel current activity indicating loss of hemichannel function (Fig. 2D). We next tested whether supplying MK4 mutant astrocytes with a cell-penetrating peptide called Pep-1 composed of His-248 to Lys-287 on the Cx43 CT encompassing the 4 Ser residues modified in MK4 mice (Fig. 1), could rescue hemichannel activity. Strikingly, preincubating astrocytes isolated from MK4 mutant animals with Pep-1 rescued hemichannel activities at 200 nM $[Ca^{2+}]_i$ (Fig. 2D). As illustrated in Fig. 2E, the unitary conductance of restored hemichannel currents in MK4 mutant astrocytes was in the range of 220-240 pS, not different from the conductance in WT astrocytes. We further quantified the effect of Pep-1 on charge transfer associated with hemichannel openings and demonstrated significantly increased charge transfer at 200 nM $[Ca^{2+}]_i$ in MK4 mutant astrocytes exposed to Pep-1 peptide as compared to those in non-treated MK4 mutants (Fig. 2F).

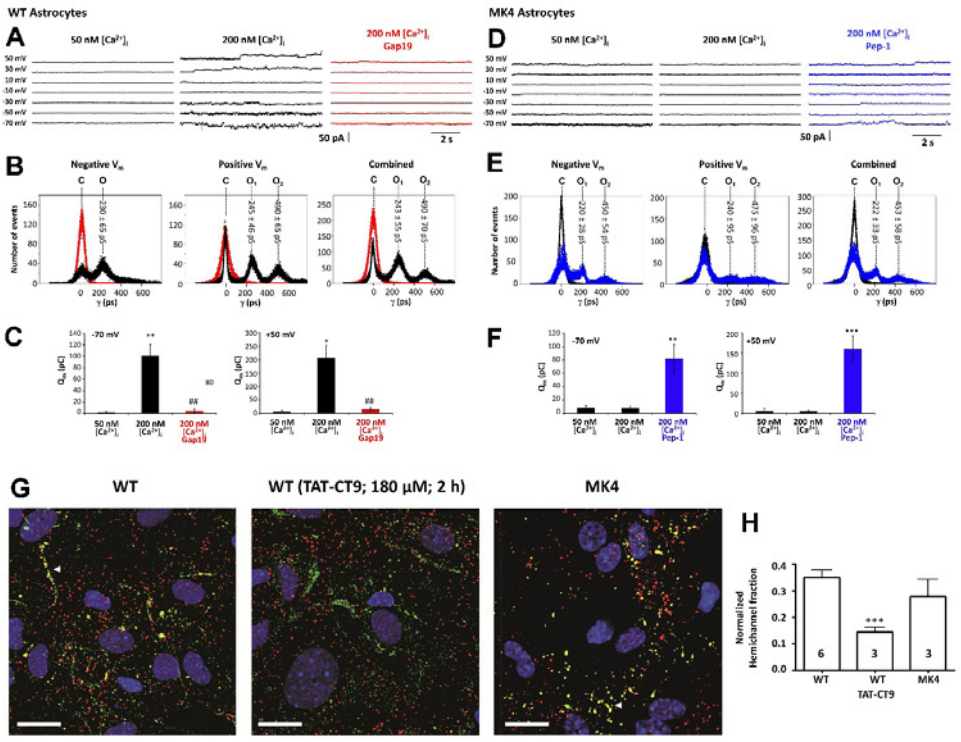

Fig. 2. Hemichannel activity is reduced in MK4 Cx43 phosphorylation null mutant astrocytes. A. *Current traces in WT astrocytes for voltage steps indicated left. Unitary current activity appeared at both negative and positive V_m when $[Ca^{2+}]_i$ was elevated from 50 nM to 200 nM. Gap19 (100 µM, added via the pipette) suppressed unitary activity (red traces).* ***B.*** *All-point histogram of current activities at negative, positive and combined V_m. Unitary conductance of one (O_1) or two open hemichannels (O_2) are indicated above each peak (mean ± s.d.). Gap19 abolished all current activity (red peak at baseline).* ***C.*** *Charge transfer (Q_m) associated with unitary current activities for recordings at -70 and +50 mV (n = 6). * P<0.05 vs 50 nM $[Ca^{2+}]_i$; ** P<0.01; ##, P<0.01 vs 200 nM $[Ca^{2+}]_i$.* ***D.*** *Current traces in MK4 mutant astrocytes. Unitary activity was absent at 200 nM $[Ca^{2+}]_i$ but pre-treatment with Pep-1 peptide (35 µM, 1 h) restored activity (blue traces).* ***E.*** *All-point histogram showing that currents restored by Pep-1 had a single channel conductance similar to WT.* ***F.*** *Q_m charge transfer data illustrating restoration of opening activities with Pep-1 (n = 6). ** P<0.01 compared to 200 nM $[Ca^{2+}]_i$; *** P<0.001.* ***G.*** *Confocal images of Duolink (red) and Cx43 (green) stainings in WT and MK4 mutant astrocytes; yellow co-localization signal corresponds to hemichannels. WT astrocytes (left) displayed clear hemichannel signal (arrowhead) that was decreased after TAT-CT9 treatment, which promotes incorporation of hemichannels into gap junctions. Hemichannel signal was also present in MK4 mutant astrocytes (right).* ***H.*** *Summary data of normalized yellow signal, demonstrating that the signal from MK4 mutant astrocytes was not different from WT. ***P < 0.001 WT vs WT (TAT-CT9). Scale bars are 20 µm. All error bars represent s.e.m.*

To exclude the possibility that the lower unitary hemichannel activity is due to a smaller pool of plasma membrane hemichannels in MK4 mutants, we performed Duolink in situ proximity ligation assays in isolated WT and MK4 mutant astrocytes. This assay reports the spatial hemichannel organization relative to gap junctions through amplification of Cx43/ZO-1 complexes that represent hemichannels (*9*). As illustrated in Fig. 2G, red Duolink fluorescence occurred throughout the cells while the yellow signal produced by red-green co-localized spots at gap junctions (arrowhead), representing hemichannels underway to gap junctions as reported for other cell types (*10*) We next tested TAT-CT9, a peptide composed of the last 9 amino acids of the Cx43 C-terminal end fused to the TAT membrane translocation sequence; this peptide promotes incorporation of hemichannels into gap junctions by competing for ZO-1 binding for which the 4 last amino acids of the C-terminal tail are crucial (*11*) WT astrocytes treated with TAT-CT9 (180 µM, 2 hr) displayed markedly less Duolink fluorescence signal, in line with its promotive effect on hemichannel assembly into gap junctions (Fig. 2G). Quantification of the yellow signal relative to the green Cx43 signal corresponding to the normalized plasma membrane hemichannel fraction, showed that the signal in MK4 mutant astrocytes was not different from the signal in WT cells (Fig. 2H). Thus, the lower hemichannel activity in MK4 mutant astrocytes is the consequence of altered gating and not the result of a decreased hemichannel pool.

The results discussed above demonstrated that MK4 Cx43 phosphorylation null mutant animals have a loss of hemichannel function in brain astrocytes. In a next step, we tested whether this is associated with a protective effect following ischemic stroke. To that purpose we collaborated with Dr. C.C. Naus (Cellular & Physiological Sciences, Faculty of Medicine, The University of British Columbia, Vancouver, Canada) and made use of various Cx43 phosphorylation null mutants generated by and Dr. P. Lampe (Translational Research Program, Fred Hutchinson Cancer Research Center, Seattle, USA). These mutants included the MK4 mutant but also a CK1 and PKC mutant; MAPK, CK1 and PKC kinases have all been shown to be active in ischemic conditions (*12-15*). To test whether disrupting CK1, PKC or MAPK phosphorylation sites of the C43 C-terminal tail impacts stroke outcome, a cohort of male and female WT and Cx43 phosphorylation null mutants for CK1, PKC and MAPK (MK4) mice were subjected to permanent occlusion of the mid-cerebral artery (pMCAO). Four days after pMCAO the CK1 and PKC Cx43 phosphorylation null mutant mice did not show significant changes in infarct volume with respect to WT controls (Fig. 3a and b). However, MK4 mutant mice exhibited a significant ($P = 0.0181$) 58.3% reduction in infarct volume compared with WT counterparts (Fig. 3a and b). In light of the compelling phenotype observed in MK4 mutant ischemic mice, a larger cohort of WT and MK4 mutant male and female animals were subjected to pMCAO. Consistent with our initial study, MK4 mutant mice exhibited a significant ($P = 0.0053$) 40.2% reduction in infarct volume compared with WT counterparts (Fig. 3c). Apoptosis triggered by an ischemic event may occur over several days and contribute to delayed neuronal death and loss of viable peri-infarct tissue (*16*). To investigate whether the difference in infarct volume found in WT and MK4 mutant ischemic mice is correlated with differences in the level of apoptosis, WT and MK4 brain sections from ischemic mice were subjected to TUNEL immunostaining. In contrast to WT mice, TUNEL staining exhibited a significant ($P = 0.0337$) 70.0% reduction in the number of apoptotic TUNEL+ cells within the infarct region of MK4 mutant brain tissue sections, 4-days after pMCAO (Fig. 3d and e).

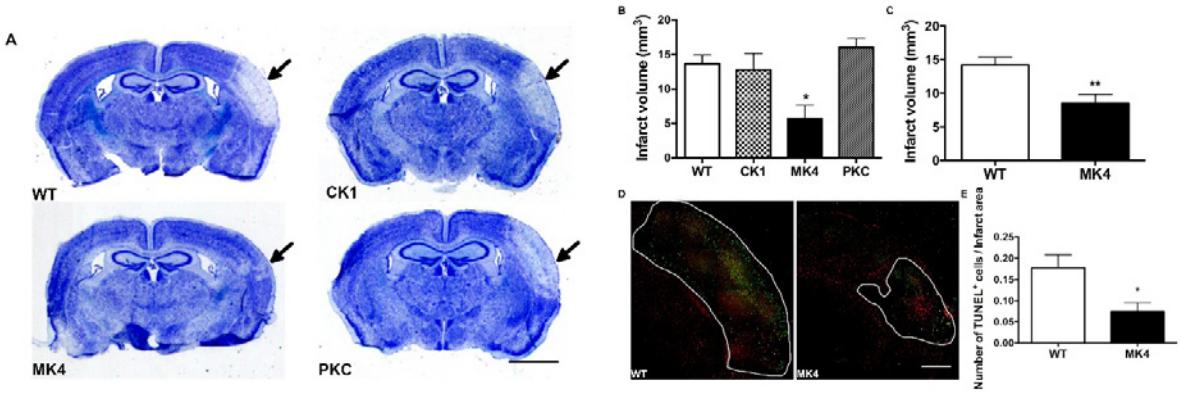

Fig. 3. Disrupting the MAPK phosphorylation sites of Cx43 C-terminus results in both a decrease in infarct volume and TUNEL staining 4-days after pMCAO. (a) *Representative photomicrographs of thionin-stained sections from WT and Cx43 null phosphorylation mutant CK1, PKC and MAPK (MK4) mutant mice, 4-days post-pMCAO. Scale bar = 2 mm.* ***(b)*** *Quantification of infarct volume from WT and Cx43 null phosphorylation mutant CK1, PKC and MAPK (MK4) thionin-stained brain sections, 4-days post-pMCAO (One-way ANOVA followed by Bonferroni post-test; *P = 0.0181; WT: n = 5 mice; CK1: n = 4; PKC: n = 4; MK4: n = 4).* ***(c)*** *Quantification of infarct volume from WT and MK4 thionin-stained brain sections, 4 days post-pMCAO (unpaired Student's t-test; **P = 0.0053; WT: n = 10 mice; MK4: n = 11 mice).* ***(d)*** *Co-immunofluorescence staining of cerebral cortex from WT (left micrograph) and MK4 (right micrograph) mice, 4 days after pMCAO, using the astrocyte marker GFAP (red) with TUNEL apoptosis marker (green). White outline on WT and MK4 micrographs delineates infarct area. Scale bar = 500 µm.* ***(e)*** *Quantification of average number of TUNEL+ cells in brain sections from WT and MK4 mice 4 days after pMCAO (unpaired Student's t-test; *P = 0.0337; WT: 4 sections, n = 5 mice; MK4: 4 sections, n = 4 mice). All error bars represent s.e.m.*

We next asked whether the decreased hemichannel activity exhibited in MK4 astrocytes is a key factor in the neuroprotective phenotype of these animals subjected to pMCAO. To test this hypothesis, we subjected WT animals to pMCAO followed by administration of either the hemichannel blocker TAT-Gap19 (*6*) or its scrambled form TAT-GAP19^{scrambled}. Fusion of Gap19 to the TAT (transactivator of transcription) sequence facilitates cellular uptake of the peptide, allowing it to cross the blood-brain barrier (*17*). Intraperitoneal (i.p.) injection of 0.75 µmol/Kg or 7.5 µmol/Kg TAT-Gap19 2hrs after pMCAO, significantly reduced infarct volume by 47.8 %, and 77.6 %, respectively 4-days after pMCAO, compared with those mice that received saline or scrambled alone (Fig. 4a and b). Mice treated with the negative control TAT-Gap19^{scrambled} did not show significant changes with respect to saline controls (Fig. 4a and b). Mice treated with 7.5 µmol/Kg TAT-Gap19 showed a significant reduction in infarct volume compared to mice treated with 0.75 µmol/Kg of TAT-Gap19 (Fig. 4b).

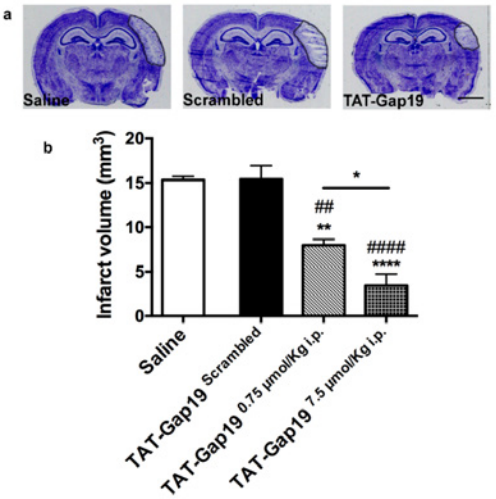

Fig. 4. TAT-Gap19 Cx43 hemichannel blocker is neuroprotective in mice subjected to pMCAO. (a) *Representative photomicrographs of thionin-stained sections, 4 days after pMCAO, in WT mice treated with either saline (left micrograph), 7.5 µmol/Kg i.p. scrambled TAT-Gap19 Scrambled (center micrograph), or 0.75 µmol/Kg i.p. hemichannel blocker TAT-Gap19 (right micrograph), 2 hrs after pMCAO. Black outline highlights infarct. Scale bar = 2 mm.* ***(b)*** *Quantification of infarct volume, 4 days after pMCAO, from WT mice treated with either saline, 7.5 µmol/Kg i.p. scrambled TAT-GAP19Scrampled, 0.75 µmol/Kg i.p or 7.5 µmol/Kg i.p.. TAT-Gap19, 2 hrs after pMCAO. (One-way ANOVA followed by Tukey's multiple comparisons test; Saline vs Scrambled: P = > 0.9999; Saline vs 0.75 µmol/Kg TAT-Gap19: **P = 0.0021; Saline vs 7.5 µmol/Kg TAT-GAP19: ****P = < 0.0001; Scrambled vs 0.75 µmol/Kg TAT-Gap19: ## P = 0.0019; Scrambled vs 7.5 µmol/Kg TAT-Gap19: #### P = < 0.0001; 0.75 µmol/Kg TAT-Gap19 vs 7.5 µmol/Kg TAT-Gap19: * P = 0.0484; Saline: n = 4 mice; 7.5 µmol/Kg TAT-Gap19scrampled: n = 4 mice; 7.5 µmol/Kg TAT-Gap19: n = 4 mice; 0.75 µmol/Kg TAT-Gap19: n = 4). All error bars represent s.e.m.*

We further characterized the functional recovery of the animals after pMCAO by the adhesive tape removal test. In WT mice, pMCAO significantly increased the time it took for mice to remove tape from the left (impaired) paw 3 days [WT = 39.78 ± 54.90 sec. vs MK4 = 7.33 ± 4.30 sec. (P = 0.0345)] after surgery (Fig. 5a). In addition, 5 and 9 days after surgery WT mice exhibited a non-significant latency in tape removal compared with MK4 animals (Fig. 5a). By 14 and 21 days post-pMCAO, WT mice became as efficient on the tape removal test as their MK4 counterparts (Fig. 5a). For the right (non-impaired) forepaw, there was no significant effect of pMCAO on tape removal latency between the two genotypes (Fig. 5b).

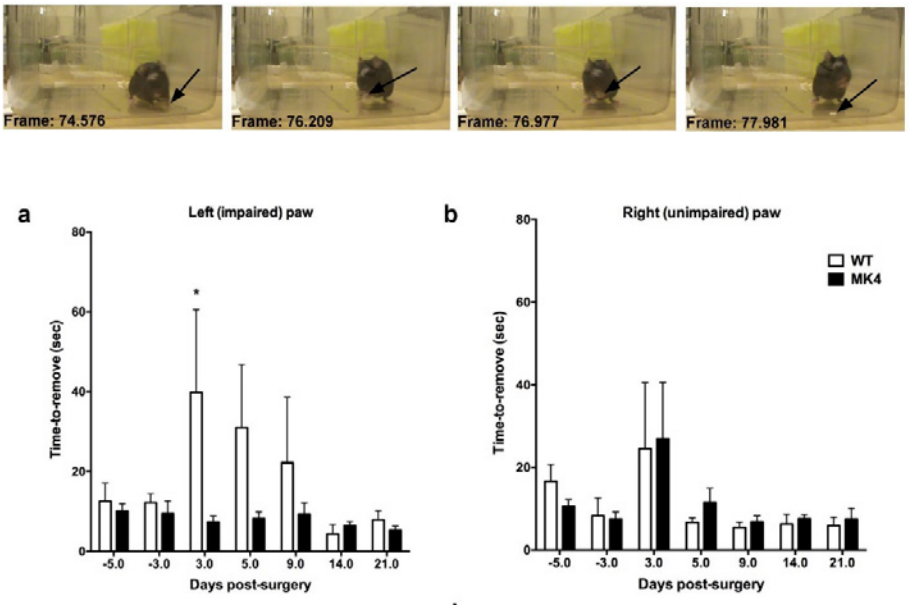

Fig. 5. MK4 mice show improved sensory function after pMCAO. (a) *Quantification of average time to remove adhesive tape from left (impaired) forepaw. Time-5 and -3 represent pre-pMCAO.* ***(b)*** *Latencies for right forepaw were unaffected by pMCAO. (Two-way ANOVA with repeated measures followed by Bonferroni's multiple comparisons test, main effect of genotype, main effect of genotype, P = 0.1200; main effect of time, P = 0.1178; subjects (matching), **P = 0.0027; interaction, P = 0.1534). The observed power for the interactions is 0.588. The effect size of interaction between time and genotype is 0.3, according to Cohen's f (medium to large effect). WT mice vs MK4 mice 3 days post-pMCAO *P = 0.0345; WT: n = 7 mice; MK4: n = 8 mice).*

4. Targeting connexin hemichannels to protect against blood-brain barrier leakage

This part is currently under review as a research paper and is therefore not shown here (DE BOCK M et al., under review - see below under publications).

5. Publications under GSKE support

Papers currently under review

– GIAUME C, NAUS CC, SAEZ JC and **LEYBAERT L**.
"Glial connexins and pannexins in the healthy and diseased brain"
Physiol Rev, revision submitted.
Impact factor: 24.0, category: PHYSIOLOGY, rank: 1/83, Vigintile: 1 (top 5%).

– DE BOCK M, DE SMET M, VERWAERDE S, VAN HAVER V, STEINHÄUSER C, VANDENBROUCKE R.E. and **LEYBAERT L**.
"Targeting gliovascular connexins prevents inflammatory blood-brain barrier leakage and astrogliosis"
Under review at JCI insight

Published papers

1. DELVAEYE T, DE SMET MAJ, VERWAERDE S, DECROCK E, CZEKAJ A, VANDENBROUCKE RE, LEMEIRE K, GONÇALVES A, DECLERCQ W, VANDENABEELE P, KRYSKO DV, **LEYBAERT L**.
"Blocking connexin43 hemichannels protects mice against tumour necrosis factor-induced inflammatory shock"
Sci Rep 9(1):16623, 2019.
2. FREITAS-ANDRADE M, WANG N, BECHBERGER JF, DE BOCK M, LAMPE PD,**LEYBAERT L*** and NAUS CC (*shared senior authorship).
"Targeting MAPK phosphorylation sites of the Connexin43 C-terminus provides neuroprotection in stroke"
J Exp Med 216(4):916-935, 2019.
Impact factor: 10.8, category: MEDICINE, RESEARCH & EXPERIMENTAL, rank: 6/133, Vigintile: 1 (top 5%).
3. DELVAEYE T, VANDENABEELE P, BULTYNCK G, **LEYBAERT L*** and KRYSKO DV (*shared senior authorship).
"Therapeutic Targeting of Connexin Channels: New Views and Challenges."
Trends Mol Med 24(12):1036-1053, 2018.
Impact factor: 11.0, category: MEDICINE, RESEARCH & EXPERIMENTAL, rank: 5/133, Vigintile: 1 (top 5%).
4. MAATOUK L, YI C, CARRILLO-DE SAUVAGE MA, COMPAGNION AC, HUNOT S, EZAN P, HIRSCH EC, KOULAKOFF A, PFRIEGER FW, TRONCHE F, **LEYBAERT L**, GIAUME C. and VYAS S.
"Glucocorticoid receptor in astrocytes regulates midbrain dopamine neurodegeneration through connexin hemichannel activity"
Cell Death Differ 26(3):580-596, 2018.
Impact factor: 8.00, category: BIOCHEMISTRY & MOLECULAR BIOLOGY, rank: 26/292, Decile: 1 (top 10%).
5. WALRAVE L, PIERRE A, ALBERTINI G, AOURZ N, DE BUNDEL D, VAN EECKHAUT A, VINKEN M, GIAUME C, **LEYBAERT L*** and SMOLDERS I (*shared senior authorship).
"Inhibition of astroglial connexin43 hemichannels with TAT-Gap19 exerts anticonvulsant effects in rodents"
Glia 66(8):1788-1804, 2018.
Impact factor: 5.846, category: NEUROSCIENCES, rank: 33/261, Quartile: 1 (top 25%).
6. **LEYBAERT L**, LAMPE PD, DHEIN S, KWAK BR, FERDINANDY P, BEYER EC, LAIRD DW, NAUS CC, GREEN CR, SCHULZ R.
"**Connexins in Cardiovascular and Neurovascular Health and Disease: Pharmacological Implications.**" ***Pharmacol Rev*** 69(4):396-478, 2017.
Impact factor: 17.9, category: PHARMACOLOGY & PHARMACY, rank: 2/256, Vigintile: 1 (top 5%).

6. References

1. L. Leybaert, P. D. Lampe, S. Dhein, B. R. Kwak, P. Ferdinandy, E. C. Beyer, D. W. Laird, C. C. Naus, C. R. Green, R. Schulz, Connexins in Cardiovascular and Neurovascular Health and Disease: Pharmacological Implications. *Pharmacol Rev* **69**, 396-478 (2017).
2. R. Ponsaerts, E. De Vuyst, M. Retamal, C. D'Hondt, D. Vermeire, N. Wang, H. De Smedt, P. Zimmermann, B. Himpens, J. Vereecke, L. Leybaert, G. Bultynck, Intramolecular loop/tail interactions are essential for connexin 43-hemichannel activity. *FASEB J* **24**, 4378-4395 (2010).
3. M. Bol, N. Wang, M. De Bock, B. Wacquier, E. Decrock, A. Gadicherla, K. Decaluwe, B. Vanheel, H. V. van Rijen, D. V. Krysko, G. Bultynck, G. Dupont, J. Van de Voorde, L. Leybaert, At the cross-point of connexins, calcium, and ATP: blocking hemichannels inhibits vasoconstriction of rat small mesenteric arteries. *Cardiovasc Res* **113**, 195-206 (2017).
4. C. D'Hondt, J. Iyyathurai, N. Wang, R. G. Gourdie, B. Himpens, L. Leybaert, G. Bultynck, Negatively charged residues (Asp378 and Asp379) in the last ten amino acids of the C-terminal tail of Cx43 hemichannels are essential for loop/tail interactions. *Biochem Biophys Res Commun* **432**, 707-712 (2013).
5. J. Iyyathurai, N. Wang, C. D'Hondt, J. X. Jiang, L. Leybaert, G. Bultynck, The SH3-binding domain of Cx43 participates in loop/tail interactions critical for Cx43-hemichannel activity. *Cell Mol Life Sci*, (2017).
6. N. Wang, E. De Vuyst, R. Ponsaerts, K. Boengler, N. Palacios-Prado, J. Wauman, C. P. Lai, M. De Bock, E. Decrock, M. Bol, M. Vinken, V. Rogiers, J. Tavernier, W. H. Evans, C. C. Naus, F. F. Bukauskas, K. R. Sipido, G. Heusch, R. Schulz, G. Bultynck, L. Leybaert, Selective inhibition of Cx43 hemichannels by Gap19 and its impact on myocardial ischemia/reperfusion injury. *Basic Res Cardiol* **108**, 309 (2013).
7. J. E. Contreras, J. C. Saez, F. F. Bukauskas, M. V. Bennett, Gating and regulation of connexin 43 (Cx43) hemichannels. *Proc Natl Acad Sci U S A* **100**, 11388-11393 (2003).
8. N. Wang, M. De Bock, G. Antoons, A. K. Gadicherla, M. Bol, E. Decrock, W. H. Evans, K. R. Sipido, F. F. Bukauskas, L. Leybaert, Connexin mimetic peptides inhibit Cx43 hemichannel opening triggered by voltage and intracellular Ca2+ elevation. *Basic Res Cardiol* **107**, 304 (2012).
9. J. M. Rhett, J. Jourdan, R. G. Gourdie, Connexin 43 connexon to gap junction transition is regulated by zonula occludens-1. *Mol Biol Cell* **22**, 1516-1528 (2011).
10. J. A. Palatinus, J. M. Rhett, R. G. Gourdie, The connexin43 carboxyl terminus and cardiac gap junction organization. *Biochim Biophys Acta* **1818**, 1831-1843 (2012).
11. C. Jin, K. D. Martyn, W. E. Kurata, B. J. Warn-Cramer, A. F. Lau, Connexin43 PDZ2 binding domain mutants create functional gap junctions and exhibit altered phosphorylation. *Cell Commun Adhes* **11**, 67-87 (2004).
12. N. Kaneko, J. Y. Hwang, M. Gertner, F. Pontarelli, R. S. Zukin, Casein kinase 1 suppresses activation of REST in insulted hippocampal neurons and halts ischemia-induced neuronal death. *J Neurosci* **34**, 6030-6039 (2014).
13. S. V. Demyanenko, S. N. Panchenko, A. B. Uzdensky, Expression of neuronal and signaling proteins in penumbra around a photothrombotic infarction core in rat cerebral cortex. *Biochemistry (Mosc)* **80**, 790-799 (2015).
14. M. Freitas-Andrade, P. Carmeliet, D. B. Stanimirovic, M. Moreno, VEGFR-2-mediated increased proliferation and survival in response to oxygen and glucose deprivation in PlGF knockout astrocytes. *J Neurochem* **107**, 756-767 (2008).
15. Z. Jiang, Y. Zhang, X. Chen, P. Y. Lam, H. Yang, Q. Xu, A. C. Yu, Activation of Erk1/2 and Akt in astrocytes under ischemia. *Biochem Biophys Res Commun* **294**, 726-733 (2002).
16. T. Nakase, G. Sohl, M. Theis, K. Willecke, C. C. Naus, Increased apoptosis and inflammation after focal brain ischemia in mice lacking connexin43 in astrocytes. *Am J Pathol* **164**, 2067-2075 (2004).
17. V. Abudara, J. Bechberger, M. Freitas-Andrade, M. De Bock, N. Wang, G. Bultynck, C. C. Naus, L. Leybaert, C. Giaume, The connexin43 mimetic peptide Gap19 inhibits hemichannels without altering gap junctional communication in astrocytes. *Front Cell Neurosci* **8**, 306 (2014).

Geneeskundige Stichting Koningin Elisabeth
Fondation Médicale Reine Elisabeth
Königin-Elisabeth-Stiftung für Medizin
Queen Elisabeth Medical Foundation

Final report of the research group of

Dr. Laurent Nguyen, PhD &
dr. Brigitte Malgrange

Université de Liège (ULg)

Dr. Laurent Nguyen, PhD

Laboratoire de régulation moléculaire de la neurogenèse
GIGA-Neurosciences
ULiège
4000 Liège
Belgium
Tel.: 32 4 366 59 87
Fax: 32 4 366 59 12
E-mail: lnguyen@ulg.ac.be
www.giga.ulg.ac.be

Dr. Brigitte Malgrange

Unité de Neurobiologie du développement
GIGA-Neurosciences
ULiège
4000 Liège
Belgium
Tel.: 32 4 366 59 87
Fax: 32 4 366 59 12
E-mail: bmalgrange@ulg.ac.be
www.giga.ulg.ac.be

Deciphering the role of protein ubiquitination in human cortical malformation and hearing impairment

1. State of the art and objectives

The cerebral cortex is an evolutionary advanced brain structure that contains different classes of neurons distributed within layers that are regionally organized into sensory, motor and association areas[1]. Cortical layering arises inside-out as progenitors give birth to successive waves of pyramidal projection neurons in the dorsal telencephalon[2] and, GABAergic interneurons in the ventral forebrain[3]. Projection neurons migrate radially to settle in appropriate cortical layers and they grow axonal projections towards cortical or sub-cortical targets. Interneurons migrate from the ganglionic eminences along multiple tangential paths to integrate local cortical networks. More generally, the development of the cortex implies a continuous rearrangement of a primordial structure that progresses through successive steps including, proliferation, specification, migration, and neuronal differentiation. Disrupting the completion of one or several of these events often lead to Malformations of Cortical Development (MCD). MCDs correspond to a heterogeneous group of focal or diffuse anatomical brain abnormalities with wide spectrum of clinical presentations, developmental delay or motor and intellectual disabilities. They usually occur during the first two trimesters of human pregnancy and involve cells that contribute to the formation of the cortex [4,5]. They are frequently associated with drug-resistant epilepsy, and more surprisingly, to neuro-sensory deafness and treatments are generally limited to symptom relief (reviewed in [6]). Most MCD are believed to have a genetic origin and their classification arises from diagnoses established by histopathological analyses, magnetic resonance imaging (MRI), electro-clinical studies and further identification of mutation in genes involved in cortical development.

Ubiquitination is a biochemical process that affect proteins in many ways: it can act as a signal for their degradation via the proteasome, change their cellular location, or modify their activity [7]. This process involves the covalent attachment of ubiquitin to a target protein, and is carried out by three enzymes: ubiquitin activating enzyme, E1, ubiquitin conjugating enzyme, E2, and ubiquitin ligase, E3. Each E3 enzyme targets a small number of proteins for ubiquitin modification but the exact substrates are mostly unknown and their identification continues to be a challenge. Regulation of protein turnover is essential for cellular homeostasis in all tissues, including the brain and the inner ear [8-10]; therefore the mutation of any enzyme involved in this process may affect brain and inner ear development. Most studies have thus focused on its role in renal (Liddle syndrome or pseudohyperaldostéronism) and pulmonary physiology and pathology but recent findings show that Nedd4-2 mutations can lead to bilateral periventricular nodular heterotopia (PNH), associated with other development abnormalities. Broix et al. showed that PNH-related mutants and excess wild-type Nedd4-2 affect projection neurons genesis, positioning and terminal translocation1. In human pathology, impaired cINs are known to be involved in seizure pathophysiology but nothing is known about their involvement in MCDs such as PNH associated with Nedd4-2 mutations. Along this line, our collaborator, Professor Jamel Chelly (IGBMC, Strasbourg, France), has identified novel human NEDD4-2 (a E3 ubiquitin ligase) mutations (c.2690G>A, p.Glu893Lys and c.2677G>A, p.Glu893Lys) in patients suffering from intellectual disabilities, MCD (the main feature being PNH), epilepsy as well as hearing impairment [11]. Identification of this novel MCD gene is important for diagnosis and genetic counselling of patients and their families, but also to better understand the molecular processes of corticogenesis and cochlear development in health and disease.

Outstanding questions and objectives

The aim of our proposal is to characterise the physiological functions of E3 ubiquitin ligases in the development of the cerebral cortex (WP1) and the formation of the cochlea, the auditory portion of the inner ear (WP2). For this purpose, we will focus on the pathophysiological mechanisms trigger by novel mutations in the HECT domain of *Nedd4-2* that lead to MCD and hearing impairment in patients. The Nguyen laboratory will focus on cortical interneurons whose contribution to MCD remains poorly understood and the Malgrange laboratory will study the mechanisms of deafness associated with *Nedd4-2* mutations. The project will combine mouse genetics with molecular and cell biology to decipher the physiological functions of *Nedd4-2,* as well as its closely related gene *Nedd4-1,* and to further untangle the pathomechanisms downstream its patient-related mutations.

2. Research program

WP1. Deciphering the role of Nedd4-1/-2 in the developing cerebral cortex in health and disease

The molecular connections existing between MCD and ubiquitination defects remain largely unknown. *Nedd4-2* codes for a HECT-domain E3-ubiquitin ligase, a protein involved in substrate ubiquitination whose mutation is associated with some MCD.

Our current project uncovers both the physiological role of *Nedd4-2* and the impact of its MCD-associated mutations on the biology of cortical interneurons using the mouse as a model.

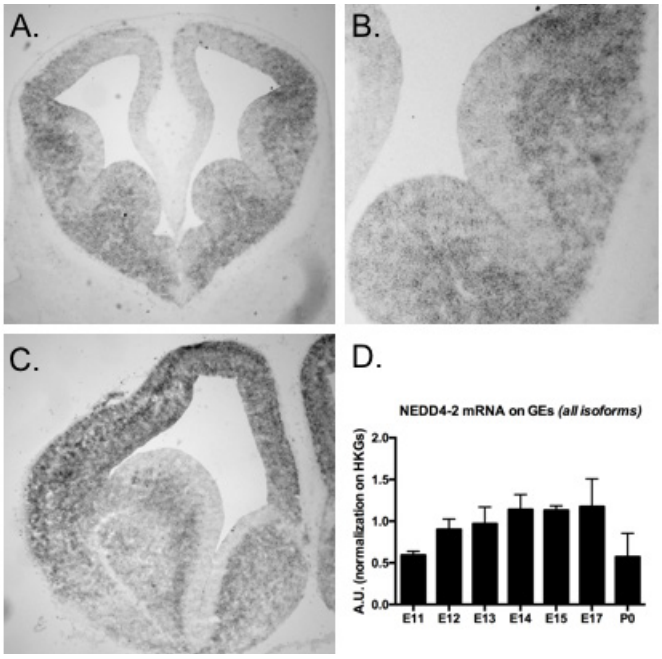

Fig.1. *Nedd4-2* expression pattern **A, B.** E12.5 MF1 mouse, whole brain coronal slice (A) and higher magnification focusing on medial (MGE) and lateral (LGE) ganglionic eminences (B), ISH. *Nedd4-2* mRNAs are expressed in the subventricular zone of both MGE and LGE, **C.** E14.5 MF1 mouse, one hemisphere coronal slice, ISH. Expression of Nedd4-2 now expands towards the cortex **D.** qRT-PCR performed on whole GE extracts. Nedd4-2 is expressed throughout embryonic stages in the brain and drops at birth.

We have first established the spatial (using ISH) and temporal (by qRT-PCR) expression patterns of Nedd4-2 messengers (Fig.1A-1D) Our findings are consistent with the expression of Nedd4-2 in post-mitotic interneurons during their tangential migration into the cortex (Fig. 1A, 1B). Our collaborators demonstrated earlier a role of Nedd4-2 in projection neuron migration (Broix et al. Nat Genet. 2016 Nov;48(11):1349-1358). According to its expression pattern in the ventral forebrain (Fig.1B), Nedd4-2 is likely also expressed by newborn migrating cortical interneurons (cINs). This will be confirmed by IHC on

brain section from WT mouse embryos. While impaired migration or maturation of cINs can contribute to the physiopathology of epilepsy (several mutations carriers suffer from seizure), poor migration and differentiation of cINs in MCD remains to be assessed. In order to address this question, we generated a conditional knockout (cKO) mouse model to genetically invalidate *Nedd4-2* in newborn cINs. For this purpose, we crossed *Nedd4-2*$^{flox/flox}$ mice (collaboration with H. Kawabe, Max Planck Institute of Experimental Medicine, Göttingen, Germany) with *Dlx5,6*:CRE-GFP mice (available in our laboratory) to generate cKO embryos. Due to high sequence homology between *Nedd4-2* and *Nedd4-1*, the ancestral member of the NEDD family, and to exclude any compensatory mechanisms, we also generated and analysed cKO cINs, using *Nedd4-1*$^{flox/flox}$ and *Nedd4-1* $^{flox/flox}$ */Nedd4-2*$^{flox/flox}$.

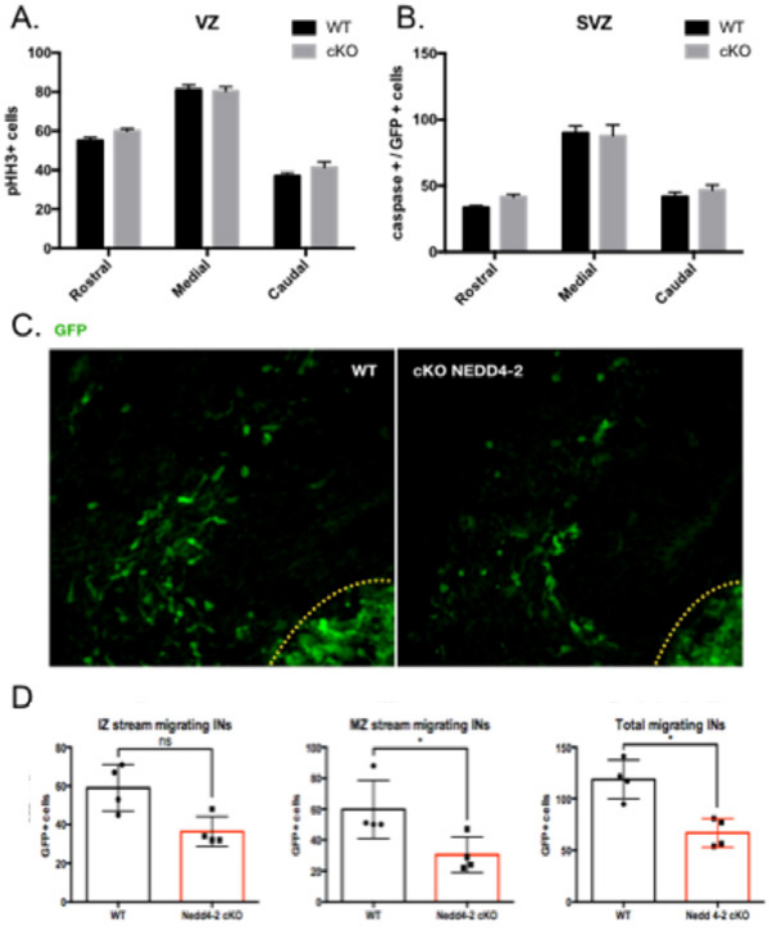

Fig. 2. Analysis of cell biological parameters in the cerebral cortex of Nedd4-2 cKO and WT mouse embryos **A.** IHC quantification. No significant difference in number of phospho-histone H3 positive cells in the ventricular zone of E14.5 embryos GEs. **B.** IHC quantification. No significant difference in number of caspase/GFP double positive cells in the subventricular zone of E14.5 embryos GEs. C. Confocal microscopy analyses of the cerebral cortex of E13.5 mice. Yellow dotted lines delineate GE/cortex border. **D.** Quantification of data shown in **C.** Non-parametric tests were applied due to too low a number of animal in each group. Number of animals needs to be increased to perform parametrical ttest.

The analyse of these different cKO mouse lines did not revealed any developmental impairment of proliferation or survival of cINs and their progenitors (Fig. 2A, 2B). We next performed time lapse recording on cultured brain slices from embryonic day (E14.5) mice to further explore the migration of the cINs in the cortical wall. We observed a defect of migration marked at early stages ***by a decreased number of cINs exiting the ganglionic eminences*** (GEs ; Fig. 2C, 2D). The positioning of the migration front of cINs at later stages was also affected upon loss of *Nedd4-2* expression (data not shown).
In order to perform a fine analysis of the morphological remodelling of cINs during migration, we performed time lapse recordings on explants culture of medial GEs (MGEs) Migrating cINs exhibit a peculiar migratory pattern known as nucleokinesis. The cell develops an expansion known as the

leading process, senses the environment and then, upon correct positioning of this leading process, the nucleus jumps forward. During those recordings, many parameters of migration were measured: average cell migration speed (Fig. 3B, 3C), frequency (Fig. 3D) and amplitude of nucleokinesis (Fig. 3E) as well as migration persistence - the ability to follow a straight line - of migrating cINs (Fig. 3.F).
Neither nucleokinesis amplitude nor migration persistence were affected by the genetical loss of *Nedd4-2* expression. ***However, our results underline a decreased frequency of nucleokinesis in Nedd4-2 cKO cINs resulting in a reduced speed of migration***. This defect may account for the migration phenotype observed in brain slices (Fig. 2C, 2D) Importantly, we couldn't find any migration defects in Nedd4-1 cKO cINs.

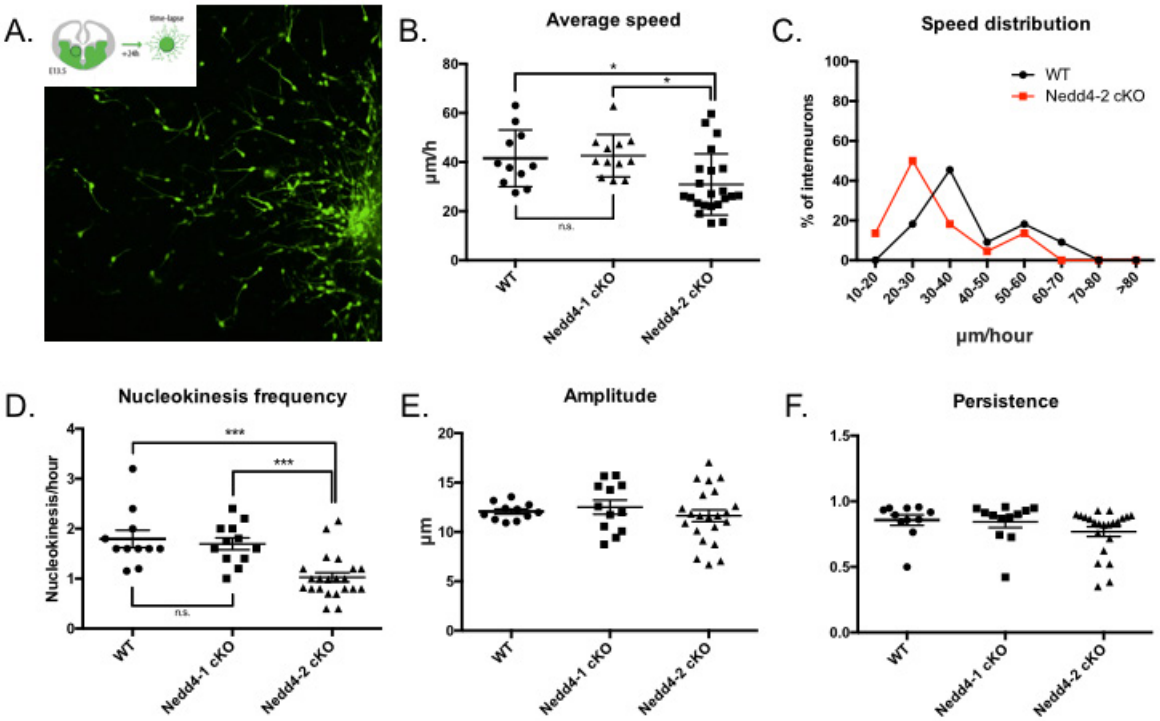

Fig. 3. *Ex vivo* imaging **A.** GE explants of E13.5 embryos are micro-dissected and cultured on cortical feeder. Five-hour recordings are held 24 to 48 hours later under controlled conditions. **B-F.** Quantification of migration features (see text). (*) P value < 0.05 (***) P value < 0.001

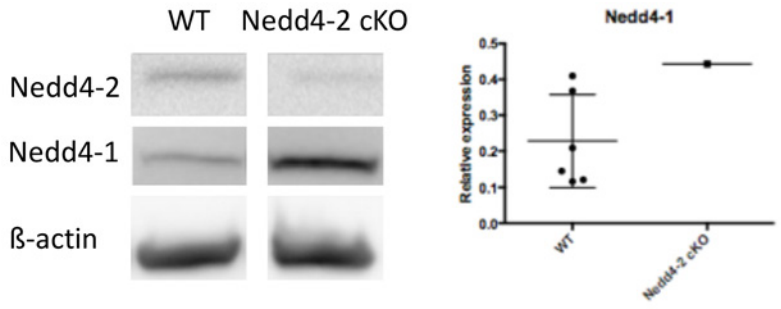

Fig. 4. *Western blotting showing the expression level of Nedd4-1, Nedd4-2 and beta-actin in cortical exttacts from WT or Nedd4-2 cKO. These are preliminary data as only one Nedd4-2 cKO animal has been analysed.*

Preliminary western blotting analyses performed on cortical extracts from E14.5 WT and Nedd4-2 cKO mouse embryos suggested the existence of a compensatory upregulation of the closely related protein Nedd4-1 (Fig. 4). In order to decipher whether the migration defects seen upon the conditional loss of Nedd4-2 may partly arise from the upregulation of Nedd4-1, we performed overexpression of Nedd4-1 in WT cINs and measured they migratory parameters. We could

not see any differences when compared with WT cINs transfected with empty vectors (data not shown), suggesting that the migratory defects seen upon loss of Nedd4-2 are resulting from loss of its activity towards direct targets. We are currently consolidating this hypothesis by knocking down acutely Nedd4-1 in Nedd4-2 cKO cINs and further testing whether this would rescue the migration defects seen upon loss of Nedd4-2.
We are currently refining the analysis of neuron migration by studying the dynamic branching of their leading process as excessive branching can slow down cINs migration[12]. More specifically, we will study the splitting frequency of the growth cone-like structure at the tip of the leading process, its branching complexity and the branch half-life [13,14]. During cINs migration, nucleokinesis and leading process branching are paced by cytoskeleton remodelling. The fine regulation of the actomyosin contractility that take place behind the nucleus (to propel it forward) and in the growth cone (to allow spitting and branch formation) are pivotal to support cINs migration. Therefore, we will monitor the actin-based contractions by analizing LifeAct-GFP in transfected WT and Nedd4-2 cKO cINs cultured in explant [15].
Membrane depolarization triggers voltage-gated calcium channel (VGCC) opening and transient calcium influx. These changes in calcium homeostasis tune myosin II activity, inducing actomyosin contractions that support nucleokinesis and branching. We will thus monitor the calcium influxes in migrating cINs (explant culture) upon expression of GCAMP8. This will allow a correlation between the possible calcium influx defects and nucleokinesis or branching phenotype observed in migrating Nedd4-2 cKO cINs. These methodological approaches are all mastered by the Nguyen laboratory.
Ultimately, genetic replacement experiments integrating MCD-related mutated proteins into *Nedd4-2* cKO cINs will be performed in order to decipher their pathophysiological implication. We will also assess cINs migration in the NEDD4-2 R897Q (K5810) "humanized" mouse and compare their migration parameters to the Nedd4-2 cKO cINs to measure the impact of the MCD-mutation on the migration of interneurons.
Since Nedd4-2 is an E3 ligase, we will next study the level of expression of relevant proteic substrates, by first focussing on ion channels (as impaired membrane depolarization defect may explain why cINs are not migrating properly).
For this purpose, we will combine UbiScan on FACS-isolated cells with western-blot and IHC in the developing mouse cortex in both WT and Nedd4s cKO mice. Co-immunoprecipitation between Nedd4-2 and the strongest candidates will be assessed in cell culture.

In conclusion and to further contextualize our work, identification of novel genes whose mutations lead to MCD is not only important for diagnosis and genetic counselling of patients and their families, but also to better understand the molecular processes of cerebral cortical development. Here, we could originally underline the involvement of both ubiquitination and interneurons migration defects in neurodevelopmental disorders characterized by MCD.

WP2. Deciphering the role of Nedd4-1/-2 in the developing inner ear and age-related hearing loss

Nedd4-1 and Nedd4-2 mRNAs are expressed in the mouse developing cochlea starting at E14.5. While both are expressed at E17.5 in the organ of Corti, the stria vascularis and in the spiral ganglion (Table 1, Fig. 5), Nedd4.2 is not any more present postnatally.
We next performed preliminary experiments at the cellular level. We start in the organ of Corti and performed immunohistochemistry in E17.5 cochlea (Fig.6). We found that Nedd41/2 are more specifically expressed at cellular junctions between hair cells and supporting cells.
To further decipher the roles of Nedd4-1/2 during cochlear development, we made use of a conditional knockout strategy: Nedd4-1lox/lox; Nedd4-2lox/lox mice were crossed to a Foxg1:Cre transgenic mouse line that express the Cre recombinase in the early otocyst to obtain Nedd4-2-cKO and Nedd4-1/2-cKO mice.

	E14.5	E17.5	P0	P3	P7
Cochlear duct	**+++/+++**	**++/++**	**++ / -**	**++ / -**	**++ / -**
Hair cells	NA	**++/++**	**++ / -**	**++ / -**	**++ / -**
Spiral ganglion	**+ / ++**	**+++/++**	**++ / -**	**++ / -**	**++ / -**
Stria vascularis	NA	**++/++**	**++ / -**	**++ / -**	**++ / -**

Table 1: Developmental pattern of expression of Nedd4.1 and Nedd4.2 in the developing cochlea

Because Nedd4.2 is highly expressed during embryonic stages and its levels decline postnatally, we first analysed the integrity of the cochlear sensory epithelium at birth. Our phenotypic analysis of 5 neonatal (P0) Nedd4-2 cKO cochleae suggested an epithelium disorganization and misalignment of hair cells within the plane of the epithelium. We performed a series of measurements for each HC row (IHC, OHC1, OHC2 and OHC3), in a total of 8 animals per genotype but we did not observe a significant difference in the HC polarity between WT and Nedd4-2 cKOs. In parallel, we also checked the polarity integrity by performing immunohistochemistry on several actors of the core planar cell polarity (Vangl2) and the cell intrinsic polarity (Lgn), our results did not reveal any mislocalization of these proteins in the sensory epithelium, further confirming that the polarized processes involved in the sensory cell architecture and the mechanosensory bundle localization at the apical plane of HCs is not significantly affected by the loss of embryonic Nedd4-2.

Next, we analysed the cochlear tissue of WT and Nedd4-2 cKOs at various postnatal stages (from postnatal day 15 to 90) by performing Scanning Electron Microscopy (SEM) and immunohistochemistry on the sensory epithelium. Actin labellings reveal the progressive loss of some actin-rich hair bundles, normally present at the apical surface of HCs, which suggests an early degeneration of the hair cells in the absence of Nedd4-2 (Fig. 7, see white arrowheads). This result was further confirmed by SEM analysis that clearly demonstrates the lack of protruding mechanosensory hair bundle from some cochlear cells (data not shown). Tehrefore, Nedd4-2 is crucial for the maintenance of cochlear sensory cells. Interestingly, cochlear cell loss in Nedd4-2 cKO animals follows a base-to-apex gradient along the cochlea that is similar to what occurs in age-related or sound-induced hearing loss. We can thus speculate HC survival is affected in humans presenting Nedd4-2 mutations and that cochlear sensory cell loss could be responsible for the early-onset and rapidly progressing hearing loss.

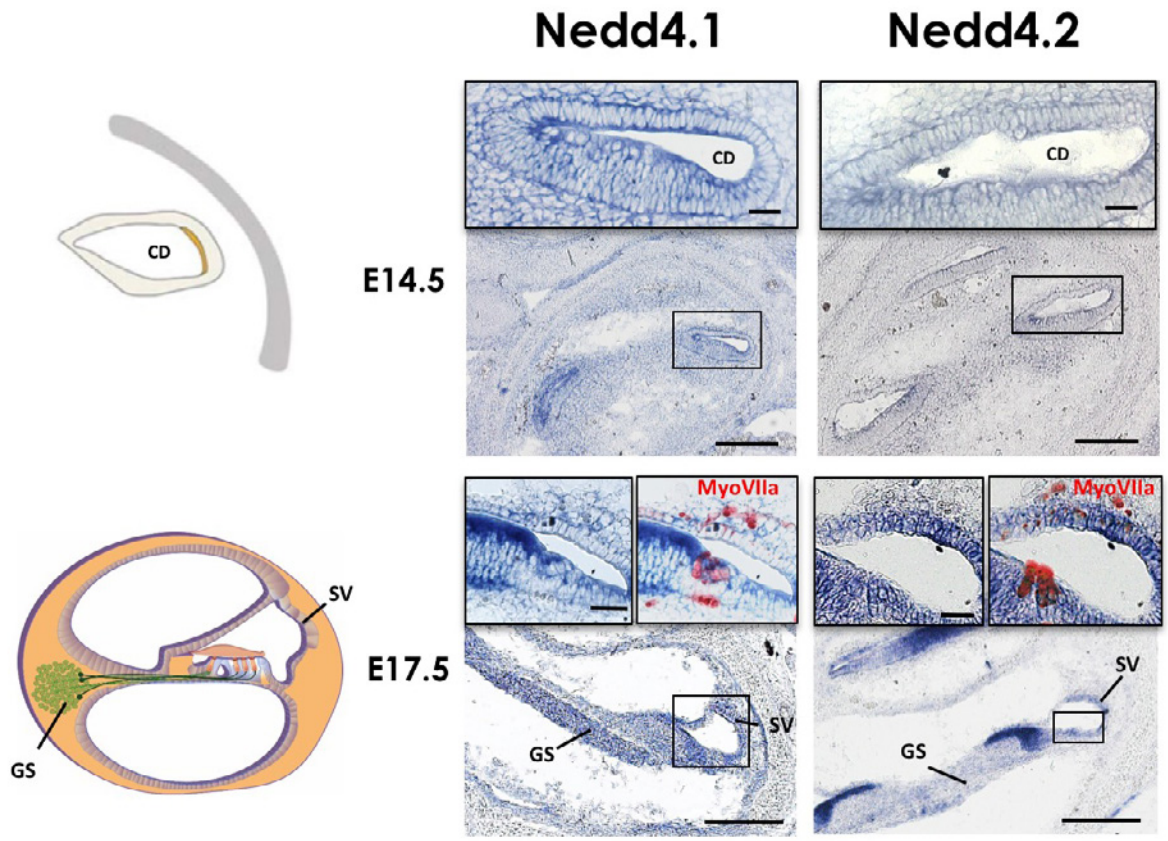

Fig. 5 Nedd4.1 and Nedd4.2 mRNA expression pattern in the developing cochlea. SV=stria vascularis, GS= spiral ganglion, CD= cochlear duct.

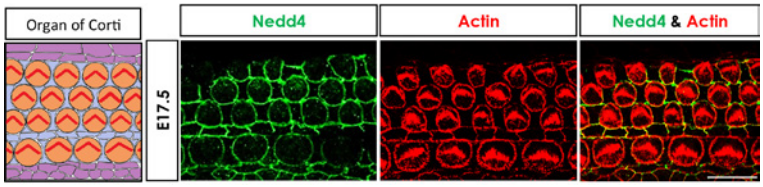

Fig. 6 Nedd4.1/2 are specifically expressed in cell junctions in the developing organ of Corti.

The progressive hair cell loss in the Nedd4-2 cKO mice might be explained by a defect of ion concentration in the endolymph. Indeed, the low sodium and high potassium concentrations in the cochlear canal are generated by the stria vascularis and are crucial for the mechanotransduction of the sound by the hair cells. It has been described that Nedd4-2 is associated to transport proteins and ion channels causing their ubiquitylation. Therefore, we studied the stria vascularis of Nedd4-2cKO cochleae by semi-thin sections (Fig. 8) and observed some defects (swollen cells and cytoplasmic protrusions) that we are currently quantifying. In addition, we have measured the thickness of the SV and our preliminary results obtained on 3 animals of each phenotype suggest a difference that we plan to confirm in the future by increasing the number of animals. To further confirm these results, we made use of another conditional knockout strategy in which we delete Nedd4.2 only in the future sensory epithelium using Sox2-Cre-ERT2 mouse line. Our preliminary results show that in these mice we also observed a progressive degeneration of hair cells. Altogether, these results demonstrate a major contribution of the ubiquitin ligase Nedd4-2 in the maintenance of mouse cochlear integrity in a cell autonomous manner and suggest that Nedd4-2 mutations in humans could lead to progressive hearing loss following premature sensory HC loss.

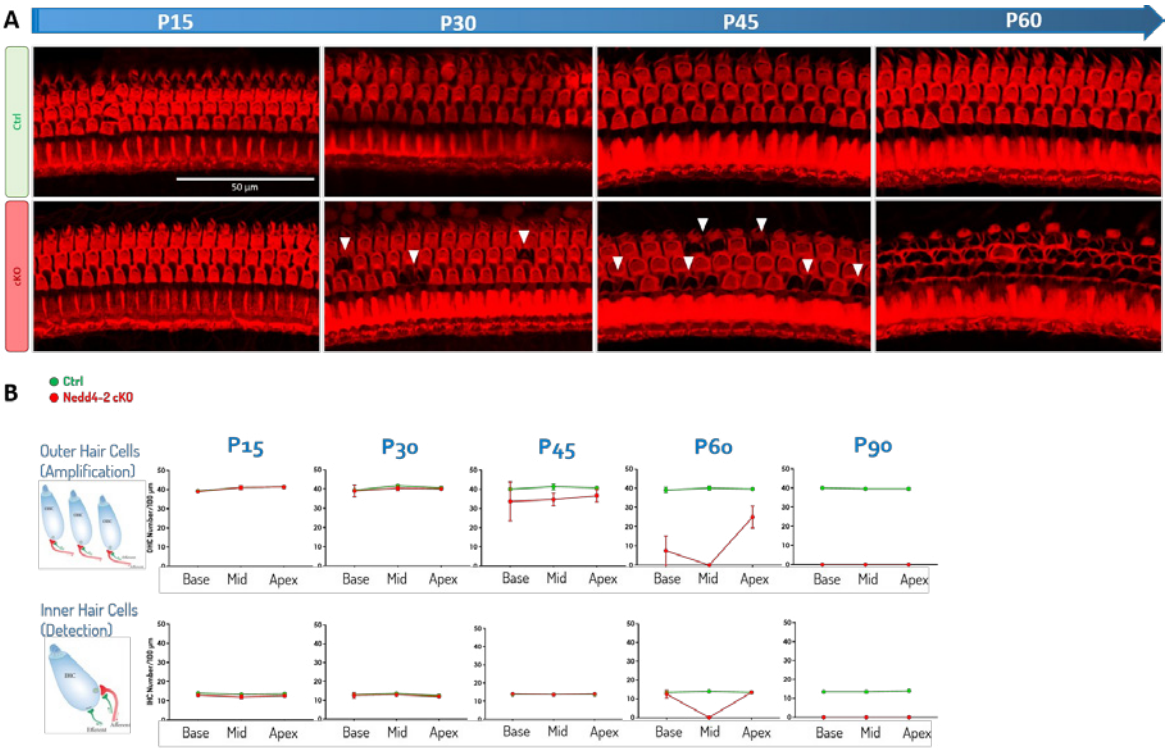

Figure 7: Analysis of the hair bundle of adult Nedd4-2 cKO cochleae. A: Actin staining of organs of Corti from controls and Nedd4-2 cKO animals at various stages (postnatal day 15, 30, 45 and 60). The white arrowheads indicate missing hair cells. B: Quantification of hair cell density in each cochlear turn at different postnatal stages.

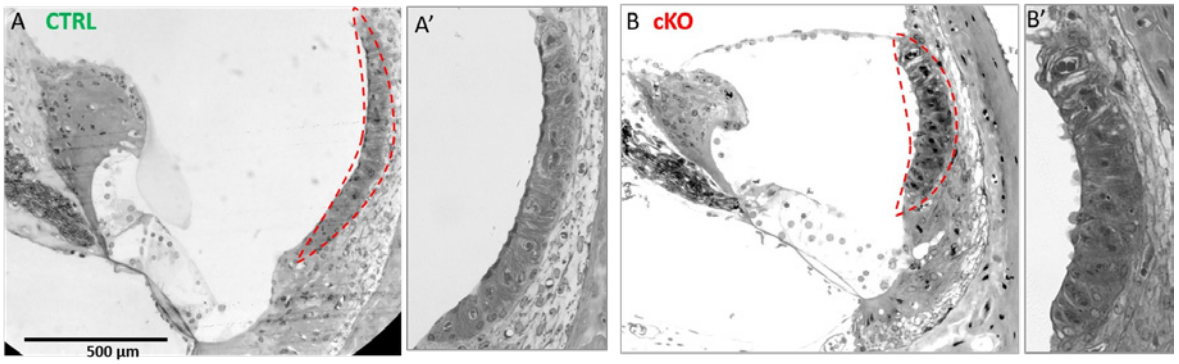

Figure 8: Semi-thin sections of the stria vascularis labelled by toluidine blue. Semi-thin section showing the cochlear canal of a control (A) and a Nedd4-2 cKO (B). The red dotted ellipse highlight the stria vascularis of a control (A') and a Nedd4-2 cKO mutant (B'). Stage = P55.

3. Publications of the laboratory in 2017 and 2019 supported by the F.M.R.E.

- Morelli, g., Avila, A., Ravanidis, S., Aourz, N., Neve, R.L., Rigo, J.-M.*, **Nguyen, L**.*, and Brône, B*. : Cerebral cortical circuitry formation requires functional glycine receptors.
  Cereb Cortex (2017), 27(3):1863-1877 (I.F. 2015= 6.559) *equal contribution
- Van den Ackerveken, P., Mounier, A., Huyghe, A., Sacheli, R., Vanlerberghe, P.-B., Volvert, M.-L., Delacroix, L., **Nguyen, L.**, and **Malgrange, B.**: The miR183/ItgA3 axis is a key regulator of prosensory area during early inner ear development
  Cell Death Differ (2017), 24(12):2054-2065. (I.F. 2016= 8.339)
- Laguesse, S., Close, P., Van Hees, L., Chariot, A., **Malgrange, B.**, and **Nguyen, L** . : Loss of Elp3 impairs the acetylation and distribution of connexin-43 in the developing cerebral cortex.
  Front Cell Neurosci (2017), (11:#122). doi: 10.3389/fncel.2017.00122. eCollection 2017.8 (I.F. 2016= 4.555)
- Agirman, G. Broix, L., and **Nguyen L**. : Cerebral cortex development: an outside-in perspective.
  FEBS Lett (2017) 591(24): 3978-3992 (I.F. 2016= 3.623.)
- Gladwyn-Ng, I., Cordon Barris, L., Alfano, C., Creppe, C., Couderc, T., Morelli, G., Thelen, N., America, M., Bessières, B., Ench-Razavi, F., Bonnière, M., Susuki, I., Flamand, M., Vanderhaeghen, P., Lecuit, M., and **Nguyen, L** . : Loss of Stress-induced unfolded protein response contributes to Zika virus-associated microcephaly.
  Nature Neuroscience (2018), 21(1):63-71 (I.F. 2018= 19.912)
- Silva, C. G., Peyre, E., Adhikari, M. H., Tielens, S., Tanco, S., Van Damme, P., Magno, L., Krusy, N., Agirman, G., Magiera, M. M., Kessaris, N., **Malgrange, B.**, Andrieux, A., Janke, C., and **Nguyen, L**.: Cell intrinsic control of interneuron migration drives cortical morphogenesis.
  Cell (2018), 172(5): 1063-78 (I.F. 2018= 31.398)
- Morelli, G., Even, A., Gladwyn-Ng, I., Le Bail, R., Shilian, M., Godin, J.D., Peyre, E., Hassan, B., Besson, A., Rigo, J.-M., Weil, M., Brône, B., Janke, C., and **Nguyen, L**.: p27Kip1 modulates axonal transport by regulating α tubulin acetyltransferase 1 stability.
  Cell Reports (2018), 23(8): 2429-2442 (I.F. 2018= 7.815)
- Marlier, Q., Jibassia, f., Verteneuil, S., Linden, J., Kaldis, P., Meijer, L., **Nguyen, L**., Vandenbosch, R., and **Malgrange, B.**: Genetic and pharmacological inhibition of Cdk1 provides neuroprotection towards ischemic neuronal death.
  Cell death discovery (2018), 4(43) doi: 10.1038/s41420-018-0044-7. eCollection 2018 (I.F. 2018= n.a.)
- Morelli, G., Even, A., Gladwyn-Ng, I., Le Bail, R., Shilian, M., Godin, J.D., Peyre, E., Hassan, B., Besson, A., Rigo, J.-M., Weil, M., Brône, B., Janke, C., and **Nguyen, L**.: p27Kip1 modulates axonal transport by regulating α tubulin acetyltransferase 1 stability.
  Cell Reports (2018), 23(8): 2429-2442 (I.F. 2018= 8.032)
- Caron, N. Genin, E.C., Marlier, Q., Verteneuil, S., Beukelaers, P., Morel, L., Hu, M. G., Hinds, P. W., Meijer, L., **Nguyen, L**., Vandenbosch, R., and **Malgrange, B.**
  Cell Mol Lifes Sci (2018), 75(20): 3817-3827 (I.F. 2018= 6.721)
- Uzquiano, A., Gladwyn-ng, I., **Nguyen L.**, Reiner, O., Götz, M., Matsuzaki, F., and Francis, F. : Cortical progenitor biology: key features mediating proliferation versus differentiation.
  J Neurochem (2018) 146(5): 500-525 (I.F. 2017= 4.609.)
- Lecuit, M., and **Nguyen L**. : Lessons learnt from the emergence of Zika virus.
  Nature Microbiology (2018) 591(24): 3978-3992 (I.F. 2017= 14.174.)
- Even, A., * Morelli, G., * Broix, L., * Scaramuzzino, C., Turchetto, S., Gladwyn-Ng, I., Le Bail,R., Shilian, M., Freeman, S., Magiera, M.M., Hassan, B., A.S., J. Krusy, N., Malgrange, B., Brône, B., Dietrich, P., Dragatsis, I., Janke, C., Saudou, F., Weil, M., * and **Nguyen, L**. *: ATAT1-enriched vesicles promote microtubule acetylation via axonal transport.
  Science Advances (2019) 5(12):eaax2705 (I.F. 2018= 12.804)

4. Other publications of the laboratory in 2017 and 2018

- Broix, L., Asselin, L., Silva, C. G., Ivanova, E. L., Tilly, P., Gilet, J. G., Lebrun, N., Jagline, H., Muraca, G., Saillour, Y., Drouot, N., Reilly, M. L., Francis, F., Benmerah, A., Bahi-Buisson, N., Belvindrah, R.,
  Nguyen, L., Godin, J. D., Chelly, J., and Hinckelmann, M. V.: Ciliogenesis and cell cycle alteraions to
- KIF2A-related malformations of cortical development
  Hum Mol Genet (2017), in press, Oct 25. doi: 10.1093/hmg/ddx384. (I.F. 2016= 5.340)
- Bento-Abreu, A., Jager, G., Swinnen, B., Rué, L., Hendrickx, S., Jones, A., Staats, K. A.,Taes, I., Eykens, C., Nonneman, A., Nuyts, R., Timmers, M., Silva, L., Chariot, A., **Nguyen,L.**, Ravits, J., Lemmens, R., Cabooter, D., Ludo, VDB, Van Damme, P., Al-Chalabi, A.,Bystrom, A., and Robberecht, W. : Elongator subunit 3 (ELP3) modifies ALD trough tRNA Modification.
  Hum Mol Genet (2018), *in press* (I.F. 2018= 4.902).

– Nganou, G., Silva, C.G., Gladwyn-Ng, I., Engel, D., Coumans, B., Delgado-Escueta, A.V., Tanaka, M., **Nguyen, L.**, Grisar, T., de Nijs, L., and Lakaye, B. : Importin-8 modulates division of apical progenitors, dendritogenesis and tangential migration during development of mouse cortex
Front Cell Neurosci (2018), (9, #129): 1-18 (I.F. 2018= 4.300)
– Kum, D.B., Mishra, N., Boudewijns, R., Gladwyn-Ng, I., Alfano, C., Ma, J., Schmid, M.A., Marques, R.E., Schols, D., Patein, S., **Nguyen, L.**, Neyts, J., and Dallmeier, K. : A yellow fever virus 17D based chimeric Zika virus vaccine cabndidate that protects against lethal Zika infection and congenital malformation in mice
NPJ Vaccines (2018), 3:56 (I.F. 2018= 3.143)
– Beaufrère, A., Bessières, B., Bonnière, M., Driessen, M., Alfano, C., Couderc, T., Thiry, M., Thelen, N., Lecuit, M., Attiè-Bitach, T., Vekemans, M., Ville, Y., **Nguyen, L.**, Leruez-Ville, M., and Encha-Razavi, F.,: A clinical and histopathological study of malformations observed in fetuses infected by the Zika virus.
Brain Pathol (2019), 29(1):114-125 (I.F. 2018= 6.187)
– Ortega, G., Falk, S., Johansson, P. A., Peyre, E., Broix, L., Sahu, S. K., De Juan Romero, C., Draganova, K., Vinopal, S., Chinnappa, K., Gavranovic, A., Karakaya, T., Merl-Pham, J., Geerlof, A., Feederle, R., Shao, W., Shi, S., Hauck, S. M., Bradke, F., Borrell, V., Tiwari, V. K., Huttner, W., Wilsch-Bräuninger, **Nguyen, L.**, and Götz, M. : A new centrosome protein regulates neurogenesis and microtubule organization.
Nature (2019) 567(7746):113-117 (I.F. 2018= 41.577)
– Telley, L.,* Agirman, G.*, Prados, J., Oberst, P., Vitali, I., **Nguyen, L.**, Dayer, A., and Jabaudon, D. : Single-cell transcriptional dynamics in the developing mouse neocortex.
Science (2019) 364(6440) (I.F. 2018= 41.058)

1. Rash, B. G. & Grove, E. A. Area and layer patterning in the developing cerebral cortex. *Curr Opin Neurobiol* **16**, 25-34 (2006).
2. Gupta, A., Tsai, L. H. & Wynshaw-Boris, A. Life is a journey: a genetic look at neocortical development. *Nat Rev Genet* **3**, 342-355 (2002).
3. Anderson, S. A., Eisenstat, D. D., Shi, L. & Rubenstein, J. L. Interneuron migration from basal forebrain to neocortex: dependence on Dlx genes. *Science* **278**, 474-476 (1997).
4. Sarnat, H. B. & Flores-Sarnat, L. A new classification of malformations of the nervous system: an integration of morphological and molecular genetic criteria as patterns of genetic expression. *European journal of paediatric neurology : EJPN : official journal of the European Paediatric Neurology Society* **5**, 57-64 (2001).
5. Sarnat, H. B. & Flores-Sarnat, L. Neuroembryology and brain malformations: an overview. *Handbook of clinical neurology* **111**, 117-128, doi:10.1016/B978-0-444-52891-9.00012-9 (2013).
6. Spreafico, R. & Tassi, L. Cortical malformations. *Handbook of clinical neurology* **108**, 535-557, doi:10.1016/B978-0-444-52899-5.00047-2 (2012).
7. Mateo Sanchez, S., Freeman, S. D., Delacroix, L. & Malgrange, B. The role of post-translational modifications in hearing and deafness. *Cell Mol Life Sci*, doi:10.1007/s00018-016-2257-3 (2016).
8. Nelson, R. F. *et al.* Selective cochlear degeneration in mice lacking the F-box protein, Fbx2, a glycoprotein-specific ubiquitin ligase subunit. *J Neurosci* **27**, 5163-5171, doi:10.1523/JNEUROSCI.0206-07.2007 (2007).
9. Kazmierczak, M. *et al.* Progressive Hearing Loss in Mice Carrying a Mutation in Usp53. *J Neurosci* **35**, 15582-15598, doi:10.1523/JNEUROSCI.1965-15.2015 (2015).
10. Narimatsu, M. *et al.* Regulation of planar cell polarity by Smurf ubiquitin ligases. *Cell* **137**, 295-307, doi:10.1016/j.cell.2009.02.025 (2009).
11. Broix, L. *et al.* Mutations in the HECT domain of NEDD4L lead to AKT-mTOR pathway deregulation and cause periventricular nodular heterotopia. *Nat Genet* **48**, 1349-1358, doi:10.1038/ng.3676 (2016).
12. Kappeler, C. *et al.* Branching and nucleokinesis defects in migrating interneurons derived from doublecortin knockout mice. *Hum Mol Genet* **15**, 1387-1400 (2006).
13. Godin, J. D. *et al.* p27(Kip1) is a microtubule-associated protein that promotes microtubule polymerization during neuron migration. *Dev Cell* **23**, 729-744, doi:10.1016/j.devcel.2012.08.006 (2012).
14. Tielens, S. *et al.* Elongator controls cortical interneuron migration by regulating actomyosin dynamics. *Cell research* **26**, 1131-1148, doi:10.1038/cr.2016.112 (2016).
15. Silva, C. G. *et al.* Cell-Intrinsic Control of Interneuron Migration Drives Cortical Morphogenesis. *Cell* **172**, 1063-1078 e1019, doi:10.1016/j.cell.2018.01.031 (2018).

Geneeskundige Stichting Koningin Elisabeth
Fondation Médicale Reine Elisabeth
Königin-Elisabeth-Stiftung für Medizin
Queen Elisabeth Medical Foundation

Final report of the research group of

Prof. dr. Timmerman Vincent, PhD

Universiteit Antwerpen (UA)

Principal investigator:

Prof. dr. Timmerman Vincent, PhD
Peripheral Neuropathy Research Group,
University of Antwerp – CDE,
Parking P4, Building V, Room 1.30,
Universiteitsplein 1
2610 Antwerpen
Belgium
E-mail: vincent.timmerman@uantwerpen.be

Team members who have contributed to this GSKE project report:
Postdoc: Manisha Juneja, PhD (period covered 2017-2018)
PhD students: Michiel Krols (2017), Mansour Haidar (2018), Elias Adriaenssens (2017-2019), Leen Vendredy (2018-2019), Angela Sisto (2019) and Jonas Van lent (2019)
Lab technician: Vicky De Winter (2017-2019)

Unravelling the novel molecular pathways contributing to distal Hereditary Motor Neuropathy caused by mutant HSPB8, with the aim to identify potential therapeutic targets

1. Research report:

1.1. State of the art:

Charcot-Marie-Tooth (CMT) neuropathies comprise a clinically diverse and genetically heterogeneous group of monogenic disorders affecting the peripheral nervous system. It is a progressive debilitating condition that can result in muscle weakness, sensory loss, foot deformities, fatigue, pain and injury. Found in both genders and in all populations, it affects an estimated 1 in 2500 (or 2.8 million) people worldwide. An important group of genes mutated in CMT are those coding for small heat shock proteins (HSPBs). Although constitutively expressed by every cell, mutations in three of these HSPBs cause exclusive degeneration of the peripheral nervous system. As molecular chaperones, HSPBs are regulated by various types of stress and responsible for protein quality control and protein folding. In addition, they play a role in many essential cellular processes such as apoptosis, autophagy, splicing and translation, cytoskeleton dynamics and neuronal survival.

1.2. Aims of the GSKE project 2017-2018-2019:

The development of induced pluripotent stem cells (iPSC) has brought together the genetic accuracy of a patient-derived model and the possibility of having the disease-specific cell type. This model promises to influence modern medicine and drug development particularly for neurological disorders by providing an unlimited access to patient-derived neurons. We will take advantage of the iPSC model along with a knock-in/knock-out mouse model that we have recently developed for distal hereditary motor neuropathy (dHMN), caused by mutations in the small heat shock protein HSPB8, to identify and validate translationally relevant pathway(s) leading to axonal degeneration, and with the ambition to select and test promising therapeutic targets.

1.3. Results obtained:

We made a survey of all published mutations in HSPBs; so far 32 mutations occur in HSPB1 and were reported in 169 patients, nine mutations have been described in HSPB8 in 68 patients, and one mutation in HSPB3 in two patients. The phenotypic spectrum of HSPB mutations may not be restricted to axonal CMT disease (CMT2) or distal hereditary motor neuropathy (dHMN), but mutations were also reported in three sporadic patients with amyotrophic lateral sclerosis (ALS) or distal myopathy. This indicates that mutations in multifunctional HSPBs can give rise to multiple neurodegenerative and neuromuscular phenotypes (Adriaenssens et al 2017).

Since we first described the K141N missense mutation in the *HSPB8* gene (Irobi et al 2004), **we and others reported additional patients and families with *HSPB8* mutations** (Echaniz-Laguna et al 2017a). Interestingly, most mutations target the same lysine residue (K141E, K141M, K141N, K141T) in the highly conserved α-crystallin domain of the HSPB8 protein. The spectrum of diseases caused by mutations in the *HSPB8* gene was recently expanded to myofibrillar myopathy (MFM) (Adriaenssens et al 2017, Echaniz-Laguna et al 2017b, Ghaoui et al 2016). **To delineate the molecular deficits and functional consequences of *HSPB8* mutations, we generated a knock-in mouse model for the K141N mutation mimicking the dHMN phenotype** (Bouhy et al 2018). We observed that homozygous knock-in mice (*Hspb8*$^{K141N/K141N}$) develop a progressive axonopathy resulting in locomotor deficits. At the ultrastructural level, mice accumulate the mutant Hspb8 protein and display degenerative patterns similar to dHMN patients. Interestingly, these animals also develop a progressive MFM phenotype as observed in some patients with HSPB8 mutations (Ghaoui et al 2016).

Our mouse model allowed us to also generate a *Hspb8* knock-out using the same targeting construct. The homozygous *Hspb8* knock-out animals (*Hspb8*$^{-/-}$) do not show any sign of axonopathy and display only minor (subclinical) muscle irregularities. The knock-out mice are indistinguishable from the wild type mice on the Rotarod and therefore present with a much milder phenotype than the *Hspb8* knock-in animals (Bouhy et al 2018). Although we did not expect that deletion of *Hspb8* would be so well tolerated, this may actually offer an attractive therapeutic strategy. Based on these findings, we expect that reducing the expression of Hspb8 in the knock-in mice may improve the dHMN and MFM phenotype (i.e. phenocopying the *Hspb8*$^{-/-}$ mouse). PhD student L. Vendredy was attracted thanks to this GSKE project within our research team and she obtained a competitive FWO-SB fellowship (starting from 1/1/2018) to explore this approach.

To this end, Leen Vendredy tested compounds from a high-throughput screen that was performed in the lab of our collaborator Prof. A. Poletti (Crippa et al 2016). In this published screen, an FDA/EMA approved library was used to identify compounds that, as a side-effect, up- or down-regulate the expression of human HSPB8. **As we aim to downregulate the expression of HSPB8, we performed a dose-response study for the top 10 expression inhibitors.** In HeLa cells, meclofenamate sodium (MFS) treatment resulted in a dose-dependent decrease of HSPB8. Unfortunately, the drug was unable to reproduce and inhibit the HSPB8 expression in NSC34 or C2C12 cells (two murine cell lines). The high-throughput screen mentioned above was performed with the human HSPB8 gene promoter, and although these drugs are working for human cell lines, these might not be effective for the mouse *Hspb8* promoter. Since our aim is to validate these drugs on our published *Hspb8* mouse model, it is a prerequisite for them to be effective on the mouse *Hspb8* promoter. **We therefore started with the development of a novel reporter line that can be used for a new high-throughput screen.** The new screen will be performed on mouse embryonal fibroblasts (MEF) derived from the abovementioned mouse model (CRISPR/Cas9-edited to tag Hspb8 with eGFP-P2A-mCherry) ensuring that the identified compounds are effective on both human and murine cells. We are currently looking for funding sources that would help us to cover the costs of the new high-throughput screening and allow us to embark this last part of the project. Lead compounds that are identified in the high-throughput screen will be validated *in vivo* in the Hspb8 knock-in mouse model as well as on human iPSC-derived motor neurons, thereby ensuring the translation to human.

The careful characterization of the mouse model helped us to identify a first therapeutic target for HSPB8-associated forms of CMT disease. However, **with the help of this GSKE-funding, we were able to identify two more pathways which are altered by mutant HSPB8 and which could form interesting therapeutic targets**. What is appealing about these two additional targets is that they are not only affected by mutations in HSPB8 but also by mutations in HSPB1, another member of the HSPB family. As such, targeting these molecular pathways may allow us to develop a single therapeutic approach that would benefit a spectrum of HSPB-associated CMT patients.

The first shared pathway we identified, highlighted in a review of emerging common pathomechanisms in inherited peripheral neuropathies, is autophagy (Haidar & Timmerman 2017). **Mutations in both HSPB1 and HSPB8 impair the formation and degradation of autophagosomes** (Guilbert et al 2018, Haidar et al 2019). Our molecular work showed that the function of HSPB1 and HSPB8 converges at the formation of *sequestosome 1* (SQSTM1/p62) puncta. The SQSTM1/p62 acts as a selective receptor for ubiquitinated proteins and clusters them in small dense round formations (known as p62 bodies). These p62 bodies undergo phase-separation and thereby promote the engulfment of these toxic aggregates by autophagic membranes. After the engulfment, the cargo is degraded by autophagosomes which fuse with lysosomes. **Our results show that both HSPB1 and HSPB8 interact and/or promote p62-puncta formation and thereby regulate one of the initial steps of autophagosome formation.** CMT causing mutations in HSPB1 and HSPB8 impair this function and lead to a decreased autophagic

flux which could be detrimental for terminally differentiated cells like motor neurons. We found that in both our models, iPSC-derived motor neurons and the knock-in *Hspb8* mouse model, the autophagic pathway was impaired. As this is the first time that the two HSPBs, HSPB1 and HSPB8, evidently share the same pathomechanism (as their activities merge in SQSTM1/p62 modulation), this pathway arises as a promising new drug target for the group of HSPB-related CMT patients.

Thanks to the GSKE project we attracted Angela Sisto as a second PhD student who will proceed with this project and screen for FDA/EMA-approved molecules that are able to reverse the autophagic deficits caused by mutant HSPB1 and HSPB8. We will validate the effect of the selected drugs in motor neurons differentiated from patient-derived iPSCs with the aim to improve the neurodegenerative phenotype. In the perspective of a preclinical study, we also crossed-bred the knock-in *Hspb8* mouse model with the GFP-LC3 mouse (Mizushima 2009), a standard model to monitor autophagy in mammals, to obtain a *Hspb8/GFP-LC3* double transgenic mouse model. This not only allows us to expand the knowledge on the mouse phenotype regarding the autophagic deficits in the murine tissues (muscles and peripheral nerves), it also provides a powerful platform to validate the most effective compound *in vivo.* In parallel with the drug screening, we will characterize the molecular interplay further, thereby providing insights in the mechanism-of-action of new drugs. So Angela Sisto, who recently also obtained a competitive FWO-SB fellowship (starting from 1/11/2019), will proceed to explore autophagy as a novel target and the first shared pathomechanism between these two genes. **Thanks to the support of the GSKE-grant we have every model available to proceed in this direction and we hope to identify a small molecule in the high-throughput screen that can reverse the autophagic deficits.**

In addition to autophagy, we identified one more pathomechanism that is shared by both HSPBs. Data obtained with the support of a previous GSKE-grant demonstrated that mitochondrial transport was severely compromised in a mutant HSPB1 transgenic mouse model (in collaboration with Prof. L. Van Den Bosch, KULeuven). In this study we were able to identify a potential novel treatment for HSPB1-related neuropathy as restoration of mitochondrial transport led to amelioration of the phenotype (d'Ydewalle et al 2011). However, why abundant cytosolic chaperones like HSPB1 would cause a mitochondrial transport defect remained enigmatic. The work from PhD student Elias Adriaenssens now identified a possible answer to this question. **Unexpectedly, HSPBs were found to translocate into mitochondria**. This raised the possibility that mutations in HSPB1 are the direct cause of mitochondrial dysfunction. Indeed, mutations in the highly conserved alpha-crystallin domain of HSPB1 were found to increase mitochondrial residence as a consequence of binding stronger to molecular client proteins inside mitochondria. A mutation (P182L) in the C-terminal domain of HSPB1, which is associated with one of the most severe dHMN phenotypes, even prohibited HSPB1 from being imported into the mitochondria. These results may thus form part of the explanation as for why restoring mitochondrial transport was beneficial in a mutant HSPB1 mouse model (full data are reported in the PhD thesis of Elias Adriaenssens in December 2019, and a manuscript is in preparation).

Our data suggest that HSPB8 is also imported into the mitochondria and mitochondrial transport defects may thus also form a shared disease mechanism. Indeed, patient-derived iPSC-lines show a clear axonal transport problem in HSPB8 mutant neuronal cells (**Figure 1A**). Moreover, in addition to a deficit in their axonal transport, also the morphology of the mitochondria is altered (higher circularity and higher solidity compared to healthy control lines) (**Figure 1B**). Also in our knock-in *Hspb8* mouse, mitochondrial abnormalities were reported further supporting the notion that mitochondrial deficits are an underlying pathomechanism. Given the positive results obtained in a transgenic mutant *HSPB1* mouse model, where we found in collaboration with Prof. L. Van Den Bosch (KULeuven) that the rescue of axonal transport led to an amelioration of the phenotype, we are encouraged to explore this pathway further and evaluate whether restoration of axonal transport in the *Hspb8* knock-in mice can also ameliorate the neuropathy phenotype.

1.4. Outlook for the future:

In summary, where we still had to identify molecular targets for HSPB8-associated CMT at the start of this GSKE-project, **we now have identified three potential therapeutic targets (Figure 2)**. The successful identification of these molecular pathways and therapeutic targets forms a big leap forward for this untreatable disease. With the planned high-throughput screens we hope to identify compounds that can either downregulate the expression of HSPB8, rescue the autophagic deficits, or rescue the mitochondrial defects and as such allow us to test the first treatment strategies for HSPB8-related CMT in our new disease models (knock-in mouse model and patient iPSC-derived motor neurons). The successful identification of such compounds will accelerate the therapy development for this rare disorder and may finally bring the first therapies towards the clinical stage.

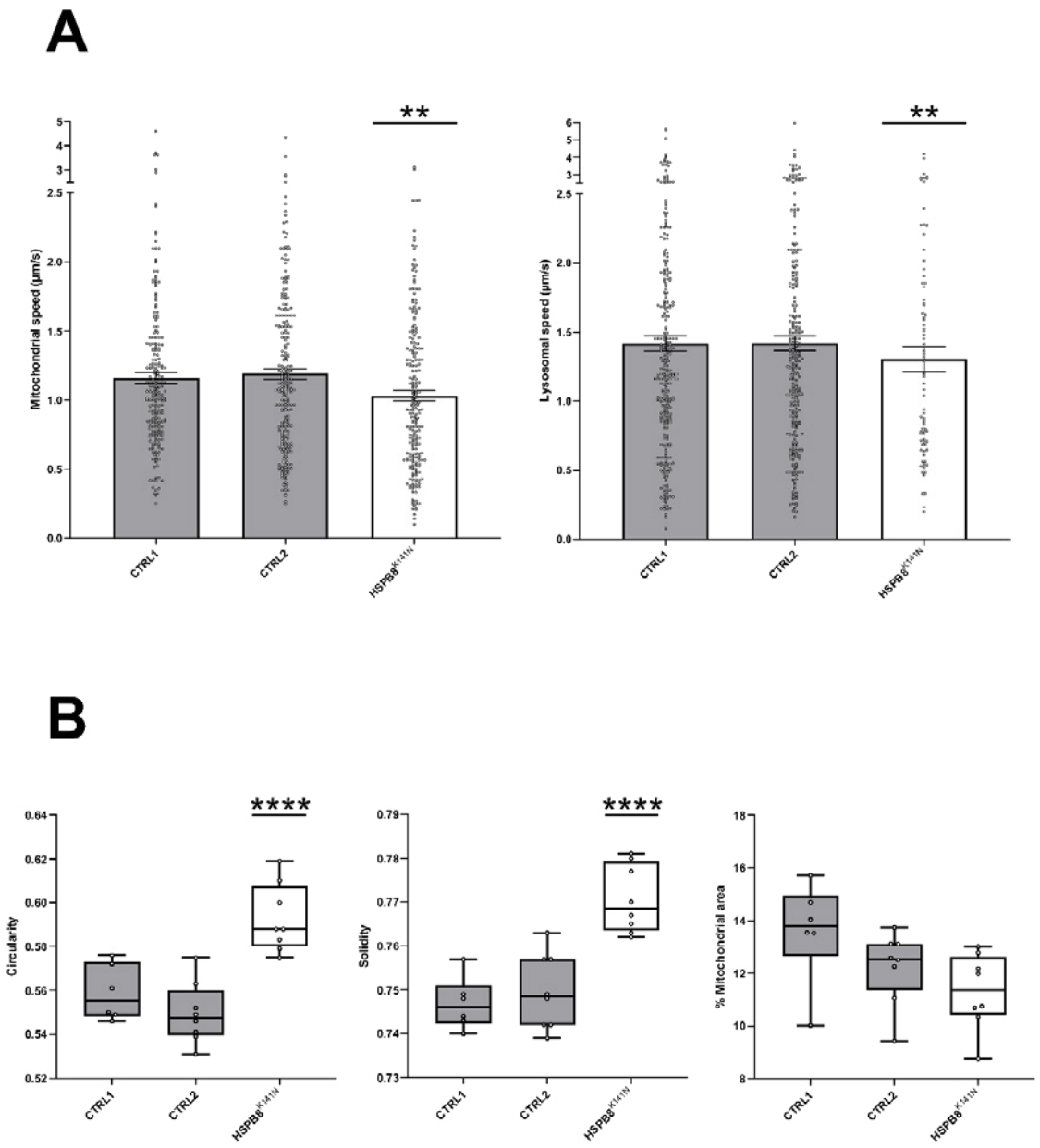

Figure 1: **Characterization of derived motor neurons from the HSPB8^{K141N} patient iPSC line.** (A) Quantification of mitochondrial (left) and lysosomal (right) speed (µm/s). (B) Quantification of mitochondrial morphology parameters: circularity (left), solidity (middle) and % mitochondrial area (right). Data values represent mean ± SEM. One-way ANOVA with post-hoc Dunnett test is used to compare the patient line with the average of both two controls; *, **, *** for *P* values of 0.05, 0.01, and 0.001, respectively (*unpublished results generated by PhD student Jonas Van lent*).

Graphical summary

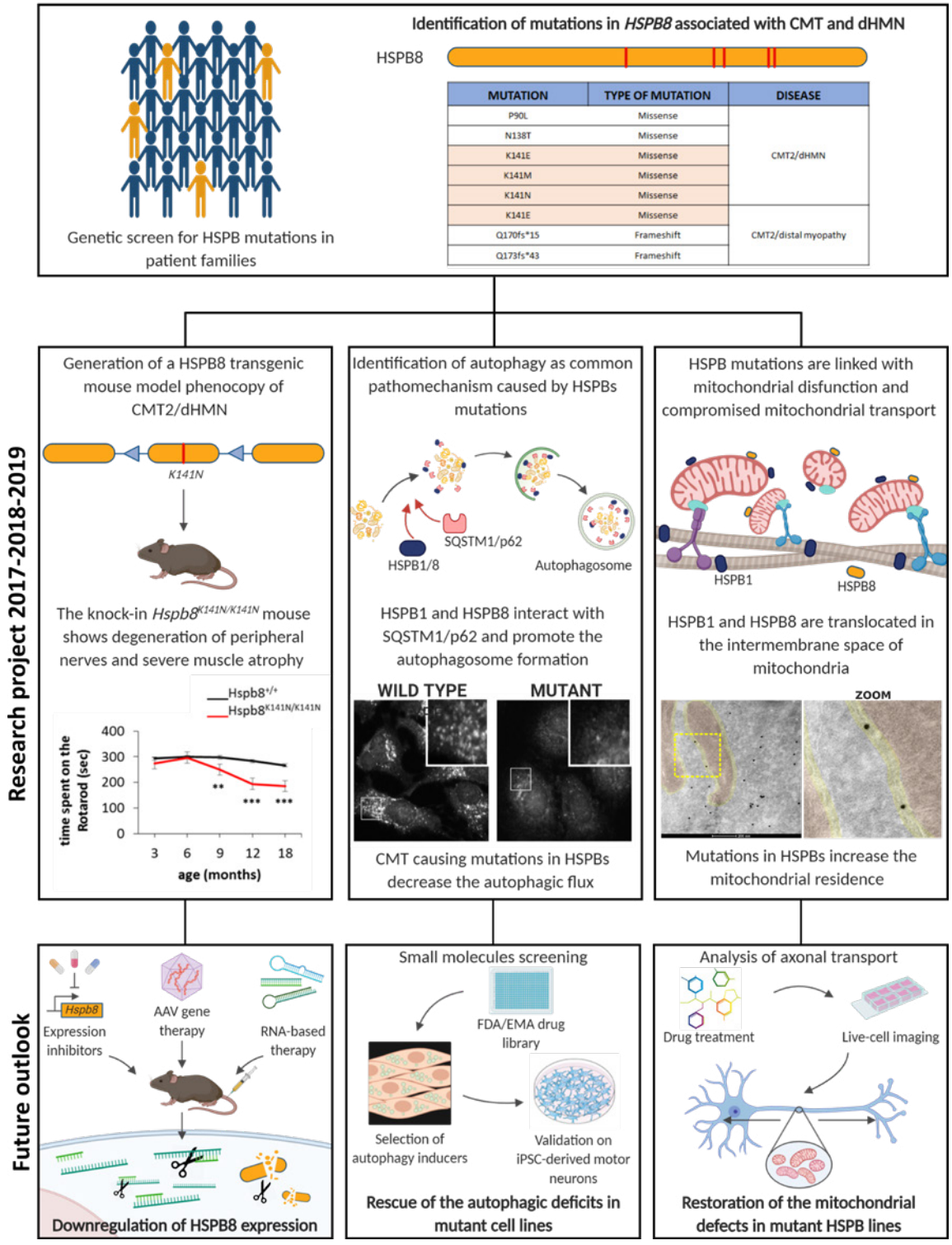

Figure 2: Schematic representation of the main results obtained in the past 3 years of the GSKE project (2017-2018-2019), complemented with future perspectives.

2. Research Activities 2017-2018-2019:

Articles published in International Journals – Acknowledging the GSKE:

1. Beijer D., Sisto A., Van lent J., Baets J., Timmerman V.; Invited Review: Defects in axonal transport in inherited neuropathies. Journal of Neuromuscular Diseases 6:401-419 (2019) Epub: 2019-09-20 (PMID: 31561383) (I.F.: 2.44, new journal and first IF)
2. Wu,J., Ma,S., Sandhoff,R., Ming,Y., Hotz-Wagenblatt,A., Timmerman,V., Bonello-Palot,N., Schlotter-Weigel,B., Auer-Grumbach,M., Seeman,P., Löscher,W., Reindl,M., Weiss,F., Mah,E., Weisshaar,N., Madi,A., Mohr,K., Schlimbach,T., Velasco Cárdenas,R.M-H., Koeppel,J., Grünschläger,F., Müller,L., Baumeister,M., Brügger,B., Schmitt,M., Wabnitz,G., Samstag,Y., Cui,G.: Loss of neurological disease HSAN-I-associated gene SPTLC2 impairs CD8+ T cell responses to infection by inhibiting T cell metabolic fitness. Immunity 50(5): 1218-1231 (2019) Epub: 23-Mar-2019 (PMID: 30952607) (I.F.: 21.522)
3. Haidar,M., Asselbergh,B., Adriaenssens,E., De Winter,V., Timmermans,J-P., Auer-Grumbach,M., Juneja,M., Timmerman,V.: Neuropathy-causing mutations in HSPB1 impair autophagy by disturbing the formation of SQSTM1/p62 bodies. Autophagy 15(6): 1051-1068 (2019) Epub: 23-Jan-2019 (PMID: 30669930) (I.F.: 11.059)
4. Bernard-Marissal,N., van Hameren,G., Juneja,M., Pellegrino,C., Louhivuori,L., Bartesaghi,L., Rochat,C., El Mansour,O., Médard,J-J., Croisier,M., Maclachlan,C., Poirot,O., Uhlén,P., Timmerman,V., Tricaud,N., Schneider,B.L., Chrast,R.: Altered interplay between endoplasmic reticulum and mitochondria in Charcot-Marie-Tooth type 2A neuropathy. PNAS 116(6): 2328-2337 (2019) Epub: 18-Jan-2019 (PMID: 30659145) (I.F.: 9.58)
5. Juneja,M., Burns,J.M., Saporta,M.A., Timmerman,V.: Challenges in modelling the Charcot-Marie-Tooth neuropathies for therapy development. Journal of Neurology, Neurosurgery and Psychiatry 90(1): 58-67 (2019) Epub: 17-Jul-2018 (PMID: 30018047) (I.F.: 8.272)
6. Krols,M.*, Asselbergh,B.*, De Rycke,R., De Winter,V., Seyer,A., Muller,F-J., Kurth,I., Bultynck,G., Timmerman,V.*, Janssens,S.* (* equal contribution): Sensory neuropathy-causing mutations in ATL3 affect ER-mitochondria contact sites and impair axonal mitochondrial distribution. Human Molecular Genetics 28(4): 615-627 (2019) Epub: 18-Oct-2018 (PMID: 30339187) (I.F.: 4.544)
7. Bouhy,D., Juneja,M., Katona,I., Holmgren,A., Asselbergh,B., De Winter,V., Hochepied,T., Goossens,S., Haigh,J.J., Libert,C., Ceuterick-de Groote,C., Irobi,J., Weis,J., Timmerman,V.: A knock-in/knock-out mouse model of HSPB8-associated distal hereditary motor neuropathy and myopathy reveals toxic gain-of-function of mutant Hspb8. Acta Neuropathologica 135(1): 131-148 (2018) Epub: 05-Aug-2017 (PMID: 28780615) (I.F.: 18.174)
8. Juneja,M., Azmi,A., Baets,J., Roos,A., Jennings,M.J., Saveri,P., Pisciotta,C., Bernard-Marissal,N., Schneider,B.L., Verfaillie,C., Chrast,R., Seeman,P., Hahn,A., De Jonghe,P., Maudsley,S., Horvath,R., Pareyson,D., Timmerman,V.: PFN2 and GAMT as common molecular determinants of axonal Charcot-Marie-Tooth disease. Journal of Neurology, Neurosurgery and Psychiatry 89(8): 870-878 (2018) Epub: 15-Feb-2018 (PMID: 29449460) (I.F.: 8.272)
9. Haidar,M., Timmerman,V.: Review: Autophagy as an emerging common pathomechanism in inherited peripheral neuropathies. Frontiers in Molecular Neuroscience 10: 143- (2017) Epub: 11-May-2017 (PMID: 28553203) (I.F.: 5.076)
10. Adriaenssens,E.*, Geuens,T.*, Baets,J., Echaniz-Laguna,A., Timmerman,V. (* equal contribution): Novel insights in the disease biology of mutant small heat shock proteins in neuromuscular diseases. Brain 140(10): 2541-2549 (2017) Epub: 01-Oct-2017 (PMID: 28969372) (I.F.: 10.84)
11. Geuens,T., De Winter,V., Rajan,N., Achsel,T., Mateiu,L., Almeida-Souza,L., Asselbergh,B., Bouhy,D., Auer-Grumbach,M., Bagni,C., Timmerman,V.: Mutant HSPB1 causes loss of translational repression by binding to PCBP1, an RNA binding protein with a possible role in neurodegenerative disease. Acta Neuropathologica Communications 5(1): 5 (2017) Epub: 11-Jan-2017 (PMID: 28077174) (I.F.: 5.414)
12. Echaniz-Laguna,A.*, Geuens,T.*, Petiot,P., Péréon,Y., Adriaenssens,E., Haidar,M., Capponi,S., Maisonobe,R., Fournier,E., Dubourg,O., Degos,B., Salachas,F., Lenglet,T., Eymard,B., Delmont,E., Pouget,J., Morales,R.J., Goizet,C., Latour,P., Timmerman,V.*, Stojkovic,T.* (* equal contribution): Axonal neuropathies due to mutations in small heat shock proteins: clinical, genetic and functional insights into novel mutations. Human Mutation 38(5): 556-568 (2017) Epub: 01-Feb-2017 (PMID: 28144995) (I.F.: 5.359)

Manuscripts under review with acknowledgements to the GSKE:

1. Alderson, R.T., Adriaenssens, E., Asselbergh, B., Pritišanac, I., Gastall, H.Y., Wälti, M., Louis, J.M., Timmerman, V.*, Baldwin, A.J.*, Benesch, J.L.P*. Dysregulation of HSP27 oligomerization and interactions by a neuropathy-causing mutation in the IPV motif. *Manuscript under revision for EMBO Journal (* corresponding authors). bioRxiv preprint first posted online Jul. 19, 2019; doi: http://dx.doi.org/10.1101/708180*
2. Adriaenssens, E. *, Tedesco, B. *, Mediani, L. *, Asselbergh, B., Crippa, V., Antoniani, F., Carra, S., Poletti, A., Timmerman, V. BAG3 Pro209 mutants associated with myopathy and neuropathy sequester chaperones of the CASA-complex in aggresomes. *Manuscript under revision for Scientific Reports. (* equal contributions) bioRxiv preprint first posted online Nov. 24, 2019; http://dx.doi.org/10.1101/853804*

3. Vendredy, L*., Adriaenssens, E*., Timmerman, V. Small heat shock proteins in neurodegenerative diseases. Invited book chapter for: "The big book on small heat shock proteins: II", editor Robert M. Tanguay (* equal contributions).

Awards and fellowships:

1. **Angela Sisto**: FWO-SB PhD fellowship started on 1st November 2019
2. **Jonas Van Lent**: DOCPRO4 PhD fellowship started in 1st October 2019
3. **Leen Vendredy**: FWO-SB PhD fellowship started on 1st January 2018
4. **Angela Sisto**: BOF-FWO-SB "opvangmandaat" from the Research Council of the University of Antwerp started on 1st January 2019 till 30 October 2019
5. **Leen Vendredy, Elias Adriaenssens, Angela Sisto, Jonas Van lent**: PNS fellowships to attend the Annual Meeting of the Peripheral Nerve Society (PNS and CMTR consortium meeting), Genova, Italy 22-25 June 2019
6. **Elias Adriaenssens**: 2019 Rotary 'Hope-in-Head' Grant
7. **Leen Vendredy, Elias Adriaenssens, M. Juneja:** PNS fellowships to attend the Annual Meeting of the Peripheral Nerve Society (PNS and CMTR consortium meeting), Baltimore, 21-25 July 2018
8. **Elias Adriaenssens**: FWO travel fellowship to attend the 3rd CSSI workshop on Small Heat Shock Proteins, Québec City, USA, 26-29 August 2018
9. **Mansour Haidar**: Travel fellowship to attend the Annual Meeting of the Peripheral Nerve Society (PNS and CMTR consortium meeting), Sitges-Barcelona, Spain, 8-12 July 2017

PhD theses:

1. **Elias Adriaenssens**: *The regulation and dysregulation of small heat shock proteins and an associated co-chaperone in health and disease;* PhD in Biochemistry and Biotechnology, Universiteit Antwerpen, 13 December 2019
2. **Mansour Haidar**: *Autophagy in inherited peripheral neuropathies: focus on the small heat shock protein HSPB1*; PhD in Biochemistry and Biotechnology, Universiteit Antwerpen, 29 March 2018
3. **Michiel Krols:** *Mutations in Atlastin-3: implications for ER membrane fusion and crosstalk with mitochondria*; PhD in Biochemistry and Biotechnology, Universiteit Antwerpen, 13 June 2017

Master theses:

1. **Tine Logghe:** *How is mitochondrial import of small heat shock proteins regulated?* Master in Biomedical Sciences, June 2019
2. **Rik van den Boom**: *Exploring the RNAi toolbox to reduce (mutant) HSPB8 expression.* Master in Biochemistry & Biotechnology, June 2019
3. **Jonas Van lent:** *Molecular phenotyping of neurons using CMT2 patient-derived iPSCs.* Master in Biochemistry & Biotechnology, January 2019
4. **Rani Boons:** *The role and import of small heat shock protein HSPB1 in mitochondria*. Master in Bioscience Engineering, Cell- and Gene technology, KULeuven, June 2018
5. **Liedewei Van de Vondel:** *Functional genomics and pathogenic validation of ARHGEF15 de novo mutation in epileptic encephalopathy*. ERASMUS Master in Biochemistry & Biotechnology, University of Barcelona, June 2018
6. **Kim Claes:** *Functional analysis of the interaction between HSPB1 and SLC25A12.* Master in Biomedical Sciences, June 2017
7. **Lotte Conings:** *Investigating the actin cytoskeleton as a common pathomechanism in axonal CMT using iPSC-derived models*. Master in Biomedical Sciences, June 2017

Chair and organizational activities:

1. **Vincent Timmerman**: (re)elected as secretary of the CMTR consortium at the Annual Meetings of the Peripheral Nerve Society (PNS) in Genova, 22-25 June 2019, Baltimore, 21-25 July 2018 and Sitges-Barcelona, Spain, 8-12 July 2017 (will be continued until 2021)
2. **Manisha Juneja**: chair at the CMTR consortium meeting at the Annual Meeting of the Peripheral Nerve Society (PNS), Baltimore, 21-25 July 2018
3. **Manisha Juneja**: co-organizer of the Thermo Fisher Scientific, Technical Stem Cell Workflow and Research Seminar, at the University of Antwerp, with a lecture: *Modeling CMT using iPSC derived motor neurons*, Antwerp, 19 October 2017

Invited research seminars:

1. **Vincent Timmerman**: *Searching for common signatures pathways associated with axonal CMT neuropathies*. Research seminar organized by Prof. R. Martini, University of Wurzburg, Germany, 6 December 2019
2. **Elias Adriaenssens**: *An introduction to CRISPR/Cas9 gene editing*, MosaCell 3rd annual meeting, University of Maastricht (Netherlands), 7 May 2019

3. **Vincent Timmerman:** *Can we find common pathomechanisms in CMT neuropathies?* Research seminar organized by Prof. V. Delague, Université Aix-Marseille, France, 6 December 2018
4. **Vincent Timmerman**: *The pathophysiology of small heat shock protein mutations causing peripheral neuropathy*. Research seminar organized by Prof. R. Horvath at the Institute of Genetic Medicine, Newcastle University, Newcastle, UK, 14 March 2017
5. **Manisha Juneja**: *Identifying common molecular determinants of axonal CMT.* TREAT-NMD, Freiburg, Germany, 27-29th November 2017

Invited lectures at international meetings:

1. **Vincent Timmerman**: *Molecular genetics and mechanisms of hereditary peripheral neuropathies.* Kongress des Medizinisch-Wissenschaftlichen Beirates der Deutschen Gesellschaft für Muskelkranke (DGM) e.V., Göttingen, Germany, 9-10 May 2019
2. **Vincent Timmerman:** *Small heat shock protein (HSPB8) related neuropathy and myopathy.* 246th ENMC workshop on Protein Aggregated Myopathies, Hoofddorp, The Netherlands, 24-26 May 2019.
3. **Vincent Timmerman**: *HSPB1/HSPB8 in axonal neuropathy and distal myopathy*, published in: 234th ENMC International Workshop: Chaperone dysfunction in muscle disease, Naarden, The Netherlands, 8-10 December 2017, by Weihl CC, Udd B, Hanna M; ENMC workshop study group. Workshop report published in Neuromuscular Disorders 2018;28(12):1022-1030.
4. **Vincent Timmerman:** *Identification of common molecular determinants of axonal Charcot-Marie-Tooth disease*. 4th joint meeting of the Belgian-Dutch neuromuscular study club and German Reference Center for Neuromuscular Diseases of the DGNN, Naarden, Netherlands, May 25-26, 2018.
5. **Vincent Timmerman**: *New genes and mechanisms in inherited neuropathies*. Plenary lecture at the 15th International Congress on Neuromuscular Diseases (ICNMD 2018), Vienna, Austria, July 6-10, 2018
6. **Vincent Timmerman**: *Disease mechanisms in the inherited neuropathies*. Educational lecture at the Peripheral Nerve Society (PNS 2018), Baltimore, USA, 21-25 July, 2018

Slide presentations selected at international meetings:

1. **Angela Sisto**: *Mutations in the small heat shock proteins HSPB1 and HSPB8 impair the autophagic flux* (platform session). Peripheral Nerve Society (PNS 2019), Genova, Italy, 22-25 June 2019
2. **Jonas Van Ient:** *Unravelling hallmarks of axonal degeneration in Charcot-Marie-Tooth type 2 using induced pluripotent stem cells* (oral poster). Peripheral Nerve Society (PNS 2019), Genova, Italy, 22-25 June, 2019
3. **Manisha Juneja**: *Molecular phenotyping of neurons derived from CMT2 patient-iPSC lines* (oral poster). Peripheral Nerve Society (PNS 2018), Baltimore, USA, 21-25 July, 2018
4. **Elias Adriaenssens**: *How does mitochondrial dysfunction contribute to the CMT2F pathogenesis caused by HSPB1 mutations.* CMTR and Peripheral Nerve Society (PNS 2018), Baltimore, USA, 21-25 July, 2018
5. **Leen Vendredy:** *A preclinical study to treat neuromuscular diseases caused by mutations in the small heat shock proteins HSPB8*. 3rd CSSI workshop on Small Heat Shock Proteins, Québec City, USA, 26-29 August 2018 [workshop report see below reference]
6. **Elias Adriaenssens:** *Small heat shock proteins operate as chaperones in the mitochondrial intermembrane space*. 3rd CSSI workshop on Small Heat Shock Proteins, Québec City, USA, 26-29 August 2018 [workshop report published in Carra, S., Alberti, S., Benesch, J.L.P., Boelens, W., Buchner, J., Carver, J.A., Cecconi, C., Ecroyd, H., Gusev, N., Hightower, L.E., Klevit, R.E., Lee, H.O., Liberek, K., Lockwood, B., Poletti, A., **Timmerman, V.**, Toth, M.E., Vierling, E., Wu, T., Tanguay, R.M.: Small heat shock proteins: multifaceted proteins with important implications for life. Cell Stress and Chaperones 24(2): 295-308 (2019)]
7. **Manisha Juneja**: *Exploring axonal CMT through iPSC derived neurons*. FP7 NeurOmics final meeting, Berlin, Germany, 3-5th May 2017
8. **Vincent Timmerman**: *A knock-in/knock-out mouse model for small heat shock protein HSPB8 mimicking distal hereditary motor neuropathy and myofibrillar myopathy.* Annual Meeting of the Peripheral Nerve Society, Sitges-Barcelona, Spain, 8-12 July 2017
9. **Mansour Haidar:** *Impairment of autophagy as a possible pathomechanism for CMT causing mutations in HSPB1.* Annual Meeting of the Peripheral Nerve Society, Sitges-Barcelona, Spain, 8-12 July 2017

Poster presentations at international meetings:

1. **Leen Vendredy**: *A CRISPR/Cas9 knock-out screen to identify regulators of Hspb8 expression and stability.* Peripheral Nerve Society (PNS 2019), Genova, Italy, 22-25 June, 2019
2. **Angela Sisto**: *Mutations in the small heat shock proteins HSPB1 and HSPB8 impair the autophagic flux*. Peripheral Nerve Society (PNS 2019), Genova, Italy, 22-25 June 2019
3. **Jonas Van Lent**: *Unravelling hallmarks of axonal degeneration in Charcot-Marie-Tooth type 2 using induced pluripotent stem cells.* Peripheral Nerve Society (PNS 2019), Genova, Italy, 22-25 June, 2019
4. **Elias Adriaenssens**: *Myopathies and neuropathies associated with Pro209 mutations in BAG3 have comparable molecular deficits*. Peripheral Nerve Society (PNS 2019), Genova, Italy, 22-25 June, 2019
5. **Leen Vendredy**: *A CRISPR/Cas9 knock-out screen to identify regulators of Hspb8 expression and stability*. EMBO Workshop-Protein quality control: from mechanisms to disease, Costa de la Calma, Spain, 28 April-3 May 2019
6. **Elias Adriaenssens**: *The small heat shock proteins operate as chaperones in the mitochondrial intermembrane space*. EMBO Workshop-Protein quality control: from mechanisms to disease, Costa de la Calma, Spain, 28 April-3 May 2019
7. **Angela Sisto**: *The shaping function of small heat shock proteins in autophagosome formation.* EMBO Workshop-Protein quality control: from mechanisms to disease, Costa de la Calma, Spain, 28 April-3 May 2019
8. **Angela Sisto**: *The adverse effect of mutations in small heat shock proteins HSPB1 and HSPB8 in autophagosome formation.* 3rd Nordic Autophagy Society (NAS) Conference, 22-24 May 2019
9. **Jonas Van Lent:** *Unravelling hallmarks of axonal degeneration in Charcot-Marie-Tooth type 2 using induced pluripotent stem cells.* 7th Molecular Mechanisms of Axon Degeneration meeting, Loch Lomond, Scotland, 11-14 March, 2019
10. **Manisha Juneja:***Molecular phenotyping of neurons derived from CMT2 patient-iPSC lines.* Peripheral Nerve Society (PNS 2018), Baltimore, USA, 21-25 July, 2018
11. **Elias Adriaenssens:** *How does mitochondrial dysfunction contribute to the CMT2F pathogenesis caused by HSPB1 mutations.* Peripheral Nerve Society (PNS 2018), Baltimore, USA, 21-25 July, 2018
12. **Leen Vendredy:** *A preclinical study to treat neuromuscular diseases caused by mutations in the small heat shock proteins HSPB8.* Peripheral Nerve Society (PNS 2018), Baltimore, USA, 21-25 July, 2018
13. **Manisha Juneja:** *Identification of common molecular players involved in the prognosis and pathogenesis of axonal CMT subtypes*. Annual Meeting of the Peripheral Nerve Society (PNS 2017), Sitges-Barcelona, Spain, 8-12 July 2017
14. **Elias Adriaenssens:** *How does mitochondrial dysfunction contribute to the CMT2F pathogenesis caused by HSPB1 mutations*. EMBO/FEBS Course: Mitochondria in life, death and disease, Fasano, Italy, 9-13 October 2017

Slide presentations selected at national meetings:

1. **Angela Sisto:** *Autophagy: Big responsibility for small molecular chaperones.* Selected speaker at WOG meeting, KU Leuven (Belgium), 28 November 2019
2. **Leen Vendredy:** *Can we treat CMT2L by downregulating HSPB8?* Selected speaker at WOG meeting, KU Leuven (Belgium), 28 November 2019
3. **Elias Adriaenssens:** *A novel role for small heat shock proteins: entering the mitochondrial territory.* Selected speaker at WOG meeting, KU Leuven (Belgium), 28 November 2019
4. **Elias Adriaenssens:** *CRISPR/Cas9: everything you need to know.* Invited speaker at KVCV meeting, KU Leuven (Belgium), 20 February 2019
5. **Elias Adriaenssens:** *CRISPR/Cas9: Everything you need to know.* Invited speaker at KVCV seminar Antwerp, 22 February 2017
6. **Elias Adriaenssens:** *CRISPR/Cas9: Everything you need to know.* Invited speaker at KVCV seminar Ghent, 8 November 2017
7. **Elias Adriaenssens:** *CRISPR/Cas9: recent developments in the field.* ThermoFisher Scientific, Technical Stem Cell Workflow and Research Seminar, at the University of Antwerp, 19 October 2017
8. **Elias Adriaenssens:** *How does mitochondrial dysfunction contribute to the CMT2F pathogenesis caused by HSPB1 mutations.* FBD Faculty Research Day, Universiteit Antwerpen, Antwerp, 27 October 2017

Poster presentations at national meetings:

1. **Manisha Juneja:** *Molecular phenotyping of neurons derived from CMT2 patient-iPSC lines*. Belgian Society for Stem Cell Research (BeSSCR 2018), Leuven, Belgium, 26 October, 2018
2. **Mansour Haidar:** *The role of HSPB1 in autophagy and its implications in peripheral neuropathy.* VIB Conference: ER Stress, Autophagy & Immune System, Bruges, 26-27 January 2017
3. **Elias Adriaenssens:** *How does mitochondrial dysfunction contribute to the CMT2F pathogenesis caused by HSPB1 mutations*. RBSM2017 symposium (P2N), Antwerp, 7 September 2017
4. **Mansour Haidar:** *Impairment of Autophagy as a Possible Pathomechanism for CMT Causing Mutations in HSPB1.* RBSM2017 symposium (P2N), Antwerp, 7 September 2017

Societal activities:

1. **Elias Adriaenssens**: "*Mijn onderzoek naar de ziekte van Charcot-Marie-Tooth*" Rotary Kempenland, Zandhoven, 14/02/2019
2. **Jonas Van lent**: *"Stamcelonderzoek: veelbelovend?"* CMT studie- en contactdag, Antwerpen, 20/10/2018
3. **Vincent Timmerman**: "*Resultaten voorgesteld tijdens het CMT-congres in Baltimore*" CMT studie- en contactdag, Antwerpen, 20/10/2018
4. **Elias Adriaenssens**: "*Het HspB8 muismodel weerspiegelt het ziektebeeld bij de mens*". CMT studie- en contactdag, Antwerpen LO, 4/11/2017

Valorisation of research findings:

1. EP17195108-PTC/EP2018/077133: "*Biomarkers for Charcot-Marie-Tooth disease*" (inventors **M. Juneja** and **V. Timmerman**)

References to the literature cited in the Research Report (part 1).

- Adriaenssens E, Geuens T, Baets J, Echaniz-Laguna A, Timmerman V. 2017. Novel insights in the disease-biology of mutant heat shock proteins in neuromuscular diseases. *Brain* 140: 2541-49
- Bouhy D, Juneja M, Katona I, Holmgren A, Asselbergh B, et al. 2018. A knock-in/knock-out mouse model of HSPB8-associated distal hereditary motor neuropathy and myopathy reveals toxic gain-of-function of mutant Hspb8. *Acta Neuropathol* 135: 131-48
- Crippa V, D'Agostino VG, Cristofani R, Rusmini P, Cicardi ME, et al. 2016. Transcriptional induction of the heat shock protein B8 mediates the clearance of misfolded proteins responsible for motor neuron diseases. *Sci Rep* 6: 22827
- d'Ydewalle C, Krishnan J, Chiheb DM, Van Damme P, Irobi J, et al. 2011. HDAC6 inhibitors reverse axonal loss in a mouse model of mutant HSPB1-induced Charcot-Marie-Tooth disease. *Nat.Med.* 17: 968-74
- Echaniz-Laguna A, Geuens T, Petiot P, Pereon Y, Adriaenssens E, et al. 2017a. Axonal Neuropathies due to Mutations in Small Heat Shock Proteins: Clinical, Genetic, and Functional Insights into Novel Mutations. *Hum Mutat* 38: 556-68
- Echaniz-Laguna A, Lornage X, Lannes B, Schneider R, Bierry G, et al. 2017b. HSPB8 haploinsufficiency causes dominant adult-onset axial and distal myopathy. *Acta Neuropathol* 134: 163-65
- Ghaoui R, Palmio J, Brewer J, Lek M, Needham M, et al. 2016. Mutations in HSPB8 causing a new phenotype of distal myopathy and motor neuropathy. *Neurology* 86: 391-8
- Guilbert SM, Lambert H, Rodrigue MA, Fuchs M, Landry J, Lavoie JN. 2018. HSPB8 and BAG3 cooperate to promote spatial sequestration of ubiquitinated proteins and coordinate the cellular adaptive response to proteasome insufficiency. *FASEB J*: fj201700558RR
- Haidar M, Asselbergh B, Adriaenssens E, De Winter V, Timmermans JP, et al. 2019. Neuropathy-causing mutations in HSPB1 impair autophagy by disturbing the formation of SQSTM1/p62 bodies. *Autophagy* 15: 1051-68
- Haidar M, Timmerman V. 2017. Autophagy as an Emerging Common Pathomechanism in Inherited Peripheral Neuropathies. *Front Mol Neurosci* 10: 143
- Irobi J, Van Impe K, Seeman P, Jordanova A, Dierick I, et al. 2004. Hot-spot residue in small heat-shock protein 22 causes distal motor neuropathy. *Nat.Genet.* 36: 597-601
- Mizushima N. 2009. Methods for monitoring autophagy using GFP-LC3 transgenic mice. *Methods Enzymol* 452: 13-23

Geneeskundige Stichting Koningin Elisabeth
Fondation Médicale Reine Elisabeth
Königin-Elisabeth-Stiftung für Medizin
Queen Elisabeth Medical Foundation

Final report of the research group of

Prof. Fadel Tissir, PhD

Université Catholique de Louvain
(UCLouvain)

Principal investigator

Prof. Fadel Tissir, PhD, Maître de Recherches FNRS
Institute of Neuroscience, Developmental Neurobiology group
Université Catholique de Louvain
Avenue E. Mounier 73, Box B1.73.16
B1200 Bruxelles
Belgium
Tel.: +32 2 764 73 84
Fax: +32 2 764 74 85
E-mail: Fadel.Tissir@uclouvain.be

Cortical development and malformations

The cerebral cortex is the seat of higher brain functions. Development of the mammalian cerebral cortex requires the production and positioning of the correct number and diversity of neurons. At initial stages of cortical development, the dorsal telencephalon is organized in a pseudostratified epithelium consisting of neural stem cells (NSCs, also known as neuroepithelial cells) that undergo multiple rounds of symmetric division to expand the initial pool of progenitors. Once neurogenesis begins, the neocortex comprises two germinal zones: the ventricular zone (VZ), which forms the lining of lateral ventricles and contains radial glial cells (RG), also known as apical neural progenitor cells (aNPC), and the adjacent subventricular zone (SVZ), located dorsally to the VZ and containing basal progenitors (BP). In VZ, aNPC undergo several rounds of divisions to self-renew and generate glutamatergic neurons. aNPC cells can also give rise to BP cells, which delaminate from the VZ and translocate to SVZ where they divide a limited number of rounds to increase the final output of neurons. Hence, a delicate balance between proliferation and differentiation of aNPC must be preserved during neurogenesis. This balance is regulated by intrinsic and extrinsic factors, and involves rearrangements of the cytoskeleton to support a rigorous sequence of fate decisions. Given the remarkable expansion of the cerebral cortex during evolution, but also the tight relationship between dysfunctions of cortical development and neurological disorders, a hot topic of neuroscience is to understand how the proliferation and differentiation of aNPC are orchestrated at the molecular and cellular levels and to identify genes and genetic pathways that control these processes. Given the remarkable expansion of the cerebral cortex during evolution, and the tight relationship between dysfunctions of cortical development and neurological disorders, a hot topic of neuroscience is to understand how the proliferation and differentiation of aNPC are orchestrated at the molecular and cellular levels and to identify genes and genetic pathways that control these processes.

During the last 3 years, we have made a tremendous progress on how 1) Celsr1 regulates the proliferation versus differentiation of NSC and how its loss affects cortical function and behavior (Boucherie et al, 2018), 2) Diaphanous (DIAPH) 3 secures survival of NSC (Lau), and 3) Lack of DIAPH3 triggers neoplastic transformation and gliobstomas.

1. Celsr1 in cortical development and function

Celsr1 (Cadherin EGF LAG Seven-Pass G-Type Receptor 1) is a member of the flamingo subfamily, part of the cadherin superfamily, which consists of 3 nonclassic-type cadherins; a subpopulation that does not interact with catenins. The flamingo cadherins are located at the plasma membrane and have nine cadherin domains, seven epidermal growth factor-like repeats and two laminin G-type repeats in their ectodomain. They also have seven transmembrane domains, a characteristic unique to this subfamily. It is assumed that these chimeric proteins are actually adhesion G protein coupled receptors ‘adhesion GPCRs’ involved in contact-mediated communication, with cadherin domains acting as homophilic binding regions and the EGF-like domains involved in cell adhesion and receptor-ligand interactions. Celsr1 is developmentally regulated and plays a critical role in early embryogenesis particularly during neural tube closure. Mutations in the Celsr1 genes have been systematically associated with a variety of neural tube closure defects ranging from the mild forms of spina bifida to “craniorachischis totalis” where the neural tube is completely open. Our expression analysis revealed that the Celsr1 transcript remains heavily expressed by NPC after neural tube closure. Yet, its function in these cells has not been assessed.

Using the Celsr1 conditional knockout mice along with a combination of cellular, molecular, and imaging approaches, we showed that the communication between forebrain meninges and aNPC is essential to cortical development, and that the basal compartment of aNPC is key to this communication process. We found that Celsr1 controls branching of aNPC basal processes abutting the meninges and thereby regulates retinoic acid-dependent neurogenesis. Loss-of-function of Celsr1 results in a decreased number of endfeet, modifies RA-dependent transcriptional activity, and biases aNPC commitment towards self-renewal at the expense of basal progenitor and neuron production. The mutant cortex has a reduced number of neurons, and *Celsr1* mutant mice exhibit microcephaly and behavioral abnormalities. These results were published in *Molecular Psychiatry*.

In addition to his role in embryonic neurogenesis, we have discovered novel functions of Celsr1 in formation of the corpus callosum, and in neuronal migration especially in the adult forebrain. Loss of function of Celsr1 in mouse leads to agenesis of corpus callosum (Fig. 1), and periventricular heterotopias (Fig. 2). Importantly, we also found mutations in CELSR1 in patients from 8 families and associated these mutations with cortical dysplasia, hypoplasia of the corpus callosum, periventricular heterotopias, intellectual disability, and epilepsy. A manuscript is being finalized and will published in 2020.

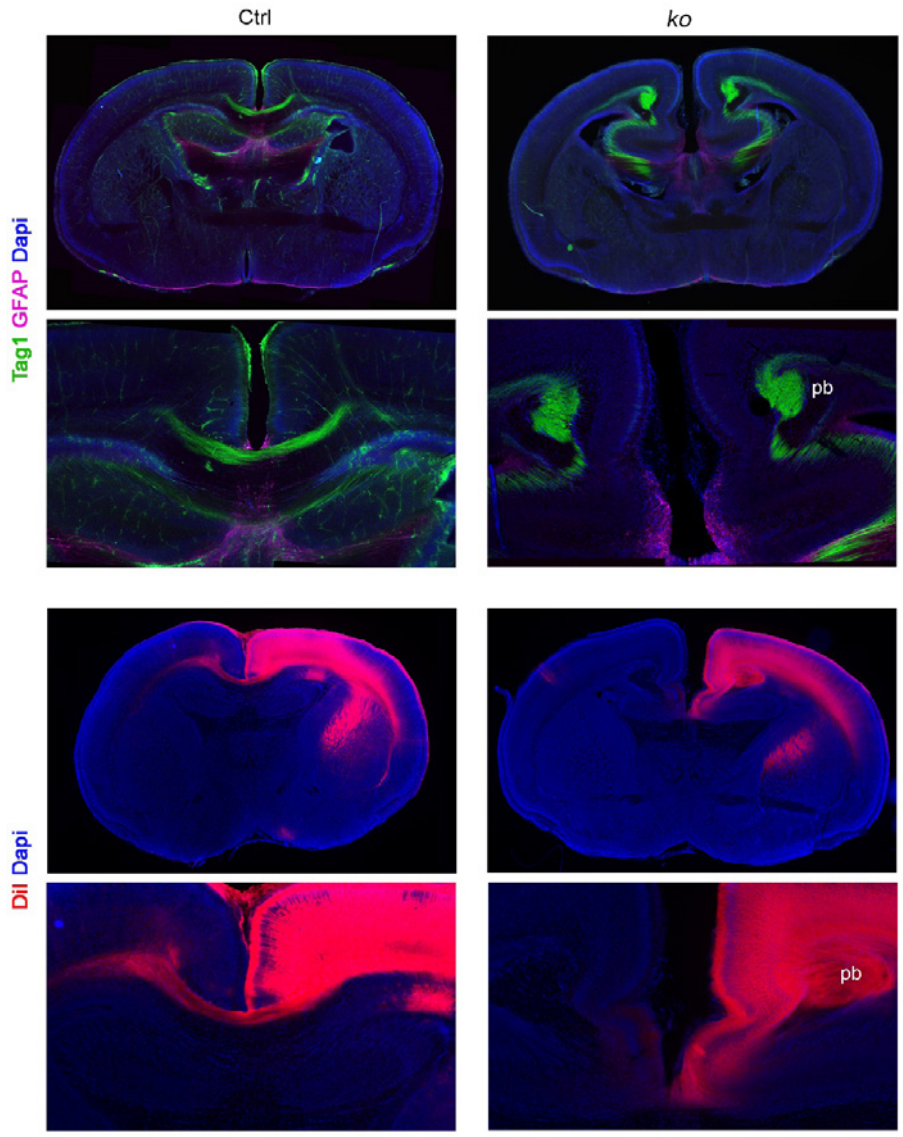

Figure 1: Agenesis of the corpus callosum and in the Celsr1 Knockout (ko) mice. Callosal axons, stained either with anti-Tag1 antibodies (green, upper panels and), or axonal tracer DiI (red in lower panels) fail to cross the midline and form the so called Probst bundle (pb).

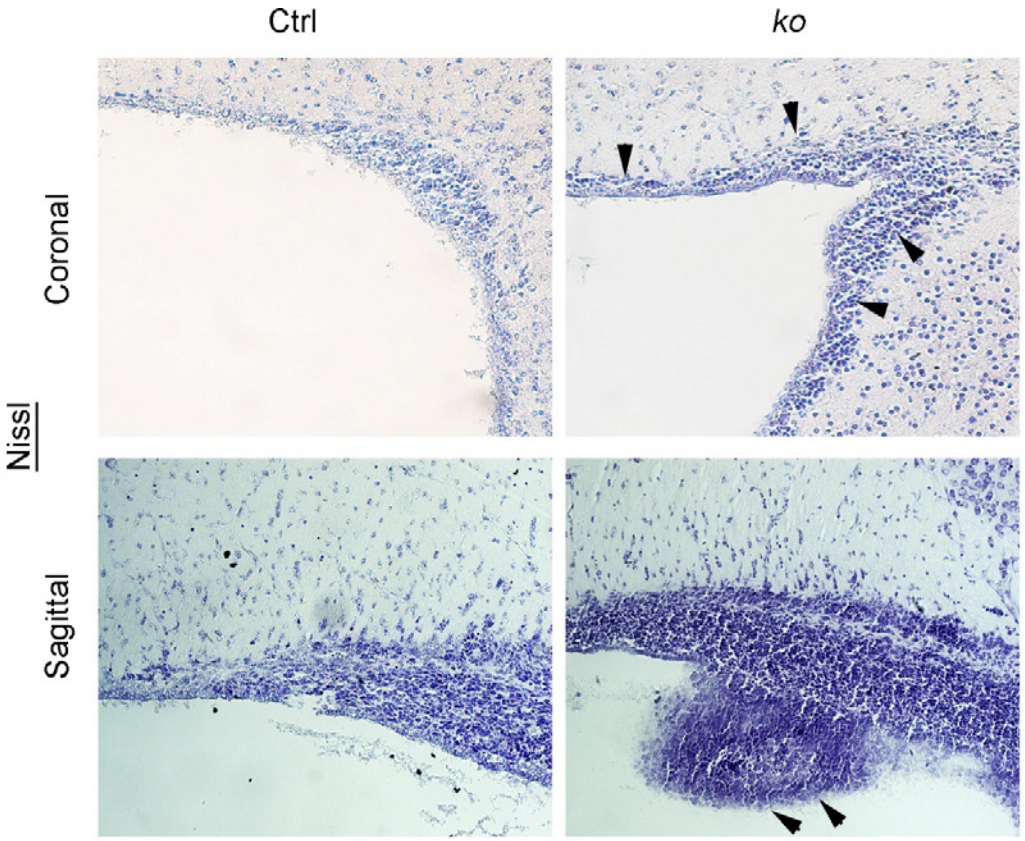

Figure 2: Nissl staining of forebrain sections from control (left) and Celsr1 KO mice depicting periventricular heterotopias (arrowheads).

2. DIAPH3 maintains NSC

DIAPH3 is a member of the diaphanous subfamily of formins. These proteins have the capacity to nucleate and elongate actin filaments, and therefore to remodel cytoskeleton. DIAPH3 is essential for cytokinesis as its dysfunction disrupts the contractile ring and produces multinucleated cells. We have shown that the loss of DIAPH3 in the developing brain causes aneuploidy and apoptosis of neural progenitors. However, the role of DIAPH3 in cortical histogensis and cortical function in the adult brain could not be assessed because of early embryonic lethality of the knockout mice. We have now used a conditional approach and we show that the specific inactivation of the *Diaph3* gene in cerebral cortex profoundly alters neurogenesis depleting cortical progenitors and neurons, and leading to microcephaly, and altered locomotor and social behavior. Mechanistically, we show that DIAPH3 localizes at the centrosome during mitosis and regulates the assembly of microtubules and bipolarity of the spindle. DIAPH3-deficient cells display supernumerary centrosomes, multipolar spindles, and disorganised cytoskeleton. DIAPH3-deficiency disrupts the expression and/or stability of polarity proteins GPSM2, PAR3, NUMB, and microtubule associated proteins SPAG5 and KNSTRN. SPAG5 and DIAPH3 have similar/identical expression patterns in the developing cortex and overlapping subcellular localization during mitosis. Knockdown of SPAG5 phenocopies the DIAPH3 deficiency, whereas its overexpression rescues the DIAPH3 phenotype. Our data uncover a new function of DIAPH3 in cortical development and function, and provide evidence that this protein belongs to a molecular toolbox that links cell polarity and cytoskeletal dynamics on the one hand and fate determination and to survival of cortical progenitors on the other hand. These results have been compiled in the attached manuscript (Lau et al, to be submitted for publication by the end of January 2020).

3. Role of DIAPH3 in glioblastoma

Since mitotic errors and aneuploidy occurred in *Diaph3* knockout mice, we further asked if aneuploid cells would trigger neoplastic transformation. To address this, we generated *Diaph3*$^{Emx1\text{-}Cre}$ /*p53*$^{Emx1\text{-}Cre}$ double cKO mice (dcKO). Using MRI, we detected in the dcKO but in control mice (Fig. 3A, B). dcKO mice exhibit a reduced lifespan and die between the ages of 4.5 and 12 months (Fig. 3C). H&E staining, CD44, GFAP, and vimentin immunostainings strongly showed that the tumours are glioblastoma multiform (GBM) (Fig. 8D-K). The tumour tissues from different stages of the tumour (MRI scanning can detect tumours of less than 2 mm^3) have been isolated. The mRNA was sequenced and will be used to perform a transcriptome profiling of tumours as they progress from grade II to grade VI Astrcytomas.

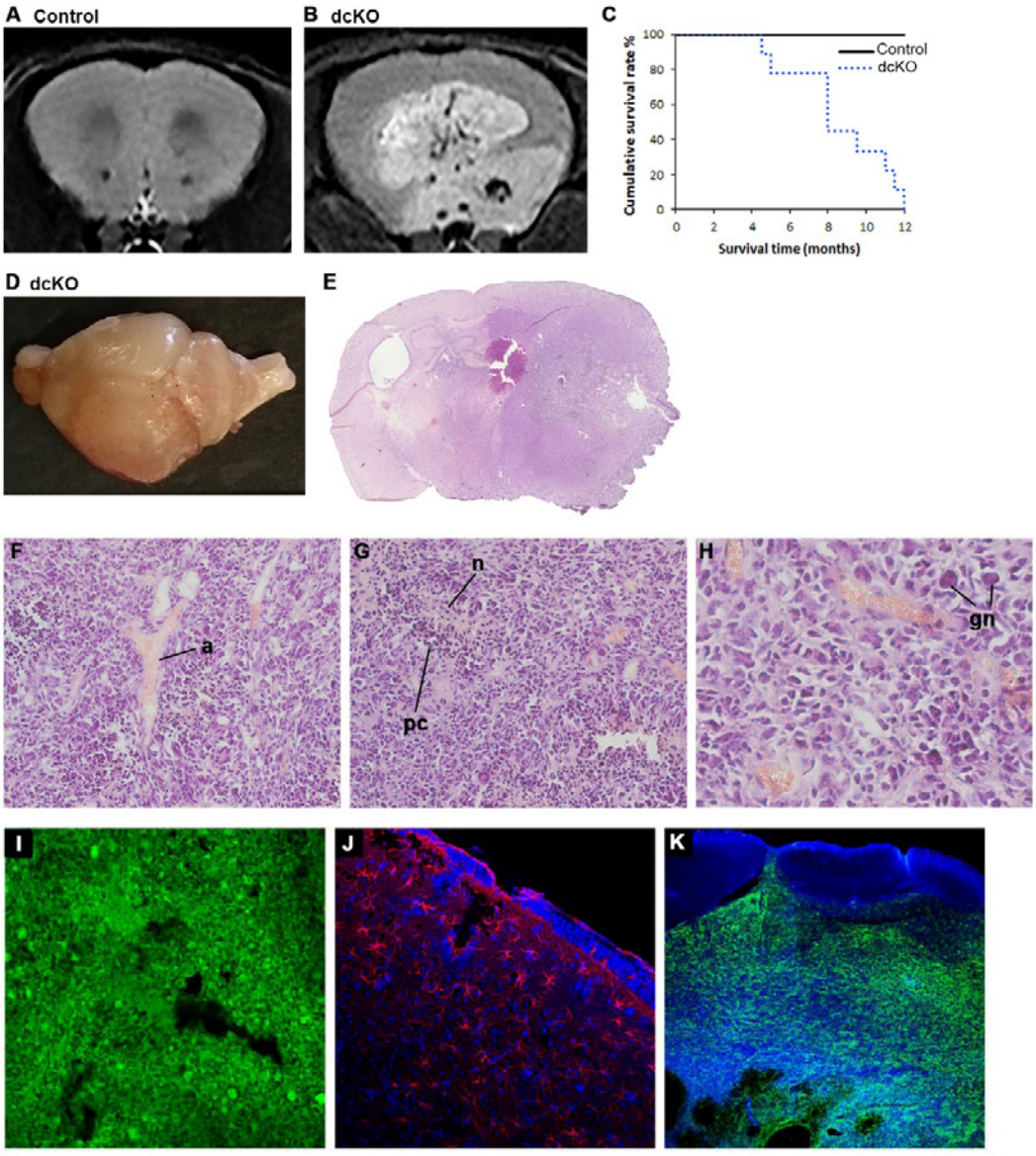

Figure 3 *Diaph3*$^{Emx1\text{-}Cre}$/*p53*$^{Emx1\text{-}Cre}$ double mutant (dcKO) mice exhibit glioblastoma (A,B) MRI images of control and dcKO mice brain show tumor in the frontal cortex of dcKO. (c) Survival curve of control vs dcKO mice (n=9 pairs). (D) Dissected brain of a *Diaph3*$^{Emx1\text{-}Cre}$/*p53*$^{Emx1\text{-}Cre}$ mouse exhibiting a metastatic brain tumour. (E) Hematoxylin-eosin staining of a coronal section at the level the forebrain depicting the progression of the tumor in the right hemisphere. Note the absence of key structures as the hippocampus and internal capsule in this hemisphere. (F-H) Hematoxylin-eosin staining of a tumor section. Typical features of glioblastoma like angiogenesis (a in F panel), palisading cells (pc in G) surrounding necrotic zones (n in G) and giant nuclei (gn in H) are observed. (I-K) Brain sections stained with CD44 (I, green), GFAP (J, red), and Vimentin (K, green) antibodies. Immunoreactivity is seen in the tumor tissue. Note the absence of reactive astrogliosis and Vimentin immunoreactivity in the "healthy" tissue illustrated by the DAPI counterstain (blue).

Geneeskundige Stichting Koningin Elisabeth
Fondation Médicale Reine Elisabeth
Königin-Elisabeth-Stiftung für Medizin
Queen Elisabeth Medical Foundation

Final report of the research group of

Prof. dr. Vandenberghe Wim, MD. PhD

Katholieke Universiteit Leuven (KU Leuven)

Principal investigator

Prof. dr. Vandenberghe Wim, MD. PhD
University Hospitals Leuven, Department of Neurology
KU Leuven, Department of Neurosciences
Herestraat 49
3000 Leuven
Belgium
Tel.: +32 16 34 42 80
Email: wim.vandenberghe@uzleuven.be

LRRK2, Rab10 and mitochondrial quality control in Parkinson's disease

1. Background

Parkinson disease (PD) is a highly prevalent, disabling neurodegenerative disorder for which no cure exists yet. The number of PD patients in the western world is expected to double over the next two decades, presenting a huge medical, social and economic challenge.
Approximately 5% of PD cases have a mendelian cause [1]. Mutations in the gene encoding LRRK2 (leucine rich repeat kinase 2) are by far the most common monogenic cause of PD, accounting for ~10% of autosomal dominant familial cases [1]. *LRRK2* mutations are also found in ~4% of apparently sporadic PD cases [1]. In addition, genome-wide association studies identified polymorphisms in the *LRRK2* locus as a risk factor for sporadic PD, indicating that pathogenic pathways may be shared between familial and sporadic forms [1]. *LRRK2* encodes an enzyme with a kinase domain and a GTPase domain. A recent phosphoproteomics study identified RAB10 and several related members of the RAB family as LRRK2 kinase substrates [2]. The RAB family comprises ~70 small GTPases that cycle between an inactive GDP-bound and an active GTP-bound state as well as between the cytosol and membranes [3]. RABs regulate vesicle formation, trafficking and fusion [3]. PD-causing *LRRK2* mutations increase phosphorylation of RAB10, which may disturb its membrane-cytosol equilibrium [2]. How this leads to neurodegeneration, is unknown.
Accumulating evidence implicates impairment of mitophagy as a pathogenic mechanism in PD [4]. Mitophagy is a form of selective autophagy in which damaged mitochondria are specifically labeled with ubiquitin and taken up by autophagosomes for degradation in lysosomes. The E3 ubiquitin ligase parkin and the mitochondrial kinase PINK1, both encoded by genes linked to autosomal recessive PD, are critically involved in mitophagy of damaged mitochondria [4]. PINK1 accumulates on damaged mitochondria and phosphorylates both parkin and ubiquitin, hereby activating parkin. Parkin-mediated ubiquitination of outer mitochondrial membrane proteins in combination with PINK1-mediated ubiquitin phosphorylation triggers recruitment of autophagy receptors, such as optineurin, that tether ubiquitinated mitochondria to LC3 on nascent autophagosomes [4]. Loss-of-function mutations in the parkin or PINK1 genes disrupt mitophagy *in vivo* and *in vitro*, leading to deficient mitochondrial quality control, accumulation of dysfunctional mitochondria, oxidative stress and apoptosis.
The starting point for our project was our discovery that mitophagy is not only disrupted in fibroblasts from parkin- and PINK1-deficient PD patients, but also in fibroblasts from PD patients with the 2 most common clinical *LRRK2* mutations (G2019S and R1441C). The mitophagy defect in the LRRK2 mutant fibroblasts was rescued by pharmacological inhibition of LRRK2 kinase activity and by overexpression of RAB10. Moreover, we had found that RAB10 translocates to depolarized mitochondria in wild–type fibroblasts, but much less so in *LRRK2* mutant fibroblasts.

2. Aim

The aim of this project was to elucidate the mechanisms by which PD-linked *LRRK2* mutations disturb mitophagy.

3. Results of the project

In this project we have succeeded in uncovering the role of RAB10 in mitophagy in great molecular detail. The results have been published in 2019 in the journal *Autophagy* [5]. The results are summarized below (more details and figures can be found in the publication):

- **Confirmation of the mitophagy defect in human *LRRK2* mutant fibroblasts**
  Using a variety of state-of-the-art mitophagy assays (e.g. live mito-Keima imaging [6,7]) we confirmed that the G2019S and R1441C mutant fibroblasts have a mitophagy defect with a magnitude similar to that observed in *parkin* and *PINK1* mutant fibroblasts. The mitophagy defect of the *LRRK2* mutant fibroblasts was corrected by siRNA-mediated knockdown of LRRK2 as well as by treatment with LRRK2 kinase inhibitors, indicating that the defect was mediated by LRRK2 kinase activity.
- ***LRRK2* mutant fibroblasts display mitochondrial dysfunction**
  Mitophagy contributes to mitochondrial quality control. As expected in cells with impaired mitophagy, mitochondrial quality in G2019S and R1441C mutant fibroblasts was impaired as evidenced by reduced average mitochondrial membrane potential and increased mitochondrial production of reactive oxygen species (ROS). These mitochondrial defects were also rescued by LRRK2 kinase inhibition.
- **Non-selective autophagy is preserved in *LRRK2* mutant fibroblasts**
  In addition to selective forms of autophagy such as mitophagy, cells have the capacity for non-selective (bulk) autophagy in which cytosolic components and organelles are degraded indiscriminately via mechanisms that are independent of autophagy receptors. A classical trigger for non-selective autophagy is amino acid starvation. Surprisingly, starvation-induced autophagy was preserved in *LRRK2* mutant cells.
  Once autophagosomes are completely closed around their cargo, they are probably processed similarly along their path to fusion with lysosomes irrespective of whether they have been formed by selective or non-selective autophagy. Our finding of impaired mitophagy and preserved non-selective autophagy in *LRRK2* mutant cells therefore suggested that *LRRK2* mutations disrupted mitophagy at a site upstream of closure of autophagosomal membranes around the mitochondria.
- **Optineurin recruitment to depolarized mitochondria is impaired in patients with *LRRK2* mutations**
  We then determined at which step mitophagy was disrupted by *LRRK2* mutations. The first steps in the mitophagy pathway (accumulation of PINK1 on depolarized mitochondria and ubiquitination of outer mitochondrial membrane proteins by activated parkin) were perfectly intact in *LRRK2* mutant fibroblasts. However, the next step in the pathway, i.e. recruitment of the autophagy receptor optineurin to ubiquitinated mitochondria was substantially impaired in G2019S and R1441C mutant fibroblasts. Thus, although PINK1 accumulation and parkin activity at depolarized mitochondria were preserved in *LRRK2* mutant fibroblasts, these mutations interfered with optineurin recruitment.
- **Increased phosphorylation of RAB10 in *LRRK2* mutant fibroblasts**
  It was recently shown in animal models that wild-type LRRK2 phosphorylates RAB10 on residue T73 and that the G2019S and R1441C mutations further enhance RAB10 phosphorylation. As LRRK2 kinase inhibition rescued mitophagy in the G2019S and R1441C mutant cells (cfr. supra), we wondered if RAB10 or other RAB substrates of LRRK2 were involved in the mitophagy defect of these cells.
  Using a novel monoclonal antibody against RAB10 phosphorylated at T73 [8], we were able to demonstrate for the first time that *LRRK2* mutations enhance RAB10 phosphorylation in human cells. The phospho-RAB10 signal was dissipated after treatment with LRRK2 kinase inhibitors, confirming the specificity of the antibody.
- **RAB10 mitigates defects in optineurin recruitment, mitophagy and mitochondrial function in *LRRK2* mutant cells**
  To explore whether RAB10 was involved in the mitophagy defect of the *LRRK2* mutant fibroblasts, we overexpressed RAB10 and several other RAB substrates of LRRK2: RAB3A, RAB5B, RAB12 and

RAB29. In addition to these LRRK2 substrates, we also overexpressed RAB7A because of its reported functional link. If the mitophagy defect of *LRRK2* mutant cells was due to enhanced phosphorylation of RAB10, we reasoned that overexpression of RAB10 might mitigate the mitophagy defect, because the low abundance of endogenous LRRK2 protein would be too limiting to phosphorylate the excess of overexpressed substrate. Indeed, overexpression of FLAG-tagged RAB10 in *LRRK2* mutant cells caused a large increase in total RAB10, but only a mild increase in phospho-RAB10, implying that it mostly enhanced the amount of non-phosphorylated RAB10.

Interestingly, overexpression of RAB10 mitigated the mitophagy deficit of G2019S and R1441C mutant fibroblasts. Overexpression of RAB3A also had a significant, although smaller, rescuing effect, whereas RAB5B, RAB7A, RAB12 and RAB29 had no effect. RAB10 overexpression in G2019S and R1441C fibroblasts also improved recruitment of optineurin, ameliorated mitochondrial membrane potential and mitigated mitochondrial ROS production.

- **RAB10 facilitates mitophagy in wild-type cells**

  We knocked down RAB10 in wild-type fibroblasts to determine whether endogenous RAB10 regulated mitophagy. RAB10 knockdown in wild-type cells indeed impaired mitophagy. Conversely, RAB10 overexpression enhanced mitophagy in wild-type cells.

- **RAB10 accumulates on depolarized mitochondria in wild-type cells**

  To search for the mechanism underlying facilitation of mitophagy by RAB10, we analyzed its subcellular localization in wild-type cells. In baseline conditions, RAB10 had a predominantly cytosolic localization. After mitochondrial depolarization, however, RAB10 formed puncta that showed striking colocalization with mitochondria. Accumulation of RAB10 on depolarized mitochondria was also confirmed by western blotting after mitochondrial fractionation. By contrast, RAB12 did not show detectable translocation to depolarized mitochondria. RAB10 specifically accumulated on depolarized mitochondria that also showed strong parkin accumulation, whereas it was not detectable on mitochondria that were devoid of parkin signal.

  Membrane association of RAB proteins is ensured by posttranslational modification of C-terminal cysteine residues with lipophilic geranylgeranyl groups that act as hydrophobic membrane anchors [3]. To assess the role of C-terminal geranylgeranylation in RAB10 recruitment to mitochondria, we deleted the 2 C-terminal cysteine residues of RAB10 (C199 and C200). This ΔCC RAB10 construct accumulated substantially less on depolarized mitochondria than full-length RAB10 despite similar expression levels, suggesting that C-terminal prenylation is important for RAB10 recruitment to mitochondria. Interestingly, overexpression of ΔCC RAB10 did not rescue mitochondrial recruitment of optineurin in the *LRRK2* mutant fibroblasts, in contrast to wild-type RAB10 overexpression. Thus, rescue of mitochondrial optineurin recruitment in *LRRK2* mutant cells required RAB10 that was capable of being tethered to the membrane via its C-terminal lipid anchor.

- **RAB10 interacts with optineurin, colocalizes with optineurin on depolarized mitochondria and promotes mitochondrial optineurin recruitment in wild-type cells**

  Interestingly, the RAB10 puncta on depolarized mitochondria in wild-type fibroblasts strongly colocalized with optineurin. Moreover, siRNA-mediated knockdown of RAB10 reduced optineurin recruitment to depolarized mitochondria in wild-type cells, indicating that RAB10 is required for optimal optineurin accumulation on damaged mitochondria.

  The colocalization of RAB10 and optineurin on depolarized mitochondria and the facilitating effect of RAB10 on mitochondrial recruitment of optineurin suggested that the two proteins might physically interact. Moreover, optineurin was previously reported to interact with RAB8A and RAB8B, the two RAB GTPases with the strongest sequence similarity to RAB10. We expressed FLAG-tagged RAB10 in control fibroblasts and found that it co-immunoprecipitated with endogenous optineurin. The interaction already occurred in basal conditions and only marginally increased after mitochondrial depolarization, suggesting that a pre-existing RAB10-optineurin complex is recruited to depolarized mitochondria.

Next, we generated Q68L (GTP-locked, constitutively active) and T23N (GDP-locked, constitutively inactive) mutant RAB10 constructs. Co-immunoprecipitation (Co-IP) experiments showed that GTP-locked RAB10 interacted more with optineurin than GDP-locked RAB10, indicating that RAB10 activity promotes binding with optineurin. This is again reminiscent of the interaction between optineurin and RAB8, which is also enhanced by RAB8 activation.

- **RAB10 interaction with optineurin and accumulation on depolarized mitochondria are impaired in patients with *LRRK2* mutations**

  To assess the effect of LRRK2-dependent RAB10 phosphorylation on the RAB10-optineurin interaction, we performed parallel Co-IP experiments in wild-type, G2019S mutant and R1441C mutant fibroblasts. Significantly less optineurin co-immunoprecipitated with RAB10 in the G2019S and R1441C mutant cells than in control cells. The interaction increased after pharmacological inhibition of LRRK2 kinase activity, further supporting the idea that T73 phosphorylation of RAB10 impairs the interaction with optineurin.

  In G2019S and R1441C LRRK2 mutant fibroblasts, RAB10 accumulation on depolarized mitochondria was substantially reduced. Interestingly, RAB10 accumulation on depolarized mitochondria was also largely abrogated in fibroblasts from PD patients with *PINK1* and *parkin* mutations. Thus, recruitment of RAB10 to depolarized mitochondria requires intact function of PINK1 and parkin and is inhibited by PD-causing *LRRK2* mutations.

  Importantly, LRRK2 knockdown with two different siRNAs and pharmacological LRRK2 kinase inhibition each rescued the accumulation of RAB10 and optineurin on depolarized mitochondria in G2019S or R1441C mutant fibroblasts, in parallel with the rescue of the mitophagy defect.

  To further test whether T73 phosphorylation of RAB10 impeded its interaction with optineurin, its translocation to depolarized mitochondria and mitophagy, we generated a phosphomimetic T73E mutant version of RAB10. Co-IP experiments in control fibroblasts showed that RAB10^{T73E} indeed interacted less well with optineurin than wild-type RAB10. Moreover, the T73E mutation impaired RAB10 translocation to depolarized mitochondria, and overexpression of RAB10^{T73E} failed to rescue mitophagy in G2019S and R1441C mutant cells, in contrast to overexpression of wild-type RAB10.

  We also made a non-phosphorylatable T73A version of RAB10, but protein levels of FLAG-RAB10^{T73A} were much lower than those of wild-type FLAG-RAB10 and FLAG-RAB10^{T73E}, despite extensive optimization of transfection conditions. This made it difficult to perform Co-IP experiments with the T73A construct and to compare its subcellular distribution with that of wild-type RAB10 and RAB10^{T73E}. However, despite its much lower abundance, RAB10^{T73A} rescued the mitophagy defect of *LRRK2* mutant fibroblasts as potently as wild-type RAB10, in contrast to the lack of rescue by RAB10^{T73E}. This further supported the conclusion that phosphorylation of RAB10 at T73 impaired its facilitating role in mitophagy.

We can summarize our data in the following model (Fig. 1). In basal conditions optineurin forms a complex with RAB10 in wild-type cells. This complex translocates to mitochondria after mitochondrial depolarization. Optimal accumulation of optineurin on mitochondria requires both binding to mitochondrial ubiquitin chains and interaction with RAB10 that is capable of insertion into the membrane via its C-terminal lipid anchor. In *LRRK2* mutant cells, enhanced T73 phosphorylation of RAB10 impairs the interaction with optineurin. Some recruitment of optineurin to mitochondria is still possible (e.g. via binding of optineurin to ubiquitin), but accumulation of optineurin on mitochondria is reduced because the interaction with membrane-inserted RAB10 is lacking (Fig. 1).

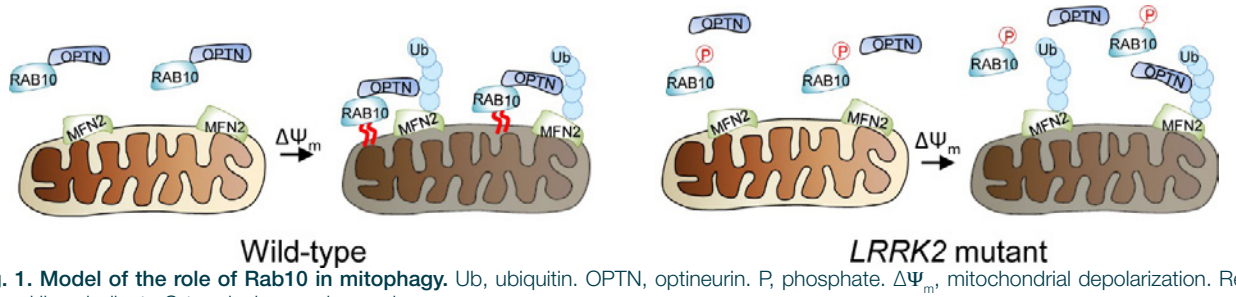

Fig. 1. Model of the role of Rab10 in mitophagy. Ub, ubiquitin. OPTN, optineurin. P, phosphate. $\Delta\Psi_m$, mitochondrial depolarization. Red curved lines indicate C-terminal geranylgeranyl groups.

These data connect LRRK2 with PINK1/parkin-mediated mitophagy via its substrate RAB10 and the RAB10 interactor optineurin, and demonstrate that the pathogenic effects of mutations in multiple PD genes all converge on a common mitochondrial quality control pathway. This convergence greatly increases the attractiveness of this pathway as a target for disease-modifying therapies for PD.

4. Impact of the results and personal evaluation

- We have achieved our aim and have succeeded in elucidating the role of RAB10 and LRRK2 in mitophagy in great mechanistic detail. The data have been published in a high-impact journal (*Autophagy*, impact factor: 11.1).
- This research has increased our understanding of the molecular basis of Parkinson's disease. In particular, the project has demonstrated a convergence of the pathogenic effects of mutations in multiple PD genes on the mitophagy pathway. This convergence makes it very likely that this pathway is fundamentally important in the pathogenesis of PD. The results also highlight the importance of LRRK2 kinase activity in PD pathogenesis.
- An exciting translational extension of this project is that I am now principal investigator on a Phase 1b, multicenter, randomized, placebo-controlled, double-blind clinical trial with the LRRK2 kinase inhibitor DNL151 (ClinicalTrials.gov identifier: NCT04056689). It is very gratifying that we are now part of the first clinical program to test the disease-modifying effects of LRRK2 kinase inhibitors in PD patients and to hopefully develop these compounds for the clinic.
- Funding from this GSKE project has also allowed us to optimize methods to differentiate patient fibroblast-derived iPSCs to dopaminergic neurons, in collaboration with the lab of Catherine Verfaillie. We are now able to generate iPSC-derived cultures in which 20-45 % of cells are dopaminergic neurons based on staining for the marker tyrosine hydroxylase. The cells also express other midbrain dopaminergic neuron markers such as LMX1A or FOXA2. PhD student Dorien Imberechts is currently developing assays to measure mitophagy and dissect the sequential steps of this process in the iPSC-derived neurons. In addition, we reprogrammed fibroblasts from two PD patients with the G2019S LRRK2 mutation and one PD patient with the R1441C mutation to iPSCs and generated an isogenic control iPSC line for one of G2019S mutant lines. Dorien Imberechts is currently determining to what extent our key findings on LRRK2 and RAB10 in fibroblasts can be confirmed in neurons. This iPSC-derived human neuronal model and the assays to analyze mitophagy in neurons were not included in our *Autophagy* publication, but will be an invaluable resource for our future research into the molecular pathogenesis of PD.

5. References

1. Corti O et al. (2011) What genetics tells us about the causes and mechanisms of Parkinson's disease. *Physiol Rev* 91:1161-1218.
2. Steger M et al. (2016) Phosphoproteomics reveals that Parkinson's disease kinase LRRK2 regulates a subset of Rab GTPases. *eLife* 5:e12813.
3. Zhen Y, Stenmark H (2015) Cellular functions of Rab GTPases at a glance. *J Cell Sci* 128:3171-3176.
4. Pickrell AM et al. (2015) The roles of PINK1, Parkin and mitochondrial fidelity in Parkinson's disease. *Neuron* 85:257-73.
5. Wauters F*, Cornelissen T* et al. (2019). LRRK2 mutations impair depolarization-induced mitophagy through inhibition of mitochondrial accumulation of RAB10. *Autophagy*. doi: 10.1080/15548627.2019.1603548. * Equal contribution.
6. Katayama H et al. (2011) A sensitive and quantitative technique for detecting autophagic events based on lysosomal delivery. *Chem Biol* 18:1042-52.
7. Cornelissen T et al. (2018) Deficiency of parkin and PINK1 impairs age-dependent mitophagy in *Drosophila*. *eLife* 7:e35878.
8. Lis P et al. (2018) Development of phosphor-specific Rab protein antibodies to monitor in vivo activity of the LRRK2 Parkinson's disease kinase. *Biochem J* 475:1-22.

6. Publications in 2017-2019 by W. Vandenberghe on topics related to this proposal (Parkinson's disease)

- Wauters F, Cornelissen T, Imberechts D, Martin S, Koentjoro B, Sue C, Vangheluwe P, **Vandenberghe W** (2019) LRRK2 mutations impair depolarization-induced mitophagy through inhibition of mitochondrial accumulation of RAB10. *Autophagy.* DOI: 10.1080/15548627.2019.1603548 (citations: 7) (impact factor: 11.1)
- Delva A, Van Weehaeghe D, van Aalst J, Ceccarini J, Koole M, Baete K, Nuyts J, **Vandenberghe W**, Van Laere K (2019). Quantification and discriminative power of 18F-FE-PE2I in patients with Parkinson´s disease. *Eur J Nucl Med Mol Imaging.* DOI: 10.1007/s00259-019-04587-y (citations: 0) (impact factor: 7.2)
- Van Weehaeghe, D., Koole, M., Schmidt, M.E., Deman, S., Jacobs, A.H., Souche, E., Serdons, K., Sunaert, S., Bormans, G., **Vandenberghe, W.**, Van Laere, K. (2019). [C-11]JNJ54173717, a novel P2X7 receptor radioligand as marker for neuroinflammation: human biodistribution, dosimetry, brain kinetic modelling and quantification of brain P2X7 receptors in patients with Parkinson's disease and healthy volunteers. *Eur J Nucl Med Mol Imaging* 46:2051-2064. DOI: 10.1007/s00259-019-04369-6 (citations: 0) (impact factor: 7.2)
- Ceccarini, J., Casteels, C., Ahmad, R., Crabbé, M., Van de Vliet, L., Vanhaute, H., Vandenbulcke, M., **Vandenberghe, W.**, Van Laere, K. (2019). Regional changes in the type 1 cannabinoid receptor are associated with cognitive dysfunction in Parkinson's disease. *Eur J Nucl Med Mol Imaging.* DOI: 10.1007/s00259-019-04445-x. (citations: 0) (impact factor: 7.2)
- Cornelissen T, Verstreken P, **Vandenberghe W** (2018) Imaging mitophagy in the fruit fly. *Autophagy* 14:1656-1657. (citations: 2) (impact factor: 11.1)
- Tinkhauser G, Torrecillos F, Duclos Y, Tan H, Pogosyan A, Fischer P, Carron R, Welter ML, Karachi C, **Vandenberghe W**, Nuttin B, Witjas T, Régis J, Azulay JP, Eusebio A, Brown P (2018) Beta burst coupling across the motor circuit in Parkinson's disease. *Neurobiol Dis* 117:217-225. (citations: 21) (impact factor: 5.2)
- Cornelissen T, Vilain S, Vints K, Gounko N, Verstreken P, **Vandenberghe W** (2018) Deficiency of parkin and PINK1 impairs age-dependent mitophagy in *Drosophila*. *Elife* pii: e35878. doi: 10.7554/eLife.35878. (citations: 25) (impact factor: 7.6)
- Nackaerts E, Michely J, Heremans E, Swinnen SP, Smits-Engelsman BCM, **Vandenberghe W**, Grefkes C, Nieuwboer A (2018) Training for Micrographia Alters Neural Connectivity in Parkinson's Disease. *Front Neurosci* 12:3. (citations: 3) (impact factor: 3.9)
- Nackaerts E, Michely J, Heremans E, Swinnen S, Smits-Engelsman B, **Vandenberghe W**, Grefkes C, Nieuwboer A (2018) Being on Target: Visual Information during Writing Affects Effective Connectivity in Parkinson's Disease. *Neuroscience* 371:484-494. (citations: 3) (impact factor: 3.4)
- Nackaerts E, Nieuwboer A, Broeder S, Swinnen S, **Vandenberghe W**, Heremans E (2018) Altered effective connectivity contributes to micrographia in patients with Parkinson's disease and freezing of gait. *J Neurol* 265:336-347. (citations: 4) (impact factor: 3.8)
- Nackaerts E, Broeder S, Pereira MP, Swinnen SP, **Vandenberghe W**, Nieuwboer A, Heremans E (2017) Handwriting training in Parkinson's disease: A trade-off between size, speed and fluency. *PLoS One* 12:e0190223. (citations: 11) (impact factor: 2.8)
- Desmet AS, Cirillo C, Tack J, **Vandenberghe W***, Vanden Berghe P* (2017) Live calcium and mitochondrial imaging in the enteric nervous system of Parkinson patients and controls. *Elife* pii: e26850. * Equal contribution. (citations: 7) (impact factor: 7.6)

– Strouwen C, Molenaar EA, Münks L, Keus SH, Zijlmans JC, **Vandenberghe W**, Bloem BR, Nieuwboer A (2017) Training dual tasks together or apart in Parkinson's disease: results from the DUALITY trial. *Mov Disord* 32:1201-1210. (citations: 45) (impact factor: 8.3)
– Koole M, Van Laere K, Ahmad R, Ceccarini J, Bormans G, **Vandenberghe W** (2017) Brain PET imaging of phosphodiesterase 10A in progressive supranuclear palsy and Parkinson's disease. *Mov Disord* 32:943-945. (citations: 1) (impact factor: 8.3)
– Nackaerts E, Heremans E, Smits-Engelsman BC, Broeder S, **Vandenberghe W**, Bergmans B, Nieuwboer A (2017) Validity and reliability of a new tool to evaluate handwriting difficulties in Parkinson's disease. *PLoS One* 12:e0173157. (citations: 9) (impact factor: 2.8)

7. Use of the GSKE grant

2017:
- 30000 € Salary of PhD student Fieke Wauters for 9 months (Jan-Sep 2017)

2018:
- 22290 € Salary of postdoc Tom Cornelissen for 3 months (Oct-Dec 2018)
- 7710 € Reagents for cell culture, molecular biology, antibodies…

2019:
- 30000 € Salary of postdoc Tom Cornelissen for 4 months (Jan-April 2019)

Geneeskundige Stichting Koningin Elisabeth
Fondation Médicale Reine Elisabeth
Königin-Elisabeth-Stiftung für Medizin
Queen Elisabeth Medical Foundation

Final report of the research group of

Prof. dr. Vangheluwe Peter, PhD

Katholieke Universiteit Leuven (KU Leuven)

Principal investigator

Prof. dr. Vangheluwe Peter, PhD
Laboratory of Cellular Transport Systems (LCTS)
Department Cellular & Molecular Medicine
Faculty of Medicine, KU Leuven
Campus Gasthuisberg, ON1 box 802
Herestraat 49
B-3000 Leuven
Belgium
Tel.: +32 16 33 07 20
Fax: +32 16 34 59 9.
E-mail: Peter.Vangheluwe@kuleuven.be
gbiomed.kuleuven.be/english/research/50000618

Neuroprotection by lysosomal transport mechanisms in Parkinson's disease

I would like to express my sincere gratitude to the Queen Elisabeth Foundation for supporting our research. It has been a true honor to interact with the Foundation, which offered important exposure to my team and provided important support to conduct pioneering research that is now being published in high impact factor journals. We obtained ground-breaking discoveries in cell transport biology, disease mechanisms in neurodegeneration, which culminated in drug discovery programs. We identified the transporters ATP13A2 and ATP10B as important mediators of lysosomal functionality and membrane integrity by preventing toxic substrate accumulation in the lysosome. Both transporters are implicated in Parkinson's disease. As such, our work opened possibilities for drug discovery in Parkinson's disease, which occurs in collaboration with CD3 and pharmaceutical companies.

1. Aims of the Project

Parkinson's disease (PD) is one of the most common neurodegenerative disorders. The neurons in PD patients accumulate protein aggregates and impaired mitochondria, which contributes to cell death. Lysosomes provide protection by efficiently removing damaged proteins and mitochondria, and are disturbed in PD. Genetic evidence points to two lysosomal transport systems that are impaired in PD, which are the subject of this project: ATP13A2/PARK9 and ATP10B, a novel, candidate PD gene. Both ATP10B and ATP13A2 belong to the P-type ATPase family of active transporters.

The overall aim of the study is to unravel and compare the transport function and cellular implications of ATP13A2 and ATP10B in endo-/lysosomes, establish their role in PD onset and assess their value as therapeutic targets.

2. Progress report ATP13A2

At the end of the program we managed to reach all major project goals. In short, we established ATP13A2 as a lysosomal polyamine exporter and ATP10B as a lysosomal glucosylceramide exporter. These two transport systems are critical for lysosomal and mitochondrial functionality. Our study offers novel insights into lysosomal biology, reveals new disease pathways in neurodegeneration and validates ATP13A2 and ATP10B as two interesting drug targets.

2.1. ATP13A2 results

(a) Results obtained from this part of the study were reported in a research article accepted in Nature.

Sarah van Veen*, Shaun Martin*, Chris Van den Haute, Veronick Benoy, Joseph Lyons, Roeland Vanhoutte, Jan Pascal Kahler, Jean-Paul Decuypere, Géraldine Gelders, Eric Lambie, Jeffrey Zielich, Johannes V. Swinnen, Wim Annaert, Patrizia Agostinis, Bart Ghesquière, Steven Verhelst, Veerle Baekelandt, Jan Eggermont, Peter Vangheluwe (*equal contribution). ATP13A2 deficiency disrupts lysosomal polyamine export. **Nature**, accepted Dec 2nd 2019, anticipated e-publication Jan 29th 2020. (IF 43.07).

Summary of our research findings:

ATP13A2 (PARK9) is a late endo-lysosomal transporter of unknown function that is genetically implicated in a spectrum of neurodegenerative disorders, including Kufor-Rakeb syndrome, a parkinsonism with dementia and early-onset Parkinson's disease (PD). ATP13A2 offers protection against genetic and

environmental risk factors of PD, whereas loss of ATP13A2 compromises lysosomal function. The lysosomal transport function of ATP13A2 remained unclear, but here, we establish ATP13A2 as a lysosomal polyamine exporter with highest affinity for spermine. Polyamines stimulate the activity of purified ATP13A2, while disease mutants are functionally impaired to a degree that correlates with the disease phenotype. ATP13A2 promotes cellular polyamine uptake via endocytosis and transports polyamines into the cytosol, which highlights a role for endo-lysosomes in cellular polyamine uptake. At high concentrations, polyamines induce cell toxicity, which is exacerbated by ATP13A2 loss due to lysosomal dysfunction, lysosomal rupture and cathepsin B activation. This phenotype is recapitulated in neurons and nematodes with loss of ATP13A2 or its orthologues. Thus, defective lysosomal polyamine export is a new mechanism for lysosome-dependent cell death that may be implicated in neurodegeneration. Our findings further shed light on the molecular identity of the elusive mammalian polyamine transport system.

(b) In a follow-up study, we report the mitochondrial phenotype of ATP13A2 loss of function models. We found that impaired lysosomal polyamine export following ATP13A2 loss of function reduces the cells anti-oxidative capacity and sensitizes cells to mitochondrial-derived oxidative stress. This highlights that polyamines are important ROS scavengers in cells.
Stephanie Vrijsen*, Laura Besora-Casals*, Sarah van Veen, Jeffrey Zielich, Chris Van den Haute, Christian Fischer, Patrizia Agostinis, Veerle Baekelandt, Jan Eggermont, Eric Lambie#, Shaun Martin#, Peter Vangheluwe#. (equal * first and # last contribution). ATP13A2-mediated endo-lysosomal polyamine export provides a mitochondrial antioxidant response. Under review in **PNAS** (IF 9.58).

Summary of our research findings:
Loss-of function mutations in ATP13A2 are implicated in neurodegenerative disorders, including Parkinson's disease (PD). We recently discovered that the late endo-/lysosomal ATP13A2 exports endocytosed polyamines into the cytosol, whereas ATP13A2 dysfunction causes lysosomal accumulation of polyamines and rupture. Here, we reveal how ATP13A2 provides protection against mitochondrial toxins such as rotenone, an environmental PD risk factor. Rotenone promoted mitochondrial-generated superoxide (mitoROS), which was exacerbated by ATP13A2 deficiency in SH-SY5Y neuroblastoma cells and patient derived fibroblasts, disturbing mitochondrial functionality and inducing toxicity. Moreover, following ATP13A2 knockdown rotenone induced an ATF4-CHOP dependent stress response that was blocked with MitoTempo, a mitochondrial antioxidant. The impact of ATP13A2 on mitoROS can be explained by the anti-oxidant properties of the polyamine spermine. Indeed, the polyamine transport activity of ATP13A2 is required for lowering the mitoROS levels. Supplementation of exogenous spermine quenched rotenone-induced mitoROS production, which requires ATP13A2. Moreover, pharmacological inhibition of the intracellular polyamine synthesis increased mitoROS accumulation when ATP13A2 is deficient. These results support a model of endocytic spermine uptake that is subsequently transported in the cytosol via ATP13A2 to quench mitoROS. Importantly, our cellular observations were recapitulated *in vivo*, in a *Caenorhabditis elegans* strain deficient in the ATP13A2-orthologue *catp-6*. These animals exhibited elevated mitoROS, induction of an ATF4-dependent stress marker and mitochondrial dysfunction in basal conditions, which was reversed with MitoTempo. Moreover, this strain was hypersensitive to rotenone toxicity and rescued by catp-6 expression. Our study reveals a novel, conserved and protective antioxidant response that depends on ATP13A2-mediated lysosomal spermine export.

2.2. ATP13A2 impact

(a) ATP13A2 belongs to the enigmatic polyamine transport system in mammalian cells, which remained unknown for several decades, despite intensive research. This is highly relevant since polyamines are vital and abundant molecules that are important for cell survival and proliferation, and determine longevity of organisms.

(b) ATP13A2 is implicated in Parkinson's disease, and loss of ATP13A2 causes lysosomal dysfunction, which causes cell death, and reduces the anti-oxidant capacity in cells, contributing to oxidative stress. This represents a new disease mechanism in neurodegeneration that will be highly influential in the field of Parkinson's research.

(c) ATP13A2 is a member of four isoforms belonging to the P5-type ATPases. Based on sequence comparison these related isoforms ATP13A2-5 are most likely polyamine transporters that together may represent the mammalian transport system. Several of these isoforms are implicated in a broad range of major human diseases, ranging from cancer, neurodegeneration, neurodevelopmental and cardiovascular diseases. Our findings are therefore relevant to study impaired polyamine homeostasis and P5-type ATPases in multiple diseases.

2.3. ATP13A2 perspectives for drug discovery

We identified a drugable activation mechanism of ATP13A2, which may be targeted by small molecules as a possible treatment of PD. ATP13A2 activation may improve lysosomal function and decrease oxidative stress, i.e. targeting two major defects in PD.
Two patents were filed based on these discoveries, and a project with the Center for Drug Design and Discovery (CD3) for high throughput screening of ATP13A2 activator molecules is initiated started, which will be funded by the Michael J. Fox Foundation.

3. Progress report ATP10B

3.1. Results

(a) The results obtained from this part of the study were summarized in a research article currently in revision in Acta Neuropathologica.
Shaun Martin*, Stefanie Smolders*, Chris Van den Haute, Bavo Heeman, Sarah van Veen, David Crosiers, Igor Beletchi, Aline Verstraeten, Helena Gossye, Géraldine Gelders, Philippe Pals, Norin Hamouda, Sebastiaan Engelborghs, Jean-Jacques Martin, Jan Eggermont, Peter Paul De Deyn, Patrick Cras, Veerle Baekelandt, Peter Vangheluwe#, Christine Van Broeckhoven# (shared * first and # last co-authors). Mutated ATP10B increases Parkinson's disease risk by compromising lysosomal glucosylceramide export. Under review in **Acta Neuropathologica (IF 18,17)**.

Several PD-associated mutations were identified in the ATP10B gene, a P-type ATPase with unknown function (Prof. C. Van Broeckhoven, joint patent WO2016166373A1). We established that the *ATP10B* gene encodes a late endo-lysosomal lipid flippase that translocates the lipids glucosylceramide (GluCer) and phosphatidylcholine (PC) towards the cytosolic membrane leaflet. The PD associated ATP10B mutants are catalytically inactive and fail to provide cellular protection against the environmental PD risk factors rotenone and manganese. In isolated cortical neurons, loss of ATP10B leads to general lysosomal dysfunction and cell death. Impaired lysosomal functionality and integrity is well known to be implicated in PD pathology and linked to multiple causal PD genes and genetic risk factors. Our results indicate that loss of function mutations in ATP10B increase risk for PD by disturbed lysosomal export of GluCer and PC. Both ATP10B and glucocerebrosidase, encoded by the PD risk gene GBA1, reduce lysosomal GluCer levels, emerging lysosomal GluCer accumulation as a potential PD driver.

3.2. ATP10B impact

(a) We discovered that GluCer transporters are implicated in PD. We found that ATP10B transports GluCer from the lysosomal compartment in cells, which is a novel insight, opening a novel and highly relevant research area about the translocation and redistribution of GluCer in mammalian cells, and how this may be implicated in PD.

(b) GBA1 mutations are the most common PD risk factor affecting 10% of the PD population. GBA1 encodes for GCase that degrades GluCer in lysosomes. Since loss of either GBA1 or ATP10B leads to an increased lysosomal GluCer content, lysosomal GluCer accumulation emerges as a critical regulator of neuronal health and survival, which is an important message for the PD field.

(c) Based on similarities between both studies lysosomal substrate accumulation is emerging as a likely driver for PD, which is a key finding and novel insight in PD.

3.3. ATP10B perspectives for drug discovery

Our study shows that ATP10B modulators may be of therapeutic interest to improve lysosomal dysfunction and prevent accumulation of glucosylceramide in lysosomes, which is of interest for GBA1-associated PD (10% of the PD population). With our established biochemical and cellular assays, we're preparing for a high throughput screening to identify ATP10B modulators, which occurs in collaboration with the Center for Drug Design and Discovery (CD3). A patent on ATP10B in neurodegeneration was filed.

4. Publications and Events (2017-2019)

4.1. Events and media coverage

- On November 23rd 2017, Princess Astrid visited the Laboratory of Cellular Transport Systems of Prof. Dr. Peter Vangheluwe and the Laboratory of Ion Channel Research of Prof. Dr. Thomas Voets in the Department of Cellular and Molecular Medicine, KU Leuven. This event has been covered by the press to inform the broad public about our research activities:
  http://www.robtv.be/nieuws/leuven/prinses-astrid-bezoekt-laboratoria-ku-leuven;
  http://www.nieuwsblad.be/cnt/dmf20171123_03203478;
  https://www.hln.be/regio/leuven/prinses-astrid-bezoekt-gasthuisberg~aeaaf126/;
  https://nieuws.kuleuven.be/nl/2017/prinses-astrid-bezoekt-leuvense-labos;
  https://www.facebook.com/ROBtv.be/videos/10154952286531825/;
  https://www.monarchie.be/nl/agenda/vib-center-for-brain-disease-research;
  http://www.fmre-gske.be/pages/nl/bezoekKULeuven3.html

- **Ernest Solvay prize**, Queen Elisabeth Foundation (€ 25,000) - Prof. Dr. Peter Vangheluwe (KU Leuven) - Neuroprotection by lysosomal transport mechanisms in Parkinson's disease
  - Award ceremony at the Palace, 26/04/2018
  - https://gbiomed.kuleuven.be/english/research/50000618/spotlight/ernest-solvay-prijs-voor-prof-peter-vangheluwe-voor-zijn-onderzoek-neuroprotection-by-lysosomal-transport-mechanisms-in-parkinsons-disease-1
  - Video interview and coverage of the research topic (by Reinout Goddyn)
  - https://vimeo.com/266308386

- Press release highlighting our findings reported in the Nature paper, currently scheduled January 29th 2020, subject to change.

4.2. Patents

– A novel gene in neurodegenerative disease; inventors: Christine Van Broeckhoven, Jessie Theuns, Aline Verstraeten, Bavo Heeman, Peter Vangheluwe, Filing date: April 18th 2016; ZL990060
– Screening Methods and Pharmaceutically active compounds for neurodegenerative diseases; inventors: Peter Vangheluwe, Veerle Baekelandt, Patrizia Agostinis, Chris Van den Haute, Sarah van Veen, Shaun Martin, Jan Eggermont. Filing date: July 3rd 2017; ZL916077
– Screeningsmethode ATP13A2; inventors: Peter Vangheluwe. Filing data: December 18th 2019; ZL919090

4.3. Publications in 2017-2019 (*** directly related to the project and with GSKE acknowledgement)

2019

- *** van Veen, S.*, Martin, S.* Van den Haute, C., Benoy, V., Lyons, J., Vanhoutte, R., Kahler, J.P., Decuypere, J.-P., Gelders, G., Lambie, E., Zielich, J., Swinnen, J.V., Annaert, W., Agostinis, P., Ghesquière, B., Verhelst, S., Baekelandt, V., Eggermont, J., Vangheluwe, P. (*equal contribution) ATP13A2 deficiency disrupts lysosomal polyamine export. *NATURE,* accepted Dec 2, 2019 (Impact factor: 43.07)
- Chen, J., Sitsel, A., Benoy, V., Sepúlveda, M.R., Vangheluwe, P. (2019). Primary Active Ca2+ Transport Systems in Health and Disease. *Cold Spring Harb Perspect Biol*. doi: 10.1101/cshperspect.a035113 (Impact factor: 9.11)
- Herrmann, A-K., Wuellner, V., Moos, S., Graf, J., Chen, J., Kieseier, B., Kurschus, F.C., Albrecht, P., Vangheluwe, P., Methner, A. (2019). Dimethyl fumarate alters intracellular Ca2+ handling in immune cells by redox-mediated pleiotropic effects. *FREE RADICAL BIOLOGY AND MEDICINE*, *141*, 338-347. doi: 10.1016/j.freeradbiomed.2019.07.005 (Impact factor: 5.66)
- Chen, J., Smaardijk, S., Mattelaer, C-A., Pamula, F., Vandecaetsbeek, I., Vanoevelen, J., Wuytack, F., Lescrinier, E., Eggermont, J., Vangheluwe, P. (2019). An N-terminal Ca2+-binding motif regulates the secretory pathway Ca2+/Mn2+-transport ATPase SPCA1. *JOURNAL OF BIOLOGICAL CHEMISTRY*, *294* (19), 7878-7891. doi: 10.1074/jbc.RA118.006250 (Impact factor: 4.11) Open Access
- Gorski, P.A., Jang, S.P., Jeong, D., Lee, A., Lee, P., Oh, J.G., Chepurko, V., Yang, D.K., Kwak, T.H., Eom, S.H., Park, Z-Y., Yoo, Y.J., Kim, D.H., Kook, H., Sunagawa, Y., Morimoto, T., Hasegawa, K., Sadoshima, J., Vangheluwe, P., Hajjar, R.J., Park, W.J., Kho, C. (2019). Role of SIRT1 in Modulating Acetylation of the Sarco-Endoplasmic Reticulum Ca2+-ATPase in Heart Failure. *Circ Res*, *124* (9), e63-e80. doi: 10.1161/CIRCRESAHA.118.313865 (Impact factor: 15.86)
- *** Wauters, F., Cornelissen, T., Imberechts, D., Martin, S., Koentjoro, B., Sue, C., Vangheluwe, P., Vandenberghe, W. (2019). LRRK2 mutations impair depolarization-induced mitophagy through inhibition of mitochondrial accumulation of RAB10. *AUTOPHAGY*. doi: 10.1080/15548627.2019.1603548 (citations: 2) (Impact factor: 11.06)
- Sitsel, A., De Raeymaecker, J., Drachmann, N.D., Derua, R., Smaardijk, S., Andersen, J.L., Vandecaetsbeek, I., Chen, J., De Maeyer, M., Waelkens, E., Olesen, C., Vangheluwe, P.*, Nissen, P.* (*equal contribution) (2019). Structures of the heart specific SERCA2a Ca2+-ATPase. *EMBO JOURNAL*, *38* (5), Art.No. ARTN e100020. doi: 10.15252/embj.2018100020 (citations: 4) (Impact factor: 11.23) Open Access

2018

- Bittremieux, M., La Rovere, R.M., Schuermans, M., Luyten, T., Mikoshiba, K., Vangheluwe, P., Parys, J.B., Bultynck, G. (2018). Extracellular and ER-stored Ca2+ contribute to BIRD-2-induced cell death in diffuse large B-cell lymphoma cells. *CELL DEATH DISCOVERY*, *4*, Art.No. ARTN 101. doi: 10.1038/s41420-018-0118-6 (citations: 3) Open Access
- Pessina, F., Gamberucci, A., Chen, J., Liu, B., Vangheluwe, P., Gorelli, B., Lorenzini, S., Spiga, O., Trezza, A., Sgaragli, G., Saponara, S. (2018). Negative chronotropism, positive inotropism and lusitropism of 3,5-di-t-butyl-4-hydroxyanisole (DTBHA) on rat heart preparations occur through reduction of RyR2 Ca2+ leak. *BIOCHEMICAL PHARMACOLOGY*, *155*, 434-443. doi: 10.1016/j.bcp.2018.07.026 (citations: 1) (Impact factor: 4.83)
- Smaardijk, S., Chen, J., Kerselaers, S., Voets, T., Eggermont, J., Vangheluwe, P. (2018). Store-independent coupling between the Secretory Pathway Ca2+ transport ATPase SPCA1 and Orai1 in Golgi stress and Hailey-Hailey disease. *BIOCHIMICA ET BIOPHYSICA ACTA-MOLECULAR CELL RESEARCH*, *1865* (6), 855-862. doi: 10.1016/j.bbamcr.2018.03.007 (citations: 6) (Impact factor: 4.74) Open Access
- *** Sorensen, D.M.*, Holemans, T.*, van Veen, S., Martin, S., Arslan, T., Haagendahl, I.W., Holen, H.W., Hamouda, N.N., Eggermont, J., Palmgren, M., Vangheluwe, P. (*equal contribution) (2018). Parkinson disease related ATP13A2 evolved early in animal evolution. *PLOS ONE*, *13* (3), Art.No. ARTN e0193228. doi: 10.1371/journal.pone.0193228 (citations: 2) (Impact factor: 2.78) Open Access
- Mikkelsen, S.A., Vangheluwe, P., Andersen, J.P. (2018). A Darier disease mutation relieves kinetic constraints imposed by the tail of sarco(endo)plasmic reticulum Ca-ATPase 2b. *Journal of Biological Chemistry*, *293* (11), Art.No. jbc.RA117.000941, 3880-3889. (citations: 2) (Impact factor: 4.11) Open Access

2017

- Martin, S., Dudek-Peric, A.M., Garg, A., Roose, H., Demirsoy, S., Van Eygen, S., Mertens, F., Vangheluwe, P., Vankelecom, H., Agostinis, P. (2017). An autophagy-driven pathway of ATP secretion supports the aggressive phenotype of BRAF(V600E) inhibitor-resistant metastatic melanoma cells. *Autophagy*, *13* (9), Art.No. 10.1080/15548627.2017.1332550, 1512-1527. (citations: 13) (Impact factor: 11.06) Open Access
- Demirsoy, S., Martin, S., Motamedi, S., van Veen, S., Holemans, T., Van den Haute, C., Jordanova, A., Baekelandt, V., Vangheluwe, P., Agostinis, P. (2017). ATP13A2/PARK9 regulates endo-/lysosomal cargo sorting and proteostasis through a novel PI(3, 5)P2-mediated scaffolding function. *Human Molecular Genetics*, *26* (9), Art.No. 10.1093/hmg/ddx070, 1656-1669. (citations: 10) (Impact factor: 4.54)

- Chen, J., De Raeymaecker, J., Hovgaard, J.B., Smaardijk, S., Vandecaetsbeek, I., Wuytack, F., Møller, J.V., Eggermont, J., De Maeyer, M., Christensen, S.B., Vangheluwe, P. (2017). Structure/activity Relationship of Thapsigargin Inhibition on the Purified Golgi/secretory Pathway Ca2+/Mn2+ Transport ATPase (SPCA1a). *Journal of Biological Chemistry*, *292* (17), Art. No. jbc.M117.778431, 6938-6951. (citations: 8) (Impact factor: 4.11) Open Access
- Smaardijk, S., Chen, J., Wuytack, F., Vangheluwe, P. (2017). SPCA2 couples Ca influx via Orai1 to Cauptake into the Golgi/secretory pathway. *Tissue & Cell*, *49* (2), Art.No. S0040-8166(16)30097-0, 141-149. doi: 10.1016/j.tice.2016.09.004 (citations: 10) (Impact factor: 1.55) Open Access
- Bittremieux, M., Gerasimenko, J.V., Schuermans, M., Luyten, T., Stapleton, E., Alzayady, K.J., De Smedt, H., Yule, D.I., Mikoshiba, K., Vangheluwe, P., Gerasimenko, O.V., Parys, J., Bultynck, G. (2017). DPB162-AE, an inhibitor of store-operated Ca2+ entry, can deplete the endoplasmic reticulum Ca2+ store. *Cell Calcium*, *62*, 60-70. doi: 10.1016/j.ceca.2017.01.015 (citations: 8) (Impact factor: 3.93)
- Estrada-Cuzcano, A., Martin, S., Chamova, T., Synofzik, M., Timmann, D., Holemans, T., Andreeva, A., Reichbauer, J., De Rycke, R., Chang, D-I., van Veen, S., Samuel, J., Schöls, L., Pöppel, T., Sorensen, D.M., Asselbergh, B., Klein, C., Zuchner, S., Jordanova, A., Vangheluwe, P.*, Tournev, I.*, Schüle, R.* (*equal contribution) (2017). Loss-of-function mutations in the ATP13A2/PARK9 gene cause complicated hereditary spastic paraplegia (SPG78). *Brain*, *140* (2), 287-305. (citations: 39) (Impact factor: 11.81)
- Tharkeshwar, A.K., Trekker, J., Vermeire, W., Pauwels, J., Sannerud, R., Priestman, D.A., Te Vruchte, D., Vints, K., Baatsen, P., Decuypere, J-P., Lu, H.Q., Martin, S., Vangheluwe, P., Swinnen, J., Lagae, L., Impens, F., Platt, F.M., Gevaert, K., Annaert, W. (2017). A novel approach to analyze lysosomal dysfunctions through subcellular proteomics and lipidomics: the case of NPC1 deficiency. *Scientific Reports*, *7*, Art.No. 10.1038/srep41408. (citations: 24) (Impact factor: 4.01)

4.4. Publications in revision (*** directly related to the project and with GSKE acknowledgement)

- *** Stephanie Vrijsen*, Laura Besora-Casals*, Sarah van Veen, Jeffrey Zielich, Chris Van den Haute, Christian Fischer, Patrizia Agostinis, Veerle Baekelandt, Jan Eggermont, Eric Lambie#, Shaun Martin#, Peter Vangheluwe#. (equal * first and # last contribution). ATP13A2-mediated endo-lysosomal polyamine export provides a mitochondrial antioxidant response. Under review in **PNAS**.
- *** Shaun Martin*, Stefanie Smolders*, Chris Van den Haute, Bavo Heeman, Sarah van Veen, David Crosiers, Igor Beletchi, Aline Verstraeten, Helena Gossye, Géraldine Gelders, Philippe Pals, Norin Hamouda, Sebastiaan Engelborghs, Jean-Jacques Martin, Jan Eggermont, Peter Paul De Deyn, Patrick Cras, Veerle Baekelandt, Peter Vangheluwe#, Christine Van Broeckhoven# (shared * first and # last co-authors). Mutated ATP10B increases Parkinson's disease risk by compromising lysosomal glucosylceramide export. Under review in **Acta Neuropathologica**.

Geneeskundige Stichting Koningin Elisabeth
Fondation Médicale Reine Elisabeth
Königin-Elisabeth-Stiftung für Medizin
Queen Elisabeth Medical Foundation

Final report of the research group of

Prof. Vanhollebeke Benoit, PhD

Université Libre de Bruxelles (ULB)

Principal investigator

Prof. Vanhollebeke Benoit, PhD
Head of the Laboratory of Neurovascular Signaling
Department of Molecular Biology
Neuroscience Institute Faculty of Sciences
University of Brussels (ULB)
Tel.: +32 2 650 97 61
Fax: +32 2 650 97 50
E-mail: Benoit.Vanhollebeke@ulb.ac.be
nvasc.ulb.be/vanhollebekelab/

Organ-wide analysis of brain neurovascular communication in real-time and at single-cell resolution

1. State of the Art

Blood vessels are more than passive conduits for blood flow and that tissue-specific vascular beds not only match the metabolic demands of the perfused organs, but also act as important signaling centers releasing angiocrine factors that contribute to organ development, maintenance and repair. Accordingly, proper brain function relies on elaborate communications between the neural and vascular system and this organ serves as a paradigm for extensive crosstalk between the vascular system and its local microenvironment. Central nervous system (CNS) neurovascular development has been best studied in the developing mouse CNS and a number of genetic regulators of neurovascular development have been uncovered, with a subset of them further organized into networks. Despite this progress, an integrated picture of how, when and to what extent neural and vascular development are coordinated is lacking. Building this model will critically rely on the combined capacity to (i) scrutinize the cellular modalities of the intrinsically highly dynamic processes of vascular and neural development in real-time and to (ii) identify experimental settings where the signaling and circulatory functions of the intracerebral blood vessels can be, at least partially, uncoupled. Every aspect of neurovascular development and function, from blood vessels morphogenesis and BBB formation to neural cell metabolism, is indeed exquisitely sensitive to reduced tissue oxygen tension. The hypoxia response that invariably accompanies defective vascular development is a confounding factor severely blunting the scope of approachable investigations in the field.

Our previous work identified and validated the optically-clear zebrafish embryonic brain as uniquely endowed with these distinctive attributes, through the startling observation that zebrafish brains remain normoxic throughout organogenesis even in the total absence of intracerebral blood vessels and that, after prolonged periods of impaired vascular development, blood vessels invade and branch within the neural system in stereotypical patterns, implying long-prevailing physiological conditions.

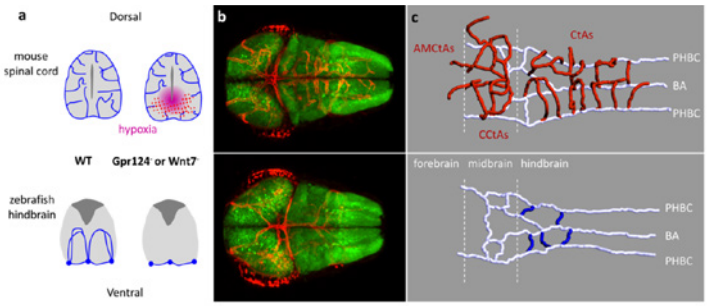

A normoxic and transparent setting to explore CNS neurovascular interactions. (**a**) Cross-section through the mouse and zebrafish central nervous system with or without impaired vascular development. (**b**) z-projection of a dorsal confocal scan through the zebrafish brain, with post-mitotic neurons labeled in green and endothelial cells in red. (**c**) Wire-diagram representation of WT and mutant zebrafish brain vasculature in dorso-lateral views. Red vessels represent the intra-cerebral BBB network.

Through the combined increase in spatio-temporal resolution, best suited to comprehend the intrinsically dynamic processes of neurovascular development and function, and the absence of confounding hypoxic signaling cascades, some fundamental questions seem now within reach: Through which cellular and molecular mechanisms is CNS vascular invasion and maturation controlled by neural signals? Reciprocally, how does the developing vascular system impact on brain patterning and function?

The physical and genetic constraints imposed to the study of the dynamic cellular mechanisms governing sprouting angiogenesis have restricted their investigation to a limited number of *in vivo* settings, most notably the postnatal mouse retina and the zebrafish ISVs. In recent years, a coherent model integrating controlled behaviors of VEGF-selected tip cells and notch-induced stalk cells within nascent sprouts has been derived from those prototypical settings. Hierarchical organization of differentially-fated endothelial cells (ECs) during sprouting angiogenesis and organ-specific adaptations are viewed as consecutive, and hence distinct, aspects of vascular development. However, through live imaging of mosaic animals, an integrated control was recently shown to operate under the control of CNS-derived signals. Neural progenitor-derived Wnt7 ligands, well-known inducers of brain EC maturation, govern CNS EC invasion through selective modulation of tip cell function within the parental perineural vessels.

2. Objectives

A major aim of our project is to address how the neural and vascular systems communicate to assemble functional neurovascular units. In particular, we study how perineural endothelial cells (ECs) selectively respond to neural-derived Wnt7 ligands during the process of brain angiogenesis.

From the initial discovery of Frizzled as Wnt receptors two decades ago to the recent crystallographic insights into their interaction mechanism, it has remained unknown how cells discriminate between multiple Wnt ligands within complex biological systems. The Wnt/Frizzled interaction chemistry is indeed incompatible with mono-specific recognition and, accordingly, when tested in pair-wise combinations, multiple Wnt ligands compete for binding to various Frizzled receptors. We are exploring a novel molecular mechanism that enables cells to bind and respond to Wnt7 ligands with strict specificity.

Our previous findings indeed identified Adgra2/Gpr124, an orphan member of the adhesion class of G protein-coupled receptors as an essential co-factor of Wnt7 signaling in CNS ECs. Adhesion G protein-coupled receptors (aGPCRs) constitute the second largest group of GPCRs in humans. Most aGPCRs are orphan receptors with no identified ligands that function through remarkably diverse mechanisms. They differ from other GPCRs by long N-terminal extensions preceding a membrane-proximal GPCR autoproteolysis-inducing (GAIN) domain containing the highly conserved GPCR proteolytic site (GPS). These N-terminal sequences typically comprise multiple protein-protein interaction domains involved in cell-cell and cell-matrix contacts. This structural hallmark significantly broadens the signaling potential and complexity of this class of GPCRs that, context-dependently, behave as adhesion molecules or signal transducing GPCRs. Gpr124, a member of this branch of GPCRs has gained considerable interest since the discovery of its essential role in brain vascular development (Kuhnert et al., 2010). Upon genetic inactivation, vascularization and blood-brain barrier maturation are impaired in all or parts of the zebrafish and mouse central nervous system, respectively (Anderson et al., 2011; Cullen et al., 2011; Kuhnert et al., 2010; Vanhollebeke et al., 2015). This receptor promotes angiogenic sprouting through endothelial cell (EC)-autonomous Wnt/β-catenin signaling stimulation upon contact with neural progenitor-derived Wnt7 ligands (Posokhova et al., 2015; Vanhollebeke et al., 2015; Zhou and Nathans, 2014).

Genetic studies in zebrafish have shown that in order to recognize these ligands, and hence to be competent for brain invasion, ECs must additionally express Reck, a GPI-anchored glycoprotein (Ulrich et al., 2016; Vanhollebeke et al., 2015). Consistently, EC-specific invalidation of RECK in the mouse leads to CNS-specific vascular defects, thereby demonstrating the evolutionary conserved role of RECK in cerebrovascular development (de Almeida et al., 2015). Gpr124 and Reck have been proposed to interact at the plasma membrane to assemble a potent and Wnt7-specific Wnt/β-catenin co-activator complex (Vanhollebeke et al., 2015). The complex also operates in neural crest-derived cells to promote

dorsal root ganglia (DRG) neurogenesis in zebrafish embryos (Vanhollebeke et al., 2015). Defective DRG neurogenesis is accompanied by metamorphic pigmentation alterations in the adult Gpr124 mutant skin (Vanhollebeke et al., 2015).

While the genetic interaction between *gpr124* (also known as *adgra2*) and *reck* is well supported by studies in the zebrafish model as well as cell culture experiments, their activation and signaling mechanisms are poorly characterized, in part as a result of a lack of *in vivo* models where structure-function relationships can be probed.

3. Results

3.1. Identification of an *in vivo* model of *gpr124/adgra2*-dependent neurovascular dysfunction (Bostaille et al. *Development*)

Malmquist *et al.* (2013) phenotypically characterized the *ouchless* mutant that was recovered from an F3 forward genetic screen for defective dorsal root ganglion (DRG) neurogenesis in zebrafish. While the initial dorsoventral migration of neural crest-derived cell clusters towards presumptive DRG locales appears unaffected in *ouchless* mutants, the neurogenic program leading to the generation of *neurog1:*EGFP+ cells within the ganglion is defective, resulting in a severe reduction of DRG numbers in 72 hours post fertilization (hpf) *ouchless* mutants. *ouchless* mutants are viable but exhibit reduced growth rates and interrupted melanophore stripes in the adult skin. The *ouchless* mutation was mapped by bulk segregation analysis to a 342 kb genomic region of chromosome 8, harboring the *sorbs3* gene. No causative mutation could be identified within the coding sequence of *sorbs3*, but a mutation was suspected to reside within cis-regulatory elements, accounting for the reduced *sorbs3* transcript levels observed in *ouchless* mutants. Antisense *sorbs3* morpholino knockdown experiments, as well as BAC and mRNA rescue experiments, further supported the model that *sorbs3* regulates DRG neurogenesis and that *sorbs3* dysfunction drives the *ouchless* phenotypes (Malmquist et al., 2013).

The *ouchless* phenotypes are remarkably analogous to the DRG defects reported in *gpr124* knock-out mutants (Vanhollebeke et al., 2015). Of note *gpr124* has been renamed to *adgra2*. Along with Reck, Gpr124/Adgra2 has been shown to control DRG formation by activating Wnt signaling in neural crest-derived sox10:mRFP+ ganglion cells (Vanhollebeke et al., 2015). Given the phenotypic similarities, we therefore set out to test whether *adgra2* and *ouchless* (presumably *sorbs3*) co-operate during the process of DRG neurogenesis and brain vascularization.

We first demonstrated that **adgra2/gpr124** and **ouchless** genetically interact by functional gene dosage experiments (**Figure 1**).

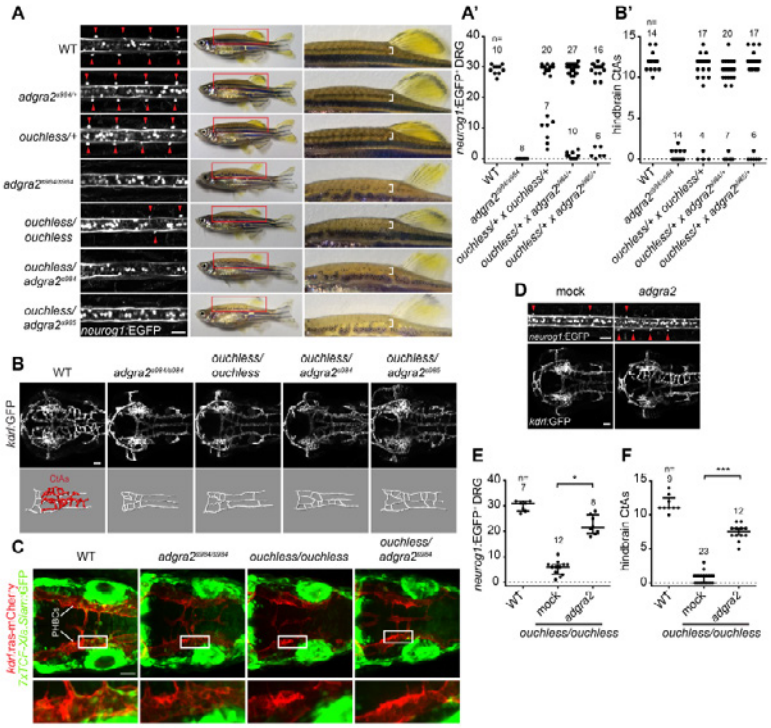

Figure 1 *gpr124/adgra2* and *ouchless* mutations fail to complement. (**A** and **A'**) Fish heterozygous for **ouchless** were crossed with the previously described **adgra2** heterozygotes, **adgra2**$^{s984/+}$ and **adgra2**$^{s985/+}$, and the offspring were assessed at 72 hpf for defects in DRG neurogenesis. From these crosses, ~25% of the offspring (annotated as **ouchless/adgra2**^{s984} and **ouchless/adgra2**^{s985}) showed an almost complete lack of **neurog1**:EGFP^{+} DRG. When raised to adulthood, these fish could be distinguished from their siblings by discontinuous dorsal melanophore stripes on their skin (brackets). (**B** and **B'**) Cerebral vasculatures of 60 hpf embryos derived from **ouchless** heterozygotes incrosses and outcrosses to **adgra2** heterozygotes. 25% of the offspring of each of the crosses displays highly penetrant brain vascular defects, characterized by a complete absence of central arteries (CtAs), similar to **adgra2** mutants. (C) Defective endothelial Wnt/β-catenin signaling in the perineural primordial hindbrain channel (PHBC) ECs. (D-F) When **ouchless** mutants are injected at the one-cell stage with mRNA encoding wild-type (WT) Adgra2, significant restoration of **neurog1:**EGFP^{+} DRG and cerebral blood vessels is observed.

The lack of complementation between *ouchless* and *adgra2*, together with the discovery of vascular phenotypes in *ouchless* mutants that mimic those of *adgra2* mutants, indicates that *ouchless* constitutes a new allele of *adgra2*. The re-evaluation of the genomic region known to harbour the *ouchless* mutation revealed that the *adgra2* gene resides within the critical interval, spanning the ca-48 and ca-37 genomic markers. In *ouchless* mutants, *adgra2* displays an essential splice site mutation inactivating Adgra2 through the in-frame deletion of a single LRR in the ectodomain of this adhesion G-protein coupled receptor (**Figure 2**).

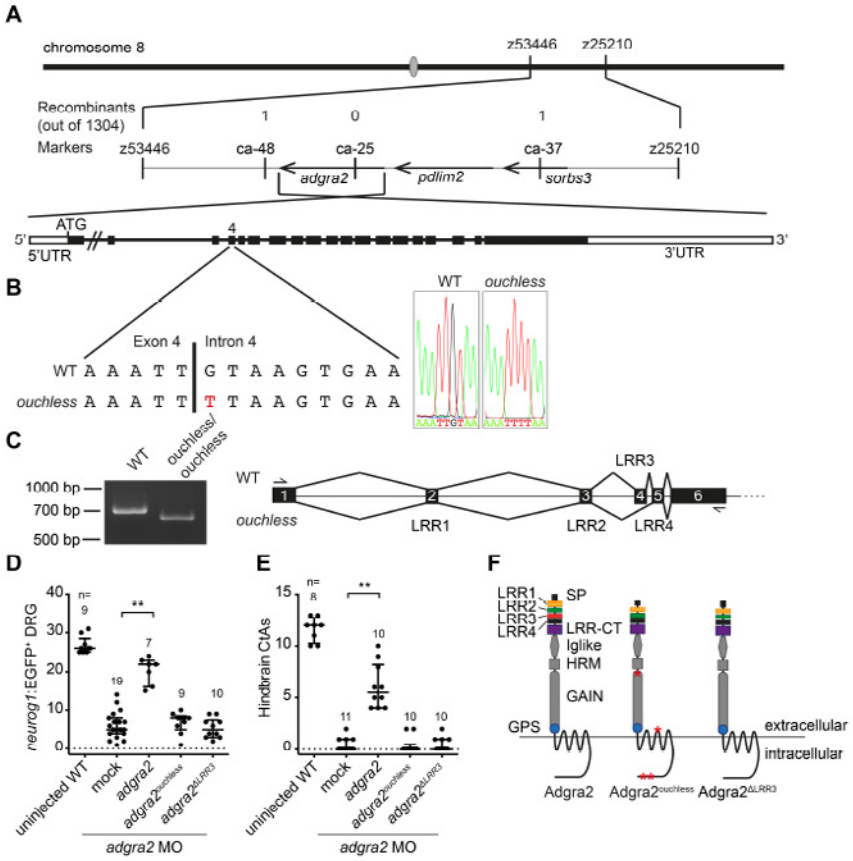

Figure 2 adgra2 is mutated in ouchless mutants. (**A**) Representation of the *ouchless* locus genetic map on chromosome 8. The number of recombinants among 1304 meioses as determined by Malmquist et al. (2013) is indicated above the markers utilized for mapping. (**B**) Sanger sequencing of the exon 4-intron 4 boundary of *adgra2* in WT and *ouchless* mutant embryos. The G→T change in the *ouchless* 5′ splice donor sequence appears in red. (**C**) RT-PCR splicing analysis of *adgra2* in 48 hpf WT and *ouchless* mutant embryos. The amplification primers hybridize to exon 1 and exon 6, as illustrated in the panel on the right. (**D, E**) The capacity of the full-length *adgra2* coding sequence from *ouchless* mutants to rescue DRG and CtA defects in *adgra2* morphants was evaluated by mRNA injection at the one-cell stage. While mRNA encoding the WT receptor (annotated as *adgra2*) partially suppressed both phenotypes, the *ouchless* variant (annotated as *adgra2*^{ouchless}) did not affect either. (**F**) Comparison of a reference WT *adgra2* allele with the *adgra2* coding sequence recovered from *ouchless* mutant embryos. Four non-synonymous single nucleotide polymorphisms (SNPs; M429V, S895P, A1282V and A1302G) as well as an in-frame 72 bp deletion corresponding to exon 4 are found in *ouchless*. While all four *adgra2* SNPs identified in *ouchless* mutants had been previously identified in functionally validated *adgra2* alleles derived from mixed AB/TL genetic backgrounds, alternative splicing resulting in exon 4 skipping is absent from any known zebrafish, mouse or human *ADGRA2* isoform. When probed in zebrafish, alternative splicing of the exon 1-exon 6 sequences is undetectable by RT-PCR (C). Exon 4 corresponds precisely to the third leucine-rich repeat (LRR) unit of the LRR/CT domain of Adgra2, which comprises an array of four 24-residue-long LRR units followed by a LRR cysteine-rich C-terminal motif (LRR-CT).

Altogether, this work reveals that *ouchless* and *adgra2* mutants are allelic and that the *ouchless* phenotypes result from an essential splice site mutation inactivating Adgra2 through the in-frame deletion of a single LRR in the ectodomain of this adhesion G-protein coupled receptor (GPCR). The zebrafish *ouchless* mutant thereby constitutes the first *in vivo* model of *adgra2* N-terminal domain-specific variation.

3.2. Molecular insights into Adgra2/Gpr124 and Reck intracellular trafficking (Bostaille *et al.* Biology Open)

Taking advantage of the above-described mutation in *adgra2*, we undertook to better define the cellular and molecular modalities of the Gpr124/Reck synergistic interaction. In particular, the stoichiometry of the Gpr124/Reck complex and the molecular determinants of its trafficking, assembly and signal transduction still needed to be investigated. The N-terminal domains of Gpr124 are likely contributors to several, if not all, of these processes. Indeed, cell culture and *in vivo* experiments have revealed that Gpr124 function critically relies on its extracellular domain architecture. N-terminal truncations or substitution of the ectodomain of Gpr124 with the equivalent domain derived from the closely related

Gpr125, abrogate receptor signaling (Posokhova et al., 2015; Vanhollebeke et al., 2015). Moreover, the Gpr124 potential interaction interface with Reck, a cell surface exposed GPI-anchored glycoprotein, is restricted to the extracellular parts of the receptor.

As is typically found in aGPCRs, the extracellular N-terminus of Gpr124 comprises multiple protein-protein interaction domains whose contributions to receptor function remain largely elusive. Specifically, the Gpr124 ectodomain is sequentially composed of an N-terminal LRR/CT domain, an Ig-like domain and a hormone receptor motif (HRM) preceding the membrane-proximal GPS-containing GAIN domain. The Gpr124 LRR/CT domain contains four leucine-rich repeat (LRR) units which are 20-29 residue-long structural units that assemble in a superhelical manner with tandemly arranged repeats to form curved solenoid structures acting as protein interaction frameworks. As found in Gpr124, extracellular LRR motifs are often flanked by cysteine-rich C-terminal domains (LRR-CTs) that are integral parts of the LRR domain and shield the hydrophobic core of the last LRR motif. Building a proper understanding of Gpr124 function will benefit from delineating the contribution of each N-terminal domain to receptor function.

The *adgra2* variant found in *ouchless* mutants differs from *adgra2* reference sequences by four non-synonymous SNPs as well as a 72 bp deletion corresponding to exon 4 (**Figure 3A**). While the SNPs represent naturally occurring variations, the exon 4 skipping event is caused by an ENU-induced essential splice-site mutation at the exon 4–intron 4 boundary and was shown to result in Adgra2^{ouchless} inactivation (Bostaille et al., 2017). Exon 4 encodes the third LRR motif (LRR3) of the LRR/CT domain. In order to determine how the absence of LRR3 mechanistically impairs Adgra2 function, we generated C-terminal EGFP-tagged versions of wild-type (WT) Adgra2 as well as *ouchless* (Adgra2^{ouchless}) and ΔLRR3 (Adgra2$^{\Delta LRR3}$) variants. This latter variant reproduces the exon 4 deletion found in *ouchless* in a WT allele of *adgra2*, and hence lacks the *ouchless*-associated SNPs (Bostaille et al., 2017). We first evaluated the functionality of the fusion proteins in brain angiogenic assays in zebrafish by mRNA injections at the one-cell stage. While ectopic restoration of either EGFP-tagged or untagged versions of WT Adgra2 could restore angiogenic sprouting in *adgra2*$^{s984/s984}$ hindbrains (red arrowheads in **Figure 3C**), the equivalent Adgra2^{ouchless} and Adgra2$^{\Delta LRR3}$ variants were inactive (**Figure 3B,C**). These observations extend and confirm previous findings indicating that C-terminal fusions are compatible with receptor function *in vivo* and that, in the absence of LRR3, Adgra2 is non-functional (Vanhollebeke et al., 2015, Bostaille et al., 2017).

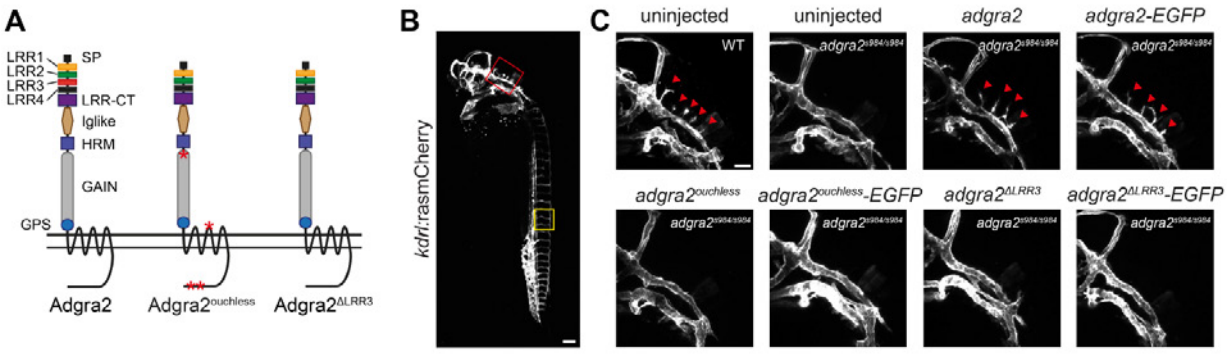

Figure 3. Adgra2^{ouchless} mislocalizes to the endoplasmic reticulum. (**A**) Schematic representation of Adgra2, Adgra2^{ouchless} and Adgra2$^{\Delta LRR3}$ topology and domain organization. Adgra2^{ouchless} and Adgra2$^{\Delta LRR3}$ lack the third LRR motif (red rectangle). The positions of the residue variations resulting from naturally occurring SNPs in *adgra2*^{ouchless} are designated by red asterisks. (**B**) Maximal intensity projection of a confocal z-stack of a WT *Tg(kdrl:ras-mCherry)* embryo at 36 hpf in lateral view. The red and yellow boxes define, respectively, the magnified areas of the hindbrain vasculature shown in C and the intersegmental vessels shown in E. Scale bar: 100 µm. (**C**) Maximal intensity projection of a confocal z-stack of WT and *adgra2*$^{s984/984}$ *Tg(kdrl:ras-mCherry)* embryos at 36 hpf in lateral view after injection of 100 pg of *adgra2*, *adgra2-EGFP*, *adgra2*^{ouchless}, *adgra2*^{ouchless}*-EGFP*, *adgra2*$^{\Delta LRR3}$ or *adgra2*$^{\Delta LRR3}$*-EGFP* mRNA at the one-cell stage. The red arrowheads point to the CtAs invading the hindbrain rhombomeres. Scale bar: 50 µm.

We then analyzed the stability and subcellular distribution of the EGFP-tagged variants in different cell types. When examined in the large and cobblestone-shaped enveloping layer cells of the 5 h post fertilization (hpf) zebrafish blastula, WT Adgra2-EGFP labeled the plasma membrane where it colocalized with a membrane-tethered lyn-RFP marker. By contrast, the mutant fusion proteins accumulated in an intracellular reticulate compartment reminiscent of the ER. Similarly, when analyzed in ECs of mosaic transgenic zebrafish, the WT fusion decorated the EC plasma membranes, including the numerous filopodial extensions of the tip cells, while the mutant variants showed strong intracellular and perinuclear signals that did not colocalize with the ras-mCherry EC membrane marker. Finally, in order to streamline quantitative colocalization studies, we imaged the cellular distribution of the EGFP fusion proteins in cultured HEK293T cells. Whereas the WT fusion protein accumulated at the plasma membrane marked by GPI-RFP as anticipated, the mutant versions failed to reach this compartment but instead accumulated intracellularly. The accumulating compartment was identified as the ER with the help of the mCherry-fused ER protein translocation apparatus component SEC61β. This was further quantitatively evaluated by Pearson's colocalization coefficient (PCC) analysis. Moreover, a perfect correlation was observed between the capacity of the LRR chimera variants to reach the plasma membrane and their ability to support vascular sprouting in the zebrafish hindbrain or to induce the formation of DRG neurons.

When overexpressed in cultured cells, Adgra2 and Reck colocalize at the plasma membrane and proximity ligation assays further suggest that the proteins may directly interact within this compartment to assemble a receptor complex (Vanhollebeke et al., 2015). It remains to be determined whether the partners recognize and assist each other during their progression within the secretory pathway or instead meet at the plasma membrane after independent trafficking events. We took advantage of the ER retention of the LRR/CT variants to address this question. As revealed by indirect immunofluorescence assays in non-permeabilized HEK293T cells, HA-Reck reached the plasma membrane independently of the nature and trafficking status of the co-expressed Adgra2 receptor (**Figure 4A**). In addition, when expressed individually in HEK293T cells, Reck and Adgra2 localized to the plasma membrane (Vanhollebeke et al., 2015). These results suggest that Reck does not require Adgra2 in order to reach the plasma membrane and vice versa. However, as HEK293T cells express low levels of endogenous *ADGRA2* and *RECK* (Vanhollebeke et al., 2015; Zhou and Nathans, 2014), this endogenous protein pool might be sufficient to accompany ectopic Reck and/or Adgra2 during secretion. We therefore engineered *ADGRA2*$^{-/-}$ and *RECK*$^{-/-}$ HEK293T cells through CRISPR/Cas9 approaches and re-evaluated Adgra2 and Reck trafficking in these genetic backgrounds (**Figure 4B**). As in WT cells, both proteins accumulated at the plasma membrane when expressed individually, indicating that each partner can reach its final destination independently (**Figure 4C,D**).

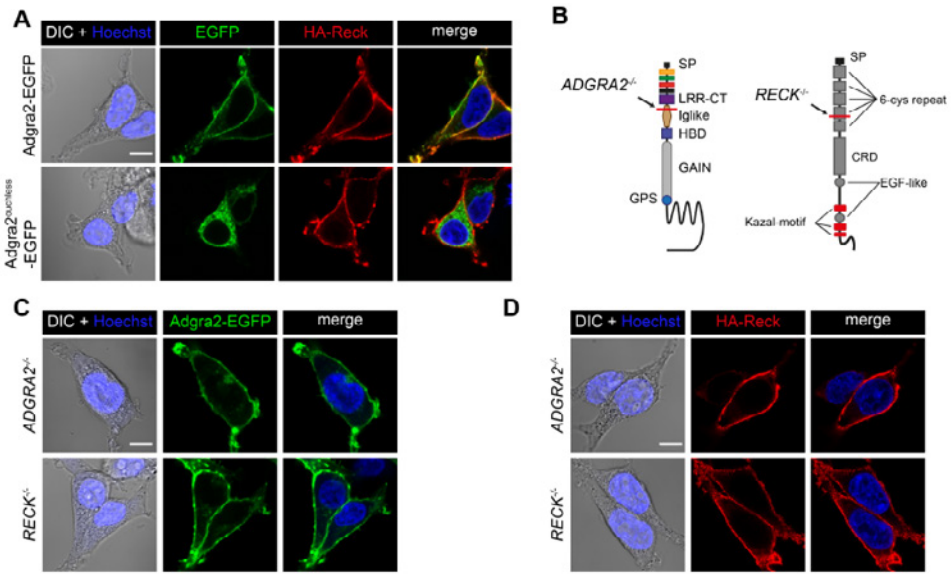

Figure 4 Independent trafficking of Reck and Adgra2 to the plasma membrane. (**A**) Single-plane confocal images of non-permeabilized HEK293T cells 48 h after transfection with *HA-reck* and *adgra2-EGFP* variants, as indicated. (**B**) Schematic representation of the genetic lesions of *ADGRA2*$^{-/-}$ and *RECK*$^{-/-}$ cells. The position of the frame-shift mutation is indicated by the red line. (**C,D**) Single-plane confocal images of non-permeabilized *ADGRA2*$^{-/-}$ and *RECK*$^{-/-}$ HEK293T cells 48 h after transfection with *adgra2-EGFP* (**C**) and *HA-reck* (**D**) constructs. In all panels, EGFP is detected by direct fluorescence and the HA-Reck fusion by anti-HA indirect immunofluorescence. Cells were additionally transfected with a *Wnt7a* (mouse gene) expression construct. Nuclei were counterstained with Hoechst. Scale bars: 10 µm.

When assessed 48 h post transfection in saponin-permeabilized HEK293T cells, a minor fraction of HA-Reck can be immunodetected in the ER and as such co-distributes with Adgra2^{ouchless} (**Figure 5A**, arrows) and presumably with a fraction of WT Adgra2 transiting through this compartment. To test whether Adgra2 is able to interact with Reck under these conditions, we performed proximity ligation assays as described previously (Vanhollebeke et al., 2015). As shown in **Figure 5B**, no interaction could be detected between HA-Reck and FLAG-Adgra2^{ouchless}, in contrast to the plasma membrane-localized signal readily detected in HA-Reck and FLAG-Adgra2 co-expressing cells. These results suggest that either the ER is not permissive for the formation of the complex or that the LRR deletion in Adgra2 impairs its interaction with Reck.

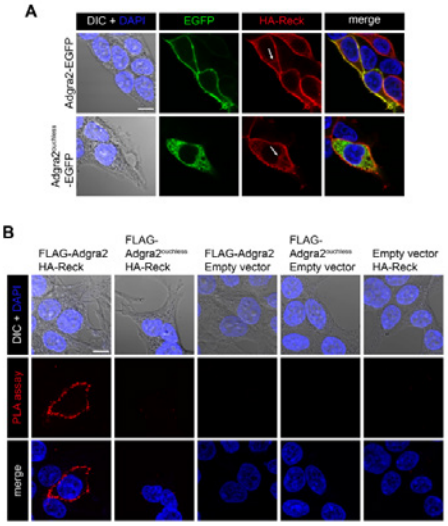

Figure 5 Cellular distribution of Adgra2 and Reck interaction. (A) Single-plane confocal images of saponin-permeabilized HEK293T cells 48 h after transfection with *HA-reck* and *adgra2-EGFP* variants, as indicated. Nuclei were counterstained with DAPI. EGFP is detected by direct fluorescence and the HA-Reck fusion by anti-HA indirect immunofluorescence. Arrows point to the ER. (B) Proximity ligation assays in HEK293T cells 48 h after transfection with *FLAG-adgra2*, *FLAG-adgra2*^{ouchless} and *HA-reck* constructs, as indicated. Nuclei were counterstained with DAPI. In all panels, cells were additionally transfected with a *Wnt7a* (mouse gene) expression construct. Scale bar: 10 µm.

This study characterized the functionally null mutation of *adgra2* recently identified in zebrafish *ouchless* mutants. The genetic lesion results in *adgra2* alternative splicing and we show that this receptor variant localizes to the ER instead of the plasma membrane. This unprecedented occurrence of an aberrantly routed Adgra2 prompted us to evaluate whether the intracellular trafficking of Reck and Adgra2 are interdependent. When co-expressed with the ER-retained Adgra2 variant, Reck still reached the plasma membrane. Extending this analysis in CRISPR/Cas9 engineered cells, Reck was shown to accumulate at the plasma membrane in both WT and *ADGRA2*$^{-/-}$ HEK293T cells and, similarly, Adgra2 trafficking to the plasma membrane was unaffected by the presence or absence of RECK. These data indicate that the partners, when expressed individually, are able to traffic independently. When co-expressed in HEK293T cells, their close proximity can be detected by PLA assays at the plasma membrane but not within the endomembrane compartments of the secretory pathway through which they transit. These combined observations indicate that the partners first meet at the plasma membrane and that their synergy is likely restricted to the events occurring subsequently at the cell surface, in agreement with the current model (Vanhollebeke et al., 2015). It is conceivable that the interaction between Adgra2 and Reck is only made possible within plasma membrane microdomains of specific proteolipidic composition or that a yet to be defined component induces complex formation within this compartment. The selective association of Reck and Adgra2 at the plasma membrane could also result from the higher concentrations reached within this final membrane compartment favoring the potentially transient encounters of the partners.

While this study describes the role of the LRR/CT domain in promoting Adgra2 progression through the ER, it does not exclude additional roles for this domain in the Adgra2/Reck signaling pathway. The LRR/CT domain might, for instance, be additionally implicated in the interactions with Reck, Wnt7 or Fzd/Lrp5/6 occurring at the plasma membrane.

3.3. Defining the molecular mechanism for Wnt ligand-specific signaling controlling brain vascularization in vertebrates (Eubelen et al. Science)

As outlined above, Wnt signaling is an ancient signaling pathway that has accompanied the emergence of metazoans and is key to many developmental, physiological, and disease processes. Similar to other signaling pathways, gene families for both Wnt ligand and its corresponding Frizzled receptor have undergone extensive expansion during metazoan evolution. Vertebrate genomes harbor 19 closely related Wnt genes as well as 10 Frizzled genes. Gene duplication is typically considered a major driving force in the evolution of new biological functions through neo- or subfunctionalization of emerging paralogs. How this functional diversification of Wnt ligands is structurally and molecularly organized, however, remains poorly understood. The Wnt/Frizzled molecular interaction is mediated by residues conserved across both families. This promiscuous interaction is incompatible with monospecific recognition and, accordingly, when tested in pair-wise combinations, multiple Wnt ligands compete for binding to various Frizzled receptors.

These observations raise the questions of how Wnt ligands achieve functional diversification and how cells interpret the intermingled expression patterns of simultaneous and sometimes conflicting Wnt signals. In some biological settings, cells may integrate all signaling inputs non discriminately and trigger appropriate responses by considering their total net balance. However, other biological processes exhibit strict Wnt ligand selectivity, despite complex Wnt/Frizzled expression landscapes. A prototypical example is provided by the exclusive control of mammalian forebrain and ventral spinal cord angiogenesis by Wnt7a and Wnt7b.
Within this neurovascular unit, in order to respond to neural progenitor–derived Wnt7 by activating Wnt/b-catenin signaling, cerebral endothelial cells must express a membrane protein complex consisting of the adhesion G protein–coupled receptor (GPCR) Gpr124 (Adgra2) and the glycosylphosphatidylinositol-anchored glycoprotein Reck. This Gpr124/Reck complex was recently reported to promote Wnt7-specific responses.

Using a combination of biophysical approaches and ligand-binding assays in genetically engineered cells, we demonstrated that ligand selectivity is conferred by Reck, which mediates Wnt7-specific binding in a Frizzled-independent manner. Reck orchestrates Wnt ligand discrimination by engaging the structurally disordered and highly divergent linker domain of Wnt7. The presence of Gpr124 is required to deliver Reck-bound Wnt7 to Frizzled by assembling higher-order Reck/Gpr124/Frizzled/Lrp5/6 complexes. This Gpr124 tethering function does not rely on its GPCR structure but instead on its combined capacity to interact with Reck extracellularly and recruit the Dishevelled scaffolding protein intracellularly. By bridging Gpr124 and Frizzled, Dishevelled recruitsWnt7, via its association with Reck, into dynamic Wnt/Frizzled signalosomes, resulting in increased local concentrations of ligand available for Frizzled signaling.

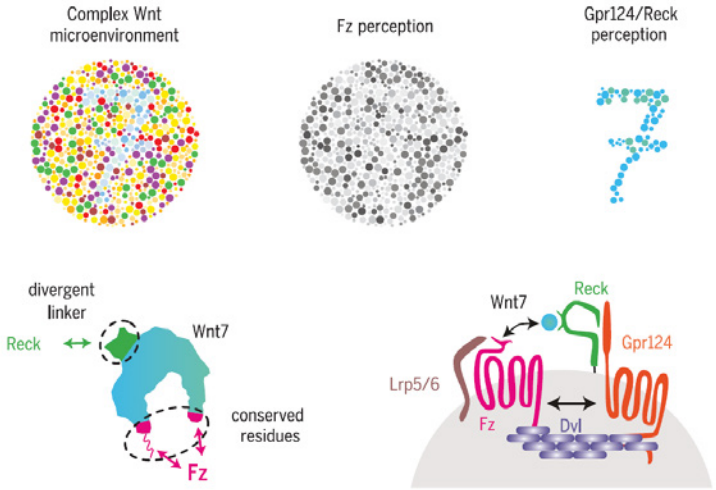

Figure 6 Task sharing for orchestrated Wnt7-specific cellular responses. (Top) Gpr124 and Reck cooperatively alter the cell's perception of its Wnt microenvironment by selectively potentiating Wnt7 signals (cyan-tinted dots). (Bottom) Reck decodes Wnt ligands by establishing monospecific contacts with the highly divergent Wnt7 linker domain. Gpr124 links Reck-bound Wnt7 to Dishevelled. Dishevelled polymers by interacting simultaneously with Gpr124 and Fz assemble Wnt7-enriched signalosomes that trigger signaling through Fz receptors and Lrp5/6 co-receptors.

Our data reveal that cells are equipped with "Wnt-decoding modules" that distinguish between Wnt ligands that are otherwise very similar. They also reveal a critical role for the linker domain in Wnt ligand evolution and functional diversification. These mechanistic insights into the Wnt decoding capacities of vertebrate cells predict that additional Wnt decoding modules exist, enabling fine-tuning of cellular behaviors in response to other Wnt or Frizzled family members. These modules expand the diversity of proximal events in Wnt signaling, opening new therapeutic opportunities for conditions in which Wnt stimulation or inhibition are desirable at the membrane level. In particular, the mechanisms uncovered here provide an opportunity for the targeted treatment of human central nervous system neurovascular disorders.

3.4. Probing the function of endothelial Wnt/β-catenin in brain vessel anastomosis and maturation (Hübner et al. Nat. Commun. 2018)

The above mentioned Wnt/β-catenin signaling mechanism is essential for brain vascular invasion. Upon disruption, vertebrate brains exhibit profound CNS-specific vascular defects. This signaling pathway is considered as a master regulator of CNS vascular biology and further functions are suspected at later steps of the establishment of the cerebrovasculature. In search for these functions, we contributed to a study that investigated the subsequent requirements of Wnt/β-catenin signaling during CNS blood vessel morphogenesis and maturation. Canonical Wnt signaling is crucial for vascularization of the central nervous system and blood-brain barrier (BBB) formation. BBB formation and modulation are

not only important for development, but also relevant for vascular and neurodegenerative diseases. However, there is little understanding of how Wnt signaling contributes to brain angiogenesis and BBB formation. Here we show, using high resolution in vivo imaging and temporal and spatial manipulation of Wnt signaling, different requirements for Wnt signaling during brain angiogenesis and BBB formation. In the absence of Wnt signaling, premature Sphingosine-1-phosphate receptor (S1pr) signaling reduces VE-cadherin and Esama at cell-cell junctions (Figure 7). We suggest that Wnt signaling suppresses S1pr signaling during angiogenesis to enable the dynamic junction formation during anastomosis, whereas later S1pr signaling regulates BBB maturation and VE-cadherin stabilization. Our data provides a link between brain angiogenesis and BBB formation and identifies Wnt signaling as coordinator of the timing and as regulator of anastomosis.

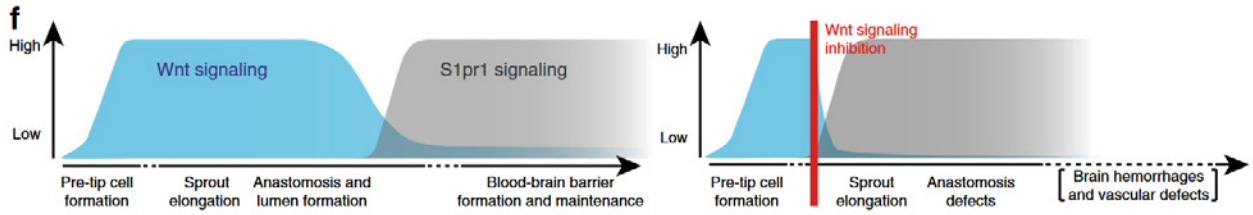

Figure 7. Illustration of Wnt and S1pr1 signaling during brain vascularization in wild type and Wnt-depleted embryos.

3.5. Probing the function of endothelial Wnt/β-catenin in BBB maintenance (Jensen et al. ATVB. 2019)

Besides the early functions described in 3.4, we contributed to a study that analyzed the later aspects of BBB maintenance under control of Wnt/β-catenin signaling. The Wnt/β-catenin pathway orchestrates development of the blood-brain barrier, but the downstream mechanisms involved at different developmental windows and in different central nervous system (CNS) tissues have indeed remained elusive. Here, we create a new mouse model allowing spatiotemporal investigations of Wnt/β-catenin signaling by induced overexpression of Axin1, an inhibitor of β-catenin signaling, specifically in endothelial cells (Axin1 iEC-OE). AOE (Axin1 overexpression) in Axin1 iEC- OE mice at stages following the initial vascular invasion of the CNS did not impair angiogenesis but led to premature vascular regression followed by progressive dilation and inhibition of vascular maturation resulting in forebrain-specific hemorrhage 4 days post-AOE. Analysis of the temporal Wnt/β-catenin driven CNS vascular development in zebrafish also suggested that Axin1 iEC- OE led to CNS vascular regression and impaired maturation but not inhibition of ongoing angiogenesis within the CNS. Transcriptomic profiling of isolated, β-catenin signaling-deficient endothelial cells during early blood-brain barrier-development (E11.5) revealed ECM (extracellular matrix) proteins as one of the most severely deregulated clusters. Among the 20 genes constituting the forebrain endothelial cell-specific response signature, 8 (Adamtsl2, Apod, Ctsw, Htra3, Pglyrp1, Spock2, Ttyh2, and Wfdc1) encoded bona fide ECM proteins. This specific β-catenin-responsive ECM signature was also repressed in Axin1 iEC- OE and endothelial cell-specific β-catenin-knockout mice (Ctnnb1-KOiEC) during initial blood-brain barrier maturation (E14.5), consistent with an important role of Wnt/β-catenin signaling in orchestrating the development of the forebrain vascular ECM. These results of this study suggest a novel mechanism of establishing a CNS endothelium-specific ECM signature downstream of Wnt-β-catenin that impact spatiotemporally on blood-brain barrier differentiation during forebrain vessel development.

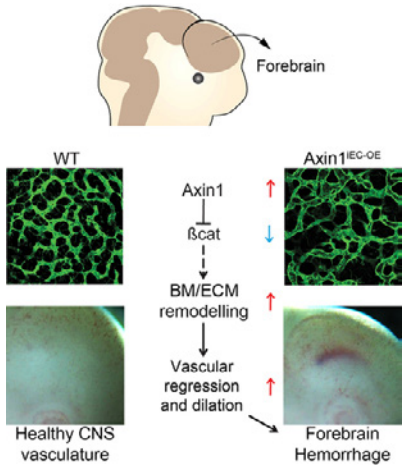

Figure 8. Wnt signaling inhibition in CNS endothelial cells triggers basement membrane/extracellular matrix remodelling that lead to vascular regression and dilation

3.6. Assessing the spatial heterogeneity of endothelial cell maturation signaling in the vertebrate brain (Benz et al, eLife 2019).

Not all blood vessels in the brain develop BBB properties, in particular those that mediate communication with the periphery in secretory or sensory circumventricular organs. In this collaborative study we started to characterize how blood vessels in these organs escape from the BBB-inductive signaling events. The circumventricular organs (CVOs) in the central nervous system (CNS) lack a vascular blood-brain barrier (BBB), creating communication sites for sensory or secretory neurons, involved in body homeostasis. Wnt/β-catenin signaling is essential for BBB development and maintenance in endothelial cells (ECs) in most CNS vessels. Here we show that in mouse development, as well as in adult mouse and zebrafish, CVO ECs rendered Wnt-reporter negative, suggesting low level pathway activity. Characterization of the subfornical organ (SFO) vasculature revealed heterogenous claudin-5 (Cldn5) and Plvap/Meca32 expression indicative for tight and leaky vessels, respectively. Dominant, EC-specific β-catenin transcription in mice, converted phenotypically leaky into BBB-like vessels, by augmenting Cldn5+vessels, stabilizing junctions and by reducing Plvap/Meca32+ and fenestrated vessels, resulting in decreased tracer permeability. Endothelial tightening augmented neuronal activity in the SFO of water restricted mice. Hence, regulating the SFO vessel barrier may influence neuronal function in the context of water homeostasis.

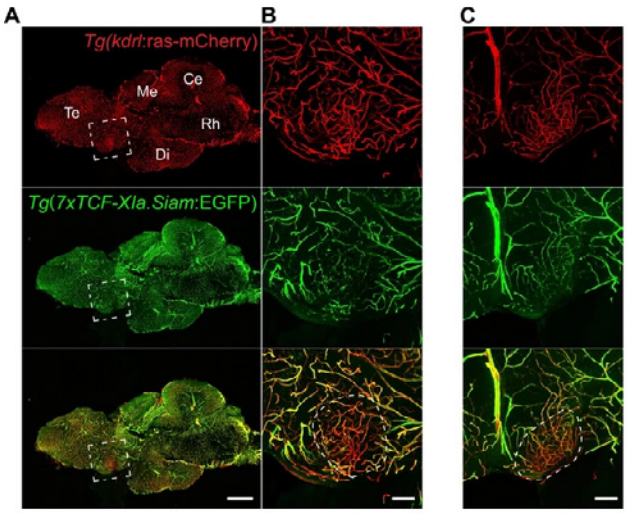

Figure 9. Low Wnt/β-catenin signaling in the adult circumventricular organs allows for efficient communication between the CNS and the peripheral organs, as illustrated here for the OVLT (organum vasculosum of the lamina terminalis) of adult zebrafish.

4. Outlook

Based on the previous findings, our project will continue to study brain angiogenesis and blood-brain barrier formation at the single-cell and real-time resolution in order to unravel the mechanisms through which neural signaling molecules couple brain vascular invasion and barriergenesis**.**

5. Publications

- Jensen LD, Hot B, Ramsköld D, Germano RFV, Yokota C, Giatrellis S, Lauschke VM, Hubmacher D, Li MX, Hupe M, Arnold TD, Sandberg R, Frisén J, Trusohamn M, Martowicz A, Wisniewska-Kruk J, Nyqvist D, Adams RH, Apte SS, Vanhollebeke B, Stenman JM, Kele J. Disruption of the Extracellular Matrix Progressively Impairs Central Nervous System Vascular Maturation Downstream of β-Catenin Signaling. ***Arterioscler Thromb Vasc Biol***. 2019 Jul;39(7):1432-1447.
- Morgan RK, Anderson GR, Araç D, Aust G, Balenga N, Boucard A, Bridges JP, Engel FB, Formstone CJ, Glitsch MD, Gray RS, Hall RA, Hsiao CC, Kim HY, Knierim AB, Kusuluri DK, Leon K, Liebscher I, Piao X, Prömel S, Scholz N, Srivastava S, Thor D, Tolias KF, Ushkaryov YA, Vallon M, Van Meir EG, Vanhollebeke B, Wolfrum U, Wright KM, Monk KR, Mogha A. The expanding functional roles and signaling mechanisms of adhesion G protein-coupled receptors. ***Ann N Y Acad Sci***. 2019 Nov;1456(1):5-25.
- Campenhout CV, Cabochette P, Veillard AC, Laczik M, Zelisko-Schmidt A, Sabatel C, Dhainaut M, Vanhollebeke B, Gueydan C, Kruys V. Guidelines for optimized gene knockout using CRISPR/Cas9. ***Biotechniques***. 2019 Jun;66(6):295-302.
- Benz F, Wichitnaowarat V, Lehmann M, Germano RF, Mihova D, Macas J, Adams RH, Taketo MM, Plate KH, Guérit S, Vanhollebeke B, Liebner S. Low wnt/β-catenin signaling determines leaky vessels in the subfornical organ and affects water homeostasis in mice. ***Elife***. 2019 Apr 1;8. pii: e43818.
- Bonnin E[§], Cabochette P[§], Filosa A, Jühlen R, Komatsuzaki S, Hezwani M, Dickmanns A, Martinelli V, Vermeersch M, Supply L, Martins N, Pirenne L, Ravenscroft G, Lombard M, Port S, Spillner C, Janssens S, Roets E, Van Dorpe J, Lammens M, Kehlenbach RH, Ficner R, Laing NG, Hoffmann K, Vanhollebeke B[#], Fahrenkrog B[#]. Biallelic mutations in nucleoporin NUP88 cause lethal fetal akinesia deformation sequence. ***PLoS Genet.*** 2018 Dec 13;14(12):e1007845. doi: 10.1371/journal.pgen.1007845. [§] co-first authors, [#] co-corresponding authors.
- Hübner K, Cabochette P, Diéguez-Hurtado R, Wiesner C, Wakayama Y, Grassme KS, Hubert M, Guenther S, Belting HG, Affolter M, Adams RH, Vanhollebeke B, Herzog W. Wnt/β-catenin signaling regulates VE-cadherin-mediated anastomosis of brain capillaries by counteracting S1pr1 signaling. ***Nat Commun.*** 2018 Nov 19;9(1):4860. doi: 10.1038/s41467-018-07302-x.
- Eubelen M[§], Bostaille N[§], Cabochette P, Gauquier A, Tebabi P, Dumitru AC, Koehler M, Gut P, Alsteens D, Stainier DYR, Garcia-Pino A, Vanhollebeke B. A molecular mechanism for Wnt ligand-specific signaling. ***Science.*** 2018 Aug 17;361(6403). pii: eaat1178. doi: 10.1126/science.aat1178. [§] co-first authors
- Guerra A, Germano RF, Stone O, Arnaout R, Guenther S, Ahuja S, Uribe V, Vanhollebeke B, Stainier DY, Reischauer S. Distinct myocardial lineages break atrial symmetry during cardiogenesis in zebrafish. ***eLife***. 2018 May 15;7. pii: e32833. doi: 10.7554/eLife.32833.
- Bostaille N, Gauquier A, Stainier DY, Raible DW, Vanhollebeke B. Defective adgra2 (gpr124) splicing and function in zebrafish ouchless mutants. ***Development.*** 2017 Jan 1;144(1):8-11.
- Bostaille N, Gauquier A, Twyffels L, Vanhollebeke B. Molecular insights into Adgra2/Gpr124 and Reck intracellular trafficking. ***Biol Open.*** 2016 Dec15;5(12):1874-1881.
- Fontaine F, Lecordier L, Vanwalleghem G, Uzureau P, Van Reet N, Fontaine M, Tebabi P, Vanhollebeke B, Büscher P, Pérez-Morga D, Pays E. APOLs with low pH dependence can kill all African trypanosomes. ***Nat Microbiol.*** 2017 Nov;2(11):1500-1506.
- Horáková E, Changmai P, Vancová M, Sobotka R, Van Den Abbeele J, Vanhollebeke B, Lukeš J. The Trypanosoma brucei TbHrg protein is a heme transporter involved in the regulation of stage-specific morphological transitions. ***J Biol Chem.*** 2017 Apr 28;292(17):6998-7010.
- De Muylder G, Vanhollebeke B, Caljon G, Wolfe AR, McKerrow J, Dujardin JC. Naloxonazine, an Amastigote-Specific Compound, Affects Leishmania Parasites through Modulation of Host-Encoded Functions. ***PLoS Negl Trop Dis.*** 2016 Dec 30;10(12):e0005234.

6. Additional References

- Anderson K. D., Pan L., Yang X., Hughes V. C., Walls J. R., Dominguez M. G., Simmons M. V., Burfeind P., Xue Y., Wei Y. et al. (2011). Angiogenic sprouting into neural tissue requires Gpr124, an orphan G protein-coupled receptor. ***Proc. Natl. Acad. Sci. USA*** 108, 2807-2812. 10.1073/pnas.1019761108
- Bostaille N., Gauquier A., Stainier D. Y. R., Raible D. W. and Vanhollebeke B. (2017). Defective *adgra2 (gpr124)* splicing and function in zebrafish *ouchless* mutants. ***Development***, doi:10.1242/dev.146803. 10.1242/dev.146803
- Bostaille N, Gauquier A, Twyffels L, Vanhollebeke B. Molecular insights into Adgra2/Gpr124 and Reck intracellular trafficking. ***Biol Open.*** 2016 Dec15;5(12):1874-1881.
- Cullen M., Elzarrad M. K., Seaman S., Zudaire E., Stevens J., Yang M. Y., Li X., Chaudhary A., Xu L., Hilton M. B. et al. (2011). GPR124, an orphan G protein-coupled receptor, is required for CNS-specific vascularization and establishment of the blood-brain barrier. ***Proc. Natl. Acad. Sci. USA*** 108, 5759-5764. 10.1073/pnas.1017192108
- de Almeida G. M., Yamamoto M., Morioka Y., Ogawa S., Matsuzaki T. and Noda M. (2015). Critical roles for murine Reck in the regulation of vascular patterning and stabilization. ***Sci. Rep.*** 5, 17860 10.1038/srep17860
- Kuhnert F., Mancuso M. R., Shamloo A., Wang H.-T., Choksi V., Florek M., Su H., Fruttiger M., Young W. L., Heilshorn S. C. et al. (2010). Essential regulation of CNS angiogenesis by the orphan G protein-coupled receptor GPR124. ***Science*** 330, 985-989. 10.1126/science.1196554
- Malmquist, S. J., Abramsson, A., McGraw, H. F., Linbo, T. H. and Raible, D. W. (2013). Modulation of dorsal root ganglion development by ErbB signaling and the scaffold protein Sorbs3. ***Development*** 140, 3986-3996. doi:10.1242/dev.084640
- Posokhova E., Shukla A., Seaman S., Volate S., Hilton M. B., Wu B., Morris H., Swing D. A., Zhou M., Zudaire E. et al. (2015). GPR124 functions as a WNT7-specific coactivator of canonical β-catenin signaling. ***Cell Rep***. 10, 123-130. 10.1016/j.celrep.2014.12.020
- Ulrich F., Carretero-Ortega J., Menendez J., Narvaez C., Sun B., Lancaster E., Pershad V., Trzaska S., Veliz E., Kamei M. et al. (2016). Reck enables cerebrovascular development by promoting canonical Wnt signaling. ***Development*** 143, 147-159. 10.1242/dev.123059
- Vanhollebeke B., Stone O. A., Bostaille N., Cho C., Zhou Y., Maquet E., Gauquier A., Cabochette P., Fukuhara S., Mochizuki N. et al. (2015). Tip cell-specific requirement for an atypical Gpr124- and Reck-dependent Wnt/β-catenin pathway during brain angiogenesis. ***eLife*** 4, e06489 10.7554/eLife.06489
- Zhou Y. and Nathans J. (2014). Gpr124 controls CNS angiogenesis and blood-brain barrier integrity by promoting ligand-specific canonical Wnt signaling. ***Dev. Cell*** 31, 248-256. 10.1016/j.devcel.2014.08.018

Geneeskundige Stichting Koningin Elisabeth
Fondation Médicale Reine Elisabeth
Königin-Elisabeth-Stiftung für Medizin
Queen Elisabeth Medical Foundation

Final report of the research group of

Prof. dr. Geert van Loo, PhD

Universiteit Gent (UGent)

Principal investigator

Prof. dr. Geert van Loo, PhD

Co-investigators

Prof. Dr. Mohamed Lamkanfi

Inflammation Research Center
VIB – Gent University
Technologiepark 927
9052 Gent-Zwijnaarde
Belgium
Tel.: +32 9 331 37 61
Fax: +32 9 221 76 73
E-mail: geert.vanloo@irc.vib-ugent.be

Microglia, inflammasomes and multiple sclerosis

Neuroinflammation and neurodegeneration often result from the aberrant deposition of aggregated host proteins that can activate inflammasomes. Inflammasomes function as intracellular sensors of both microbial pathogens and foreign as well as host-derived danger signals. Upon activation, they induce an innate immune response by secreting the inflammatory cytokines interleukin (IL)-1β and IL-18, and additionally by inducing pyroptosis, a lytic cell death mode that releases additional inflammatory mediators. Microglia are the prominent innate immune cells in the brain for inflammasome activation. However, additional CNS resident cell types including astrocytes and neurons, as well as infiltrating myeloid cells from the periphery express and activate inflammasomes. We recently published a review summarizing the role of inflammasomes in neurodegenerative and neuroinflammatory diseases in the journal *EMBO Molecular Medicine* (Voet et al., 2019), and a review on the role of microglia in multiple sclerosis (MS) pathology in the journal *Trends in Molecular Medicine* (Voet et al., 2019).

In our GSKE-funded project we investigated the role of the anti-inflammatory protein A20 in microglia. We found that A20 critically controls microglia activation both in steady-state as in conditions of neuroinflammation. In experimental models of neuroinflammation, we found that A20 in microglia is crucial for keeping NLRP3 inflammasome activation, important for the production and secretion of the inflammatory cytokine interleukin-1β, under control. Mice which lack A20 expression in microglia produce high levels of IL-1β and are hypersensitive to LPS-induced neuroinflammation and to experimental autoimmune encephalomyelitis (EAE), a model for multiple sclerosis. Strategies targeting microglia to suppress their activation, eventually through expression of A20, might prove useful for the treatment of neuroinflammatory diseases. These results have been published in the journal *Nature Communications* (Voet et al., 2018).

1. A20 critically controls microglia activation and inhibits inflammasome-dependent neuroinflammation

Microglia, the mononuclear phagocytes of the central nervous system (CNS), are important for the maintenance of CNS homeostasis, but also critically contribute to CNS pathology. Here, we demonstrate that the nuclear factor kappa B (NF-κB) regulatory protein A20 is crucial in regulating microglia activation during CNS homeostasis and pathology. In mice, deletion of A20 in microglia increases microglial cell number and affects microglial regulation of neuronal synaptic function. Administration of a sublethal dose of lipopolysaccharide induces massive microglia activation, neuroinflammation and lethality in mice with microglia-confined A20 deficiency. Microglia A20 deficiency also exacerbates multiple sclerosis (MS)-like disease, due to hyperactivation of the Nlrp3 inflammasome leading to enhanced interleukin-1β secretion and CNS inflammation. Finally, we confirm a Nlrp3 inflammasome signature and IL-1β expression in brain and cerebrospinal fluid from MS patients. Collectively, these data reveal a critical role for A20 in the control of microglia activation and neuroinflammation.

2. Phenotype of mice with A20 deficiency in microglia

Transcriptome analysis of purified brain cell types of mouse cortex identifies the A20 encoding gene Tnfaip3/A20 as highly expressed in microglia, in contrast to its expression in neurons, astrocytes, endothelial cells, pericytes, and oligodendrocytes in various maturation stages (Zhang et al., 2014). To investigate the importance of A20 for microglia development and function, we first examined the

expression of A20 in different microglial developmental stages, including yolk sac precursors (EMPs, A1, A2), embryonic microglia and adult microglia (Fig. 1a). Although A20 is only marginally expressed in early development, an increase in expression is seen in the later stages of embryonic development, and A20 expression is further enhanced in adult microglia. To assess its function in vivo, we crossed mice carrying a floxed A20 allele ($A20^{FL}$) (Vereecke et al., 2010) to Cx3Cr1CreErt2 transgenic mice allowing Cre-mediated gene deletion following tamoxifen (TAM) treatment. Targeting of microglia using this system is based on microglia longevity and capacity of self-renewal without any appreciable input from circulating blood cells (Goldmann et al., 2013). $A20^{Cx3Cr1CreErt2}$ mice were injected with TAM inducing A20 deletion in all Cx3Cr1 expressing cells. However, due to their short half-life, Cx3Cr1 Ert2Cre+ expressing blood-derived monocytes are gradually replaced by their monocyte precursors harboring non-rearranged A20 alleles. A20 deletion in microglia was confirmed at the protein level by Western blotting of fluorescence-activated cell sorted (FACS) microglia ex vivo (Fig. 1b) and of primary microglia cultured *in vitro* (Fig. 1c).

Mice with TAM-induced A20 deficiency in microglia (named $A20^{Cx3Cr1\text{-}KO}$) do not display overt spontaneous abnormalities, and histological analysis of brain sections of $A20^{Cx3Cr1\text{-}KO}$ mice do not reveal any gross morphological defects, astrogliosis or demyelination. However, immunohistochemical examination with the microglia marker Iba-1+ revealed a significant increase in the number of microglia both in brain ($p = 0.0286$) and spinal cord sections of $A20^{Cx3Cr1\text{-}KO}$ mice compared to control littermates (Fig. 1d-f). Quantitative morphometric three-dimensional analysis of Iba-1+ microglia in the adult cortex showed that A20-deficient microglia have an altered morphology, characterized by significantly longer processes and increased number of segments, branching and terminal points relative to microglia from control mice (Fig. 1g-h). Together, these data suggest that lack of A20 induces proliferation of adult microglia with altered morphology.

Next, to determine whether A20 deficiency in microglia affects microglia activation or its immune function under homeostatic conditions, we expression profiled sorted $CD45^{int}CD11b^{hi}$ microglia from brains of $A20^{Cx3Cr1\text{-}KO}$ and control littermate mice by quantitative deep sequencing of RNA transcripts. We observed significant differences in the mRNA profiles of microglial genes in $A20^{Cx3Cr1\text{-}KO}$ relative to control mice. In total, 216 genes were significantly upregulated and 39 genes were downregulated ($p < 0.01$ and fourfold change) in $A20^{Cx3Cr1\text{-}KO}$ microglia compared to controls. Many genes typically expressed under physiological conditions (P2ry12, Cx3cr1, Sall1, Gpr34, Fcrls, Rhob, Olfml3) are selectively downregulated in $A20^{Cx3Cr1\text{-}KO}$ microglia (Fig. 1i). Among all upregulated transcripts in $A20^{Cx3Cr1\text{-}KO}$ microglia, we identified genes linked to cell activation (Cd45, F4/80, Cd86, Cd40, Cd11c), microglia polarization (Cxcl10, C4a/C4b, Tnfsf10, Cxcl9, Ccl2, Ccl5, Tlr1, Il1b), MHC class I (H2k1, H2d1, B2m, H2q7, H2m3, H2q8), type I interferon signaling (Irf-1, Irf-7, Irf-9, Stat1, Stat2, Ifi35, Ifit1, Ifit3, IfitM3), and inflammatory signaling (Nfkb1, Nfkb2, Relb,Il1b, Il12b, Ccl2, Ccl5, Ccl12, Cxcl9, Cxcl10, Cxcl11, Cxcl13) (Fig. 1j). Next, we analysed the expression of 'disease-associated microglia' (DAM) markers that have recently been identified (Keren-Shaul et al., 2017), and demonstrate the significant upregulation of many of these DAM genes (Axl, Cst7, Ctsl, Cd9, Csf1, Itgax, Clec7a, Lilrb4, Timp2, Ctsd, Ctsb) in $A20^{Cx3Cr1\text{-}KO}$ microglia. Network analysis on differentially expressed genes identified 'Antimicrobial response, inflammatory response, cell signaling' as the most differential between both populations, and IPA canonical pathway analysis identified pathways associated with interferon signaling, pattern recognition receptor signaling, complement system and inflammatory signaling as being enriched in $A20^{Cx3Cr1\text{-}KO}$ microglia. Overall, the gene expression analysis suggests that upon A20 deletion microglia decrease their homeostatic 'surveilling' state expression profile, and acquire an inflammatory, disease-associated signature. In conclusion, morphometric 3D analysis and genome signature comparison between microglia from $A20^{Cx3Cr1\text{-}KO}$ and control animals suggests a crucial role for A20 in the control of microglia activation under steady-state conditions, and demonstrates that in the absence of A20 microglia adopt a dysfunctional phenotype.

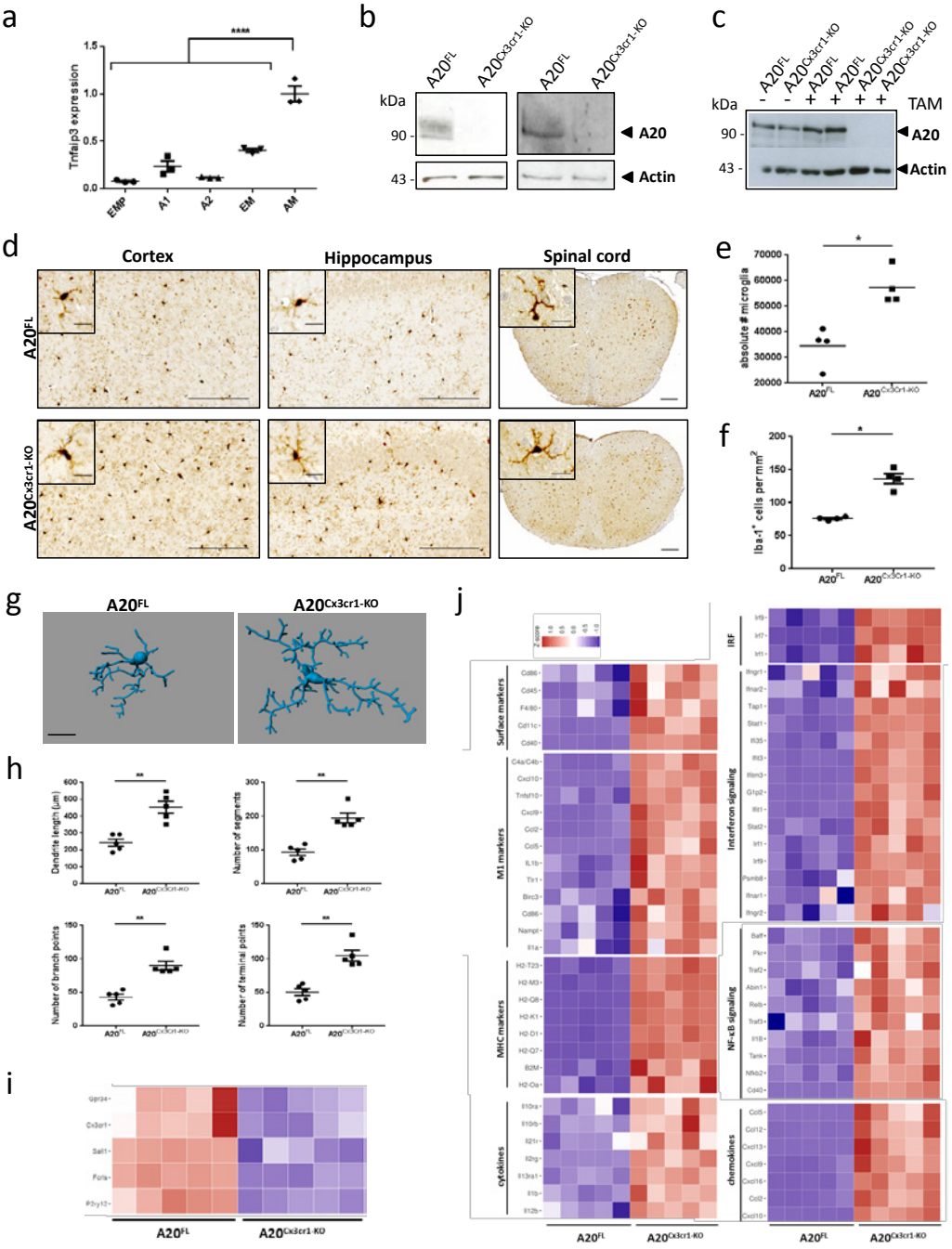

Figure 1. CNS phenotypel of A20$^{Cx3Cr1\text{-}KO}$ mice. (a) A20 expression during microglial cell development. Cells were sorted according to Kierdorf et al, 2013. EMP; Erythromyeloid precursors (yolk sac), A1; immature CD45^{+} c-kit^{lo} Cx3Cr1- cells (yolk sac), A2; mature CD45^{+} c-kit^{-} Cx3Cr1+ cells (yolk sac), EM; embryonic microglia (E14), AM; adult microglia. Each symbol represents one mouse, n=3 per group. Data presented as mean ± SEM. Significant differences determined by a one-way ANOVA with Tukey correction for multiple comparison (**** $p < 0.0001$). (b) Immunoblot for A20 expression on ex vivo FACS-sorted microglia from control (A20^{FL}) and A20$^{Cx3Cr1\text{-}KO}$ mice 4 (left) or 35 weeks (right) after TAM injection. Actin is shown as loading control. (c) Immunoblot for A20 expression on lysates from primary microglia from control (A20^{FL}) and A20$^{Cx3Cr1\text{-}KO}$ mice after stimulation with 4-OH-TAM. Actin is shown as loading control. Data are representative of two independent experiments. (d) Immunohistochemistry for Iba-1+ in the cerebral cortex, hippocampus and spinal cord of control (A20^{FL}) and A20$^{Cx3Cr1\text{-}KO}$ mice. Scale bars: 100 µm (cortex and hippocampus) and 200 µm (spinal cord), insert: 10 µm and 20 µm, respectively. Representative images are displayed. (e) Flow cytometric quantification of the number of CD11b^{+} CD45^{int} microglia in brain of control (A20^{FL}) and A20$^{Cx3Cr1\text{-}KO}$ mice 4 weeks post TAM injection. Each symbol represents one mouse. Data are representative of two independent experiments and presented as mean ± SEM. Significant differences determined by Mann-Whitney U statistical test (* $p < 0.05$). . (f) Number of Iba-1+ ramified parenchymal microglia. Each symbol represents one mouse, with four mice per group. Data presented as mean ± SEM. Significant differences determined by a Mann-Whitney U statistical test (* $p < 0.05$) (g-h) 3D reconstruction (scale bars: 10 µm) (g) and Imaris-based quantification of cell morphology (h) of cortical Iba-1+ microglia. Each symbol represents one mouse; three cells analyzed per mouse; n=5 per condition. Data presented as mean ± SEM. Significant differences determined by a Mann-Whitney U statistical test (** $p < 0.01$). (i-j) RNA sequencing on FACS-sorted microglia from TAM-injected control (A20^{FL}) and A20$^{Cx3Cr1\text{-}KO}$ mice . Each column represents microglia from one individual mouse, n=5 per group. Color code presents linear scale. (i-j) Pathway analysis of RNA-Seq datasets demonstrates downregulation of homeostatic genes (i) and upregulation of genes involved in microglia activation, polarization, MHC class I, interferon and inflammatory signaling (j) in A20$^{Cx3Cr1\text{-}KO}$ microglia.

3. A20 deficiency in microglia affects synaptic function

Previous studies indicated that alterations in microglial number or activation can result in functional and structural deficits in cortical circuits (Parkhurst et al., 2013). To evaluate the functional consequences of increased microglial number and/or activation status for neuronal function, we prepared acute slices from P30-35 control and $A20^{Cx3Cr1\text{-}KO}$ mice, and analyzed spontaneous glutamatergic synaptic transmission in layer V pyramidal neurons in S1 cortex. No changes in action potential spiking profiles or intrinsic membrane properties were found between pyramidal neurons from control and $A20^{Cx3Cr1\text{-}KO}$ mice (Fig. 2a), indicating that cell-autonomous parameters are likely unaffected in $A20^{Cx3Cr1\text{-}KO}$ mice. However, we observed a marked increase in spontaneous excitatory postsynaptic current (sEPSC) frequency in $A20^{Cx3Cr1\text{-}KO}$ S1 layer V pyramidal neurons compared to those from control mice (Fig. 2b-e). The robust increase in sEPCS frequency in $A20^{Cx3Cr1\text{-}KO}$ mice with increased microglial number and (hyper)activation is consistent with previous studies showing an increased frequency of spontaneous synaptic transmission following microglia activation18 and a decreased frequency following microglia depletion (Parkhurst et al., 2013). A small, but significant decrease in sEPSC amplitude was also observed (Fig. 2b, f-g), indicating that microglia activation could negatively influence the density of postsynaptic glutamate receptors on dendrites.

Next, to evaluate whether the observed aberrant excitatory synaptic function affects learning and memory, $A20^{Cx3Cr1\text{-}KO}$ and control littermate mice were examined in the hidden platform protocol of the Morris water maze (MWM), a very reliable and robust protocol to investigate hippocampus-dependent spatial learning and memory (Hooghe et al., 2001). Over 10 training days, 6 month old female control and $A20^{Cx3Cr1\text{-}KO}$ mice showed similar learning curves to locate the hidden platform using distal visual cues. Interspersed probe trials on day 6 and 11 showed no difference in spatial reference memory and a robust preference for the correct target quadrant (data not shown). Cognitive flexibility, a measure for executive function, was assessed in a consecutive 5 day reversal training where the platform position was relocated to the opposite quadrant. $A20^{Cx3Cr1\text{-}KO}$ and control mice showed similar learning curves (repeated measures 2-way ANOVA for factor day: $F(4,76)=16.8$; $p<0.0001$) (Fig. 2h). Interestingly, during the reversal probe trial only control mice showed a significant preference for the target quadrant over the other three quadrants (repeated measures 2-way ANOVA for factor quadrant preference: $F(3, 57)=11,4$; $p<0.0001$) (Fig. 2i) and were at any given time point significantly closer to the location of the reversal platform than to the location of the acquisition platform (expressed as total distance to target) (2-way ANOVA for factor platform location: $F(1,38)=14,36$; $p=0.0005$) (Fig. 2j). Together these findings indicate that after 5 days of reversal learning, $A20^{Cx3Cr1\text{-}KO}$ mice do not have a robust spatial representation of the platform's correct location and were not capable of forming a robust reference memory. Together, these results show that the aberrantly activated microglia in $A20^{Cx3Cr1\text{-}KO}$ mice affect excitatory synaptic function with consequences for proper cognitive function.

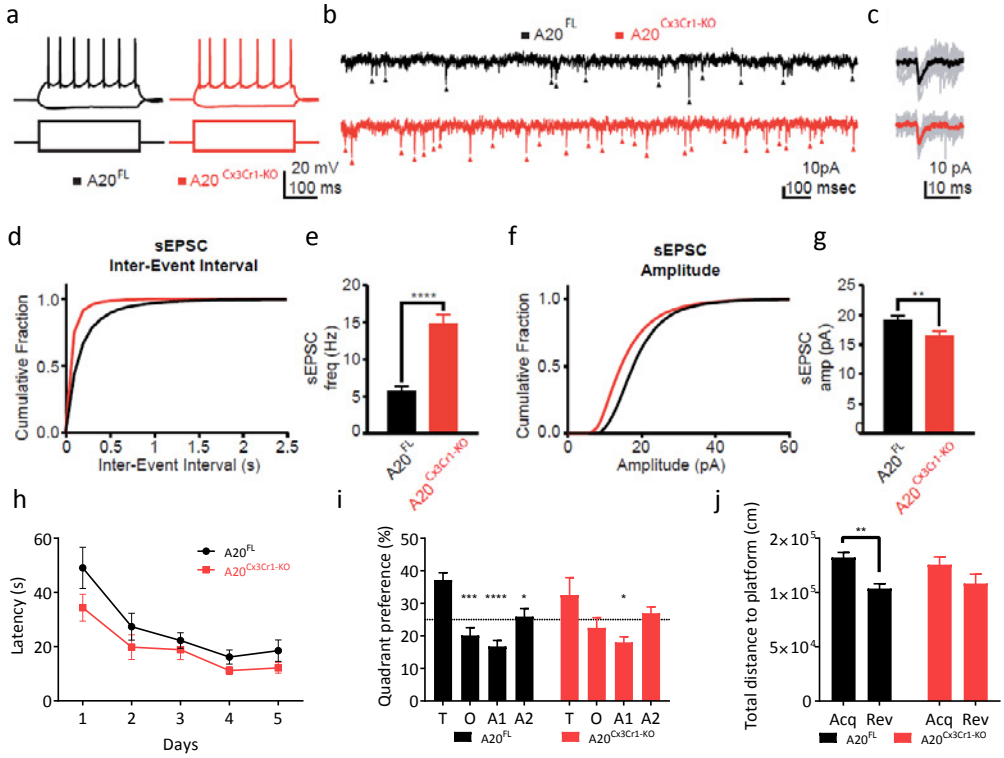

Figure 2. Effect of microglia hyperactivation on basal network activity in somatosensory pyramidal neurons. (a) Example action potential (AP) firing profiles, showing the typical regular spiking behavior of layer V S1 pyramidal neurons both in control and in A20$^{Cx3Cr1\text{-}KO}$ neurons. Responses to hyperpolarizing (-150 pA) and suprathreshold (400 pA) current injections are shown. (b) Example sEPSC traces, 2s stretches. (c) Examples of individual sEPSC events. Individual events shown in grey, averaged event shown as overlay (control, black; A20$^{Cx3Cr1\text{-}KO}$, red). (d) Cumulative probability distributions of inter-event sEPSC intervals (IEIs) for control (black) or A20$^{Cx3Cr1\text{-}KO}$ (red) cells. (e) sEPSC frequency (Control (black) 5.76 ± 0.58 Hz, n/m=21/3; A20$^{Cx3Cr1\text{-}KO}$ (red) 14.8 ± 1.29 Hz, n/m=20/3; **** $p < 0.0001$). Data represents means ± SEM. Number of cells (n), number of animals (m). Statistical differences were determined by a two-tailed Wilcoxon matched-paired t-test. (f) Cumulative probability distributions for sEPSC amplitudes in control (black) or A20$^{Cx3Cr1\text{-}KO}$ (red) cells. (g) sEPSC amplitudes. (Control 19.3 ± 0.69 pA, n/m=21/3; A20$^{Cx3Cr1\text{-}KO}$ 16.5 ± 0.87 pA, n/m=20/3; ** p=0.0013). Data represents means ± SEM. Number cells (n), number of animals (m). Statistical differences were determined by a two-tailed unpaired Mann-Whitney t-test. (h) Cognitive flexibility in Morris water maze reversal learning was similar in control (A20FL, n=12) and A20$^{Cx3Cr1\text{-}KO}$ mice (n=9). (i) In the reversal probe trial, controls displayed significant target quadrant preference, while A20$^{Cx3Cr1\text{-}KO}$ mice did not (T: target quadrant, O: opposite quadrant, A1: adjacent 1 quadrant, A2: adjacent 2 quadrant). Chance level at 25 % is indicated. (j) During the reversal probe trial, control animals searched closer to the correct reversal location for the platform than to the old location (distance to platform), while A20$^{Cx3Cr1\text{-}KO}$ mice searched at equidistance to both locations. All data (h-j) are represented as means ± SEM and statistical differences were determined by repeated-measures two-way ANOVA (h-i) and two-way ANOVA (j) using Bonferroni correction for post hoc analysis (h-j) (* $p<0.05$, ** $p<0.01$, *** $p<0.001$, **** $p<0.0001$).

4. A20 in microglia protects against LPS-induced inflammation

Microglia are the CNS-resident immune cells acting as the first responders to microbial infections of the brain (Waisman et al., 2015). To investigate the importance of A20 for microglia function in a model of neuroinflammation, A20$^{Cx3Cr1\text{-}KO}$ and control littermate mice were injected with a single sublethal dose of the TLR4 agonist lipopolysaccharide (LPS), known to induce neuroinflammation through microglia activation and expression of pro-inflammatory cytokines (Qin et al., 2007). Surprisingly, in contrast to control mice, which only exhibit a modest drop in body temperature in the first hours after systemic LPS injection, A20$^{Cx3Cr1\text{-}KO}$ mice displayed severe hypothermia (Fig. 3a) and increased mortality (Fig. 3b). Histological analysis of the CNS 10 hours after systemic LPS administration, a time point at which all A20$^{Cx3Cr1\text{-}KO}$ mice are still alive, demonstrated increased microgliosis in A20$^{Cx3Cr1\text{-}KO}$ brain and spinal cord compared to control tissue (Fig. 3c). Since A20 knockout mice with A20 deficient microglia already spontaneously display a pro-inflammatory phenotype characterized by microglia hyperproliferation (Fig. 1), no further effect on microglia proliferation is seen after LPS (Fig. 3d). Microglia morphology analysis 10 hours post LPS suggests a reactive phenotype in A20$^{Cx3Cr1\text{-}KO}$ mice compared to wild type

littermates, as evidenced by a significantly higher number of processes, branching points, terminal point and segments. (Fig 3e-f). In agreement, significantly elevated levels of inflammatory cytokines were detected in CNS tissue and cerebrospinal fluid (CSF) of $A20^{Cx3Cr1\text{-}KO}$ relative to littermate $A20^{FL}$ mice after systemic LPS challenge (Fig. 3g). Finally, microglia from LPS-injected $A20^{Cx3Cr1\text{-}KO}$ and $A20^{FL}$ control mice were isolated and global gene expression was determined by RNA sequencing. Investigation of the gene ontology enrichment network on differentially expressed genes revealed that inflammatory pathways are highly affected in LPS-stimulated microglia compared to unstimulated microglia, as expected (data not shown). However, 2774 genes were differentially expressed between $A20^{Cx3Cr1\text{-}KO}$ and control microglia isolated 10 h after systemic LPS injection (cut-off: $p < 0.01$ and at fold change ≥4; 1609 upregulated, 1165 downregulated in $A20^{Cx3Cr1\text{-}KO}$ compared to control), and LPS-stimulated $A20^{Cx3Cr1\text{-}KO}$ microglia expressed much higher levels of inflammatory cytokine and chemokine pathways compared to LPS-stimulated control microglia, demonstrating their hyperactivation (Fig. 3h). Together, these results demonstrate that A20 expression in microglia controls inflammatory CNS responses and is essential to prevent a detrimental response to LPS-induced neuroinflammation.

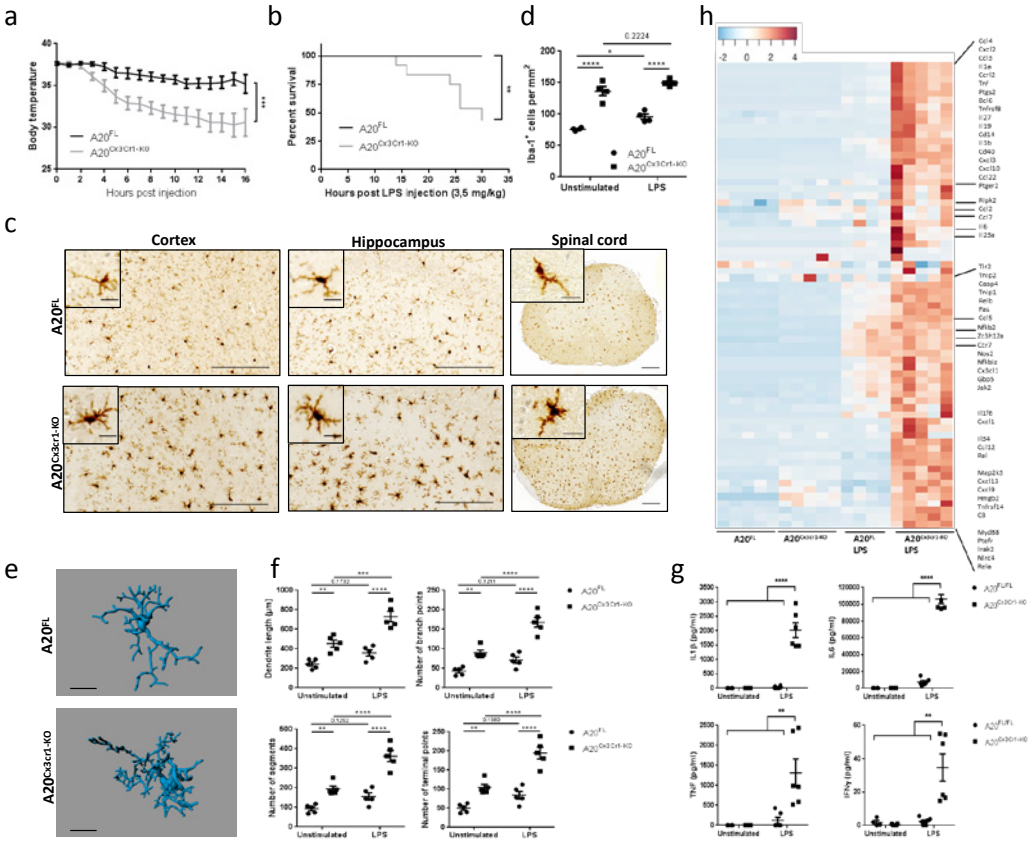

Figure 3. $A20^{Cx3Cr1\text{-}KO}$ mice are hypersensitive to LPS. (a) Rectal body temperature responses and (b) survival were analyzed in function of time in control ($A20^{FL}$; n=13) and $A20^{Cx3Cr1\text{-}KO}$ (n=14) mice after intraperitoneal injection of 3.5 mg/kg LPS. The combined results of three independent experiments are shown. Body temperature data are means ± SEM. Statistical differences were determined by a REML analysis for rectal body temperatures and a Mantel-Cox test for the survival curve (** $p < 0.01$, *** $p < 0.001$). (c) Immunohistochemistry images showing Iba-1+ expression in the cerebral cortex, hippocampus and spinal cord of control ($A20^{FL}$) and $A20^{Cx3Cr1\text{-}KO}$ mice 10 hours post LPS challenge. Scale bars represent 100 µm (cortex and hippocampus) and 200 µm (spinal cord), insert: 10µm and 20 µm, respectively. Representative images are displayed. Data are representative of two independent experiments. (d) Number of Iba-1+ ramified parenchymal microglia in brain. Each symbol represents data from one mouse, n=4 per group. Data are presented as mean ± SEM. Significant differences were determined by a two-way ANOVA with Tukey correction for multiple comparison. (* $p < 0.05$, **** $p < 0.0001$) (e-f) Three-dimensional reconstruction (scale bars represent 10 µm, e) and Imaris-based semi-automatic quantification of cell morphology (f) of cortical Iba-1+ microglia. Each symbol represents the average of three measured cells per mouse; n = 5 per group. Data are presented as mean ± SEM. Significant differences were determined by two-way ANOVA with Tukey correction for multiple comparison (** $p < 0.01$, *** $p < 0.001$, **** $p < 0.0001$). (g) Bioplex analysis of cytokine levels in CSF 10 hours post LPS. Each symbol represents one mouse. Data are representative of three independent experiments. Significant differences were determined by a one-way ANOVA with Tukey correction for multiple comparison (** $p < 0.01$, **** $p < 0.0001$). (h) RNA prepared from FACS-sorted microglia from control ($A20^{FL}$) and $A20^{Cx3Cr1}$ mice either or not injected with LPS for 10 h was submitted for RNA sequencing. Heat map of expression values for inflammatory genes that are upregulated in LPS stimulated $A20^{Cx3Cr1}$ microglia compared to LPS stimulated control microglia. Each column represents microglia data from one individual mouse, with four or five mice per group. Color code presents linear scale.

5. Nlrp3 inflammasome hyperactivation in A20-deficient microglia

An inflammatory cytokine that was significantly upregulated in microglia from LPS stimulated A20$^{Cx3Cr1\text{-}KO}$ mice and can be detected in the CSF of A20$^{Cx3Cr1\text{-}KO}$ mice was IL-1β (Fig. 3g-h). LPS induced a strong upregulation of pro-IL-1β in both control and A20$^{Cx3Cr1\text{-}KO}$ microglia compared to non-injected mice, however, this upregulation is significantly stronger in microglia from LPS-injected A20$^{Cx3Cr1\text{-}KO}$ mice compared to LPS-injected control mice (Fig. 4a). IL-1β is the prototype cytokine secreted by cells upon activation of inflammasomes, multi-protein complexes that enable the activation of caspase-1 leading to the processing and secretion of biologically active IL-1β. Also IL-18 is produced through the activation of inflammasomes (Lamkanfi and Dixit, 2014), however, no difference in IL-18 expression could be observed between FACS-sorted microglia from LPS-injected A20$^{Cx3Cr1\text{-}KO}$ and control mice (data not shown). Microglia are capable of engaging different inflammasome types in response to infectious agents and host-derived danger signals that are associated with neurological diseases (Walsch et al., 2014). To study the contribution of inflammasome signaling to inflammatory responses of A20$^{Cx3Cr1\text{-}KO}$ microglia, we assessed caspase-1 processing in primary cultured microglia isolated from A20$^{Cx3Cr1\text{-}KO}$ and control littermate mice. Secreted levels of IL-1β and IL-18 were significantly increased in LPS-primed A20$^{Cx3Cr1\text{-}KO}$ microglia that were treated with soluble (ATP and nigericin) or crystalline (silica) stimuli of the Nlrp3 inflammasome compared to control microglia (Fig. 4b). In accordance, caspase-1 autoprocessing was substantially increased in A20$^{Cx3Cr1\text{-}KO}$ relative to control microglia (Fig. 4c). Besides their roles in maturation and secretion of IL-1β and IL-18, a major effector mechanism of inflammasomes is the induction of pyroptosis, a pro-inflammatory and lytic mode of cell death occurring mainly in myeloid cells including microglia (Walsch et al., 2014). Pyroptosis induces cell swelling and rupture of the plasma membrane, causing massive leakage of cytosolic contents provoking inflammatory reactions. Similarly to the effect on caspase-1 autoprocessing and IL-1β/IL-18 secretion, the induction of cell death was also enhanced in A20$^{Cx3Cr1\text{-}KO}$ microglia (Fig. 4d). Activation of the Nlrp3 inflammasome, one of the most pleiotropic inflammasomes, requires a priming signal that results in the upregulation of Nlrp3 expression along with the inflammasome substrate proIL-1β via the pro-inflammatory transcription factor NF-κB (Bauernfiend et al., 2009). A20 negatively regulates Nlrp3 inflammasome signaling by suppressing NF-κB-dependent production of Nlrp3 and proIL-1β in macrophages (Vande Walle et al., 2014). Indeed, a pharmacological inhibitor of IKK2, TPCA-1, significantly reduced ATP-induced caspase-1 autoprocessing and IL-1β secretion in LPS-primed A20$^{Cx3Cr1\text{-}KO}$ microglia (Fig. 4e-f). Together, these results demonstrate that A20 negatively controls Nlrp3 inflammasome priming and activation in microglia.

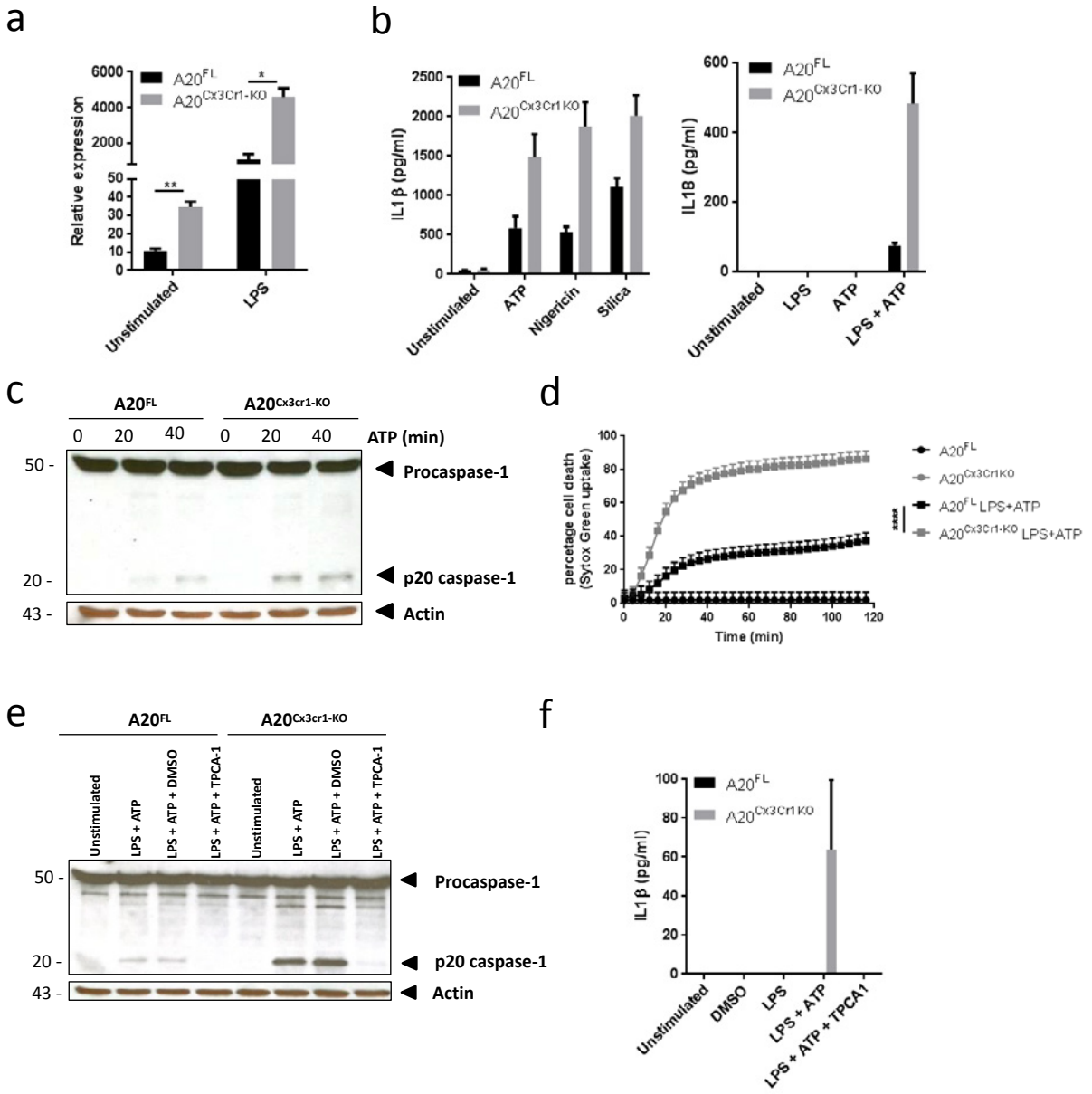

Figure 4. A20$^{Cx3Cr1-KO}$ microglia are hypersensitive to Nlrp3 inflammasome activation. (a) IL1β mRNA expression in microglia from A20$^{Cx3Cr1-KO}$ mice compared to control mice either or not injected with LPS. Each symbol represents an individual mouse. Data are presented as mean ± SEM. Significant differences were determined by a Mann-Whitney t-test (* $p < 0.05$, ** $p < 0.01$). (b) IL1β and IL18 protein levels in the supernatant of primary cultured microglia stimulated with LPS alone or together with ATP, Silica or Nigericin. Data represent the mean ± SD of three technical replicates of pooled microglial cells from control (A20^{FL}) and A20$^{Cx3Cr1-KO}$ mice. Data are representative of three independent experiments. (c) Immunoblot for procaspase-1 and cleaved caspase-1 (p20) in primary cultured microglia from control (A20^{FL}) and A20$^{Cx3Cr1-KO}$ mice stimulated with LPS and/or ATP. Actin is shown as loading control. Data are representative of two independent experiments. (d) Pyroptosis induction in primary microglia from control (A20^{FL}) and A20$^{Cx3Cr1-KO}$ mice stimulated with LPS and ATP, as measured by Sytox Green uptake. Data are presented as mean ± SEM and are representative of two independent experiments. Significant differences were determined by a REML analysis (**** $p < 0.0001$). (e) Immunoblot showing procaspase-1 and cleaved caspase-1 in primary cultured microglia from control (A20^{FL}) and A20$^{Cx3Cr1-KO}$ mice either or not pretreated *in vitro* with TPCA-1 and stimulated with LPS and/or ATP. Actin is shown as loading control. Data are representative of two independent experiments. (f) IL1β protein in supernatant of primary cultured microglia from control (A20^{FL}) and A20$^{Cx3Cr1-KO}$ mice either or not pretreated *in vitro* with TPCA-1 and stimulated with LPS and/or ATP. Data represent the mean ± SD of three technical replicates of pooled microglial cells, and are representative of two independent experiments.

6. Mice with A20-deficient microglia are hypersensitive to EAE

Based on our results, we investigated the microglia-specific function of A20 in a model of autoimmune CNS inflammation, namely experimental autoimmune encephalomyelitis (EAE). $A20^{Cx3Cr1\text{-}KO}$ and control mice were immunized with a myelin oligodendrocyte glycoprotein (MOG) peptide (MOG35-55) and disease progression was monitored by assessing clinical disease symptoms and body weight (Fig. 5a-b). Both $A20^{Cx3Cr1\text{-}KO}$ and control mice developed EAE, however, $A20^{Cx3Cr1\text{-}KO}$ mice developed earlier disease onset and exhibited a more severe disease course as compared to control mice (Fig. 5a-b), demonstrating a crucial role for microglia A20 activity in EAE pathogenesis. In contrast, A20 deletion in other CNS cell types (all CNS progenitor cells, neurons, astrocytes or oligodendrocytes) did not result in differences in EAE clinical pathology (data not shown). Clinical pathology in $A20^{Cx3Cr1\text{-}KO}$ was confirmed by histology and flow cytometry on spinal cord sections at start of the clinical manifestations, showing extensive demyelination, axonal damage, inflammation and immune cell infiltration in $A20^{Cx3Cr1\text{-}KO}$ mice, while nearly no immune cell infiltration, demyelination or axonal loss could be detected in the spinal cord of control mice at this early time-point (Fig. 5c-d). As A20 deficiency enhances the activation of the Nlrp3 inflammasome in isolated primary microglia (Fig. 4), we speculated that the hyperactivation of the Nlrp3 inflammasome is responsible for the aggravated EAE phenotype in $A20^{Cx3Cr1\text{-}KO}$ mice. Indeed, gene expression analysis of spinal cord tissue showed enhanced expression of pro-IL-1b, ASC, Nlrp3 and caspase-1 in $A20^{Cx3Cr1\text{-}KO}$ mice compared to control mice, suggesting a contribution of inflammasome activities in the observed phenotype (Fig. 5e). To test this hypothesis, Nlrp3–/– mice were crossed with $A20^{Cx3Cr1\text{-}KO}$ mice and EAE disease development was monitored. In contrast to $A20^{Cx3Cr1\text{-}KO}$ mice, which develop a more severe pathology, $A20^{Cx3Cr1\text{-}KO}$-Nlrp3–/– mice show a significantly reduced clinical pathology, comparable to control $A20^{FL}$ littermate mice (Fig. 5f). These results are in line with previous studies demonstrating a critical role for Nlrp3 in the development of EAE by mediating peripheral immune responses (Gris et al., 2010; Shaw et al., 2010). However, $Nlrp3^{-/-}$ mice lack the Nlrp3 protein ubiquitously, and the specific contribution of inflammasome signaling inside the CNS to EAE pathogenesis is unknown. To study the specific function of inflammasomes within microglia during EAE, caspase-1 conditional knockout mice having a floxed allele (Caspase-1^{FL}) were generated (Van Gorp et al., 2016) and crossed with $A20^{Cx3Cr1\text{-}KO}$ mice to produce mice lacking both A20 and caspase-1 in microglia (caspase-1-$A20^{Cx3Cr1\text{-}KO}$). In contrast to single $A20^{Cx3Cr1\text{-}KO}$ mice, caspase-1/$A20^{Cx3Cr1\text{-}KO}$ mice developed less severe disease upon immunization with MOG35-55 peptide (Fig. 5g). Together, these results demonstrate the role of A20 in the control of Nlrp3 inflammasome activation locally in microglia, and indicate the importance of this microglial A20/Nlrp3 inflammasome axis in EAE pathogenesis.

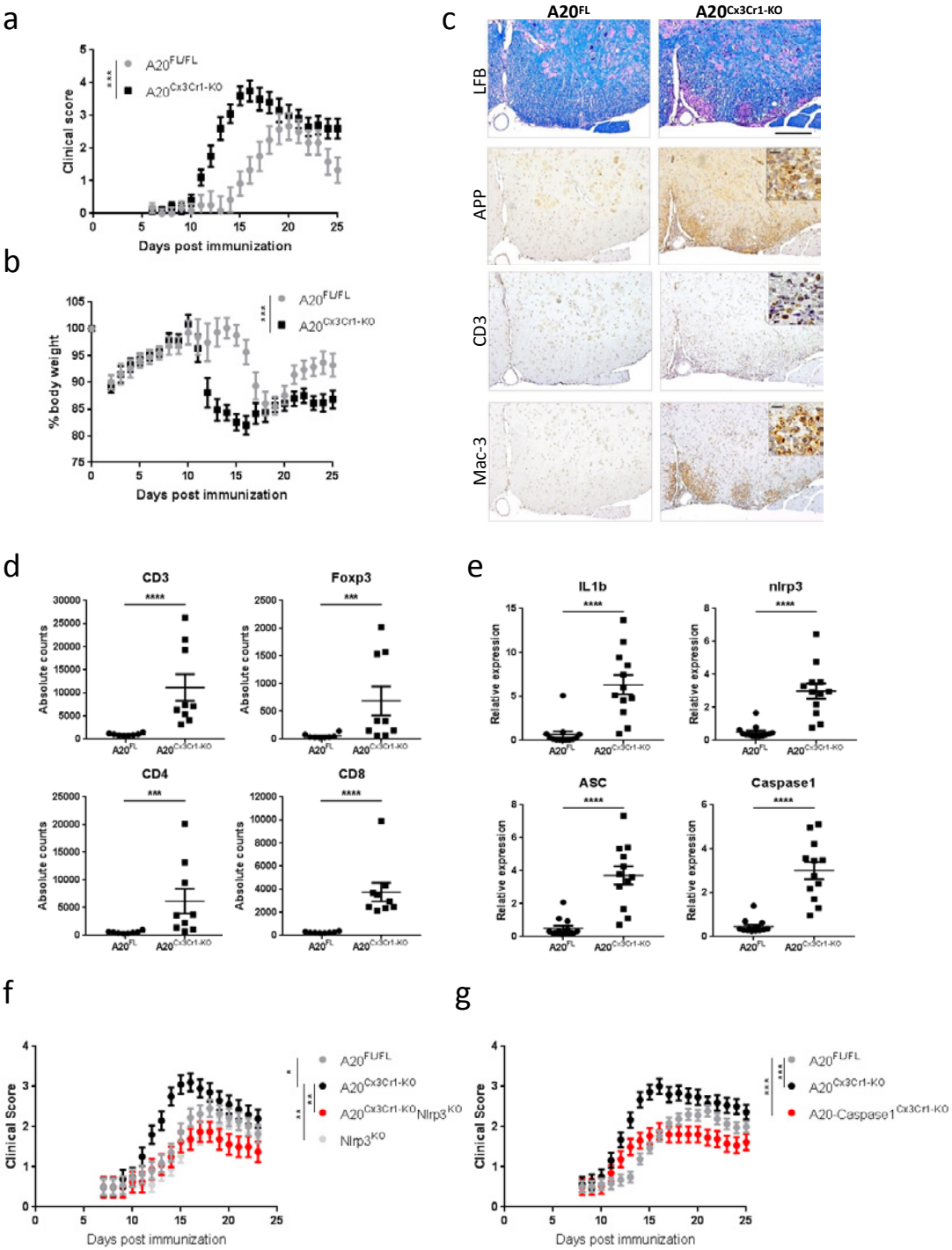

Figure 5. Microglia A20 deficiency aggravates autoimmune CNS inflammation due to Nlrp3 inflammasome hyperactivation. (a-b) EAE was induced by active immunization of control A20^{FL} (n=6) and A20$^{Cx3Cr1\text{-}KO}$ mice (n=10) with MOG peptide, and clinical disease development (a) and body weight (b) was followed over time. Each data point represents the mean ± SEM as estimated by the REML analysis. Changes in clinical score and relative body weight differ significantly (*** $p < 0.001$; F-test) between genotypes across the time span. Data are representative of three independent experiments. (c) Representative images of spinal cord of control (A20^{FL}) and A20$^{Cx3Cr1\text{-}KO}$ mice 13 days post-immunization using LFB, APP, CD3 and MAC-3 antibodies. Scale bars represent 200 µm (overview) and 20 µm (zoom). Representative images from at least four mice per group are displayed. (d) Assessment of immune cell (CD3, CD4 and CD8 T cell, Treg) infiltration in the CNS of control (A20^{FL}) and A20$^{Cx3Cr1\text{-}KO}$ mice by flow cytometry just before disease onset. Each symbol represents one mouse. Data are expressed as mean ± SEM and significant differences are determined by a Mann-Whitney U statistical test (*** $p < 0.001$, **** $p < 0.0001$). (e) Expression of inflammasome-associated factors in the spinal cord of TAM-injected control (A20^{FL}) and A20$^{Cx3Cr1\text{-}KO}$ mice 12 days post immunization. Each symbol represents one mouse. Data are expressed as the ratio of the mRNA expression normalized to endogenous housekeeping genes and expressed as mean ± SEM. Significant differences are determined by a Mann-Whitney U statistical test (**** $p < 0.0001$). (f-g) Active immunization of control (A20^{FL}, n=11), A20$^{Cx3Cr1\text{-}KO}$ (n=10), Nlrp3^{KO} (n=18) and A20$^{Cx3Cr1\text{-}KO}$-Nlrp3^{KO} (n=8) mice (f) and of control (A20^{FL}, n=28), A20$^{Cx3Cr1\text{-}KO}$ (n=15) and A20/Caspase1$^{Cx3Cr1\text{-}KO}$ (n=13) mice (g), and clinical disease development over time. Each data point represents the mean ± SEM as estimated by the REML analysis. Changes in clinical score and relative body weight differ significantly between genotypes across the time span(* $p < 0.05$, ** $p < 0.01$, *** $p < 0.001$; F test). Graph represents combined data from three independent experiments.

Finally, to investigate the relevance of our findings to human CNS pathology, post-mortem brain tissue and CSF of multiple sclerosis (MS) patients were analyzed for expression of A20 and for the presence of an inflammasome 'signature'. Expression of A20/TNFAIP3, as well as the expression levels of IL-1β and NLRP3 were significantly increased in MS plaques compared to NAWM (Normal appearing white matter), and a trend, albeit not significant, in enhanced IL-18 and caspase-1 in MS plaques could be observed (Fig. 6a-b). Higher IL-18 and IL-1β protein levels were also detected in CSF of MS patients compared to controls, suggestive of inflammasome activation in microglia, although also other immune cells may have contributed to this (Fig. 6c). Our data analyzing the expression levels of inflammasome mediators in brain plaques isolated from normal and MS patients show that brain tissue affected by MS clearly exhibits enhanced activation of the NLRP3 inflammasome, as shown in previous studies.

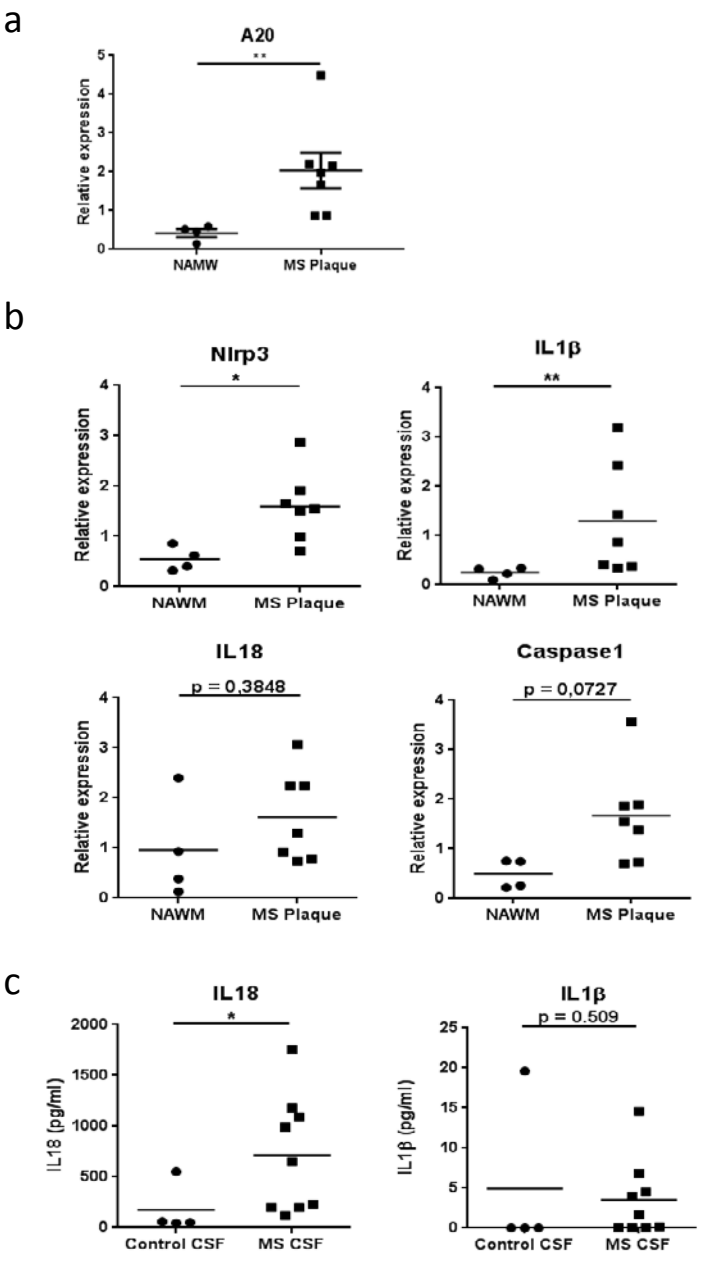

Figure 6. (a-b) Relative gene expression levels of A20/TNFAIP3 (a) and of inflammasome-associated factors (b) in plaques of post-mortem MS patients (Plaque) or post-mortem control tissue (NAWM). Each symbol represents one patient. Data are expressed as the ratio of the mRNA expression normalized to endogenous housekeeping genes (Sdha and Tbp) and expressed as mean ± SEM. Significant differences are determined by Mann-Whitney U statistical test (* $p < 0.05$, ** $p < 0.01$). (c) IL1β and IL18 cytokine levels in the CSF of post-mortem MS patients or control samples. Each symbol represents one CSF sample. Significant differences are determined by Mann-Whitney U statistical test (* $p < 0.05$).

In summary, we found that A20 critically controls microglia activation both in steady-state as in conditions of neuroinflammation. In experimental models of neuroinflammation, the expression of A20 by microglia is crucial in keeping NLRP3 inflammasome activation at bay. These results may contribute to a better understanding and treatment of inflammatory and neurodegenerative diseases. Strategies targeting microglia to suppress their activation eventually through expression of A20 might prove useful for the treatment of these diseases.

Our ongoing studies are now investigating the importance of inflammasome activation locally in microglia for multiple sclerosis pathology. For this we have generated microglia-specific caspase-1 and caspase-11 knockout mouse lines which are being investigated in the EAE model of MS.

7. References

- Bauernfeind FG, Horvath G, Stutz A, et al. Cutting edge: NF-kappaB activating pattern recognition and cytokine receptors license NLRP3 inflammasome activation by regulating NLRP3 expression. J Immunol. 183(2), 787-791 (2009).
- Goldmann T, Wieghofer P, Müller PF, et al. A new type of microglia gene targeting shows TAK1 to be pivotal in CNS autoimmune inflammation. Nat Neurosci. 16(11), 1618-1626 (2013).
- Gris D, Ye Z, Iocca HA, et al. NLRP3 plays a critical role in the development of experimental autoimmune encephalomyelitis by mediating Th1 and Th17 responses. J Immunol. 185(2), 974-981 (2010).
- Hooge RD, Deyn PP De. Applications of the Morris water maze in the study of learning and memory. Brain Res Rev. 36(1), 60-90 (2001).
- Keren-shaul H, Spinrad A, Weiner A, et al. A Unique Microglia Type Associated with Restricting Development of Alzheimer ' s Disease. Cell. 169(7), 1276-1290 (2017).
- Kierdorf K, Erny D, Goldmann T, et al. Microglia emerge from erythromyeloid precursors via Pu.1- and Irf8-dependent pathways. Nat Neurosci. 16(3), 273-280 (2013).
- Lamkanfi M, Dixit VM. Mechanisms and functions of inflammasomes. Cell. 157(5), 1013-1022 (2014).
- Parkhurst CN, Yang G, Ninan I, et al. Microglia Promote Learning-Dependent Synapse Formation through Brain-Derived Neurotrophic Factor. Cell. 155(7), 1596-1609 (2013).
- Shaw PJ, Lukens JR, Burns S, Chi H, McGargill MA, Kanneganti T-D. Cutting edge: critical role for PYCARD/ASC in the development of experimental autoimmune encephalomyelitis. J Immunol. 184(9), 4610-4614 (2010).
- Vande Walle L, Van Opdenbosch N, Jacques P, et al. Negative regulation of the NLRP3 inflammasome by A20 protects against arthritis. Nature. 512(7512), 69-73 (2014).
- Van Gorp H, Saavedra PH V, Vasconcelos NM De, Opdenbosch N Van. Familial Mediterranean fever mutations lift the obligatory requirement for microtubules in Pyrin inflammasome activation. Proc Natl Acad Sci U S A. 113(50), 5-10 (2016).
- Vereecke L, Sze M, Guire CM, et al. Enterocyte-specific A20 deficiency sensitizes to tumor necrosis factor-induced toxicity and experimental colitis. J Exp Med. 207(7), 1513-1523 (2010).
- Waisman A, Ginhoux F, Greter M, Bruttger J. Homeostasis of Microglia in the Adult Brain: Review of Novel Microglia Depletion Systems. Trends Immunol. 36(10), 625-636 (2015).
- Walsh JG, Muruve DA, Power C. Inflammasomes in the CNS. Nat Rev Neurosci. 15(2), 84-97 (2014).
- Qin L, Wu X, Block ML, et al. Systemic LPS causes chronic neuroinflammation and progressive neurodegeneration. Glia. 55(5), 453-462 (2007).
- Zhang Y, Chen K, Sloan SA, et al. An RNA-Sequencing Transcriptome and Splicing Database of Glia, Neurons, and Vascular Cells of the Cerebral Cortex. J Neurosci. 34(36), 11929-11947 (2014).

8. Publications van Loo group 2016-2019 (acknowledging GSKE support) * Publications related to GSKE-supported research

1. * Voet, S., Srinivasan, S., Lamkanfi, M. and **van Loo, G.** (2019) Inflammasomes in neuroinflammatory and neurodegenerative diseases. EMBO Mol. Med., 11 (6) (IF : 10.29)
2. Hoste, E., van Hove, L., Vikkula, H.K., Roelandt, R., Declercq, W., Fuentes, I., Pallison, F., Gonzalez, S., Salas-Alanis, J.C., Huebener, P., Schwabe, R.F. and **van Loo, G.** (2019) Epithelial HMGB1 delays skin wound healing and drives tumor initiation by priming neutrophils for NET formation. Cell Rep., in press. (IF : 7.82)
3. Priem, D., Devos, M., Druwé, S., Martens, A., Slowicka, K., Ting, A. T., Pasparakis, M., Declerq, W., Vandenabeele, P., **van Loo, G.** and Bertrand, M. (2019) A20 protects cells from TNF-induced apoptosis through linear ubiquitin-dependent and -independent mechanisms. Cell Death Dis., 10(10), 692. (IF : 6.0)
4. * Martens, A. and **van Loo, G.** (2019) A20 at the crossroads of cell death, inflammation and autoimmunity. In : Cell Death and Survival, 2nd ed. Cold Spring Harb. Perspect. Biol., Cold Spring Harbor Press, in press. (IF : 9.25)
5. Serramito-Gómez, I., Boada-Romero, E., Slowicka, K., Vereecke, L., **van Loo, G.** and Pimentel-Muiños, F.X. (2019) The anti-inflammatory protein TNFAIP3/A20 binds the WD40 domain of ATG16L1 to control the autophagic response, NF-kB activation and intestinal homeostasis. Autophagy, 15(9), 1657-1659. (IF : 11.1)
6. Slowicka, K., Serramito-Gómez, I., Boada-Romero, E., Martens, A., Sze, M., Petta, I., Vikkula, H.K., De Rycke, R., Parthoens, E., Lippens, S., Savvides, S.N., Wullaert, A., Vereecke, L., Pimentel-Muiños, F.X. and **van Loo, G.** (2019) Physical and functional interaction between A20 and ATG16L1-WD40 domain in the control of intestinal homeostasis. Nat. Commun., 10 (1), 1834. (IF : 12.35)
7. Polykratis, A., Martens, A., Eren, O., Shirasaki, Y., Yamagishi, M., Yamaguchi, Y., Uemura, S., Miura, M., Kollias, G., Armaka, M.*, **van Loo, G.*** and Pasparakis, M.* (2019) A20 prevents inflammasome-dependent arthritis by inhibiting macrophage necroptosis through its ZnF7 ubiquitin binding domain. Nat. Cell Biol., 21, 731-742. (*equally contributed) (IF : 19.06)
8. * Voet, S., Prinz, M. and **van Loo, G.** Microglia in central nervous system inflammation and multiple sclerosis pathology. Trends in Molecular Medicine, 25 (2), 112-123. (IF : 11.0)
9. * Voet, S., Mc Guire, C., Hagemeyer, N., Martens, A., Schroeder, A., Wieghofer, P., Daems, C., Staszewski, O., Vande Walle, L., Costa Jordao, M.J., Sze, M., Vikkula, H., Demeestere, D., Van Imschoot, G., Scott, C.L., Hoste, E., Gonçalves, A., Guilliams, M., Lippens, S., Libert, C., Vandenbroucke, R., Kim, K.W., Jung, S., Callaerts-Vegh, Z., Callaerts, P., de Wit, J., Lamkanfi, M., Prinz, M. and **van Loo, G.** (2018) A20 critically controls microglia activation and inhibits inflammasome-dependent neuroinflammation. Nature Communications, 9 (1), 2036. (IF : 13.1)
10. Slowicka, K. and **van Loo, G.** (2018) Optineurin functions for Optimal immunity. Frontiers Immunology, 9, 769. (IF : 6.42)
11. Catrysse, L. and **van Loo, G.** (2018) Adipose tissue macrophages and their polarization in health and obesity. Cellular Immunology, 330, 114-119. (IF : 3.17)
12. Catrysse, L. and **van Loo, G.** (2017) Inflammation and the metabolic syndrome : the tissue specific functions of NF-κB. Trends Cell Biol., 27(6), 417-429. (IF:11.5)
13. Slowicka, K., Vereecke, L. and **van Loo, G.** (2016) Optineurin functions in health and disease. Trends Immunol. 37(9), 621-633. (IF : 10.4)
14. Catrysse,L., Farhang Ghahremani, M., Youssef, S.A., Mc Guire, C., Vereecke, L., Sze, M., Weber, A., Heikenwalder, M., De Bruin, A., Beyaert, R. and **van Loo, G.** (2016) A20 prevents chronic liver inflammation and cancer by protecting hepatocytes from death. Cell Death Dis., 7, e2250 (IF : 5.0)
15. Maelfait, J., Roose, K., Vereecke, L., Mc Guire, C., Sze, M., Schuijs, M.J., Willart, M., Ibañez, L.I., Hammad, H., Lambrecht, B.N., Beyaert, R., Saelens, X. and **van Loo, G.** (2016) A20 Deficiency in Lung Epithelial Cells Protects against Influenza A Virus Infection. PLoS Pathog., 12 (1), e1005410. (IF : 7.56)
16. Slowicka, K., Vereecke, L., Mc Guire, C., Sze, M., Maelfait, J., Kolpe, A., Saelens, X., Beyaert, R. and **van Loo, G.** (2016) Optineurin deficiency in mice is associated with increased sensitivity to Salmonella but does not affect proinflammatory NF-kB signaling. Eur. J. Immunol., 46(4), 971-980. (IF : 4.03)

Geneeskundige Stichting Koningin Elisabeth
Fondation Médicale Reine Elisabeth
Königin-Elisabeth-Stiftung für Medizin
Queen Elisabeth Medical Foundation

Final report of the research group of

Prof. dr. Verfaillie Catherine

Katholieke Universiteit Leuven (KU Leuven)

Principal investigator

Prof. dr. Verfaillie Catherine
Interdepartementaal Stamcel Instituut
Katholieke Universiteit Leuven
UZ Gasthuisberg
Herestraat 49
3000 Leuven
Belgium
Tel.: +32 16 33 02 95
Fax: +32 16 33 02 94
E-mail: catherine.verfaillie@med.kuleuven.be

Unraveling the Role of TREM2 Mutations in Alzheimer's Disease using Human Pluripotent Stem Cells

1. Summary of Key Achievements / Findings for ***AIM 1***: **Generate TREM2 mutant hPSC lines and assess their phagocytic ability**:

- Three TREM2 mutant hPSC lines have been successfully created by CRISPR/Cas9-mediated genome engineering: (1) *TREM2 R47H HE*; (2) *Heterozygous TREM2*$^{+/-}$; (3) *Homozygous TREM2*$^{-/-}$

- All three mutant lines could be differentiated to monocytes and microglia-like cells (via Yanagimachi protocol). Nonetheless, the *TREM2*$^{+/-}$ and *TREM2*$^{-/-}$ hPSC-derived monocytes and tMG showed a severe reduction of amyloid phagocytic capacity compared to *wt,* in contrast to minimal effects observed for those derived from *R47H HE* hPSC.

- Genome-wide RNA sequencing (RNAseq) analysis suggested that the produced hPSC monocytes differ from peripheral blood (PB) monocytes but more closely resemble tMG cells, which we hypothesize that this was caused by *in vitro* culture. The produced hPSC tMGs resemble microglia-like cells generated in other published studies as well as in cultured human primary microglia.

- In a migration assay using a microfluidic system, the *TREM2*$^{-/-}$ tMGs displayed a decrease in phagocytic clearance in brain slices, however no significant difference in the migration behaviour between the *TREM2*$^{-/-}$ tMGs and WT tMGs towards Aβ42 was observed.

Two publications are generated from these works:

1. Claes C, Van Den Daele J, Boon R, Schouteden S, Colombo A, Monasor LS, Fiers M, Ordovas L, Nami FA, Bohrmann B, Tahirovic S, De Strooper B, Verfaillie CM. ***Human stem cell-derived monocytes and microglia-like cells reveal impaired amyloid plaque clearance upon heterozygous or homozygous loss of TREM2***. Alzhemier's & Dementia. 2019 Mar; 15(3): 453-464. doi: 10.1016/j.jalz.2018.09.006. IF: 14.423 (citations = 8)
2. Claes C, Van den Daele J, Verfaillie CM. ***Generating tissue-resident macrophages from pluripotent stem cells: Lessons learned from microglia***. Cell Immunol. 2018 Aug;330:60-67. doi: 10.1016/j.cellimm.2018.01.019. IF: 2.995 (citations = 3)

2. AIM 2 : Compare the effect of normal donor, TREM2^{R47H} and TREM2$^{-/-}$ tMGs derived from hPSC on neuronal survival in vitro.

Neuroinflammation is known to worsen neurodegeneration due to excessive secretion of pro-inflammatory cytokines. To study this phenomenon in an *in vitro* condition that more closely recapitulating the *in vivo* brain microenvironment niche, we adopted a two-prong approach to produce 3D cellular models:

2.1. Generation of brain cortical organoids

To create 3D cortical organoids, one can allow iPSC to spontaneously develop as spheroids in stirred suspension cultures. However, the time required for maturation of the glial compartment is > 3 months; and the organoids in general are highly variable, even if a recent study suggested that more consistent organoids can be created. Additionally, Matrigel is often used to encapsulate organoids or added into medium to promote corticogenesis, which is an extracellular matrix extracted from mouse sarcoma that has variable composition, thus may contribute to the inconsistent composition of the organoids. Moreover, no microglia, which play an important role in the inflammatory component of all neurodegenerative disorders, are present in such organoids.

For this, we created so-called 'concentroids' derived from fused brain organoids derived from iPSC neural progenitors, that could be maintained for > 150 days *in vitro*. Although maturation was observed, we noticed presence of a large fraction of (radial) glia, also found in published cortical organoids (***Figure 1***). Studies are now ongoing to drive differentiation away from (radial) glia towards neurons. Once the neuronal cell fraction could be enriched in the concentroids, the three tMGs lines will be incorporated as co-culture models in order to assess neuronal cell survival (with or without the treatment with LPS to activate inflammation responses by the tMGs).

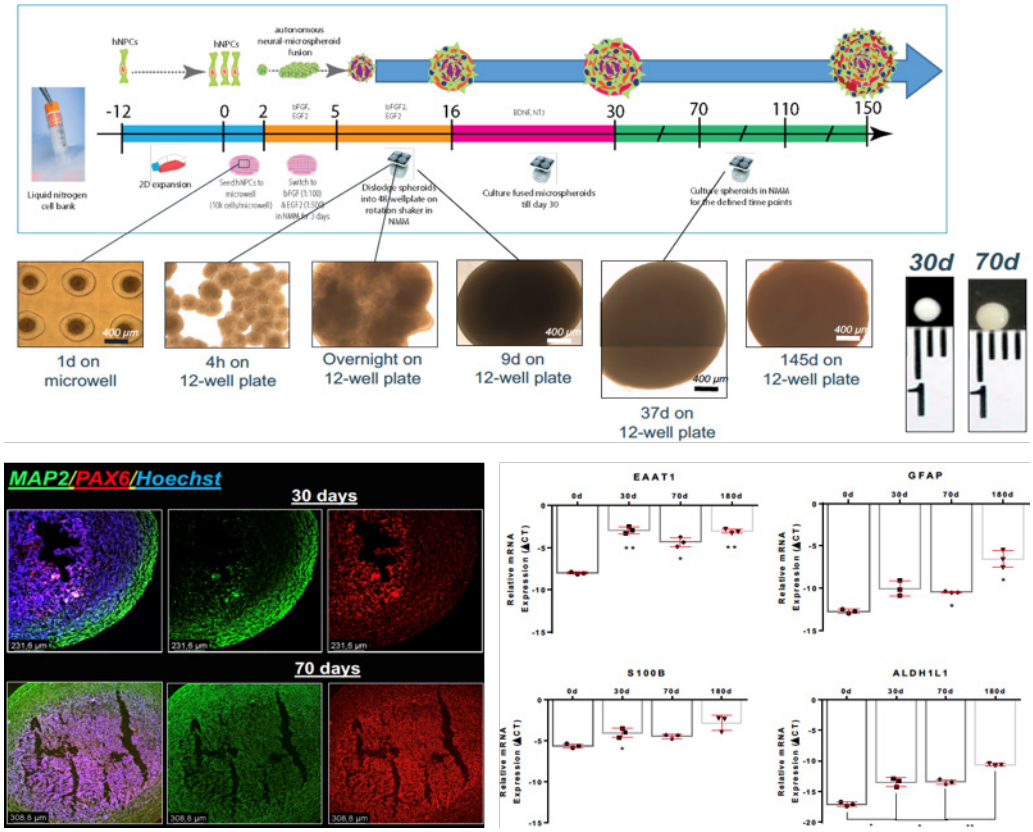

Fig. 1: Gereation of concentroids from iPSC-NPC. *Top panel; method; Lower panel: immunostaining for mature (MAP2) and immature (PAX6) neuronal, and markers; and qRT-PCR data for (radian neural) glia.*

2.2. Generation of brain-specific hydrogel

Additionally, we develop methods to replace the matrigel-based hydrogel commonly used to create cortical organoids by a defined and tunable polyethylene glycol (PEG)-based hydrogel. Different physicochemical properties were generated based on the concentration of the PEG gel, the concentration of hyaluronic acid and the degree of cross-linking. Functionalization was done with only the RGDS adhesion peptide during this initial screen. This screen demonstrated that optimal conditions for cortical neuron differentiation (assessed using a design of experiment (DOE) approach with as readout qRT-PCR for expression of ± 30 stem cell vs. neuronal vs. glial genes identified an optimal hydrogel composition with a stiffness in the range of 250 Pascal, based on specific PEG-hyaluronic acid and MMP-cleavable linker concentrations (***Figure 2***). A subsequent screen is now ongoing to determine the complement of adhesion ligands aside from RGDS that should be used to create the optimal cortical neuron conducive hydrogel. We hypothesize that the same peptide-functionalized hydrogel identified for cortical neuron will also be conducive to other brain cell types (including tMGs), thus allowing the assessment of activated tMGs on neuronal cell survival in the perspective of neurodegenerative diseases.

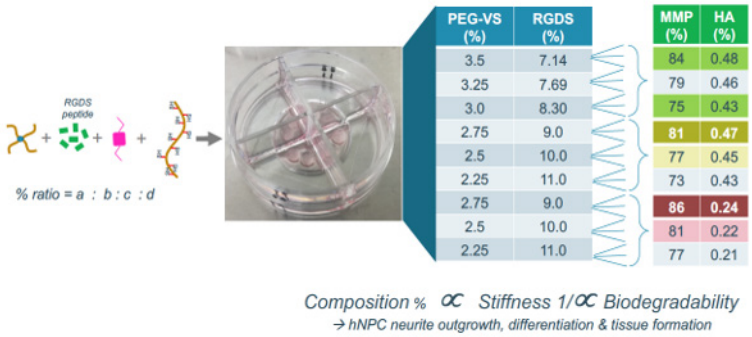

Fig. 2: *Set-up of design of experiment screen to define the physicochemical properties of a cortical neuron conducive defined hydrogel formulation.*

3. AIM 3: Assess the effect of the normal donor, TREM2R47H and TREM2$^{-/-}$ tMGs on neuronal survival in vivo in an APP, PS1$^{+/-}$ NOD-SCID and NOD-SCID mouse model.

In collaboration with the De Strooper lab (KU Leuven), we have transplanted hPSC-derived wild-type tMGs in Rag2$^{-/-}$CSF1$^{h/h}$ mice (as an improved humanized mouse model) in order to determine if the tMGs can replace the microglia in the brain *in vivo*. tMGs were GFP labeled, allowing their re-isolation from the murine brain using FACS. After 8 weeks, the grafting efficiency of hPSC-derived tMGs was estimated at 9% ± 5% of the total microglial population and they were widely distribution across multiple areas of the brain (***Figure 3a & 1b***).

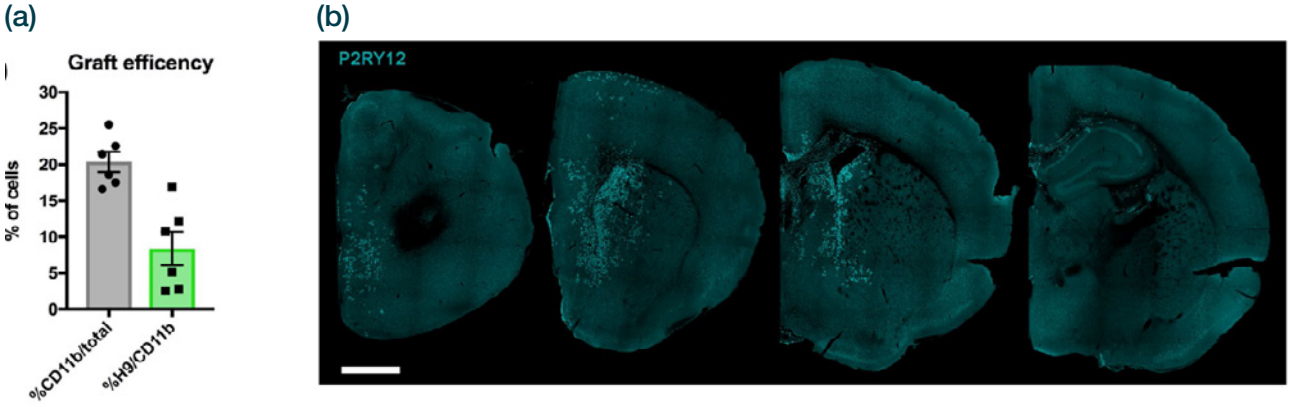

Fig. 3: (a) *hPSC-derived tMGs graft efficiency. Percentage of CD11b cells in the total sample, and proportion of human cells amongst them (mean ± s.e.m., n = 6).* ***(b)*** *hPSC-derived tMGs showed a widespread distribution across multiple areas of the brain (stained for P2RY12) across consecutive sections separated by 500* **µ***m to capture multiple anatomical areas. Scale bar, 1mm.*

We performed single cell RNAseq on the re-isolated tMGs in comparison with freshly isolated human microglia. Specifically, we compared the single-cell transcriptomic profile of 2,246 re-isolated tMGs (n = 3/1: three mice in one combined sequencing pool) versus 4,496 *in vitro* cultured MNC (n = 2/1: two differentiations in one combined sequencing pool) and 3,385 *in vitro* cultured microglia (n = 2/1), as well as 22,846 human primary microglia obtained from cortical surgical resections. The results showed that more than 97% of the *in vitro* cultured MNC and microglia were present in *in vitro* clusters, whereas 79% of primary microglia and 60% of transplanted hPSC-derived tMGs distributed into the *in vivo* HM cluster (***Figure 4a – 4c***). A smaller percentage (13%) of primary compared with transplanted hPSC-derived tMGs (35%) were present in the *in vitro* clusters. Immunohistochemistry and *in situ* hybridization confirmed that CAM cells were in proximity to blood vessels and expressed the perivascular macrophage

marker MRC1 (***Figure 4d***, ***lower panels***). The engrafted H9 cells expressed the microglia markers CX3CR1 and P2RY12 (***Figure 4d, upper panels***).

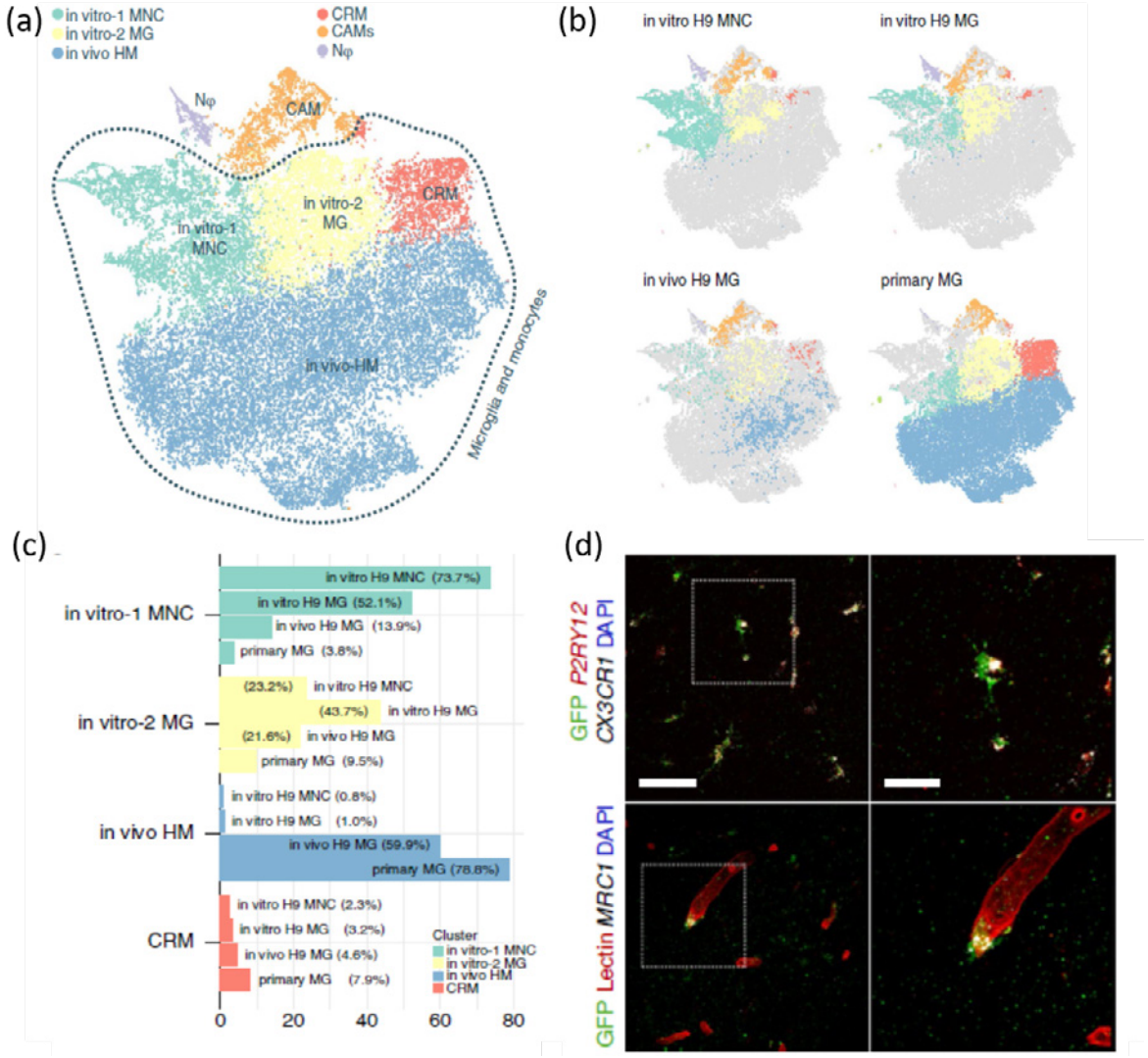

Fig. 4: hPSC-derived tMGs isolated 8 weeks after transplantation are similar to human primary microglia. (a) *t-SNE plot visualizing single cells sorted based on CD11b (primary human), CD11b hCD45 and GFP (engrafted tMGs) staining.* ***(b, c)*** *Distribution and percentage of cells from either in vitro, in vivo (engrafted) tMGs or primary human microglia across the different clusters identified.* ***(d)*** *In situ hybridization for CX3CR1 and P2RY12 (microglia) and MRC1 (perivascular macrophages) confirming the location of the two main distinct identities acquired by H9 engrafted cells (GFP) in mouse brain (n = 4 mice). Scale bars, 25 µm (left); 10 µm (right).*

Direct comparison between experimental groups revealed that *in vitro* MNC and microglia displayed >300 differentially expressed genes (logFC > 0.2) compared with microglia from surgical samples, consistent with an 'activated' profile (***Figure 5a – 5c***). In contrast, engrafted hPSC-derived tMGs displayed a comparable homeostatic signature to that of the cells isolated from human brain, with only 41 differentially expressed genes (***Figure 5a & 5c***). Therefore, the mouse CNS environment is sufficient to drive microglia from an artificial *in vitro* 'activated' toward a more natural homeostatic brain-resident phenotype. In summary, the scRNAseq analysis suggested that transplanted tMGs are highly similar to freshly isolated human primary microglia and are distinct from *in vitro* cultured MNC and tMGs.

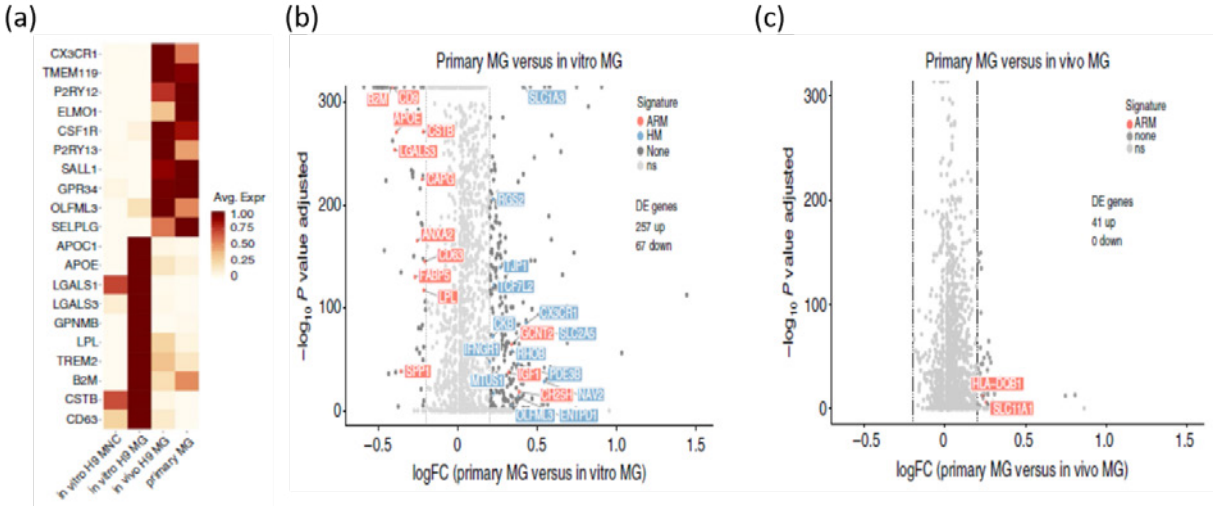

Fig. 5: (a) *Most highly expressed genes in the different samples: in vitro-1 MNC, in vitro-2 MG, in vivo (engrafted) tMGs and primary microglia.* ***(b, c)*** *Volcano plots showing gene expression differences between average gene expression in 22,846 primary versus 3,385 in vitro MG and 22,846 primary versus 2,246 engrafted tMGs (logFC > 0.2, Wilcoxon rank-sum test, P values adjusted with Bonferroni correction based on the total number of genes in the dataset).*

Additionally, we tested our humanized system with an acute Alzheimer's disease-related challenge, that is, oligomeric amyloid-β, previously shown to induce cognitive alterations. Mice were injected with oligomeric amyloid-β (Aβ) or scrambled peptide at 8–10 weeks post-transplantation, and 4,880 transplanted tMGs were isolated at 6 hour after injection. Clustering analysis revealed a homeostatic (H9.HM), a 'primed' (H9.PM) and a cytokine (H9.CRM) cluster (***Figure 6a***). The H9.HM cluster was significantly enriched with Scr-treated cells (68%, $\chi 2$ test, $P < 2.2 \times 10–250$) and showed high expression of multiple homeostatic genes. The 'primed' H9.PM cluster was very different from the previously characterized activated response in wildtype mouse microglia because it expresses an unusual mixture of homeostatic and activation genes, and consisted of a larger proportion of scrambled (65%) versus oligomeric amyloid-β cells (35%, $\chi 2$ test, $P < 10–250$; ***Figure 6a & 6b***). Finally, the H9.CRM cluster was significantly enriched in cells from oligomeric amyloid-β-treated mice (75%, $\chi 2$ test, $P < 2.2 \times 10–250$) and displayed high levels of multiple inflammatory cytokines and chemokines, such as IL1B, IL6, CCL2, CCL4 and so on. Trajectory analysis revealed a phenotypical change of hPSC-derived tMGs from homeostatic toward the cytokine response state (***Figure 6b***) with microglia from the H9.PM cluster enriched in the initial and middle phases, indicating they might represent an early response to the injection of peptides.

At the same time, we isolated and sequenced 9,942 host mouse microglia (after exclusion of CAMs and other immune or cycling cells) from the same animals to compare their reaction with that of hPSC-derived tMGs (***Figure 6c & 6d***). Although we acknowledge that the genetic background of the host might cause (unknown) developmental abnormalities, analysis of different wild-type mouse microglial datasets did not reveal expression of Rag2 or Il2ry, and although the effect of Il2ry deficiency on microglia is not documented, Rag2 deficiency does not affect microglial number, morphology or gene expression profiles. Clustering analysis yielded a homeostatic (ms.HM), a cytokine (ms.CRM) and an activated (ms.ARM) response cluster. The HM cluster was significantly enriched with control cells (70%), whereas the CRM and activated response microglia (ARM) clusters mostly consisted of cells from the mice treated with oligomeric amyloid-β (69% and 77%, $\chi 2$ test, $P < 10–250$; ***Figure 6d***). The ARM cluster showed a similar profile to that of microglia responding to amyloid-β plaques (***Figure 6c & 6d***). Trajectory analysis showed that mouse microglia transition from homeostatic to cytokine response to activated response cells (***Figure 6c***), suggesting that they form a single successive response of mouse microglia to oligomeric amyloid-β. Overall, the results suggested that the transplanted tMGs displayed a cytokine response which was quite distinct from the response of the mouse microglia.

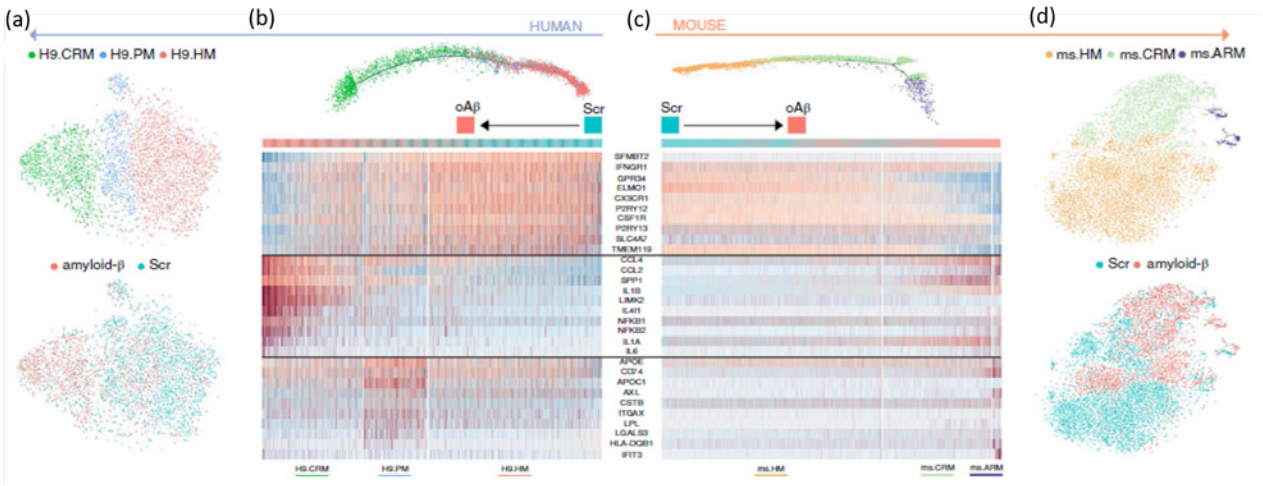

Fig. 6: Human and host mouse microglial response to oligomeric amyloid-β. (a, b) *Analysis of the response of hPSC-derived tMGs upon oligomeric amyloid-β exposure:* ***(a)*** *t-SNE plot visualizing the 4,880 tMGs passing quality control and after removal of CAM, cycling cells and doublets.* ***(b)*** *Plot of the phenotypic trajectory followed by tMGs upon oligomeric amyloid-β exposure. hPSC-derived tMGs followed a trajectory from H9.HM and H9.PM to H9.CRM.* ***(c, d)*** *Analysis of the response of endogenous (Rag2$^{-/-}$ Il2rγ$^{-/-}$) mouse microglia upon oligomeric amyloid-β challenge:* ***(c)*** *t-SNE plot visualizing the 9,942 endogenous mouse microglia passing quality control and after removal of peripheral cells, CAMs cycling cells and doublets.* ***(d)*** *Plot of the phenotypic trajectory followed by endogenous mouse microglia upon oligomeric amyloid-β exposure. Mouse microglia followed a trajectory from ms.HM to ms.CRM to ms.ARM. The heatmap shows the differential expression of representative genes from each cluster, ordered by pseudotime.*

We finally evaluated whether this chimeric model covers the human expressome better than the classical mouse models. We extracted 10,914 one-to-one, bidirectional orthologs between mouse and human and performed a correlation analysis comparing logFC in gene expression in the CRM versus HM comparison done in each species (false discovery rate (FDR) < 0.05). We observed a significant, but rather limited correlation in the response to oligomeric amyloid-β (R = 0.4, Pearson's correlation, P ≈ 0), with a number of genes changed in mouse or human alone (logFC > 0.2; ***Figure 7a***), 207 of them showing opposite behavior (***Figure 7b***), such as TYMP, NFKB, PPARG, LIMK2 and TGFBR1, an HM marker in mouse, and the Alzheimer's disease risk genes ABI3, BIN1 and PICALM. We also explored how the 8,266 human genes with no clear mouse ortholog reacted to oligomeric amyloid-β and found 79 and 127 uniquely upregulated and downregulated human genes, mainly involved in cytokine and chemokine responses. The human response was particularly strong for IL1B and CCL2 (***Figure 7a***), which have been experimentally implicated in the pathology of Alzheimer's disease (***Figure 7a***). Remarkably, 12 of the 15 Alzheimer's disease risk genes identified as lacking 1:1 mouse orthologs were expressed in primary microglia from surgical samples (***Figure 7c***), confirming the association of genetic risk for Alzheimer's disease with microglia. Reassuringly, all of these genes were also detected in the transplanted hPSC-derived tMGs (including APOC, CD33, CR1, MS4A and TREM2). The similarities in gene expression between Rag–/– Il2rγ–/– and wild-type mouse microglia (***Figure 7c***) further support the proof-of-concept study presented here.

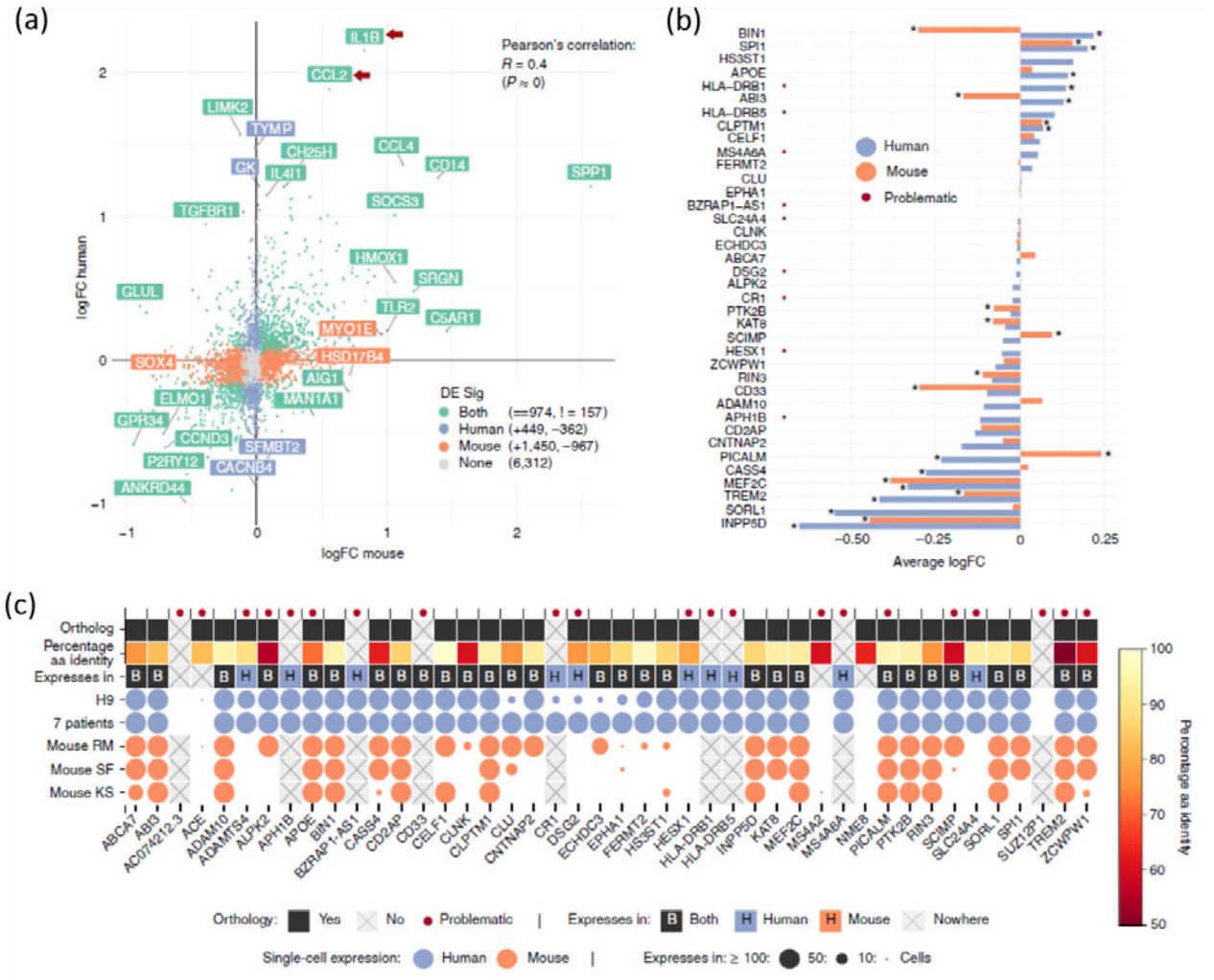

Fig. 7: (a) *Correlation analysis of the logFC in hPSC-derived (y axis) and host (Rag2$^{-/-}$ Il2rγ$^{-/-}$) mouse (x axis) microglia upon oligomeric amyloid-β challenge relative to Scr (CRM versus HM clusters, Pearson's correlation, R = 0.4).* ***(b)*** *Expression changes induced by oligomeric amyloid-β challenge in the selected candidate Alzheimer's disease risk genes.* ***(c)*** *Extension of the table shown in Fig. 1b highlighting the important number of putative Alzheimer's disease risk genes in humans that lack good orthologs in mice or show an opposite behavior upon oligomeric amyloid-β challenge (highlighted by red dots). We identified 15 genes with observed expression in human but not mouse microglia and that were also observed in hPSC-derived tMGs.*

The above data has been published in the journal "Nature Neuroscience":

– *Mancuso R, *Van Den Daele J, Fattorelli N, Wolfs L, Balusu S, Burton O, Liston A, Sierksma A, Fourne Y, Poovathingal S, Arranz-Mendiguren A, Sala Frigerio C, Claes C, Serneels L, Theys T, Perry VH, Verfaillie C, Fiers M, De Strooper B. ***Stem-cell-derived human microglia transplanted in mouse brain to study human disease.*** Nat Neurosci. 2019 Dec;22(12):2111-2116. doi: 10.1038/s41593-019-0525-x. Epub 2019 Oct 28. (***IF: 21.125***) *Joint 1st authorship.

In the meantime, we also have done graftings of hPSC-derived *TREM2R247H* and *TREM2-/-* tMGs in APPNLGF Rag2-/-CSF1h/h mice to address the effect of the mutant microglia in an AD environment, to cause in neuroinflammation and neurodegeneration in AD. Transplanted tMGs will be isolated after 3 and 6 months of grafting and single cell RNAseq will be performed. Experiments are ongoing and first isolation will take place in February.

4. Conclusion:

Within the project duration, we have made significant progress on addressing the project aims. We have provided data on the generation of three TREM2 mutant lines from hPSC that displayed different phagocytic ability and expressed transcriptome profiles that resemble the WT monocytes/microglias. We have therefore achieved the Aim 1. These findings have led to a scientific publication in an IF >10 journal of the field (*Claes C et al. Alzheimer's and Dementia; Impact factor 12.74*), 1 invited review (*Claes C et al. Cell Imunol*) and the defence of 1 PhD student (Christel Claes; defended her PhD on 24 September 2018). Considering current research development and new insights gained in the field of neurodegeneration, we dedicated efforts on developing 3D cellular models instead of the originally proposed 2D monolayer co-culture method (by the recruitment of Dr. Yoke-Chin Chai, postdoctoral fellow; contributes 50% of his time). These brain organoid model and 3D peptide-based hydrogel technology represent useful research avenues, which are largely accepted as better *in vitro* models that allow clinically-relevant disease modelling. The optimized models will eventually be highly beneficial for the study of interaction between microglia activation and neuronal cell death, thus contributes to addressing AIM 2). Encouraging research outcomes have been achieved for Aim 3 (by Johanna Van Den Daele, final year PhD student), whereby the grafting behaviour and phenotype attained (including transcriptomic profiling) by the transplanted hPSC-derived tMGs (wild type) in mouse brain are highly similar to freshly isolated human primary microglia and are distinct from *in vitro* cultured MNC and tMGs. Interestingly, they displayed a cytokine response to amyloid-β that was quite distinct from the response of the mouse microglia. Ongoing works on transplanting the three TREM2 mutant cell lines in the wild-type and neurodegenerative mouse models will provide further insights into the disease pathogenesis, thus fulfilling the Aim 3 and Aim 4. An additional PhD student (Susan Simorgh) is recently recruited and implicated in the ongoing studies.

5. PhD Thesis:

1. **Christel Claes** (defended on 24 September 2018).
   Thesis title: *Unraveling the role of TREM2 in Alzheimer's disease using human pluripotent stem cell-derived microglia-like cells.*
2. **Johanna Van Den Daele** (Final year PhD student).
   Thesis title: *3D stem cell models to study the effect of TREM2 on the hallmarks of Alzheimer's disease.*

6. References:

– Abud EM, Ramirez RN, Martinez ES, Healy LM, Nguyen CHH, Newman SA, et al. iPSC-Derived human microglia-like cells to study neurological diseases. Neuron 2017;94:278–9.
– Claes C, Van Den Daele J, Boon R, Schouteden S, Colombo A, Monasor LS, Fiers M, Ordovas L, Nami FA, Bohrmann B, Tahirovic S, De Strooper B, Verfaillie CM. Human stem cell-derived monocytes and microglia-like cells reveal impaired amyloid plaque clearance upon heterozygous or homozygous loss of TREM2. Alzheimer's & Dement. 2018. Nov. 7. http://doi.org/10.1016/j.jalz.2018.09.006
– García-León JA, Cabrera-Socorro A, Eggermont K, Swijsen A, Terryn J, Fazal R, Nami F, Ordovás L, Quiles A, Lluis F, Serneels L, Wierda K, Sierksma A, Kreir M, Pestana F, Van Damme P, De Strooper B, Thorrez L, Ebneth A, Verfaillie CM. Generation of a human induced pluripotent stem cell-based model for tauopathies combining three microtubule-associated protein tau mutations which displays several phenotypes linked to neurodegeneration. Alzheimers & Dement. 2018 Jul 20. pii: S1552-5260(18)30161-4.
– Yanagimachi MD, Niwa A, Tanaka T, Honda-Ozaki F, Nishimoto S, Murata Y, Yasumi T, Ito J, Tomida S, Oshima K, Asaka I, Goto H, Heike T, Nakahata T & Saito MK. Robust and Highly-Efficient Differentiation of Functional Monocytic Cells from Human Pluripotent Stem Cells under Serum- and Feeder Cell-Free Conditions. PLoS ONE (2013) 8: e59243

Geneeskundige Stichting Koningin Elisabeth
Fondation Médicale Reine Elisabeth
Königin-Elisabeth-Stiftung für Medizin
Queen Elisabeth Medical Foundation

Final report of the research group of

Prof. Voets Thomas

Katholieke Universiteit Leuven (KU Leuven)

Principal investigator

Prof. Thomas Voets
Laboratory of Ion Channel Research
VIB-KU Leuven Center for Brain & Disease Research
KU Leuven, Department of Cellular and Molecular Medicine
Herestraat 49 bus 802
3000 Leuven
Belgium
Tel.: +32 16 33 02 17
E-mail: Thomas.voets@kuleuven.vib.be

Other researchers:

Dr. Ine Vandewauw
Dr. Lauri Moilanen
Miss Marie Mulier
Miss Laura Vangeel

Table of contents

Unraveling the role of TRPM3 in neuropathic and inflammatory pain

1. Background

It is estimated that about 1 million Belgians suffer from moderate-to-severe chronic pain. Chronic back pain, migraine, diabetic neuropathy, osteoarthritis, cancer pain and chemotherapy-induced neuropathic pain are just a few examples of common conditions associated with persistent pain, which in many cases is very difficult to treat (Grayson, 2016; Reid et al., 2011). Indeed, about 50 % of the chronic pain sufferers report inadequate pain control. Over-the-counter analgesics such as paracetamol or nonsteroidal anti-inflammatory drugs often show limited efficacy in the treatment of severe chronic pain. Alternatives such as the gabapentinoids, which act by blocking $\alpha_2\delta$ subunit-containing voltage-dependent calcium channels, or the tricyclic antidepressants such as amitriptyline have good analgesic activity in only a minority of treated patients, and can have significant effects on the central nervous activity. Opioids such as morphine, hydrocodone or fentanyl are increasingly used as potent analgesic drugs to treat moderate to severe pain, but these cause tolerance and addiction and can have severe adverse effects including the risk of overdose (Reid et al., 2011). Of note, a dramatic increase in the use of prescription and non-prescription opioids has been observed in the last two decades, referred to as the "opioid epidemic", resulting in an alarming rise in the number of fatalities from prescription opioids and heroin (Wilson-Poe & Moron, 2017). Therefore, there is a large unmet need for newer and safer treatments for pain, which requires identification of potential druggable targets in the pain pathway (Grayson, 2016).

Recently, our research group has identified TRPM3, a member of the transient receptor potential family of cation channels, as a key player in the pain pathway and a potential novel target for pain treatment. We found that TRPM3 is highly expressed in sensory neurons, in particular in the small-diameter pain-signaling (nociceptor) neurons, and demonstrated that direct activation of TRPM3 in sensory nerve endings in the skin causes acute pain and neurogenic inflammation. In addition, we found that genetic ablation (using knockout mice) or pharmacological inhibition (using specific antagonists) of TRPM3 function leads to significant analgesia in various animal models of persistent pain, without obvious side-effects (Vriens et al., 2011). In particular, we found that pharmacological inhibition of TRPM3 causes a strong reduction of the hypersensitivity (hyperalgesia and allodynia) of inflamed/injured tissue to thermal and mechanical stimuli (Vriens et al., 2011).

2. Objective, hypothesis and specific aims

The overall *objective* of this project is to uncover the molecular and cellular mechanisms whereby TRPM3 contributes to the onset and persistence of pain and hypersensitivity, as a fundamental basis for the further development of TRPM3 antagonists as a novel class of analgesic drugs for human use.

We *hypothesized* that inflammation and peripheral nerve injury leads to a functional upregulation of TRPM3 in nociceptor neurons, either at the transcriptional or at the posttranscriptional level. Increased TRPM3 functionality then increases the excitability of these neurons and renders them more responsive to thermal and mechanical stimuli, which leads to hypersensitivity and persistent pain. Accordingly, we hypothesized that inhibiting TRPM3 activity would reduce neuronal excitability and alleviate hypersensitivity in various painful conditions.

These hypotheses were addressed using rodent models of inflammatory and neuropathic pain, and we aimed at (1) evaluating the role of TRPM3 in the detection of acute painful stimuli; (2) assessing possible alterations in TRPM3 expression and functionality in nociceptor neurons in the context of inflammation and nerve injury; and (3) analyzing the *in vivo* effects of TRPM3 inhibition in animal models of inflammatory and neuropathic pain. Finally, we also aimed at evaluating TRPM3 functionality in human sensory neurons, as an important step towards translating the fundamental findings to future treatments for patients.

3. Results

In the course of the three-year project funded by GSKE, we made important progress in elucidating the role of TRPM3 as a pain sensor and obtained exciting novel insights into its involvement in the development of pathological pain, further highlighting its role as a potential target for novel pain therapies.

3.1. Identification of the role of TRPM3 in acute heat sensing

At the onset of the project, it was well established that TRPM3 acts as a heat sensor involved in the detection of noxious heat. However, pharmacological inhibition or genetic elimination of TRPM3 in mice provokes only a minor reduction of heat responses in sensory neurons and a moderate increase in response latencies to painful heat stimuli *in vivo*, indicative of the co-existence of multiple heat sensors in these neurons (Straub et al., 2013; Vriens et al., 2014; Vriens et al., 2011). To understand how TRPM3 contributes to thermal hypersensitivity in pathological conditions such as inflammation or nerve injury, it was essential to first identify the full set of heat sensors in sensory neurons and their relative role in heat-induced pain. We initially focused on TRPV1, also known as the capsaicin/vanilloid receptor, an extensively studied heat-activated channel in sensory neurons. To this aim, we first produced and analyzed double knockout (DKO) mice lacking expression of both TRPM3 and TRPV1 ($DKO^{M3/V1}$ mice). Whereas the number of heat-sensitive sensory neurons was further reduced, we still observed robust heat responses in ~40% of $DKO^{M3/V1}$ neurons (**Figure 1a,g**).

An important breakthrough in the course of this project was our discovery that the remaining heat responses in $DKO^{M3/V1}$ neurons are mediated by TRPA1, a channel that in mammals has been implicated in the detection of noxious chemicals such as acrolein, mustard oil and H2O2 (Bautista et al., 2006), but was not associated with heat sensing. Pharmacological inhibition of TRPA1 eliminated the residual heat responses in $DKO^{M3/V1}$ neurons (**Figure 1b-d,g**), and triple knockout (TKO) mice lacking all three TRP channels also lacked neuronal responses to noxious heat (**Figure 1e,g**). Mice lacking expression of both TRPM3 and TRPA1 ($DKO^{M3/A1}$ mice) or TRPV1 and TRPA1 ($DKO^{V1/A1}$ mice) showed robust heat responses in ~35-40% of the tested neurons.

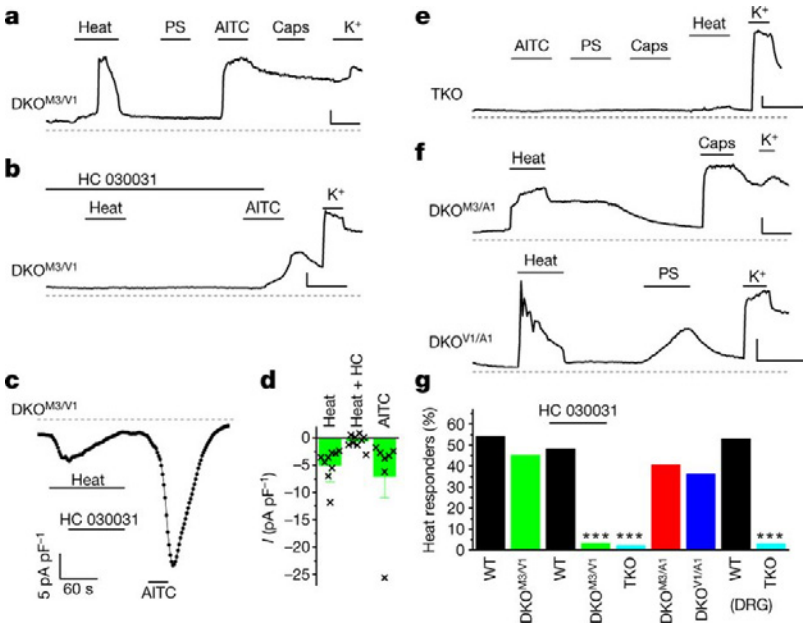

Figure 1. a, b, Responses to heat (45 °C) and AITC (50 µM) in sensory neurons from DKO$^{M3/V1}$ mice in the absence and presence of the TRPA1 antagonist HC030031 (100 µM). WT, wild-type; PS, pregnenolone sulfate; Caps, capsaicin. **c,** Example of a HC030031-sensitive heat-activated inward current in an AITC-sensitive DKO$^{M3/V1}$ neuron. **d,** Mean (± s.e.m.) current densities for experiments as in c($n = 9$ cells). **e, f,** Heat and ligand responses in sensory neurons from TKO and indicated DKO mice. Scale bars in **a, b, e, f,** 60 s/100 nM. **g,** Percentages of heat-responding sensory neurons in mice of the indicated genotypes, in the absence or presence of HC030031. ***$P < 0.00001$; Fisher's exact test with Holm–Bonferroni correction. From Vandewauw *et al.*, Nature (2018).

Strikingly, the TKO mice (DKO$^{M3/V1}$, DKO$^{M3/A1}$ or DKO$^{V1/A1}$ mice) showed a dramatic and specific deficiency in the avoidance of noxious heat. Indeed, in tail flick or hot plate experiments, TKO mice would not withdraw from the noxiously heat stimulus and obtain burn injuries unless the experiment was terminated by the experimenter (**Figure 2a-c**). In contrast, the TKO mice showed normal pain responses to cold or mechanical stimuli and normal thermal preference (**Figure 2d-k**). Taken together, these data indicate that TRPM3 is one of three redundant noxious heat sensors - as long as one of these three channels is functional, acute heat sensing is conserved.

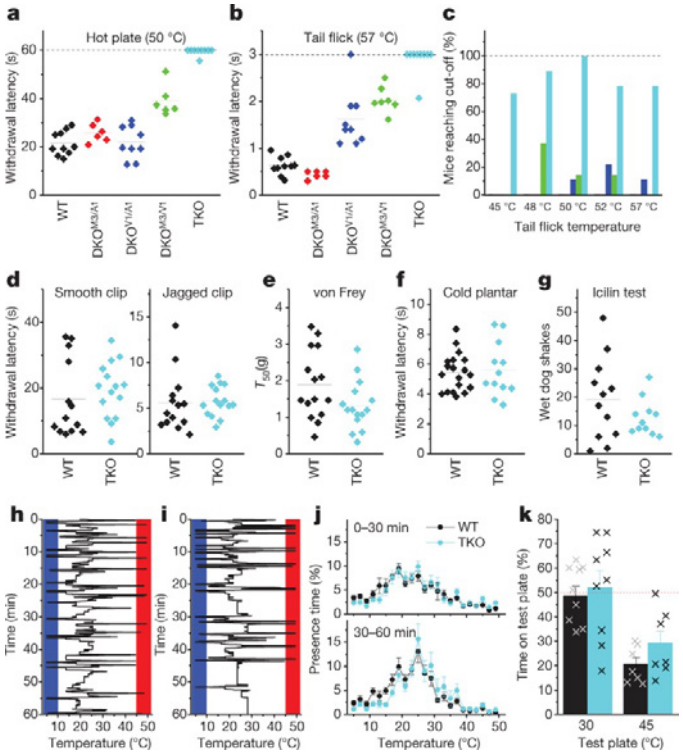

Figure 2. a, b, Withdrawal latencies of male mice in the hot-plate (**a**) and tail-flick (**b**) assays. Dotted lines indicate cut-off times. Horizontal lines in **a, b, d**–gindicate mean. **c,** Percentage of tested animals (WT: $N=16$; $DKO^{M3/A1}$: $N=12$; $DKO^{V1/A1}$: $N=15$; $DKO^{M3/V1}$: $N=12$; TKO: $N=16$) that did not withdraw their tail before the cut-off. **d,** Withdrawal latencies of wild-type ($N=13$–14) and TKO ($N=15$) mice to smooth plastic and jagged metal clips. $P=0.50$ and 0.86, respectively; two-sided Student's *t*-test. **e,** Sensitivity of wild-type ($N=15$) and TKO ($N=15$) mice to calibrated von Frey hairs ($P=0.09$; two-sided Student's *t*-test). T_{50}, 50% paw withdrawal threshold. **f,** Withdrawal latencies of wild-type ($N=19$) and TKO ($N=12$) mice in the cold plantar test ($P=0.76$; two-sided Student's *t*-test). **g,** Number of icilin-induced wet dog shakes in wild-type ($N=12$) and TKO ($N=11$) mice ($P=0.20$; two-sided Student's *t*-test). **h, i,** Representative experiments depicting the positions of a wild-type (h) and a TKO (**i**) mouse on a thermal gradient. Border zones of the gradient are red (>45 °C) and blue (<10 °C). **j,** Mean presence time ± s.e.m. in the different temperature zones during the first and second 30-min periods ($N=10$ mice for each genotype). **k,** Two-temperature choice test with control plate set at 30 °C and test plate set at 30 °C or 45 °C. Mean percentage ± s.e.m. of the total time spent on the test plate ($N=9$ mice for each genotype; $P=0.77$ at 30 °C, $P=0.16$ at 45 °C; two-sided Student's *t*-test). Both genotypes showed statistically significant avoidance at 45 °C ($P=0.001$; one-sample *t*-test versus 50%). From Vandewauw *et al.*, Nature (2018).

These findings not only represent a fundamental breakthrough in the field of pain transduction, but are also of high importance for the future development of TRPM3 antagonists for chronic pain. In particular, it has been questioned whether TRPM3 inhibition could lead to hyposensitivity to noxious heat, leading to a high risk of burn injury. However, our data indicate that as long as TRPM3 antagonists do not inhibit TRPV1 and TRPA1, acute heat sensing remains largely preserved. A manuscript describing these findings was published in *Nature* (Vandewauw et al., 2018), and further analysis of these findings is presented in a manuscript in *British Journal of Pharmacology* (Vriens & Voets, 2019). Both papers acknowledge the support of the Queen Elisabeth Medical Foundation.

3.2. Functional upregulation of TRPM3 in sensory neurons during inflammation

Based on published and unpublished data showing that pharmacological inhibition or genetic ablation of TRPM3 eliminates heat hypersensitivity in the context of inflammation and peripheral nerve injury (Vriens et al., 2011; Vriens & Voets, 2018), we hypothesized that these disease states leads to an upregulation of TRPM3 expression in nociceptor neurons, leading to increased neuronal excitability.

To test this hypothesis, with support of the Queen Elisabeth Medical Foundation, we succeeded in developing a novel combination of experimental approaches to analyze changes in TRP channel expression and functionality specifically in those nociceptive neurons that innervate injured tissue.

In a first step, we examined whether tissue inflammation alters the mRNA expression of TRPM3 and the two other heat-activated TRP channels (TRPV1 and TRPA1). We injected the retrograde label WGA-AlexaFluor647 in the hind paws of mice, which after 5 days resulted in the fluorescent staining of a subset of sensory neuron cell bodies in the lumbal L3-L6 dorsal root ganglia. Then, one hind paw was injected with complete Freund's adjuvans (CFA) leading to a strong inflammatory response associated with heat hyperalgesia, while the other paw was used as vehicle control. In the course of the project, we established the RNAscope-technology (Wang et al., 2012) to detect and quantitate the expression at the mRNA level of sensory TRP channels in dorsal root ganglia tissue. By combining this approach with the WGA-AlexaFluor647-based retrograde labeling, we were able to compare expression in cell bodies of sensory neurons innervating the inflamed *versus* the contralateral control paw (**Figure 3**). Importantly, these experiments revealed a significant increase in TRPM3-encoding mRNA in the ipsilateral DRG neurons innervating the inflamed tissue (**Figure 3**). As a complementary approach, thanks to the support from the **Prix Fonds Elisabeth Vreven**, we have also developed an assay to compare the single cell transcriptomes of sensory neurons. To achieve this, we isolate retrogradely labeled ganglia, disperse the cells, and submit them to FACS sorting based on combined AlexaFluor647 and GCaMP3 fluorescence. With the use of the BD Influx™ high-speed cell sorter, available via the VIB-KU Leuven Flow Cytometry Facility, individual cells were sorted and subjected to single-cell RNA-seq using the SMARTseq technology, available via the Genomics core (KU Leuven/UZ Leuven). We are currently in the process of analyzing this extended data set, which we expect to provide invaluable new data with regard to inflammation-induced changes in expression in sensory neurons, and the contribution of TRPM3.

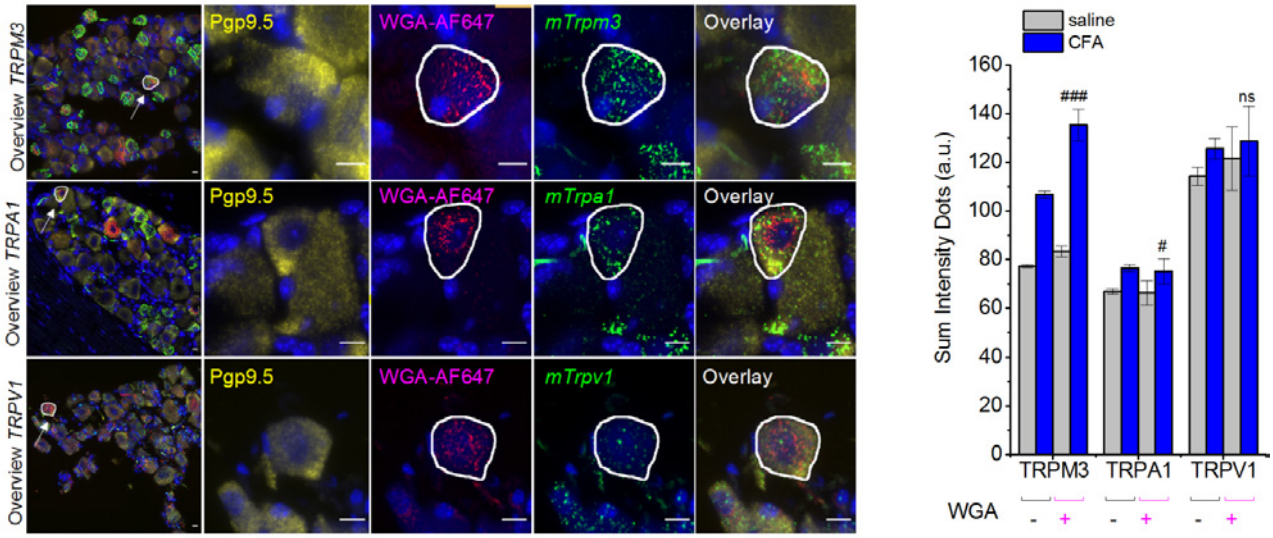

Figure 3. Multiplex fluorescent *in situ* hybridization using RNAscope probes against the neuronal marker Pgp9.5 (yellow), the retrograde label WGA-AF647 and the indicated TRP channels (green) sections of mouse dorsal root ganglia. Nuclei are stained using DAPI (blue). The leftmost pictures provide an overview of the entire section, whereas the other panels zoom in on a region including one retrogradely labeled neuron. The summary figure (right) provides a quantification of the intensity of the RNAscope dots, as a measure of the expression of the indicated TRP channels, comparing ipsi- and contralateral ganglia after CFA-induced inflammation of one hindpaw. #, ###: p<0.05, p<0.001 *versus* control (Two-way ANOVA with Sidak-Holm posthoc test). Mulier, Moilanen & Voets - unpublished results.

In a second step, to analyze whether inflammation also affect TRPM3 functionality, we made use a mouse model that expresses a genetically encoded calcium indicator in nociceptor neurons. We crossed the TRPV1-cre reporter mouse line, which expresses cre-recombinase in all heat-sensitive C and Aδ fibers, with a mouse line expressing GCaMP3 in a cre-dependent manner (GCaMP3-V1 mice), and used the retrograde label WGA-AlexaFluor647 and CFA to induced unilateral inflammation, as described above. Following development of the inflammatory response, we used spinning-disk confocal imaging to measure GCaMP3 fluorescence in intact dorsal root ganglia, and measured changes induced by application of specific agonists for TRPM3 (pregnenolone sulfate + CIM0216), TRPV1(capsaicin) and TRPA1 (Mustard Oil) (**Figure 4a,b**).

By comparing the responses in AlexaFluor647-positive neurons in the ganglia ipsilateral and contralateral to the CFA-injected paw, we were able to specifically measure alterations in functional TRP channel expression caused by inflammation. This approach revealed a strong increase the number of neurons responding to TRPM3 agonism as well as in the amplitude of the TRPM3-mediated responses in neurons innervating the inflamed paw (**Figure 4c,d)**. These responses were fully suppressed by the TRPM3 antagonist isosakuranetin. Moreover, we found that inflammation leads to an increase of the number of sensory neurons that co-express TRPV1 and TRPM3, and that pharmacological inhibition of TRPM3 also leads to a reduction of the TRPV1-mediated responses (**Figure 4c-e**). Considering the key role of TRPV1 as a pain transducer channel, these findings indicate that increased TRPM3 expression can contribute to persistent pain by increasing the excitability of TRPV1-expressing nociceptors.

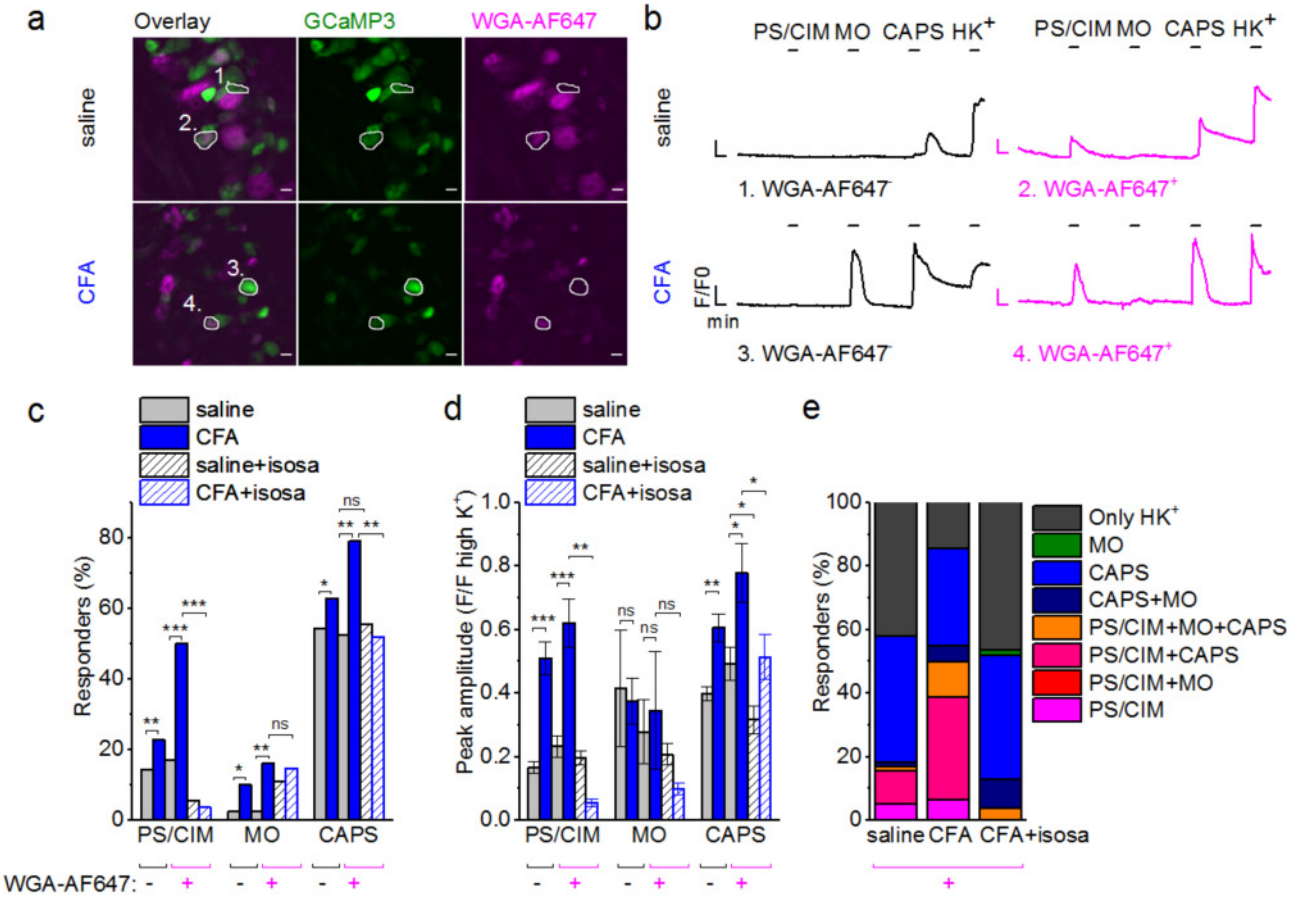

Figure 4. a, Confocal images of the retrogradely labeled DRGs from a GCaMP3-V1 mouse, containing cell bodies of neurons innervating the vehicle- and CFA-treated hind paw, respectively. **b,** Time course of GCaMP3 fluorescence of the indicated cell bodies, showing transient responses to agonists of TRPM3 (pregnenolone sulfate + CIM0216), TRPV1(capsaicin) and TRPA1 (Mustard Oil) and to a depolarising high K^+ solution. **c,d,** quantification of the percentage of responding neurons to the different stimuli (**c**) and of the normalized response amplitudes (**d**). Where indicated, the DRGs were preincubated with isosakuranetin to inhibit TRPM3. **e,** quantification of the co-activation patterns of individual neurons for the agonists of TRPM3, TRPV1 and TRPA1. *,**,***: p<0.05, 0.01, 0.001; Two-way ANOVA with Sidak-Holm posthoc test. Mulier, Moilanen & Voets - unpublished results.

A highly relevant question is whether the molecular and functional upregulation of TRPM3 at the level of the cell bodies in the dorsal root ganglia is also reflected in an increased TRPM3 activity in the sensory nerve endings, where the actual signal detection takes place. To address this question, we have established a novel assay whereby we image free nerve endings in the paw skin of GCaMP3-V1 mice. In this assay, the skin and innervated nerve is carefully dissected and imaged from the external side using spinning-disk confocal microscopy (**Figure 5a,b**), and application of agonists for TRPM3, TRPA1 or TRPV1 revealed specific calcium responses in fine nerve endings in the skin (**Figure 5c**). Importantly, using this innovative assay, we discovered a significant increase in nerve endings responding to TRPM3 agonism, and in particular in nerve endings co-expressing TRPM3 and TRPV1 (**Figure 5d**).

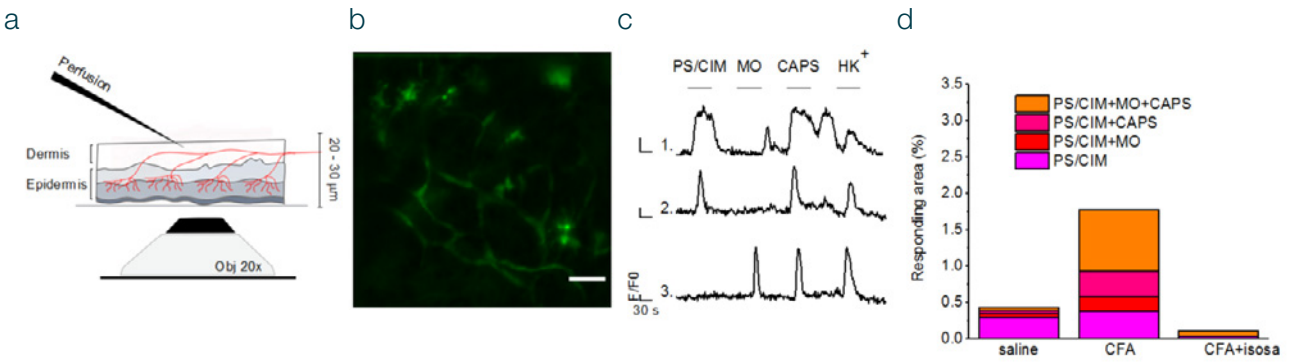

Figure 5. a, Schematics of the set-up to measure activity in sensory nerve endings in the skin. **b,** Raw fluorescence image. c, Examples of calcium responses in individual nerve endings to the same agonists as described in **Figure 4. d,** CFA treatment results in an increase in the area of nerve endings expressing functional TRPM3, and this is inhibited by the TRPM3 antagonist isosakuranetin. Mulier, Moilanen & Voets - unpublished results.

Collectively, these findings are of high relevance for our understanding of the role of TRPM3 in inflammatory pain, as they provide the first demonstration of a molecular and functional upregulation of TRPM3 in neurons that innervate inflamed tissue, both at the level of the cell bodies and in the nerve endings. These results also provide a strong rationale for the development of TRPM3 antagonists to treat hypersensitivity and persistent pain, as they indicate that upregulation of TRPM3 in neurons innervating injured tissue contributes to increased sensitivity of nociceptor nerve endings. A manuscript describing these findings is currently being drafted (Mulier *et al.*, in preparation).

3.3. Further steps towards the development of novel analgesic drugs targeting TRPM3

The ultimate goal of this line of research is the development of novel analgesic treatments for patients suffering from chronic pain, using TRPM3 as a pharmacological target. We have extensively discussed the potential importance of TRPM3 and other TRP channels as pharmacological targets for human drug development for pain and related diseases in a recent review in *Trends in Pharmacological Sciences*, acknowledging the support of the Queen Elisabeth Medical Foundation (Voets et al., 2019). Furthermore, emanating from results in this project, we also made further important steps to translate the fundamental findings towards a clinical application.

3.a Expression and functional characterization of TRPM3 in human sensory neurons

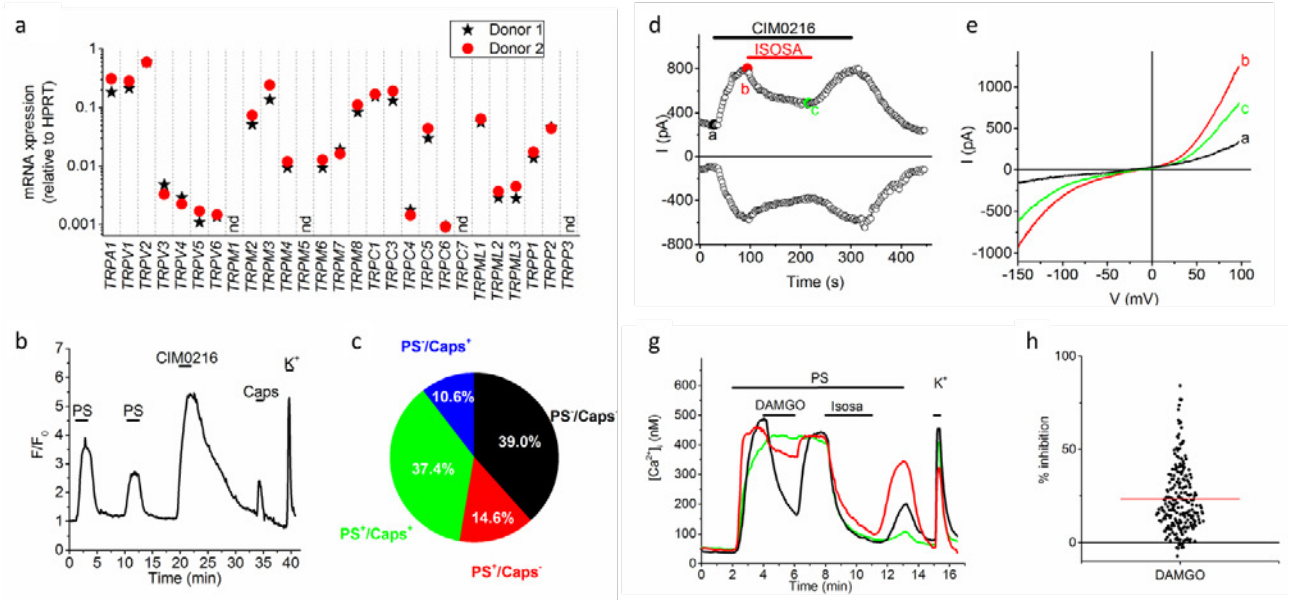

Figure 6. a, Expression levels of TRP channel mRNA in DRG neurons from two donors, determined using RT-qPCR. nd: not detected. **b,** Representative example of changes in Fluo-8-fluorescence in human DRG neurons in response to the TRPM3 agonists PS (50 μM) and CIM0216 (10 μM) and to the TRPV1 agonist capsaicin (200 nM). **c,** Pie chart showing the distribution of neurons responding to PS, capsaicin or both (n=206 hDRG neurons). **d,** Time course of inward (at -120 mV) and outward (at +80 mV) whole-cell currents in hSCDS neurons showing the effects of the TRPM3 agonist CIM0216 (1 μM) and inhibitor isosakuranetin (5 μM). **e,** IV-curves corresponding to the time points indicated in (**d**). **g,** Example intracellular calcium measurements showing variable degrees of inhibition of PS-induced responses upon activation of endogenously expressed μ-opioid receptors using DAMGO (300nM). **h,** Scatter plot showing the range of DAMGO-induced inhibition of PS responses in hSCDS neurons. Red line represents the mean percentage of TRPM3 inhibition caused by DAMGO (data from 6 experiments, with hSCDS neurons from 3 different differentiations). From Vangeel et al., British Journal of Pharmacology (2020).

While the role of TRPM3 as a noxious heat sensor and key player in acute pain sensation and inflammatory hyperalgesia is well established in rodents, little is known about the expression, function and modulation of TRPM3 in the human somatosensory system. Such knowledge is essential for further development of TRPM3-based therapies, as expression pattern, pharmacology and function can differ significantly between humans and rodents, leading to poor translation of preclinical results. We therefore analyzed the expression and function of TRPM3 in two relevant models of human sensory neurons: primary neurons isolated from human dorsal root ganglia from organ donors (hDRG neurons), and sensory neurons derived from human embryonic stem cells (hSCDS neurons). Importantly, using RT-qPCR, calcium imaging and whole-cell patch-clamp recordings, we were able to demonstrate molecular and functional expression of TRPM3 in a large fraction of hDRG and hSCDS neurons, with a large overlap with the nociceptor marker TRPV1 (**Figure 6a-c**). Important aspects of TRPM3 functionality in mouse sensory neurons, including voltage-dependence, activation by PS and CIM0216 as well as inhibition by the flavonoid antagonist isosakuranetin and by activation of the μ-opioid receptor using DAMGO, were found to be fully conserved in human sensory neurons (**Figure 6d-f**). Taken together, these findings indicate that the expression and properties of TRPM3 in human somatosensory neurons is very similar to what is known from rodents, providing confidence that results obtained in animal models may translate to humans. These results have been recently accepted for publication in *British Journal of Pharmacology* (Vangeel et al., 2020), acknowledging the support of the support of the Queen Elisabeth Medical Foundation.

3.b Efficacy of TRPM3 inhibition in models of inflammatory hypersensitivity

In addition to the CFA model described above, which is a model of acute inflammation but has no direct correlation with human disease, we have also investigated the potential role of TRPM3 in other clinically relevant rodent models of chronic pain and inflammation: the cyclophosphamide-induced (CYP) cystitis model in mice and the monoiodoacetate (MIA) model of osteoarthritis in rats.

We used the CYP model in mice to evaluate the potential contribution of TRPM3 to abdominal pain and pollakisuria (increased voiding frequency) during cystitis. Mice received intraperitoneal injections of CYP (40 mg/kg) every 2 days for 7 days, resulting in a chronically inflamed bladder associated with pain and increased voiding frequency. Importantly, we found that systemic application of the selective TRPM3 antagonist isosakuranetin (10 mg/kg; ip) completely reversed mechanical hyperalgesia, as assessed using von Frey hairs to stimulate the suprapubic area (**Figure 7a**). These results further strengthen the potential of TRPM3 antagonism to treat pain and hypersensitivity associated with visceral pathology.

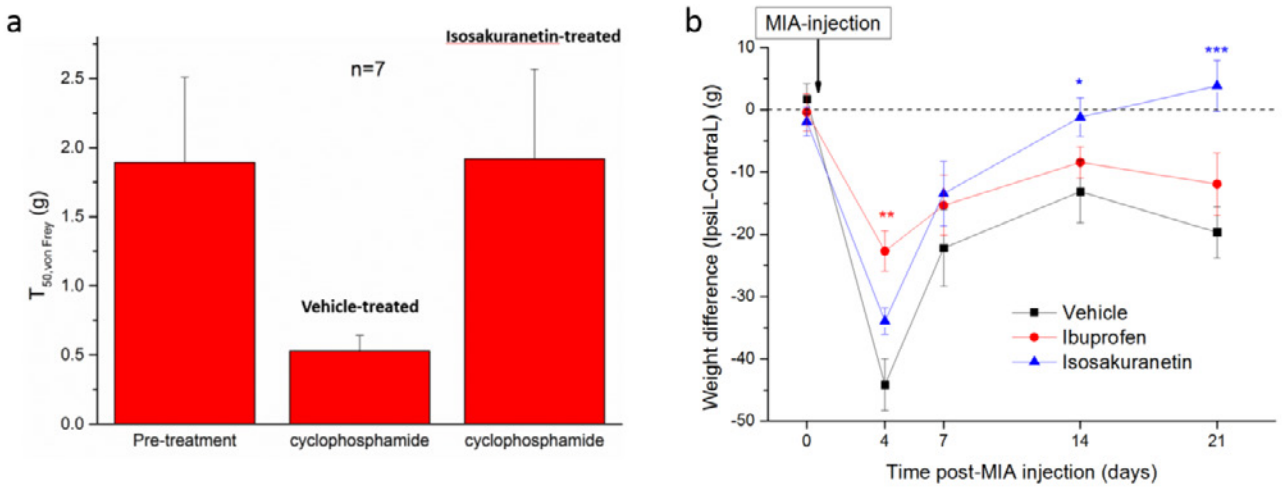

Figure 7. a, Response threshold for von Frey hairs applied in the abdominal area of mice before treatment, and after induction of CYP-induced cystitis upon treatment with vehicle of isosakuranetin (10 mg/kg; ip). **b,** Time-course of the difference in weight on the ipsi- versus contralateral paw in MIA-treated rats, treated with vehicle, the NSAID ibuprofen en the TRPM3-antagonist isosakuranetin (10 mg/kg; ip). *,**,***: p<0.05, 0.01, 0.001; Two-way repeated measurements ANOVA with Sidak-Holm posthoc test. Moilanen & Voets - unpublished results.

In the rat MIA model of osteoarthritis, injection of MIA in the knee joint leads to the development of experimental osteoarthritis, characterized by hypersensitivity and a shift of the body weight towards the non-injured hindpaw. The hypersensitivity is typically biphasic, with an initial phase that peaks at day 4, followed by a chronic phase that persists for several weeks. Using the dynamic weight bearing assay, we found that treatment with isosakuranetin (10 mg/kg; ip) had only a minor effect on the initial phase, but fully reversed the weight imbalance between the ipsi- and contralater paw in the chronic phase (**Figure 7b**).

Taken together, these findings provide strong support for the hypothesis that TRPM3 antagonism can be used to treat various forms of pain and hypersensitivity, encouraging the development of more potent and selective TRPM3 antagonists for potential clinical development.

4. Conclusions and outlook

With the financial support of the GSKE, our lab has been able to delineate the role of TRPM3 in acute heat sensing, to establish that TRPM3 is molecularly and functionally upregulated in sensory neurons under inflammatory conditions, and to demonstrate that TRPM3 antagonism shows analgesic efficacy in disease-relevant animal assays of ongoing pain and hypersensitivity.

In this study, TRPM3 activity was inhibited using isosakuranetin, a naturally occurring flavonoid that potently inhibits TRPM3 activity. However, we note that isosakuranetin represents a tool compound: it has some activity towards other ion channel, it is not orally bioavailable, and has only a very short half-life *in vivo*. Therefore, encouraged by the results from this study, we are actively collaborating with industrial partners to develop potent and selective TRPM3 antagonists with a better, drug-like profile, which we hope may result in a novel class of safe and potent analgesic drugs.

5. Publications acknowledging support from GSKE

1. Vandewauw I, De Clercq K, Mulier M, Held K, Pinto S, Van Ranst N, Segal A, Voet T, Vennekens R, Zimmermann K, Vriens J, Voets T: **A TRP channel trio mediates acute noxious heat sensing**. *Nature* 2018, **555**(7698):662-666.
2. Vangeel L, Voets T: **Transient Receptor Potential Channels and Calcium Signaling**. *Cold Spring Harb Perspect Biol* 2019, **11**(6).
3. Voets T, Vriens J, Vennekens R: **Targeting TRP Channels - Valuable Alternatives to Combat Pain, Lower Urinary Tract Disorders, and Type 2 Diabetes?** *Trends Pharmacol Sci* 2019, **40**(9):669-683.
4. Vriens J, Voets T: **Heat sensing involves a TRiPlet of ion channels**. *Brit J Pharmacol* 2019, **176**(20):3893-3898.
5. Vangeel L, Benoit M, Miron Y, Miller PE, De Clercq K, Chaltin P, Verfaillie C, Vriens J, Voets T: **Functional expression and pharmacological modulation of TRPM3 in human sensory neurons.** *Brit J Pharmacol*, in press.

In preparation:

6. Mulier M, Moilanen L, Van Ranst N, Voets T: **Molecular and functional upregulation of TRPM3 expression in TRPV1-positive neurons innervating inflamed tissue.** In preparation.

7. References

- Bautista, D. M., Jordt, S. E., Nikai, T., Tsuruda, P. R., Read, A. J., Poblete, J., . . . Julius, D. (2006). TRPA1 mediates the inflammatory actions of environmental irritants and proalgesic agents. *Cell, 124*(6), 1269-1282. doi:10.1016/j.cell.2006.02.023
- Grayson, M. (2016). Pain. *Nature, 535*(7611), S1. doi:10.1038/535S1a
- Reid, K. J., Harker, J., Bala, M. M., Truyers, C., Kellen, E., Bekkering, G. E., & Kleijnen, J. (2011). Epidemiology of chronic non-cancer pain in Europe: narrative review of prevalence, pain treatments and pain impact. *Curr Med Res Opin, 27*(2), 449-462. doi:10.1185/03007995.2010.545813
- Straub, I., Krugel, U., Mohr, F., Teichert, J., Rizun, O., Konrad, M., . . . Schaefer, M. (2013). Flavanones that selectively inhibit TRPM3 attenuate thermal nociception in vivo. *Mol Pharmacol, 84*(5), 736-750. doi:10.1124/mol.113.086843
- Vandewauw, I., De Clercq, K., Mulier, M., Held, K., Pinto, S., Van Ranst, N., . . . Voets, T. (2018). A TRP channel trio mediates acute noxious heat sensing. *Nature, 555*(7698), 662-666. doi:10.1038/nature26137
- Vangeel, L., Benoit, M., Miron, Y., Miller, P. E., De Clercq, K., Chaltin, P., . . . Voets, T. (2020). Functional expression and pharmacological modulation of TRPM3 in human sensory neurons. *Br J Pharmacol, In press*.
- Voets, T., Vriens, J., & Vennekens, R. (2019). Targeting TRP Channels - Valuable Alternatives to Combat Pain, Lower Urinary Tract Disorders, and Type 2 Diabetes? *Trends Pharmacol Sci, 40*(9), 669-683. doi:10.1016/j.tips.2019.07.004
- Vriens, J., Nilius, B., & Voets, T. (2014). Peripheral thermosensation in mammals. *Nat Rev Neurosci, 15*(9), 573-589. doi:10.1038/nrn3784
- Vriens, J., Owsianik, G., Hofmann, T., Philipp, S. E., Stab, J., Chen, X., . . . Voets, T. (2011). TRPM3 is a nociceptor channel involved in the detection of noxious heat. *Neuron, 70*(3), 482-494. doi:10.1016/j.neuron.2011.02.051
- Vriens, J., & Voets, T. (2018). Sensing the heat with TRPM3. *Pflugers Arch*. doi:10.1007/s00424-017-2100-1
- Vriens, J., & Voets, T. (2019). Heat sensing involves a TRiPlet of ion channels. *Br J Pharmacol, 176*(20), 3893-3898. doi:10.1111/bph.14812
- Wang, F., Flanagan, J., Su, N., Wang, L. C., Bui, S., Nielson, A., . . . Luo, Y. (2012). RNAscope: a novel in situ RNA analysis platform for formalin-fixed, paraffin-embedded tissues. *J Mol Diagn, 14*(1), 22-29. doi:10.1016/j.jmoldx.2011.08.002
- Wilson-Poe, A. R., & Moron, J. A. (2017). The dynamic interaction between pain and opioid misuse. *Br J Pharmacol*. doi:10.1111/bph.13873

Geneeskundige Stichting Koningin Elisabeth
Fondation Médicale Reine Elisabeth
Königin-Elisabeth-Stiftung für Medizin
Queen Elisabeth Medical Foundation

Final report of the research group of

Prof. dr. Vonck Kristl

Universiteit Gent (UGent)

Principal investigator

Prof. dr. Vonck Kristl
Reference Center for Refractory Epilepsy
Laboratory for Clincial and Experimental Neurophysiology
Institute for Neuroscience
Department of Neurology
Ghent University Hospital
De Pintelaan 185
9000 Gent
Belgium
Tel.: +32 50 61 06 51
E-mail: Kristl.Vonck@UGent.be
www.uzgent.be
H-index: 28

The role of locus coeruleus noradrenergic neurons in the mechanism of vagus nerve stimulation and the effect of selective activation of these neurons in epilepsy.

Chemogenetic modulation and electrofysiological recordings of the locus coeruleus

1. First part

1.1. Induction of DREADD expression in LC neurons using AAV viral vectors

To selectively induce DREADD expression in LC neurons of male rats, animals were injected with the adeno-associated viral vector (AAV) serotype 2/7 carrying a plasmid with the PRSx8-hM3Dq-mCherry construct (5.99E+12 GC/ml, provided by the group of Veerle Baekelandt and Chris Van Den Haute). This serotype was used instead of 2/9 as described by previous groups (Vazey and Aston-Jones 2014; Rorabaugh et al. 2017; Fortress et al. 2015; Cope et al. 2019; Kane et al. 2017)we investigated the causal relationship between LC-NE activity and general anesthetic state under isoflurane. Selective activation of LC-NE neurons produced cortical electroencephalography (EEG, because it has proven efficiency in transducing dopaminergic neurons in substantia nigra (Van der Perren et al. 2011)several serotypes have been described, with varying tropism for brain transduction. In light of the further development of a viral vector-mediated rat model for PD, we performed a comprehensive comparison of the transduction and tropism for dopaminergic neurons (DNs.

Animals (n=32; 9-10 weeks old; 309±15g body weight) were anesthetized with a mixture of medical oxygen and isoflurane (5% for induction, 2% for maintenance, Isoflo, Zoetis, UK); body temperature was controlled using a heating pad. Rats were placed in a stereotaxic frame (Stoelting, USA) and the skull was exposed. Bregma was lowered 2mm relative to lambda (15° head angle) to target the LC and avoid the transverse sinus. Using a Neuro-Syringe (Hamilton model 7001 point style 3, Hamilton company, Nevada, USA) and Quintessential Stereotaxic Injection system (flowrate 2nl/min, Stoelting, USA), injections of 10nl of AAV2/7 containing a PRSx8-hM3Dq-mCherry plasmid (n=19; 11 unilateral and 8 bilateral) or AAV2/7-PRSx8-eGFP plasmid as a control (n=13; 5 unilateral and 8 bilateral) were performed in the LC (3.9 AP, 1.15 ML relative to lambda, -5.7 DV from dura). After injection the syringe was left in place for an additional 5min and was then slowly withdrawn to avoid backflow. All animals recovered three weeks in their home cage to allow for optimal viral vector expression.

At the end of the total experiment, including unit recording sessions (cfr. Infra), animals were deeply anesthetized with an overdose of sodium pentobarbital (200 mg/kg, i.p.) and transcardially perfused with phosphate-buffered saline (PBS) followed by paraformaldehyde (4%, pH 7.4). The brains were post fixed in paraformaldehyde (4%, pH 7.4) for 24h and subsequently cryoprotected in a sucrose solution of 10-20-30% at 4°C, snap-frozen in isopentane and stored in liquid nitrogen at -196°C. After 1 hour on -20°C, coronal cryosections of 40µm were made using a cryostat (Leica, Germany). The sections were rinsed twice for 5min in distilled water (dH_2O) followed by incubation in 0.5% and 1% H_2O_2 for 30 and 60min respectively to block endogenous peroxidase activity. After washing twice for 5min in PBS, sections were incubated in blocking buffer (BB) made of PBS containing 0.4% Fish Skin Gelatin (FSG) and 0.2% Triton X for 45min to block non-specific antibody binding sites. The sections were then incubated in primary antibodies to visualize noradrenergic LC neurons and GFP or mCherry tag respectively with mouse anti-DBH (1:1000, Merck, clone 4F10.2) and chicken anti-green fluorescent protein (1:1000, Abcam, ab13970) or rabbit anti-red fluorescent protein (targeting mCherry, 1:1000, Rockland, ROCK600-901-379) diluted in BB for 1 hour at room temperature and subsequently overnight at 4°C. On the next day the sections were washed twice in blocking buffer for 10 min followed by

incubation in secondary antibodies Alexa Fluor goat anti-mouse 488 nm (1:1000, Abcam, Ab 150113) or Alexa Fluor goat anti-mouse 594 nm (1:1000, Abcam, ab150176) against DBH^+ cells and Alexa goat anti-rabbit 594 nm or Alexa fluor goat-anti chicken 488 nm (against mCherry or GFP tag) diluted in BB for 1 hour at room temperature in darkness. After washing twice in PBS for 5 min, a nuclear DAPI staining was performed and subsequent rinsing in PBS (2x5 min). Sections were mounted on glass slides and cover slipped using Vectashield H1000 mounting medium (Vector Laboratories, USA) to prevent photo bleaching.

The viral vector expression levels were determined using a fluorescence microscope (Carl Zeiss, Axiovert 200M and Nikon Eclipse TE2000-E, Germany). Pictures of DAPI, DBH and GFP or mCherry were taken with the AxioVision Microscope Software (6D acquisition) connected to the Carl Zeiss fluorescence microscope on the 10x magnification. For each animal that underwent successful electrofysiological recordings, images were taken from three slices along the anterior-posterior axis of the LC and exported as TIFF files before being analyzed in Fiji- ImageJ software. To determine hM3Dq-DBH colocalization, three sections containing LC per animal were used to quantify the number of DBH^+ LC cells by placing virtual markers on a merged image of DBH^+/DAPI. These markers were then copied on the merged image of DBH^+/mCherry to determine the number of LC cells expressing hM3Dq-mCherry. To quantify aspecific hM3Dq-mCherry expression, cells that were $DBH^-/mCherry^+$ were counted and divided by the total number of $mCherry^+$ cells.

Double label immunostaining for the mCherry tag coupled to the hM3Dq receptor and DBH was used to quantify the transduction efficiency of the viral vector in LC-NA neurons and its specificity (fig.2A).

All animals that underwent successful unit recording at least three weeks after viral vector administration showed expression of hM3Dq in LC-NA cells and adjacent axons although there was variability in the fraction of LC cells expressing hM3Dq (fig.2B-D). HM3Dq expression was evident in 20.6 ± 2.3% LC neurons (21 sections; three sections/animal; range 11-32%). Aspecific expression of hM3Dq-mCherry was also observed in cells outside the LC (26.0 ± 4.1% of mCherry positive cells was DBH negative) (fig.2C).

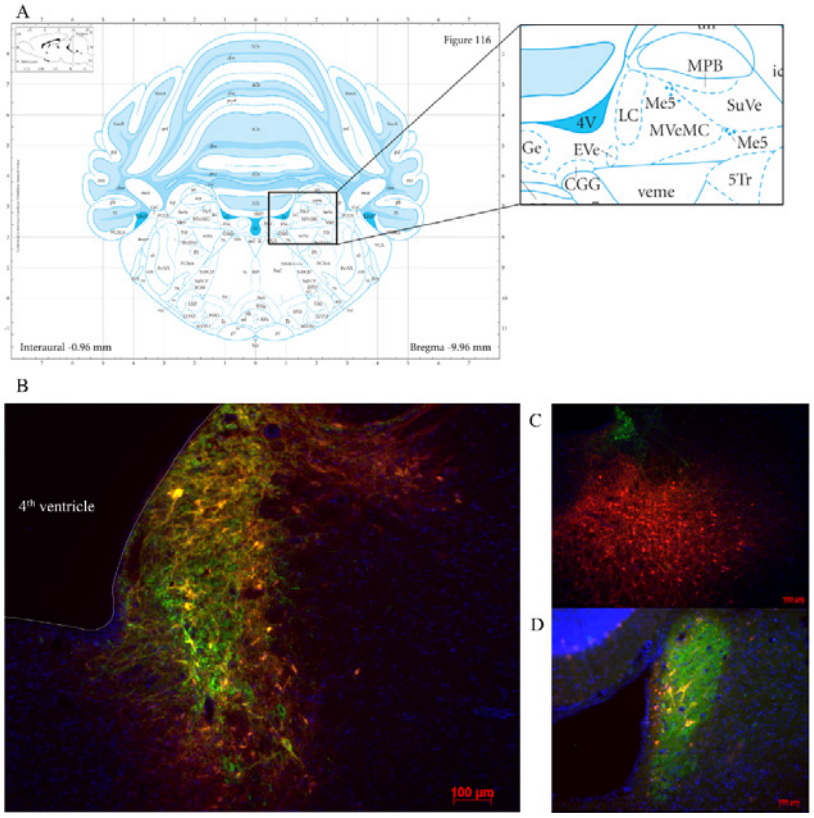

Figure 2: Visualization of hM3Dq-mCherry expression in LC injected with PRSx8-driven AAV. (A) *Stereotactical location of brainstem locus coeruleus next to the fourth ventricle.* (Watson and Paxinos 2007). ***(B)*** *LC-NA neurons are visualized using primary anti-DBH antibody (green) and expression of hM3Dq DREADD is visualized with the mCherry tag (red).* ***(C)*** *Aspecific hM3Dq expression (red) in DBH- non LCneurons.* ***(D)*** *Only a low number of transduced neurons are observed in some animals. Scale bar 100µm.*

1.2. Electrophysiological recordings in LC neurons in anesthetized rats

To validate the functionality of hM3Dq receptors expressed in LC neurons and to determine whether low doses of clozapine can be used as selective ligand to activate genetically modified LC neurons, rats were systemically injected with clozapine (0.01 and 0.1 mg/kg). We chose to use clozapine instead of clozapine-N-oxide (CNO) because of its higher specificity and affinity. Additionally a recent study by the group of Gomez et al. has shown that DREADD activation upon systemic injection of CNO is mainly due to converted clozapine since CNO does not pass the blood brain barrier (Gomez et al. 2017).

At least three weeks after viral vector injection animals (387 ± 26g body weight) were used for LC unit recordings. Rats were anesthetized with a mixture of medical oxygen and isoflurane (5% for induction, 1.5% for maintenance, n=18) or were induced with 5% isoflurane followed by an intraperitoneal injection of urethane (1.5 g/kg, n=14). For unit recording, a tungsten microelectrode (.008”/200 µm shank diameter, impedance ≥ 1.5 MΩ, FHC, USA) was implanted under electrophysiological control and audio monitoring to target LC neurons (Bouret et al. 2003). As a reference and ground, two custom made epidural scalp electrodes, consisting of an insulated copper wire attached to a stainless steel microscrew (1.75mm diameter; Plastics One, USA) were placed above the left and right frontal cortex. Electrophysiological recordings were amplified (x10 000), filtered (300Hz-3kHz) and digitized at 31 kHz using a 1401 micro and Spike2 software (Cambridge Electronic Design, UK) for online visualization of action potentials and storage for post-processing. Action potentials are detected as input signals crossing a trigger level set by the researcher. LC neurons can be visually identified online as they are characterized by the occurrence of a typical pattern called ‘a phasic burst inhibition’ following a foot pinch. After identification of LC neurons, a stable baseline period of 300s was recorded followed by subsequent subcutaneous injections of clozapine into the loose skin of the neck, starting with the lowest dose of 0.01 mg/kg and followed by 0.1 mg/kg (dissolved in 3% DMSO in saline). Action potentials were

recorded for at least 650s after each clozapine injection. After the recording period following 0.1 mg/kg clozapine administration, clonidine (0.04 mg/kg), an α2 agonist which inhibits the spontaneous firing of LC-NA neurons, was injected subcutaneously to confirm the LC identity of recorded neurons. Recording was stopped when a decrease in the firing frequency at least to baseline levels was observed.

Successful electrophysiological recordings were performed in 12 animals. A total of 12 neurons were recorded, 7 in DREADD-injected animals and 5 in control animals, all characterized by foot pinch elicited phasic bursting and decreased firing frequency after clonidine administration. A two-way repeated measures ANOVA showed no interaction between treatment and group ($F=0.212$, $p=0.655$). No significant effect of group was reported ($F=1.429$, $p=0.259$) although treatment has a significant effect on the firing frequency ($F=14.623$, $p=0.003$). Systemic administration of the 0.01 mg/kg clozapine had no significant effect on the mean firing frequency (2.72 ± 0.48 Hz, $p=0.468$) of recorded LC neurons compared to baseline (2.34 ± 0.30 Hz) whereas an increased firing rate was observed after 0.1 mg/kg clozapine (3.57 ± 0.54 Hz, $p=0.006$), irrespective whether recordings were performed in DREADD or control animals. A significant difference between the two doses of clozapine on the firing frequency was observed ($p=0.003$) (fig.1). In all LC neurons, firing frequency was reduced to baseline levels or completely inhibited after clonidine administration confirming LC identity.

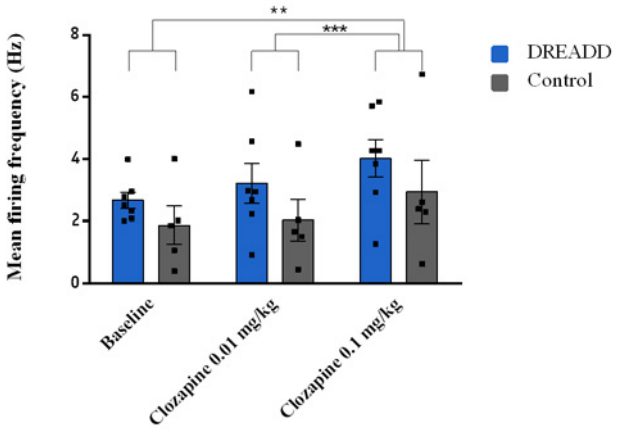

Figure 1: The effect of systemic administration of different doses of clozapine on the mean firing frequency of LC neurons in DREADD and control injected animals. *Electrophysiological recordings were performed in 12 animals (DREADD group n=7; control n=5), in each animal one neuron was recorded for a stable baseline period (300s) followed by subsequent injections of clozapine (0.01 and 0.1 mg/kg, s.c.). No difference in the effect of clozapine on the firing frequency of neurons recorded in DREADD-injected or control animals was observed ($F=14.623$, $p=0.003$). The highest dose of clozapine (0.1 mg/kg) increased the firing frequency compared to baseline ($p=0.006$) whereas the lowest dose of clozapine (0.01 mg/kg) showed no effect ($p=0.312$). A significant difference between the two doses of clozapine on the mean firing frequency was observed ($p=0.003$). Each bar represents the mean firing frequency ± SEM (firing frequencies from individual neurons represented by black squares). *$p<0.05$ and **$p<0.01$ (two way repeated measures ANOVA Bonferroni corrected).*

1.3. Conclusions

The transduction efficiency observed in this study using an AAV2/7 viral vector was significantly lower compared to previously observed transduction levels (>95%) with high specificity (Vazey et al., 2014) in other studies. The transduction efficiency is controlled by the AAV serotype, promotor and injection site. We believe that in our study the serotype of the viral vector is the primary reason for the poor expression levels and aspecificty. The transduction efficiency of an AAV is determined by AAV entry which is controlled by the AAV capsid with its proteins on the surface that determine binding specificity and entry of the virion to the cells. In contrast to other groups using AAV2/9 achieving high levels of expression, we use AAV2/7 which means that the genome of serotype 2 is encapsulated in a viral capsid formed by serotype 7. The presence of different surface proteins on the capsid in comparison to AAV2/9 particles can lead to lower lower binding affinity for the surface receptors on LC-NA cells and possible affinity for non-LC cells. This explains both the low expression levels and the observed aspecificity.

A second finding of this study was that we were not able to draw conclusions on the feasibility to chemogenetically increase LC firing frequency using clozapine. Due to a limited number of transduced LC neurons, we were unable to claim that we recorded from DREADD positive neurons. There was a significant effect of the highest dose of clozapine (0.1 mg/kg) on the firing frequency of LC neurons, however also in control animals, indicating a DREADD-independent effect. It has been shown that clozapine has affinity for a variety of endogenous receptors, also present in LC. Previous studies observed increased LC firing frequencies after clozapine administration due to a combination of NMDA receptor activation and increased glutamatergic release due to activation of clozapine sensitive receptors on glutamatergic afferents. (Coward 1992; Schwieler et al. 2008; Nilsson et al. 2005).

From this study we can conclude that the use of AAV2/7 is less desirable to induce DREADD expression in LC neurons in comparison to previously used AAV2/9 or a different type of viral vector (i.e. CAV). Due to low expression levels we cannot conclude the usability of clozapine as selective chemogenetic ligand. Optimization of the chemogenetic transduction approach is required to induce higher transduction efficiency and selectivity in combination with a technique that ensures that unit recording was performed in transduced cells to validate the effect of clozapine and characterize its suitability as selective ligand for chemogenetic activation of LC.

2. Part 2

2.1. Induction of DREADD expression in LC neurons using CAV viral vector

To optimize expression levels and specificity to chemogenetically modify LC neurons, the use of a different type of viral vector was investigated. The canine adenoviral vector (CAV) carrying a PRSx8-hM3Dq-mCherry plasmid ($2.5x10^{12}$ TU/ml, provided by the group of Prof. Pickering, Bristol University) was injected in the locus coeruleus of male rats.

In a first pilot trial male rats were injected with the CAV2-PRSx8-hM3Dq-mCherry viral vector to validate expression levels. Animals (n=4; 10 weeks old) manipulated in a similar way as described under 1.1.1 CAV2 viral vector containing a PRSx8-hM3Dq-mCherry was bilaterally injected in LC at three sites along the dorso-ventral axis (3.9 AP, 1.15 ML relative to lambda, -5.8; -5.5; -5.3 DV from dura; 300nl/site; 150 nl/min flow rate). After each injection, the syringe was left in place for an additional 5min and was then slowly withdrawn to avoid backflow. After two weeks, rats were sacrificed to determine expression levels of hM3Dq in locus coeruleus using immunofluorescence staining (as described in 1.1.1).

In all rats injected with CAV2-PRSx8-hM3Dq-mCherry hM3Dq expression was observed in both hemispheres. A difference in expression between the left LC (first injected during surgery) and right LC could be observed (fig.3). To determine hM3Dq-DBH colocalization, three sections containing LC per animal were used to quantify the number of DBH+ LC cells by placing virtual markers on a merged image of DBH+/DAPI. These markers were then copied on the merged image of DBH+/mCherry to determine the number of LC cells expressing hM3Dq-mCherry. To quantify aspecific hM3Dq-mCherry expression, cells that were DBH-/mCherry+ were counted and divided by the total number of mCherry+ cells. This manual cell count showed high and selective expression.

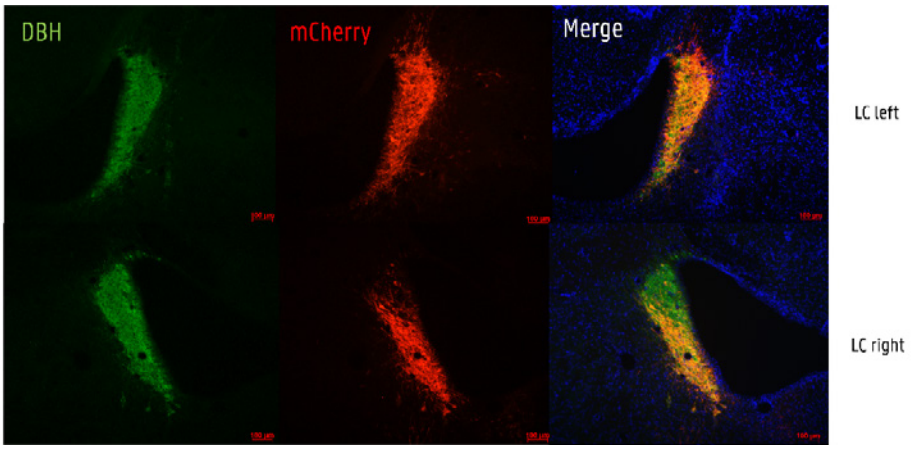

Figure 3: Visualization of hM3Dq-mCherry expression in LC injected with PRSx8-driven CAV. *Primary antibodies anti-dopamine b hydroxylase (green) and anti-red fluorescent protein (RFP, red) were used for visualization of LC-NA neurons and mCherry coupled to hM3Dq respectively. The merged image is an overlay of the DBH, mCherry and DAPI filter. Scale bar 100µm.*

2.2. Electrophysiological recording in LC neurons in anesthetized rats

Because of the high hM3Dq expression levels observed in the pilot trial compared to the previous study using a PRSx8-hM3Dq driven AAV viral vector, the next step was to validate the functionality of hM3Dq receptors expressed in LC neurons and determine whether low doses of clozapine can be used as selective ligand to activate genetically modified LC neurons. To increase the chance of recording LC and record more neurons simultaneously, a neuronexus probe (A1x32-Poly3-10mm-50-177-CM32) consisting of 32 channels was used instead of a single tungsten microelectrode.

In a first phase animals were injected as described above with the CAV2-PRSx8-hM3Dq-mCherry viral vector (DREADD, n=9). A control group (n=6) consisted of 2 naïve animals (n=2/6) and four animals injected with a control viral vector (n=4/6). At least two weeks after viral vector injection animals (DREADD n=9; control n=6) were used for LC unit recordings. Rats were anesthetized with a mixture of medical oxygen and isoflurane (5% for induction, 1.5% for maintenance). For unit recording, a neuronexus probe was implanted under electrophysiological control and audio monitoring to target LC neurons (Bouret et al. 2003). As a reference and ground, two custom made epidural scalp electrodes, consisting of an insulated copper wire attached to a stainless steel microscrew (1.75mm diameter; Plastics One, USA) were placed above the left and right frontal cortex. Electrophysiological recordings were recorded using open ephys software. LC neurons can be visually identified online as they are characterized by the occurrence of a typical pattern called 'a phasic burst inhibition' following a foot pinch. After identification of LC neurons, a stable baseline period of 30 min was recorded followed by subsequent subcutaneous injections of clozapine into the loose skin of the neck, starting with the lowest dose of 0.01 mg/kg and followed by 0.03mg/kg (dissolved in 3% DMSO in saline). Action potentials were recorded for 30 min after each clozapine injection. After the recording period following 0.03 mg/kg clozapine administration, clonidine (0.04 mg/kg), an $\alpha 2$ agonist which inhibits the spontaneous firing of LC-NA neurons, was injected subcutaneously to confirm the LC identity of recorded neurons. Recording was stopped when a decrease in the firing frequency at least to baseline levels was observed. At the end of the recording, animals were sacrificed for post-mortem visualization of hM3Dq expression levels using immunofluorescence staining (described above). DREADD expression was present in all injected animals. A manual cell count will be performed as described above, and is currently ongoing.

Successful recordings were performed in five animals (DREADD n=3; control n=2, injected animals). In two DREADD animals two LC neurons were recorded with a clear increase in firing frequency after clozapine 0.01 mg/kg administration (fig. 4). The highest dose of clozapine (0.03 mg/kg) increased firing frequency however this increase was also observed in the control animals confirming (fig.5).

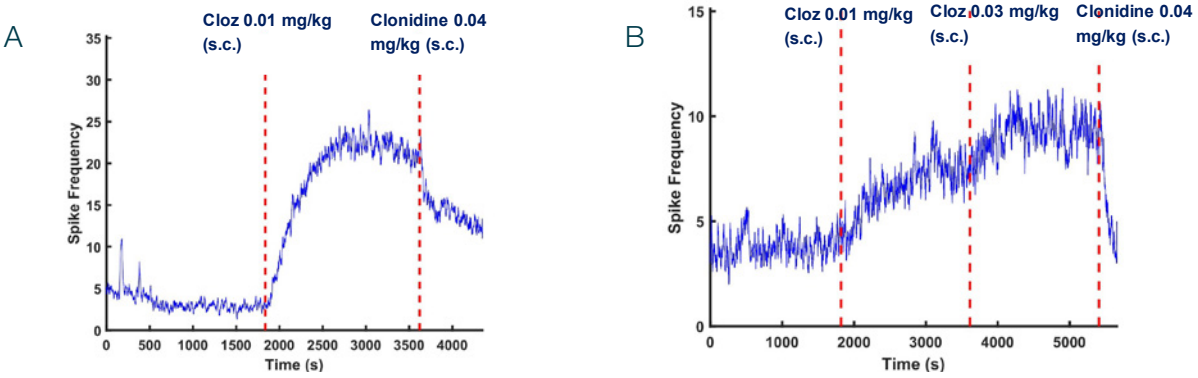

Figure 4: The effect of systemic administration of different doses of clozapine on the firing frequency in DREADD injected animals. *Electrophysiological recording performed in two DREADD injected animals, each graph represents the firing frequency (y-axis) over time (x-axis). A stable baseline period of 30 minutes was followed by subsequent injections of clozapine (0.01 and 0.03 mg/kg, s.c.). A. Clozapine 0.01 mg/kg increased the firing frequency compared to baseline. Clonidine administration decreased the firing frequency. B. Clozapine 0.01 mg/kg gradually increased the firing frequency followed by a plateau phase after 0.03 mg/kg. Clonidine decreased and inhibited the recorded neuron. Dotted lines represent the time of clozapine and clonidine administration.*

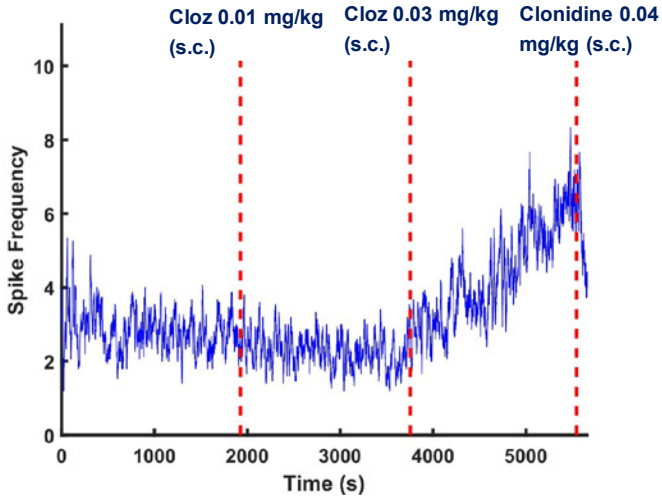

Figure 5: The effect of systemic administration of different doses of clozapine on the firing frequency in control animal. Electrophysiological recording performed in one control animal, graph represents the firing frequency (y-axis) over time (x-axis). *After a stable baseline period (± 30min) clozapine was subsequently administered starting from the lowest dose. Systemic clozapine administration (0.01 mg/kg, s.c.) has no effect on the spike frequency of LC neurons, whereas 0.03 mg/kg shows a clear increase in spike frequency. Clonidine administration decreases and inhibits the recorded neuron, confirming its LC identity. Dotted lines represent the time of clozapine and clonidine administration.*

3. Conclusion

The LC-NA pathway is believed to play an important role in the mechanism of action of vagus nerve stimulation, a neurostimulation therapy for patients with drug resistant epilepsy. To selectively investigate the role of the locus coeruleus and the noradrenergic brain input from this brainstem region, we have chosen to develop a chemogenetic strategy which would allow cell-specific modulation of LC-NA neurons. The challenge in this research field is the identification both the optimal viral vector for sufficient and selective genetic modification of the locus coeruleus and the dose-response curve of activating ligands. In vivo electrofysiological recordings were chosen as the ultimate outcome parameter to investigate the feasibility of the consecutive steps in the total experimental protocol.

Transducing LC neurons with an AAV2/7 vector for induction of DREADD expression leads to insufficient and aspecific expression. We concluded that the described approach is suboptimal to selectively modulate LC. In comparison to previously used AAV2/9 with successful transduction levels and specificity (Vazey and Aston-Jones 2014)we investigated the causal relationship between LC-NE activity and general anesthetic state under isoflurane. Selective activation of LC-NE neurons produced cortical electroencephalography (EEG, we observed rather low hM3Dq expression in combination with aspecificity. We believe that the major reason for this result is the different surface receptors present on the capsid of the virion, leading to lower affinity for LC-NA neurons and possible binding of non-LC neurons, explaining both low expression levels and aspecificity. Due to these poor expression levels, no clear conclusion could be made about the suitability of clozapine as selective ligand to activate these genetically modified LC neurons. Administration of the highest dose of clozapine (0.1 mg/kg) did increase the firing frequency of LC neurons, however this effect was also observed in control animals stating a DREADD-independent effect. It is known from previous studies that clozapine binds endogenous receptors, also present in LC, and can increase LC firing frequency due to NMDA receptor activation and increased glutamatergic release. (Schwieler et al. 2008; Nilsson et al. 2005)

We therefor investigated a second approach to chemogenetically modify the LC. In collaboration with Prof. Pickering from Bristol University, we changed our approach to using CAV viral vectors (Hirschberg et al. 2017). Recent results show that this type of viral vector leads to higher expression levels and specificity. With

the application of the neuronexus probe with 32 channels, we recorded multiple LC neurons per animal. From this study we were able to conclude that low doses of clozapine lead to selective modulation of genetically modified LC neurons using CAV viral vectors. An additional experiment, including a larger group of animals is currently undertaken. This developed experimental set-up can be used for selective modulation of LC neurons in combination with hippocampal electrophysiology recordings to investigate the effect of LC neuradrenergic modulation on hippocampal functioning.

4. References

- Bouret, Sebastien, Adam Duvel, Selim Onat, and Susan J Sara. 2003. “Phasic Activation of Locus Ceruleus Neurons by the Central Nucleus of the Amygdala.” *The Journal of Neuroscience* 23 (8): 3491–97. https://doi.org/10.1523/jneurosci.23-08-03491.2003.
- Cope, Zackary A., Elena M. Vazey, Stan B. Floresco, and Gary S. Aston Jones. 2019. “DREADD-Mediated Modulation of Locus Coeruleus Inputs to MPFC Improves Strategy Set-Shifting.” *Neurobiology of Learning and Memory* 161 (May): 1–11. https://doi.org/10.1016/J.NLM.2019.02.009.
- Fortress, Ashley M, Eric D Hamlett, Elena M Vazey, Gary Aston-Jones, Wayne A Cass, Heather A Boger, and A.-C. E Granholm. 2015. “Designer Receptors Enhance Memory in a Mouse Model of Down Syndrome.” *Journal of Neuroscience* 35 (4): 1343–53. https://doi.org/10.1523/JNEUROSCI.2658-14.2015.
- Gomez, Juan L, Jordi Bonaventura, Wojciech Lesniak, William B Mathews, Polina Sysa-Shah, Lionel A Rodriguez, Randall J Ellis, et al. 2017. “Chemogenetics Revealed: DREADD Occupancy and Activation via Converted Clozapine.” *Science* 357: 503–7. https://doi.org/10.1126/science.aan2475.
- Hirschberg, Stefan, Yong Li, Andrew Randall, Eric J Kremer, and Anthony E Pickering. 2017. “Functional Dichotomy in Spinal- vs Prefrontal-Projecting Locus Coeruleus Modules Splits Descending Noradrenergic Analgesia from Ascending Aversion and Anxiety in Rats.” *ELife* 6 (Lc): e29808. https://doi.org/10.7554/eLife.29808.
- Kane, Gary A, Elena M Vazey, Robert C Wilson, Amitai Shenhav, Nathaniel D Daw, Gary Aston-Jones, and Jonathan D Cohen. 2017. “Increased Locus Coeruleus Tonic Activity Causes Disengagement from a Patch-Foraging Task.” *Cognitive, Affective and Behavioral Neuroscience* 17 (6): 1073–83. https://doi.org/10.3758/s13415-017-0531-y.
- Nilsson, Linda K, Lilly Schwieler, Gö Ran Engberg, Klas R Linderholm, and Sophie Erhardt. 2005. “Activation of Noradrenergic Locus Coeruleus Neurons by Clozapine and Haloperidol: Involvement of Glutamatergic Mechanisms.” https://doi.org/10.1017/S1461145705005080.
- Perren, a Van der, J Toelen, M Carlon, C Van den Haute, F Coun, B Heeman, V Reumers, et al. 2011. “Efficient and Stable Transduction of Dopaminergic Neurons in Rat Substantia Nigra by RAAV 2/1, 2/2, 2/5, 2/6.2, 2/7, 2/8 and 2/9.” *Gene Therapy* 18 (5): 517–27. https://doi.org/10.1038/gt.2010.179.
- Rorabaugh, Jacki M., Termpanit Chalermpalanupap, Christian A. Botz-Zapp, Vanessa M. Fu, Natalie A. Lembeck, Robert M. Cohen, and David Weinshenker. 2017. “Chemogenetic Locus Coeruleus Activation Restores Reversal Learning in a Rat Model of Alzheimer’s Disease.” *Brain* 140 (11): 3023–38. https://doi.org/10.1093/brain/awx232.
- Schwieler, Lilly, Klas R Linderholm, Linda K Nilsson-Todd, Sophie Erhardt, and Göran Engberg. 2008. “Clozapine Interacts with the Glycine Site of the NMDA Receptor: Electrophysiological Studies of Dopamine Neurons in the Rat Ventral Tegmental Area.” *Life Sciences* 83 (5–6): 170–75. https://doi.org/10.1016/j.lfs.2008.05.014.
- Vazey, Elena M, and Gary Aston-Jones. 2014. “Designer Receptor Manipulations Reveal a Role of the Locus Coeruleus Noradrenergic System in Isoflurane General Anesthesia.” *Proceedings of the National Academy of Sciences* 111 (10): 3859–64. https://doi.org/10.1073/pnas.1310025111.
- Watson, Charles, and George Paxinos. 2007. *The Rat Brain in Stereotaxic Coordinates*.

5. Publications

- Latoya Stevens, Kristl Vonck , Wouter Van Lysbettens, Veerle Baekelandt, Chris Van Den Haute, Paul Boon, Robrecht Raedt. Genetic modification of locus coeruleus NE cells for chemogenetic activation remains challenging. **BSN meeting 2019 Brussel (poster+abstract submission); Kempenhaeghe symposium 2019 Heeze (poster)**
- Latoya Stevens, Kristl Vonck , Wouter Van Lysbettens, Veerle Baekelandt, Chris Van Den Haute, Paul Boon, Robrecht Raedt Genetic modification of locus coeruleus NE cells for chemogenetic activation remains challenging. **f-tales 2019 Antwerpen (datablitz presentation + poster)**
- Latoya Stevens, Kristl Vonck , Wouter Van Lysbettens, Veerle Baekelandt, Chris Van Den Haute, Paul Boon, Robrecht Raedt Presumed subclinical doses of clozapine not useful for chemogenetic activation of Locus Coeruleus neurons in rats. **Research Day UGent (platform presentation) + SWO midwinter meeting 2019 (abstract submission + poster)**
- Latoya Stevens, Kristl Vonck, Lars Emil Larsen, Wouter Van Lysebettens, Charlotte Germonpré, Veerle Baekelandt, Chris Van Den Haute, Evelien Carrette, Wytse Jan Wadman, Paul Boon, Robrecht Raedt. A feasibility study to investigate chemogenetic modulation of the locus coeruleus by means of single unit activity. **Manuscript under review after submission of responses to first review** Frontiers in Neuroscience.
- Latoya Stevens, Kristl Vonck, Lars Emil Larsen, Evelien Carrette, Wytse Jan Wadman, Paul Boon, Robrecht Raedt. The use of CAV viral vectors to chemogenetically modify the locus coeruleus prior to single unit recordings. **Manuscript in preparation.**

6. Financial Report

	Universiteit Gent						STI.DI2.2017.0003.01				
	Prof. Kristl Vonck						365E04517				
							GSKE				
Benaming van instelling :	Ugent										
Rechtsgeldige vertegenwoordiger :	Rector Rik Van de Walle										
Nummer van de overeenkomst :	**Neurons in Epilepsy**										
Kostenstaat voor de periode :	01/01/2018 - 31/12/2019										
	Eindverslag										
omschrijving	**Bedrag TOTAAL**										
Personeelskosten	€ 0,00										
Werkingskosten	€ 101.889,79										
OVERHEAD 17%	17.321,26										
TOTAAL PROJECT	**€ 119.211,05**										
Geert Van de Gucht, directeur Financiën, namens de Rector, rechtsgeldige vertegenwoordiger UGent,											
bevestigt dat alle hierboven vermelde uitgaven werkelijk betaald zijn binnen het betreffende onderzoek.											
	Datum :										
	Handtekening :										
	Geert Van de Gucht, directeur Financiën,										

Geneeskundige Stichting Koningin Elisabeth – G.S.K.E.

Fondation Médicale Reine Elisabeth – F.M.R.E.

Queen Elisabeth Medical Foundation – Q.E.M.F.

Mailing address:

The scientifique director:
Prof. dr. Jean-Marie Maloteaux
3, avenue J.J. Crocq laan
1020 Bruxelles - Brussel
Belgium
Tel.: +32 2 478 35 56
E-mail: jean-marie.maloteaux@uclouvain.be

and

Secretary:
Mr. Erik Dhondt
3, avenue J.J. Crocq laan
1020 Bruxelles - Brussel
Belgium
Tel.: +32 2 478 35 56
E-mail: fmre.gske@skynet.be
E-mail: erik.dhondt@skynet.be, e.l.dhondt@skynet.be
www.fmre-gske.be
www.fmre-gske.eu
www.fmre-gske.com